Adaptive Incremental Nonlinear Dynamic Inversion for Consistent Pitch Rate Control

Master of Science Thesis

B. Smit

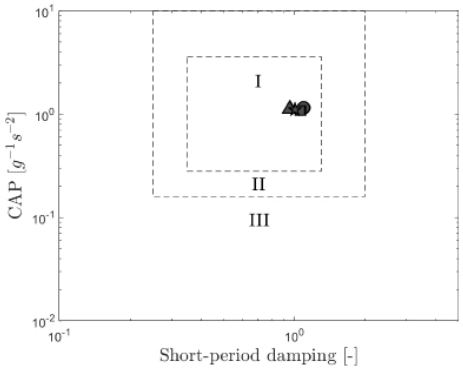

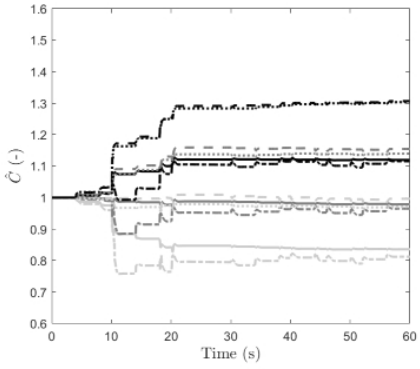

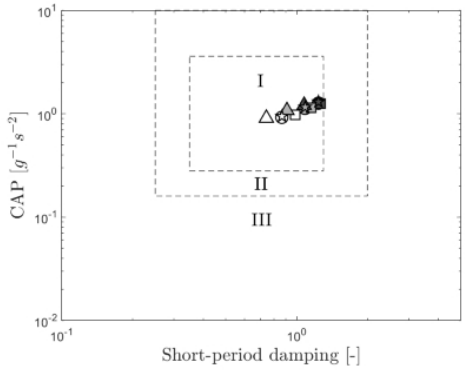

Technische Universiteit Delft

TU Delft

Adaptive Incremental Nonlinear Dynamic Inversion for Consistent Pitch Rate Control

Master of Science Thesis

by

B. Smit

to obtain the degree of Master of Science
at the Delft University of Technology,

Student number:	4289692	
Project duration:	December 9, 2019 – February 19, 2021	
Thesis committee:	Dr. ir. M. M. van Paassen,	TU Delft, chair
	Dr. ir. E. van Kampen,	TU Delft, supervisor
	Ir. T. S. C. Pollack,	TU Delft, supervisor
	Ir. M. L. Hoogendoorn,	Royal Netherlands Aerospace Centre (NLR), supervisor
	Ir. W. F. J. A. Rouwhorst,	Royal Netherlands Aerospace Centre (NLR), supervisor
	Dr. ir. E. Mooij,	TU Delft, Examiner

February 19, 2021

TU Delft

Preface

This thesis project concludes a mind-opening and inspiring study period at the faculty of Aerospace Engineering at the Delft University of Technology. I would like to thank to my parents, brother, sister, girlfriend and friends for their unconditional support during this time. Furthermore, as this thesis was performed during the Covid-19 pandemic, I have mainly been working at home. Therefore, I would also like to thank my roommates and girlfriend for being my necessary rubber duckies from time to time.

Furthermore, I would like to express my gratitude to my thesis supervisors Dr. ir. Erik-Jan van Kampen and Ir. Tijmen Pollack from the Delft University of Technology, and Ir. Marijn Hoogendoorn and Ir. Wilfred Rouwhorst from the Royal Netherlands Aerospace Centre (NLR) for giving me the necessary insights and expertise during this master's thesis project. In addition, I would like to thank Marijn Hoogendoorn and Wilfred Rouwhorst for giving me the opportunity to perform the thesis research at NLR.

Beau Smit
Delft, February 2021

Synopsis

Control augmentation systems based on Incremental Nonlinear Dynamic Inversion (INDI) are able to provide high-performance nonlinear control without the need for a model of the complete system. Considering a pitch rate control law for a fixed-wing high-performance aircraft, only a model for the elevator control effectiveness (CE) and sensor feedback of the pitch acceleration are required to close the inversion loop. Despite the increased robustness against model error compared to control laws based on Nonlinear dynamic inversion (NDI), INDI-based control laws could still suffer from performance variation when the on-board CE model deviates from the actual CE.

In this thesis it is demonstrated by simulations that CE model mismatches will induce variations in the control performance of an INDI-based pitch rate control law for a high-performance aircraft. The causes for CE model mismatches considered in this research are centre of gravity (CG) shifts, inertia changes and aerodynamic model error. The main goal of this thesis it to evaluate the most suitable method which could make the INDI-based pitch rate control law more robust against the aforementioned causes of model mismatch. Before the evaluation of the most suitable method, this thesis will study and analyse several methods from the adaptive control domain. Following from this analysis one adaptive INDI-based control law is selected and further investigated using handling quality and stability (HQ&S) guidelines.

In the initial verification study, four adaptive forms of the INDI-based pitch rate control law are analysed and compared. The considered adaptive applications are based on Recursive-Least-Squares (RLS) online system identification estimation, Least-Mean-Squares (LMS) online system identification estimation, Model Reference Adaptive Control (MRAC) and Immersion & Invariance (I&I) adaptive control.

The performance study on these adaptive INDI-based pitch rate control laws reveals that the MRAC and I&I adaptive designs considered in this thesis are unable to converge to a solution and cause an unstable closed-loop response. On the other hand, both the RLS and LMS adaptive control laws are able to obtain a better estimate of the CE model. A more elaborate verification and comparison study on the latter adaptive control laws established that the LMS approach has a more consistent performance for prolonged steady-state flight, noise and input time-delay compared to the RLS approach.

Consequently, the LMS adaptive INDI-based pitch rate control law has been selected for further investigation of the handling quality and stability (HQ&S) of a high-performance aircraft. In this part of the thesis, the non-adaptive and LMS adaptive control laws are designed using handling quality and stability guidelines. Then, for both control laws, the HQ&S variation is analysed for different combinations of forward and backward CG shifts, inertia changes and aerodynamic model mismatches. The results of this study revealed that the LMS adaptive INDI-based pitch rate control law was able to decrease the HQ&S variation. However, is was observed that large CG shifts impair the time-scale separation assumption which is used to derive the INDI-based pitch rate control law and the adaptive prediction model. Consequently, for these cases it was not possible to obtain a correct estimation of the CE model and a residual HQ&S estimation remained. Moreover, it is presumed that having a correct CE model estimate will not solve this HS&S variation.

Contents

List of Figures

List of Tables

Nomenclature

List of Abbreviations

AMDF	Average magnitude difference function
ARIMAX	Auto-regressive integrated moving average with exogenous input
ASDF	Average square difference filter
ASDF	Average square difference function
BS	Backstepping
CAP	Control anticipation parameter
CE	Certainty equivalence
CFD	Computational fluid dynamics
CG	Centre of gravity
CMSD	Cumulative moving standard deviation
DLR	German Aerospace Centre
EKF	Extended Kalman filter
EOM	Equations of motion
FBW	Fly-by-wire
FBW	Fly-by-wire
FCC	Flight control computer
FL	Fuzzy logic
FT	Fault tolerant
GARTEUR	Group for aeronautical research and technology in Europe
GMV	Generalized minimum variance
HIRM	High Incidence Research Model
I&I	Immersion and Inveriance
IBS	Incremental backstepping
ICR	Instantaneous centre of rotation
IEKF	Iterated extended Kalman filter
INDI	Incremental nonlinear dynamic inversion
ISA	International Standard Atmosphere
KF	Kalman filter
LMS	Least-mean-squares
LOES	Lower order equivalent system
LP	Linear-in-the-parameters
LPV	Linear parameter varying
LS	Least squares
LSF	Lyapunov stability function
LTI	Linear time-invariant
MAC	Mean aerodynamic chord
MAV	Micro air vehicle
MIMO	Multi-input-multi-output
MIT	Massachusetts Institute of Technology
MRAC	Model reference adaptive control
MSE	Mean square error
MUAD	Maximum unnoticeable added dynamics
NDI	Nonlinear dynamic inversion
NN	Neural networks
NP	Nonlinear-in-the-parameters
PCH	Pseudo control hedging
PE	Persistent excitation
PI	proportional-integral
PID	Proportional-integral-derivative
PIO	Pilot induced oscillations
RLS	Recursive least squares
RMS	Root-mean-square
SISO	Single-input-single-output
SM	Static margin
SMC	Sliding mode control
STC	Self-tuning control

STR	Self-tuning regulator
SVD	Singular value decomposition
TO	Tracking objective
UAV	Unmanned aerial vehicle
UKF	Unscented Kalman filter
UoM	University of Minnesota
VAAC	Vectored-thrust aircraft advanced-flight control

Symbols

α	°	Angle of attack
β	°	Angle of sideslip
β		I&I stabilization function
δ_a	°	Aileron deflection
δ_e	°	Elevator deflection
δ_r	°	Rudder deflection
Δx	m	Centre of gravity shift in x-direction
Δy	m	Centre of gravity shift in y-direction
Δz	m	Centre of gravity shift in z-direction
Δ		Incremental notation
ϵ		Estimation residual
Γ		Adaption gain matrix
γ		Adaption gain
λ		RLS forgetting factor
$\mathcal{L}$		Lebesgue space identifier
$\mathcal{M}$		I&I manifold
$\mathcal{V}$		Lyapunov stability function
μ		LMS adaption gain
ν		Virtual control input
ω	rad/s	Natural frequency
ϕ		LP model basis function
ϕ		Diffeomorphism functions
ρ		Relative degree
Σ		Residual covariance matrix
σ		I&I off-manifold error
θ		Uncertain model parameter(s)
A	m/s^2	Linear acceleration
A		A-matrix of state-space
A		Linear regression matrix
a		Function parameters
B		B-matrix of state-space
C		Aerodynamic model coefficient
CC		Computational complexity
E		Expectation operator
e		Difference between actual system output and reference model output
f		Nonlinear mapping of state to state time derivative
G		Control effectiveness
g		Nonlinear mapping of control input to state time derivative
g		Impulse response function coefficients
h		Nonlinear mapping of state to output
H		Transfer function
I		Identity matrix
I	kg·m^2	Mass moment of inertia
K		Linear control gain matrix
K		RLS update gain vector
k		Control gain
k		Discrete time index
L		Lie derivative
L	Nm	Aerodynamic moment around x-axis of body reference frame
m	kg	Mass
M	Nm	Aerodynamic moment around y-axis of body reference frame
N	Nm	Aerodynamic moment around z-axis of body reference frame
N		Number of data points in simulation
n		Number of model parameters
n_α		Change in load factor for a change in α
n_s		Number of samples in CMSD window
n_z		Load factor
p	°/s	Roll rate

P		Positive definite matrix in LSF
P		RLS covariance matrix
p		Crosscorrelation matrix
q		Internal dynamics
q	°/s	Pitch rate
Q		Positive definite design matrix in LSF
r	°/s	Yaw rate
R		Autocorreletaion matrix
S		Transfer function of sensor
s		Laplace operator
T	s	Total simulation time
t	s	time
u		Control input
v		Measurement noise
w		Input noise
x		System state
X	N	Aerodynamic force in the body reference frame x-axis direction
y		System output
Y	N	Aerodynamic force in the body reference frame y-axis direction
z		Transformed description of x
Z	N	Aerodynamic force in the body reference frame z-axis direction
z		Measurement of system output

1 Introduction

In the past decades one of the notions on high-performance military aircraft has been to improve their capabilities with respect to control characteristics Snell et al. (1992); Gal-Or (1990); Gallaway and Osborn (1985). This means higher manoeuvrability, more precise tracking, and possibility of flight at high angle-of-attack and angle-of-side-slip. Until today, most flight control system designs are based on gain scheduling control. The most used principle behind this control strategy is the *divide and conquer* approach, which assumes that the nonlinearity of the system could be grasped by a set of linear systems Leith and Leithead (2000a). To design the gain scheduling controller, linear controllers are designed for design points within the full operating envelope of the system. Each set of control gains is selected such that the control stability and performance complies with a set of design requirements. The obtained set of control gains of all controllers are then scheduled using scheduling variables to obtain a global controller (Enns et al., 1994).

The benefit of using linear descriptions of the system is the possibility of applying powerful linear methods, such as pole-placement and frequency analysis, for controller design and performance analysis (Rugh, 1991). Therefore, this design approach was regarded well suited for certification at the introduction of automatic flight control. Consequently, this design strategy became very popular since and currently still is.

However, gain-scheduling controllers have a few drawbacks. First of all, the task of determining the control gains and how to schedule them is time consuming and therefore costly (Enns et al., 1994). Furthermore, one of the fundamental assumptions is that the gain scheduling variables change slowly. As the states are often used as scheduling variable, this means that state transitions should not occur too fast (Shamma and Athans, 1992). However, high-performance military aircraft operate in a large flight envelope. Consequently, it is possible to achieve high acceleration and Mach numbers, high rotational rates, and large aerodynamic angles. These high acceleration and rotational rates result in fast changes of the scheduling variables which decreases the validity of the gain scheduling control design. Furthermore, the increased rotational rates amplify nonlinear inertial coupling effects and the behaviour of the aerodynamic forces and moments become significantly more nonlinear at high aerodynamic angles and Mach numbers. Therefore, the validity region of the linear approximation of the dynamics decreases (Snell et al., 1992; Albostan and Gökaşan, 2017). When these limitations are not considered appropriately in the control law design, it could result in increased pilot workload or an even an abort of the mission (Slotine and Li, 1991).

To relax the assumption on fast changing scheduling variables in classical gain-scheduling, approaches such as the velocity-based approach (Leith and Leithead, 2000b), a switch polytopic system approach (Hou et al., 2011), or a reformulation of the linear parameter varying (LPV) approach (Shamma and Athans, 1992) have been suggested. However, despite the ability to cope with faster changes in the scheduling variables and stronger nonlinearities, the approaches do not alleviate the design effort of the gain-scheduling controller.

To bypass the costly gain-scheduling procedure, alternative nonlinear control architectures have been investigated during the past decades. These architectures use nonlinear equations which allow them to be valid in a larger region of the flight domain. Examples of these control approaches are *Nonlinear Dynamics Inversion* (NDI), *Lyapunov redesign*, *Sliding Mode Control* (SMC), *Backstepping*, *Neural Networks* (NNs) and *fuzzy logic* (FL) control (Slotine and Li, 1991; Stengel, 1993).

Until today the NDI is probably the most used alternative approach. Due to the fact that the nonlinear properties of the system are taken into account in the control design it avoids the need for gain-scheduling. The nonlinear properties are incorporated in the controller by using the inverse nonlinear model in the feedback path of the most inner (inversion) control loop. This results in a *Linear Time Invariant* (LTI) linearization of the controlled system with respect to the outer loop which makes it possible to use a single linear controller to control the inversion loop (Khalil, 2002). The benefit of this structure becomes apparent when handling quality and stability (HQ&S) requirements need to be incorporated in the control design. The inversion loop accounts for the nonlinear system and therefore the outer loop can be designed with the focus on complying to the HQ&S requirements. Consequently, control design based on NDI could take less time for development, which means more time for prototyping or lower design cost. Moreover, due to the use of the dynamic model in this control law a NDI-based control law can be easily reconfigured for the control law of other aircraft. These aspects have led to many research projects investigating this technique including flight test in the Vectored-thrust Aircraft Advanced-flight Control (VAAC) Harrier (Smith and Berry, 2000) and the Cessna Citation II of NLR and the Delft University of Technology (Grondman et al., 2018). On top of that, the NDI approach has been applied in the flight control of the F-35 (Harris, 2018). However, The NDI design approach has a drawback. Due to the use of the complete system model in the controller, the NDI approach is sensitive to model mismatches (Sieberling et al., 2010). To make control laws based on this approach more robust for this issue, techniques based on, for example, H_∞ loop shaping, μ-synthesis and adaptive methods have been investigated (Smit and Craig, 1998; Reiner et al., 1995; Lombaerts et al., 2009). These techniques have shown to be effective, however at the expense of increased mathematical complexity of the control design. This could again lead to increased design effort and consequently less time for testing prototypes, or higher development cost.

At the end of the 1990's an inherently more robust form of feedback linearization has been introduced, called *simplified* or *modified* NDI (Smith, 1998). Today this method is known as *incremental nonlinear dynamic inversion*, or INDI (Sieberling et al., 2010). This theory has written the feedback linearization controller such that an increment of the control input is determined instead of the full control input. Furthermore, due to using a Taylor expansion for the definition the nonlinear system, the control approach is more general and therefore also valid for systems which are not input affine. Using the time-scale separation principle in the derivation of the method, the control law could be designed such that the complete system model is not required, but only the control effectiveness of the actuators. However, this reduction of model dependency comes at the drawback of requiring feedback of the ρ^{th} order time derivative of the control variables. Where ρ is the relative degree of the dynamic system equations. The concept of relative degree will be treated in section 2.1. The feedback of the ρ^{th} order time derivative of the control variables can either be obtained by using the so-called model-based approach or the sensor-based approach, see Figure 2.2. The model-based approach uses a model of the system again to determine the ρ^{th} order derivative feedback of the control variables from the state measurement while the sensor-based approach uses only sensors to obtain this feedback. In case the sensor-based approach is used and the ρ^{th} order time derivative cannot be measured directly, it is possible to use a derivative filter (Smeur et al., 2016). Furthermore, the calculation of the control increment and the lower model dependency make INDI control laws more robust against model uncertainty and has improved disturbance rejection performance compared to NDI (Wang et al., 2019b). These properties are realized without changing the controller

design complexity. Lastly, to complete the controller, the inverse of the control effectiveness model, G^+, is required. For over-actuated systems this matrix could not be inverted via the normal inverse, therefore a pseudo inverse or other control allocation approach could be applied (Smeur et al., 2016; Matamoros and de Visser, 2018).

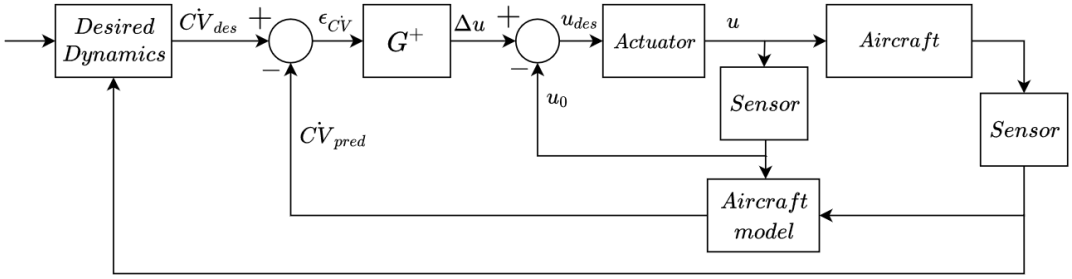

(a) Model-based INDI controller.

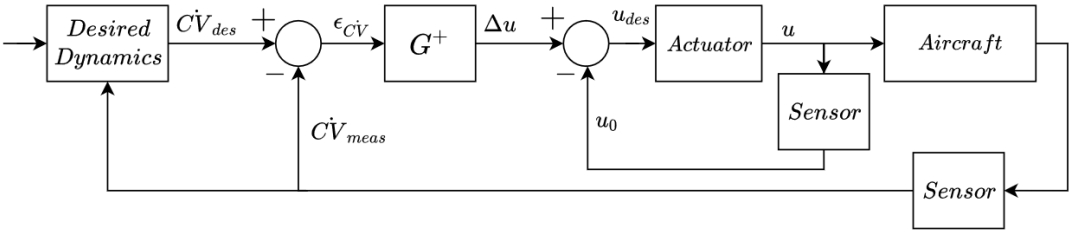

(b) Sensor-based INDI controller.

Figure 1.1: General block diagrams of INDI controller.

However, as INDI-based control laws are dependent on the control effectiveness, their performance could still be affected by model mismatches. A possible result of using an incorrect control effectiveness model has been shown in Smeur et al. (2016). Here, it is demonstrated that an underestimated control effectiveness model leads to sustained oscillations in the system response and overestimating model results in less damping and more overshoot of the system response. As this is a problem related to INDI, it can be postulated that the same effects could be found for INDI-based control laws of other aircraft. Therefore, it is likely that the control performance of high-performance aircraft will degrade under these conditions. This means that the pilot workload will change and probably increase. In addition, it might not be possible to perform the mission successfully. Consequently, there is a need for an accurate control effectiveness model.

Possible causes for deviations of aircraft models are aerodynamic model mismatches, changes in inertia (due to fuel consumption, payload release or airframe failure), centre of gravity (CG) shifts and actuator failure (Lombaerts, 2010). From these causes a discrimination can be made between failure and non-failure related causes. For example, aerodynamic model errors could result from limitations of the aerodynamic model identification techniques or from a damaged aircraft. Control systems which account for changes in the dynamic model due to failure are part of the *Fault Tolerant* (FT) control systems (Lombaerts, 2010). As a possible method to increase safety, this aspect of control research has gained significant attention during the past decades. Also for military aircraft this aspect is valuable as these aircraft have a much higher possibility to enter hazardous situations than civil aircraft. However, due to time constraints of this thesis it is impossible to adequately analyse and design a controller which could cope with system changes due to both failure and non-failure related changes in system dynamics. As adequate control of non-failure flight is regarded more important than fault tolerant control at this stage, this research project will therefore focus on non-failed flight.

Aerodynamic model mismatches, and changes in the aircraft inertia and CG location for non-

failure flight can be reduced by gathering more aerodynamic model data and developing a detailed mass model. A drawback of these solutions is that they require considerable effort and multiple resources to collect all the necessary data. Improving the aerodynamic model requires additional *computational fluid dynamics* (CFD) simulations, wind-tunnel tests or flight tests. Furthermore, high-performance military aircraft could have several store configurations, which should all be taken into account for the mass model. In addition, the amount of configurations could expand over time due to the development of new stores. Research has been conducted on inertia and CG location estimation methods which are more flexible and attempt to perform the estimations on-line. These methods are based on kinematic and kinetic approaches (Manshadi and Saghafi, 2018; Stanley, 2011; Wüest et al., 2019). Kinetic approaches for fixed-wing aircraft require an accurate aerodynamic model and either a good estimation of the CG location or inertia to function. Kinematic methods estimate the CG location and inertia based on sensor measurements (Manshadi and Saghafi, 2018). Although, the kinematic approaches allow for an estimation method that is independent of the aircraft dynamic model, the drawback is that only the CG location is determined and not the inertia. Consequently, additional methods will be required to estimate the inertia.

Next to the offline and online approaches discussed above to improve the accuracy of the dynamic model, there are also potential solutions in the control domain which allow for more robustness against model uncertainties. Methods to maintain constant control performance can be found in both the *active* and *passive* control domains (Lombaerts, 2010). Each domain adheres to a different philosophy in the handling of mismatches of the control law. Passive control architectures have fixed parameters which are selected such that the controller performance becomes insensitive to every mismatch within the bounds of the known causes. Active control methods have the ability to accommodate for the mismatches by actively monitoring the control performance and adjusting the controller if necessary. Both control augmentation strategies are viable approaches to handle model mismatches. Within these branches there are two approaches which handle on-board model mismatches of non-linear model-based control and do not consider a control horizon. These active and passive approaches are called *adaptive* and *robust* control, respectively (Lombaerts, 2010).

The fixed structure of robust control laws make them more predictable and therefore possibly easier to certify. On the other hand, systems with large uncertainty bounds could impose stringent requirements on the robustness of the control law. In the trade-off between control robustness and performance this could necessitate a reduction in control performance to achieve the desired amount of robustness (Hodel et al., 2008). For high-performance military aircraft, with large uncertainty bounds, this compromise might result into a conflict with the performance demands. On the other hand, using adaptive control laws this compromise in performance could potentially be circumvented. However, methods to evaluate the dynamic behaviour and stability of these control laws are not yet fully developed, which makes these control laws difficult to certify (Jacklin, 2008). On the other hand, regarding the novelty of robust and adaptive INDI-based control laws both these approaches are still in a proof-of-concept phase. Therefore, the aspect of certification will not be taken into account for the decision of which approach will be further investigated in this study. What is important in this decision is the potential control performance improvement which can be achieved with the robust or adaptive control law. As mentioned above, robust control laws could have reduced performance in case the known model uncertainty is large. Furthermore, it was mentioned that adaptive control laws have the ability to accommodate for these uncertainties while maintaining high control performance. From the perspective of achieving as high as possible control performance, this is a desirable characteristic. Moreover, due to the on-line adaption of the control parameters adaptive control has the potential to incorporate FT control as well. Consequently, given the high control performance demands and the characteristics of adaptive control, this research will further investigate the application of adaptive INDI-based control laws for the handling of model mismatches for high-performance military aircraft.

In this section it is established that INDI could be a suitable design strategy for the control laws of high-performance military aircraft. Furthermore, it has been substantiated that aerodynamic model mismatches, CG shifts and inertia changes negatively affect the control performance of INDI-based control laws and that adaptive forms have the potential to preserve the desired control performance. To the best knowledge of the author of this thesis, there is still a knowledge gap with respect to application of adaptive INDI in uncertain high-performance military aircraft flight control systems, especially for the accommodation of system changes due to CG and inertia changes. This is because INDI is still a relatively novel control law design methodology. Therefore, this thesis will contribute to this knowledge gap by investigating the performance of adaptive INDI-based control in handling the previously mentioned causes for changes in the system dynamics.

1.1. Research objective

This section will focus on the objective of the research performed in this Master's thesis. There is a wide range of subjects which could be of interest within the field on adaptive INDI-based control. However, due to a limited amount of time it is important to find a focus point. Therefore, only the subjects which are deemed to contribute most to the solution of the knowledge gap stated in the previous section are considered.

To evaluate whether the performance of the adaptive INDI-based control law meets the requirements for high-performance aircraft, the dynamic response will be compared to HQ&S requirements for this aircraft type. Furthermore, the HQ&S sensitivity for uncertainties related to CG shifts, inertia changes and aerodynamic model error will be analysed. However, a literature study on adaptive control will be performed first. This study will result in the selection of a compact set of adaptive INDI control architectures which will be further investigated. Furthermore, methods to evaluate the control and adaption performance of adaptive control laws will be investigated as well. Successive to the literature study, preliminary experiments will be performed in which the adaptive INDI control laws are compared. Finally, one adaptive approach is selected for further investigation of the handling qualities.

Furthermore, in van 't Veld (2016) it has been established that real-world phenomena, such as actuator dynamics, sensor/filter dynamics and signal synchronization, are important factors for the stability of INDI-based control laws. Furthermore, in Smeur et al. (2016) it has been shown that relative delay between the angular acceleration and actuator feedback significantly decreases the control performance. Consequently, to increase the fidelity of the analysis of the adaptive INDI-based control law, these real-world phenomena will be included in the simulations.

There are different layers and types of control. For example, the high level control layers are more concerned with position or altitude control and low level layers are dedicated to translation or rotation control. With respect to the model deviations considered in this study it was shown in Lombaerts (2010) that the rotational dynamics are most dominantly affected. Consequently, this research will only consider rotational control. Furthermore, this thesis is mainly concerned with the adaptive part of the INDI control law. To facilitate this, the design complexity of the INDI-based control law will be kept as low as possible. Therefore, the control objective will be to track a rate command as this requires only the design of the INDI inversion loop and a single outer loop. Moreover, to be able to perform the analysis steps for the adaptive INDI-based control laws mentioned above, the focus of the control law will be further demarcated to only controlling the pitch rate.

Lastly, a flight mission consists of multiple phases such as take-off, cruise and landing. These phases all have different requirements and characteristics which should be tested to know whether the control law performs adequate in that phase. As adaptive INDI-based control laws are still novel, the knowledge regarding the control performance in these different mission phases is not yet developed. However, due to the novelty of the INDI-based control laws there are still quite some questions to be answered before the full flight mission should be analysed. Moreover, as the time in this

research is limited, it has therefore been decided to perform all the simulations in cruise phase flight conditions. It is however recommended that the performance in the other mission phases will be analysed when the knowledge on this control law is more mature.

Considering the aforementioned knowledge gap, the methods to evaluate the adaptive INDI-based flight control law and the demarcation of the research project, the following research objective can be formulated:

The objective of this Master's thesis is to evaluate the handling qualities and stability of the most suitable adaptive INDI-based pitch rate control law for a high-performance aircraft, which could cope with control effectiveness model uncertainties due to longitudinal centre of gravity shifts, inertia changes and aerodynamic model mismatches. This will be achieved by first selecting the most suitable adaptive INDI-based control law from a literature study and preliminary experiments. Suitability will be evaluated by appropriate metrics, also obtained from literature. Finally, the performance of the selected adaptive control law will be evaluated according to handling quality and stability guidelines and compared to the non-adaptive control law.

The high-performance aircraft model used for the analysis in this study is the F-16 model described in Nguyen et al. (1979). This model is selected as it is the best publicly available model of a high-performance military aircraft. The model contains aerodynamic tables with measurements made between Mach 0.1 and 0.2. Though, from the analysis performed in Nguyen et al. (1979), this model is considered valid for an airspeed up to Mach 0.6. Furthermore, the aerodynamic model has an angle-of-attack range between -10° and +45° and sideslip angle range between -30° and +30°. The University of Minnesota (UoM) has implemented this model in the Matlab/Simulink environment which is readily available (Russel, 2003). A limitation of this model is that the CG location can only be changed in the longitudinal direction. Furthermore, structural vibrations are not included in the model either. Consequently, the control performance including structural vibrations cannot be evaluated and will be recommended for future research.

1.2. Research questions

Following from the research objective formulated in the previous section, six research questions could be defined to support this objective. These questions are stated as follows:

1. Which adaptive methods are suited for the integration in INDI-based pitch rate control of high-performance aircraft?
   (a) What are the adaptive control approaches?
   (b) What is the state-of-the-art research in the field of adaptive INDI?
   (c) Which methods are suited for INDI-based control?
2. How do longitudinal centre of gravity shifts, changes in inertia and aerodynamic model mismatches affect the INDI-based pitch rate control law?
3. Which evaluation metrics are suited for the assessment of adaptive INDI-based control?
   (a) Which metrics quantify control performance in adaptive control?
   (b) Which metrics quantify parameter estimation performance in adaptive control?
   (c) What is the appropriate metric for assessing computational complexity of adaptive control methods?

   (d) What are the appropriate handling quality and controller stability guidelines for the evaluation of the non-adaptive and adaptive INDI-based pitch rate control law?

4. How is the non-adaptive INDI-based pitch rate control performance affected when actuator dynamics, sensor dynamics, filters and computational delay are added to the system model?

5. Which adaptive INDI-based pitch rate control law is most suited for coping with aerodynamic model mismatches and system model changes due to centre of gravity shifts and inertia changes?

6. What are the differences in handling qualities and stability sensitivity between the non-adaptive and adaptive INDI-based pitch rate control law, considering aerodynamic model mismatches and system variation due to longitudinal centre of gravity shifts?

1.3. Research approach

To ultimately reach the research objective defined in the previous section and the to answer the research questions formulated above, the following research approach was followed:

1. **Construct theoretical framework on Incremental Nonlinear Dynamic Inversion and adaptive control**
   As this research will combine adaptive control with the INDI control design framework to find a solution which could cope with the aforementioned causes for model error, a literature study will be performed on the field of INDI and adaptive control. From this research a concise set of adaptive INDI-based pitch rate control laws will follow, which will be further investigated.

2. **Develop rotational equations of motion which incorporates aerodynamic model errors, longitudinal CG shifts and inertia changes**
   To obtain a better understanding about the effect of aerodynamic model mismatches and system changes related to CG shifts and inertia changes, a system model will be developed which includes these aspects. This knowledge could be used to gain understanding about how these causes for model mismatch affect the control performance of an INDI-based pitch rate control law.

3. **Develop performance analysis framework for the assessment of adaptive INDI-based control laws.**
   To be able to evaluate and compare the adaptive control laws it is required to have an appropriate set of metrics. As adaptive INDI control is a nonlinear controller it is not possible to use performance metrics based on linear control theory. Consequently, a literature review will be conducted to adaptive control performance metrics which are suited for nonlinear control evaluation. Furthermore, a literature review will be conducted on the evaluation of longitudinal control laws against handling quality guidelines.

4. **Non-adaptive and adaptive INDI-based pitch rate control law design**
   Here, the non-adaptive and adaptive INDI-based pitch rate control law designs are derived.

5. **Analysis of non-adaptive INDI-based pitch rate control law**
   To understand how the non-adaptive control law is affected by model mismatches related to system changes or aerodynamic model deviations, the non-adaptive INDI law performance will be analysed as well. Furthermore, actuator dynamics, sensor dynamics, filters and computational delay effects will be added to the system model to aid the realism of the simulation.

6. **Analysis of the adaptive INDI-based pitch rate control laws and selection of the most suitable version.**
   For the selection of the most suited adaptive INDI-based longitudinal rotational law, the performance of all adaptive control laws are tested and compared to each other. Furthermore, the sensitivity to noise and an increase in time-delay of the actuator command will be analysed.

7. **Redesign of non-adaptive and selected adaptive pitch rate control laws for handling quality and stability requirement compliance.**
   After selection of the most suited adaptive INDI-based pitch rate control law, the thesis will focus on compliance to HQ&S requirements and its sensitivity. To achieve possible compliance to these requirements, both the non-adaptive and adaptive control laws will be redesigned. This redesign phase will make sure that the control law will comply to the requirements for a nominal condition case. Compliance to the HQ&S requirements is verified at the same time to be sure that the final design meets the requirements.

8. **Handling quality and stability sensitivity analysis of the non-adaptive and selected adaptive INDI-based pitch rate control laws**
   Here, the non-adaptive and selected adaptive INDI-based control law are evaluated for its ability to maintain consistent handling qualities. Both control laws will be subjected to different cases of CG shifts, inertia changes and aerodynamic model error.

1.4. Thesis outline

The outline of the thesis is as follows. It is divided into five parts. The first part contains the scientific paper. This paper summarizes the results obtained during the process to answer the sixth research question. Furthermore, the second part focuses on the literature reviews. This part contains four chapters and treats the first three research questions of this thesis. The first chapter of the literature review, Chapter 2, considers the theory on feedback linearization, which is the foundation of the INDI control law design framework. Chapter 3 continues with the investigation into the adaptive control domain. Here, the information required to answer the first research question will be covered. Then, Chapter 4 will focus on the problem at hand. In this chapter, literature on modelling the aircraft dynamics while taking into account the influence of a centre of gravity and inertia changes on the motion will be studied. Furthermore, the obtained knowledge will be used to answer the second research question. Lastly, Chapter 5 will discuss the methods to evaluate the tracking and parameter estimation performance of nonlinear adaptive control laws. Furthermore, this chapter will treat the use of HQ&S guidelines for control performance evaluation. The analysis and synthesis of this information in this chapter will be used to answer the third research question.

The preliminary experiments part consists of three chapters. First of all, Chapter 6 will elaborate on the design of the non-adaptive INDI control law, and the theory and designs of the adaptive INDI control laws. Furthermore, Chapter 7 will focus on the change in performance of the non-adaptive INDI control performance for ideal and realistic control system models. Consequently, this chapter focuses on gathering the information to answer the fourth research question. Then, in Chapter 8, the tracking performance of the adaptive control laws will be analysed and compared to the non-adaptive INDI control law. Furthermore, the most suited adaptive INDI control law will be selected. Therefore, this chapter will cover the information required for the fifth research question.

The fourth part discusses the additional derivations and results. This part consists of chapter 9 which treats optional additional guidelines usable for a satisfactory optimization of the control law design parameters. Lastly, the fifth part wraps up this thesis with the conclusion and recommendations in Chapter 10. The conclusion treats the answers to the research questions considered in this thesis and puts the impact of the findings in this thesis in a broader perspective.

I

Scientific paper

Adaptive Incremental Nonlinear Dynamic Inversion Flight Control for Consistent Handling Qualities

B. Smit *

Control augmentation systems based on Incremental Nonlinear Dynamic Inversion (INDI) are able to provide high-performance nonlinear control without the need for a model of the complete system. Considering a pitch rate control law for a fixed-wing aircraft, only a model for the elevator control effectiveness (CE) and sensor feedback of the pitch acceleration are required for the model inversion. Despite the increased robustness against model error due to the decreased model dependency, control laws based on INDI could still suffer from performance variation when the on-board CE model deviates from the actual CE. This paper shows that longitudinal centre of gravity (CG) shifts and pitching effectiveness uncertainty could result in variation in the handling qualities and stability (HQ&S) for longitudinal flight. Furthermore, this paper investigates an adaptive solution based on online correction of the CE model using Least-Mean-Square (LMS) based parameter estimation. The results of this paper demonstrate that online parameter estimation and model correction could result in less HQ&S variation. However, it was found that higher dynamic pressure conditions together with forward and backward CG shifts could lead to violation of the time-scale separation assumption. As this assumption is used in both the INDI control law and the parameter estimation this leads to simultaneous degradation of the parameter estimation and control performance. It is presumed that omitting the time-scale separation assumption in the online parameter estimation could restore the estimation performance. However, as the INDI control law is designed using this assumption, the HQ&S variation due to large CG shifts might not be mitigated despite having a correct CE model.

Nomenclature

C	kg	Fuel tank capacity.
C	-	Correction factor.
$\bar{c}$	m	Mean Aerodynamic Chord.
$C_{m_{\delta e}}$	-	Elevator dependency of aerodynamic pitching moment coefficient.
e	deg/s	Pitch rate tracking error.
e_G	s^{-2}	Control effectiveness estimation error.
G	s^{-2}	Control effectiveness.
H	-	Transfer function.
I	$kg \cdot m^2$	Mass moment of inertia.
K	-	Control law design parameter.
M	kg	Mass.
$\mathcal{M}$	Nm	Pitching moment.
n_s	-	Number of observation window samples.
N	-	Size of data vector.
p	$deg \cdot s^{-1}$	Roll rate.
q	$deg \cdot s^{-1}$	Pitch rate.
$\bar{q}$	Pa	Dynamic pressure.
r	$deg \cdot s^{-1}$	Yaw rate.
s	-	Laplace operator.
s	s^{-4}	Cumulative Moving Standard Deviation Window variance.
S	m^2	Reference surface area.

*M.Sc student, Faculty of Aerospace Engineering, Control and Simulation Division, 2626 HS Delft, The Netherlands

t	s	Time.
T_s	s	Sampling time.
$\underline{u}$	deg	Control input vector.
$\underline{x}$	-	State vector.
α	deg	Angle-of-attack
δ_e	deg	Elevator deflection.
Δ	-	Incremental notation.
ν_q	$deg \cdot s^{-2}$	Virtual pitch control input.
μ	-	LMS adaption gain.
ϕ	$deg \cdot s^{-2}$	Regression basis function.
ζ	-	Damping coefficient.
ω	rad/s	Natural frequency.
$\|\cdot\|_\infty$	-	Infinity norm.

I. Introduction

The ongoing pursuit of increasing the flight capabilities of high-performance aircraft is driving the systems based on classical control theory to its boundaries. Higher angle-of-attack flight, velocities and agility are highly wanted improvements to enlarge the operational limits and therefore increase the platform capability.[1–3] At such flight conditions, aircraft behave significantly more nonlinear due to inertial coupling and increased nonlinearity of the aerodynamics. The consequence of this might be that the segmented linear model assumption used for classical control law design could become violated.[1, 4, 5] This problem causes degraded tracking performance which can lead to increased pilot workload or even an abort of the mission.

This limitation of classical control, together with need for more safety and less development cost of flight control systems, sparked interest in research on modern control theories which could cope with the nonlinear behaviour of the aircraft motion.[4, 6, 7] Some examples of nonlinear theories, which are thoroughly investigated during the past few decades, are Nonlinear Dynamic Inversion (NDI) and Backstepping.[4, 8] Flight control laws developed according to these theories require the complete aircraft model. The accompanying benefit of this is that the nonlinear character of the aircraft behaviour could easily be incorporated in the control law. Consequently, adequate control of the aircraft in highly nonlinear domains of the flight envelope should become possible. Another advantage of NDI and Backstepping control is that the need for complicated gain-scheduling can be avoided. Only some scheduling is still necessary to comply to the desired handling qualities and stability (HQ&S) at different flight conditions.[9]

Due to these aspects, NDI and Backstepping control are currently popular in flight control research and flight control designers, especially NDI control for high-performance aircraft.[1, 10] In the past decades several research projects have been conducted involving NDI and backstepping control which have demonstrated their high performance.[11–14] However, despite the high performance, it has been found that mismatches in the aircraft model and measurement error led to performance degradation.[15, 16] This problem stimulated research on control laws which are less dependent on the aircraft model. One of the proposed solutions is Incremental Nonlinear Dynamic Inversion (INDI).[17]

INDI is similar to NDI. It differs from NDI in the sense that the model equations are transformed into linear incremental equations before performing the inversion. Furthermore, assuming that the sampling frequency of the control system is high enough, it is possible to neglect the incremental state dependency of the linearized model. This significantly reduces the model dependency of INDI control laws. However, this comes at the expense of requiring feedback of the time derivative of the control variable, which could be difficult to obtain accurately.[16, 17] Moreover, as a consequence of the incremental model equations, this control law determines the desired incremental control effector change. Therefore, feedback of this system output should be available as well.

In some of these projects the performance of the INDI control law is shown by performing flight tests using the VAAC Harrier [18], a micro aerial vehicle (MAV) [19] and the PH-LAB Cessna Citation II of the Delft University of Technology and the Royal Netherlands Aerospace Centre (NLR) [20]. Furthermore, a recent study has theoretically proven that INDI control laws could be more robust and have better disturbance rejection than their NDI equivalents if the sampling frequency is high enough.[21] Despite this proof, flight tests with a micro aerial vehicle (MAV) in 2016 have demonstrated that an INDI flight control law, sampling at a rate of 512 Hz, could still suffer from significant performance degradation due to model mismatches.[19]

This paper will investigate the possible performance change, due to system uncertainties, of a pitch rate control law based on INDI. The performance change will be put in the context of handling qualities and stability (HQ&S) guidelines

for a high-performance (type IV) aircraft. HQ&S guidelines are developed to predict whether the workload of a pilot will be acceptable during a mission.[22] Next to compliance to these guidelines, it is preferred that the variation of the HQ&S remains small despite possible system uncertainties to retain a constant pilot workload.

Results presented in this paper will show that HQ&S variation, due to system uncertainties, can occur for an INDI-based pitch rate control law operating at a limited sampling rate (100 Hz). The system uncertainties considered in this paper originate from unanticipated longitudinal centre of gravity (CG) shifts and elevator effectiveness uncertainty. Finally, to cope with these uncertainties, this paper will investigate a possible indirect adaptive control solution based on online system identification and correction of the control effectiveness (CE) model. The premise is that an accurate CE model at all times could improve performance robustness against aforementioned issues. The online system identification algorithm used in this study is based on Least-Mean-Square (LMS) parameter estimation.[23, 24]

The outline of the paper is as follows. First, the INDI pitch rate control law and the additional online system identification algorithm derivation will be treated in Section II. This will be followed by Section III, which will elaborate on the employed design strategy to select the appropriate values for the design parameters of the INDI control law and LMS estimation algorithm. Furthermore, this section will discuss the approach to assess the HQ sensitivity of both the non-adaptive and adaptive pitch rate control law. Section IV will clarify the details of the simulation model used to perform the analysis. Then, the results and presented and discussed in Section V. Finally, this paper is concluded in Section VI.

II. Adaptive Incremental Nonlinear Dynamic Inversion pitch rate control

The control objective considered in this study is to track the pitch rate command given by the pilot. This section will elaborate on the derivation of the control law architecture using the INDI design framework. Furthermore, the online parameter estimation algorithm based on LMS is treated as well.

A. Inversion loop

To start the derivation of a pitch rate controller based on INDI consider the following model for the longitudinal rotational motion:

$$\dot{q} = \frac{I_{zz} - I_{xx}}{I_{yy}} pr + \frac{I_{xz}}{I_{yy}} \left(r^2 - p^2\right) + \frac{1}{I_{yy}} \mathcal{M} \tag{1}$$

Linearizing this equation with respect to the current time step, '0', and assuming that the control sampling rate is high enough such that time-scale separation between the control input and incremental state dependent parts is justified [17], the following result can be found:

$$\dot{q} = \dot{q}_0 + \frac{1}{I_{yy}} \frac{\partial \mathcal{M}\left(\underline{x}_0, \underline{u}_0\right)}{\partial \underline{u}} \Delta \underline{u} = \dot{q}_0 + \frac{\bar{q}_0 S \bar{c}}{I_{yy}} C_{m_{\delta_e}}\left(\underline{x}_0, \underline{u}_0\right) \Delta\delta_e = \dot{q}_0 + G_0 \Delta\delta_e \tag{2}$$

Setting $\dot{q}$ as the virtual control input, ν_q, and solving for the incremental elevator deflection, $\Delta\delta_e$, Equation (3) is obtained.

$$\Delta\delta_{e_c} = G_0^{-1}\left(\nu_q - \dot{q}_0\right) \tag{3}$$

Calculating the virtual control input, ν_q, is performed by the outer loop and will be discussed in the next section. Lastly, to complete the inversion loop the incremental elevator deflection should be added to the feedback of the elevator deflection to obtain the new commanded elevator deflection:

$$\delta_{e_c} = \delta_{e,0} + \Delta\delta_{e_c} \tag{4}$$

B. Outer loop

The architecture of the outer loop consists of a command filter and a closed loop Proportional-Integrator (PI) compensator as shown in Figure 2. A command filter is applied to directly incorporate the desired aircraft response in a transparent manner and the PI compensator is used to construct a closed loop controller which accurately follows the command filter output while being robust to system uncertainties. The command filter has the following structure:

$$\frac{q_{cf}}{q_{plt}} = \frac{K_{cf_1} s + K_{cf_3}}{s^2 + K_{cf_2} s + K_{cf_3}} \tag{5}$$

This second order command filter architecture has been selected as it has the same structure as the aircraft short period *lower order equivalent system* (LOES) model without the time delay factor.[25] If the closed loop part of the control law could accurately follow the command filter output, this control law architecture allows for convenient incorporation of desired second order short term behaviour. Together with the PI compensator, this architecture will result in sufficient design flexibility as will be seen later on. To calculate the virtual control input, a feed-forward term containing the time derivative of the command filter output is added as well. This term is added to assure that the closed loop control tracks the command filter with zero error (in absence of external disturbances) and results in the following control law:

$$\nu_q = K_P \left(q_{cf} - q_0\right) + \frac{K_I}{s} \left(q_{cf} - q_0\right) + s q_{cf} \tag{6}$$

The aircraft tracking response, assuming negligible actuator and feedback path dynamics and perfect inversion, will be as follows:

$$q = \frac{1}{s}\nu_q = \frac{1}{s}\left(K_P \left(q_{cf} - q_0\right) + \frac{K_I}{s} \left(q_{cf} - q_0\right) + s q_{cf}\right) \tag{7}$$

$$\downarrow$$

$$sq + K_p q + \frac{K_I}{s} q = s q_{cf} + K_p q_{cf} + \frac{K_I}{s} q_{cf} \tag{8}$$

$$\downarrow$$

$$\frac{q}{q_{cf}} = 1 \tag{9}$$

Furthermore, using the same assumptions, the response of the closed loop control law for a constant command to an error in the pitch rate, $e = q - q_{cf}$, is as follows:

$$\dot{e}\left(t\right) + K_p e\left(t\right) + K_I \int_0^t e\left(t\right) dt = 0 \tag{10}$$

C. Least-Mean-Square online parameter estimation

The goal of the online parameter estimation is to correct for the uncertainty in the on-board model used in the inversion loop. Considering Equation (3), the model uncertainty can be found in the term G_0^{-1}. This term is dependent on the uncertain nonlinear aerodynamic model, $C_{m_{\delta_e}}$, and the mass moment of inertia around the body reference frame Y-axis, I_{yy}, as shown in Equation (2). Both the aerodynamic model and inertia are affected by CG shifts. Furthermore, as the CE is dependent on the aerodynamic model divided by the inertia, the influence of CG shifts on the CE is likely to be nonlinear. To estimate the changes of the inertia and aerodynamic model separately, nonlinear parameter estimation algorithms are required. As these algorithms are rarely suitable for real-time applications, this study will apply another strategy.

The approach applied in this study is to model the uncertainty as lumped together in one uncertain term, $g\left(\underline{x}_0, \underline{u}_0\right) = I_{yy}^{-1} C_{m_{\delta e}}\left(\underline{x}_0, \underline{u}_0\right)$, and estimate a correction factor, $\hat{C}$, online to scale the deviating model until it closely approximates the actual CE of the aircraft. Using this strategy allows for the application of linear parameter estimation methods which have the potential of real-time operation.

The estimation algorithm applied in this study is based on LMS parameter estimation.[23, 24] Algorithms based on this theory have been applied in many adaptive filter applications and recently it has been used for the control of a UAV.[19] The attractiveness of this approach lies in the straightforward design and the low computational complexity while still being able to obtain accurate estimations.[23]

To apply the LMS parameter estimation algorithm for estimating the correction factor, the regression model for the uncertain pitching motion will be written as shown in Equation (11) and the regression basis function is defined as Equation (12).

$$\dot{q} - \dot{q}_0 = \Delta\dot{q} = \hat{C}\bar{q}_0 S\bar{c} g_{nom}\left(\underline{x}_0, \underline{u}_0\right)\Delta\delta_e = \hat{C}\phi\left(\underline{x}_0, \underline{u}_0\right) \tag{11}$$

$$\phi\left(\underline{x}_0, \underline{u}_0\right) = \bar{q}_0 S\bar{c} g_{nom}\left(\underline{x}_0, \underline{u}_0\right)\Delta\delta_e = G_{nom}\left(\underline{x}_0, \underline{u}_0\right)\Delta\delta_e \tag{12}$$

Here, $\phi\left(\underline{x}_0, \underline{u}_0\right)$ is the regression model basis function and contains the nominal CE model, $G_{nom}\left(\underline{x}_0, \underline{u}_0\right)$, that predicts the nominal increment of $\dot{q}$ from an increment in δ_e. The LMS parameter estimation algorithm is shown in Equation (13).

$$\hat{C} = \hat{C}_0 + \mu\phi\left(\underline{x}_0, \underline{u}_0\right)\left(\Delta\dot{q} - \hat{C}_0\phi\left(\underline{x}_0, \underline{u}_0\right)\right) \tag{13}$$

The estimated value of the required correction factor, $\hat{C}$, will be used to improve the model inversion in the inversion loop of the INDI control law. Consequently, the inversion loop of the LMS adaptive INDI pitch rate control law will have the following structure:

$$\Delta\delta_e = \left(\hat{C}G_{0,nom}\right)^{-1}\left(\nu_q - \dot{q}_0\right) \tag{14}$$

III. Control law design and evaluation strategy

This section elaborates on the approach for finding an appropriate set of control law design parameters and the strategy to evaluate the HQ&S sensitivity of the non-adaptive and adaptive control laws. As the adaptive control law can be considered as a non-adaptive control law with a modular adaptive element, the design phase will consist of two parts. Section III.A focuses on the selection of the parameters for the non-adaptive control, $K_p, K_I, K_{cf_1}, K_{cf_2}, K_{cf_3}$, and Section III.B treats the selection of the appropriate LMS adaption gain, μ. Lastly, Section III.C treats the HQ&S evaluation approach adopted in this study.

A. Non-adaptive control law design

The goal of this study is to analyse whether online correction of the on-board CE model could decrease the sensitivity of the HQs and control performance. To achieve this objective, the non-adaptive control law will be designed taking into account relevant HQ guidelines during the development process. This approach allows for improved realism of the design and therefore the final sensitivity results are easier to put into a practical perspective.

To be able to perform this design approach, the student version (6.0) of the software package CONDUIT® is utilized.[26] This software package allows for optimization of the control law design parameters while immediately reflecting the intermediate design iterations on the considered HQ&S specifications. However, the student version itself contains a restricted amount of specifications. Therefore, to be able to perform the optimization and analysis, several are custom made using Specmaker version 1.5.[26] These specifications are indicated with a '*' in Table 1 and 2.

Resources for relevant HQ guidelines are the military standards MIL-STD-1797A [25] and several other handling quality technical reports and best practices [26–31]. From these sources a set of handling quality guidelines as listed in Table 1 is selected. These guidelines are considered important for design and verification of longitudinal control laws of high-performance military aircraft. Although this set of guidelines is likely to be incomplete, this study only considers sources from the public domain. Nevertheless, the goal of the design phase is to find a set of parameters for which all considered handling qualities and stability characteristics are inside their specified level 1 region.

Furthermore, to guide the optimization a few extra design objectives are added to the optimization. These additional objectives are summarized in Table 2. The goals of these objectives are to monitor the design process and ensure that the control law remains stable and the broken-loop response remains robust for shifts in gain/phase margins, see the first three rows of Table 2. Furthermore, additional objectives for the LOES guidelines and command model following performance are applied to improve the second order behaviour of the closed-loop controlled aircraft (row 4 and 5 of Table 2). Lastly, the actuator activity is monitored for the pilot and disturbance input and the broken-loop cross-over frequency is evaluated.

Recommendations from Tischler [26] state that the actuator activity could be minimized to find a design that satisfies all objectives while using the least amount of control power possible. This approach could reduce actuator wear and the chance of Pilot Induced Oscillations (PIO). However, a different approach will be followed in this study and the control law will be optimized for maximal performance robustness. This robustness will be induced by maximizing the broken-loop cross-over frequency at the broken-loop location, which is at the input of the actuators as shown in Figure 1, while keeping the other requirements in their level 1 region. Approaching the control problem in this manner allows for as much control power as possible to overcome uncertainties. It should be noted that increasing the performance robustness does come at the cost of decreasing the stability robustness just as increasing the cross-over frequency (high gain control) decreases the stability margins [33]. Consequently, there is an upper limit for the performance robustness.

Table 1 Handling quality criteria for optimization.

Criterion Name	Description	Source	Comment
Short Period damping (ζ_{SP}) vs. Control Anticipation Parameter (CAP)*	Restrains CAP and LOES ζ_{SP}.	MIL-HDBK-1797A [25]	Simultaneous short term pitch rate and load factor response fit. 0.1-10 rad/s.
Equivalent Time Delay*	Evaluates the LOES fit equivalent time delay.	MIL-HDBK-1797A [25]	Simultaneous short term pitch rate and load factor response fit. 0.1-10 rad/s.
Pitch attitude Dropback*	PIO guideline. Restrains the pitch rate overshoot and pitch attitude dropback.	WL-TR-94-3162 [28]	Pitch rate unit step input held for 8 seconds.
Neal-Smith*	Evaluates pilot effort for pilot-in-the-loop closed-loop pitch attitude control.	MIL-HDBK-1797A [25] AFFDL-TR-70-74 [32]	Pilot model settings: ω_{BW} = 3.5 rad/s, T_{lag} = 0.25 s, Max. droop = -3 dB. 0.1-10 rad/s.
Pitch attitude bandwidth vs. Phase delay*	PIO guideline. Limits the pitch attitude bandwidth and phase delay.	WL-TR-94-3162 [28]	0.1 - 50 rad/s.
Gibson Phase Rate*	PIO guideline. Limits the phase rate at $\omega_{\phi=180^o}$ and limits $\omega_{\phi=180^o}$.	AGARD-CP-508 [29]	0.1 - 50 rad/s.
Flight Path Bandwidth vs. Pitch Attitude Bandwidth*	Ensures appropriate ratio of flight-path and pitch attitude bandwidth.	WL-TR-94-3162 [28]	0.1 - 50 rad/s.

* Indicates a custom criterion developed in CONDUIT Specmaker 1.5.

However, from experience gathered during this study, this approach does not lead to unstable control systems when the uncertainties are added to the nominal model. Therefore, this design strategy is regarded appropriate.

Although the INDI control design framework allows for nonlinear control law design due to the inclusion of the nonlinear CE model of the aircraft, the HQ guidelines used for the control law design here are developed for linear control systems. Consequently, the control law design and evaluation could only be performed for linear systems, which means that this process should be performed separately for a trimmed and linearized control system at each considered flight condition.

B. LMS parameter estimation algorithm design

The design phase of the LMS estimation algorithm consists of selecting an appropriate value for the adaption gain, μ. This objective will be reached by evaluating the estimation performance during time-domain simulations for different adaption gain values. The metrics used for the performance characterization are the Root-mean-square (RMS) [16, 34] and $\mathcal{L}_\infty$-norm [35–37] of the temporal error between the actual CE and the corrected CE model, and the cumulative moving standard deviation (CMSD) of the estimated correction factor, $\hat{C}$ [38]. The mathematical descriptions of these metrics are defined as described in Equation (15) until (17).

$$RMS\left(e_G\right) = \sqrt{\frac{1}{N}\sum_{i=1}^{N}\left(\hat{C}\left(i\right)G_{nom}\left(i\right) - G\left(i\right)\right)^2} \tag{15}$$

$$\left\|e_G\right\|_\infty = \max_{t\in T}\left\{\left|\hat{C}\left(t\right)G_{nom}\left(t\right) - G\left(t\right)\right|\right\} \tag{16}$$

$$CMSD\left(\hat{C}\right) = \sum_{j=n_s/2+1}^{N-n_s/2}\sqrt{\frac{1}{n_s-1}\sum_{k=0}^{n_s-1}s_j\left[k\right]}, \quad s_j\left[k\right] = \left(\hat{C}\left[j-n_s/2+k\right] - \bar{\hat{C}}_j\right)^2 \tag{17}$$

Table 2 Additional criteria for optimization.

Criterion Name	Description	Source	Comment
Eigenvalues	Ensures stable eigenvalues of control system.	Practical Methods for Aircraft and Rotorcraft Flight Control Design [26]	Max. real value: 10^{-3}.
Nichols Margins (Broken-Loop)	Ensures robustness for simultaneous shifts in broken-loop gain/phase margins	FM(AG08)-TP-088-4 [39]	0.01 - 100 rad/s. Loop broken before actuator input
Gain/Phase Margins (Broken-Loop)	Ensures robustness in broken-loop gain and phase margin	MIL-DTL-9490E [40]	0.01 - 100 rad/s. Loop broken before actuator input.
Max. Allowable LOES Cost	Limits the LOES fitting cost.	MIL-HDBK-1797A [25]	Limit set at 20. MUAD bounds are driving limits.
Model Following Cost*	Ensures closed-loop control law accurately follows the command filter output.	Practical Methods for Aircraft and Rotorcraft Flight Control Design [26]	Uses LOES equi. time delay. Simultaneous short term pitch rate and load factor response fit. 0.1 - 10 rad/s.
Actuator RMS (pilot input)	Evaluates RMS actuator position. Measure for actuator activity.	Practical Methods for Aircraft and Rotorcraft Flight Control Design [26]	0.1 - 1000 rad/s. Max. pilot input: 20 deg/s. Max. actuator deflection 25 deg.
Actuator RMS (disturbance input)	Evaluates RMS actuator position. Measure for actuator activity.	Practical Methods for Aircraft and Rotorcraft Flight Control Design [26]	0.1 - 1000 rad/s. Max. disturbance input 10 deg/s. Max. actuator deflection 25 deg.
Cross-over frequency (Broken-Loop)	Evaluates the broken-loop cross-over frequency	Practical Methods for Aircraft and Rotorcraft Flight Control Design [26]	0.1 - 40 rad/s. Loop broken before actuator input.

* Indicates a custom criterion developed in CONDUIT Specmaker 1.5.

Here, G_{nom} is the nominal on-board model used by the INDI-based pitch control law. Furthermore, s_j and $\bar{\hat{C}}_j$ are the local variance and average estimated correction factor of the data window, respectively. The RMS of the estimation history is used as metric for the spread in the error or constant bias during the simulation. Besides, as the amount of simulation time is limited, a smaller RMS value also could indicate that the parameter estimation converges close to the desired value faster. Furthermore, the $\mathcal{L}_\infty$-norm of the estimation error gives the maximum observed error value during the simulation. This metric shows whether the parameter estimation remains bounded during the simulation and could be used to analyse how this bound changes for different values of the adaption gain. Lastly, the CMSD of the estimated parameter gives an indication of the estimation activity during the simulation. A high value means that the estimated parameter still experiences significant variation despite being converged around a mean value. Too much variation is unwanted as this could affect the control performance of the complete adaptive control law again. Consequently, the value of the adaption gain will be selected such that the CMSD will be as low as possible.

The variation of these performance metrics will be analyzed for different values of the adaption gain for all deviation cases described in Section III.C. Considering the variation, an adaption gain will be selected for which the LMS parameter estimation achieves adequate performance according to the three metrics described above.

C. Handling quality sensitivity evaluation

This section will discuss process of the HQ&S sensitivity analysis. A practical approach is adopted in which different CG locations together with CE uncertainty will be considered. The CG cases will be simulated depending on the fuel distribution in the aircraft. As will be shown in Section IV.B, a fuel tank configuration consisting of one front and one rear tank will be assumed. Furthermore, using this configuration the handling qualities and stability for the nominal, most forward, most backward and a low fuel CG locations will be analysed. In addition, an elevator effectiveness deviation of -15%, 0% and +15% will be applied at each CG location. This means that a total of twelve cases will be evaluated. From these cases the one with a nominal CG position and 0% CE deviation will be used for the nominal control law design. Moreover, these cases will be analysed for different flight conditions to be able to evaluate the efficacy of the online parameter estimation at different points in the flight envelope. The considered flight conditions in this study are described in Table 3.

To analyse the handling qualities and stability for each case, the CONDUIT® software package will be used as well. This means that again only a linearized version of the control law and aircraft model can be used. For the analysis of the non-adaptive control law, only the aircraft model will change according to the considered deviations. Therefore, the change in HQs will be determined using the nominal control law design.

Determining the HQs sensitivity of the adaptive control law will require a combination of time-domain simulations and HQ&S determination using CONDUIT. The time-domain simulations will be performed with the non-linear aircraft model to verify that the parameter estimation would still function with the complete system dynamics. During the simulations, the adaptive control law will execute a pitch rate tracking task and the parameter estimator will attempt to find the desired correction factor. The tracking task will be repeated several times, each time starting with the last estimated value of the correction factor from the previous simulation. Each repetition of the tracking task is called an episode. The tracking task will be repeated until the estimation response does not show significant differences between simulations anymore. At this point convergence is achieved and the average value of the correction factor estimation response will be used for the HQs evaluation. The CE model used in the non-adaptive control law will be multiplied by this average value and the HQ&S are re-evaluated.

Table 3 Flight condition information.

		FC-1	FC-2	FC-3	FC-4
Altitude	[m]	12000	3000	7000	5000
Mach number	[-]	0.6	0.6	0.4	0.5
Velocity	[m/s]	177	197	125	160
Dynamic pressure	[Pa]	4871	17667	4599	9453

IV. F-16 aircraft model

The high-performance aircraft model which will be applied in this study is the F-16 model developed by the University of Minnesota and NASA [41]. The aerodynamic model used in this aircraft model is obtained from wind-tunnel test performed as M = 0.2. Though, from simulator studies performed in [42], it is observed that the model could be used for controller design until a Mach number of 0.6. Furthermore, the low-fidelity model is applied in this study. This means that the effect of the leading edge flap is not taken into account and the coupling between the symmetric and asymmetric motion is reduced. Besides, the low-fidelity non-linear aerodynamic model contains data for $-10 \leq \alpha \leq 45$ degree. To be able to carry out the analysis steps which are described in the preceding sections, some alterations have been made to the F-16 model and additions have been applied to the complete simulation model. This section will elaborate on these modifications. Figure 1 and 2 respectively present the block schemes of the inversion loop and outer loop containing all components described in this section.

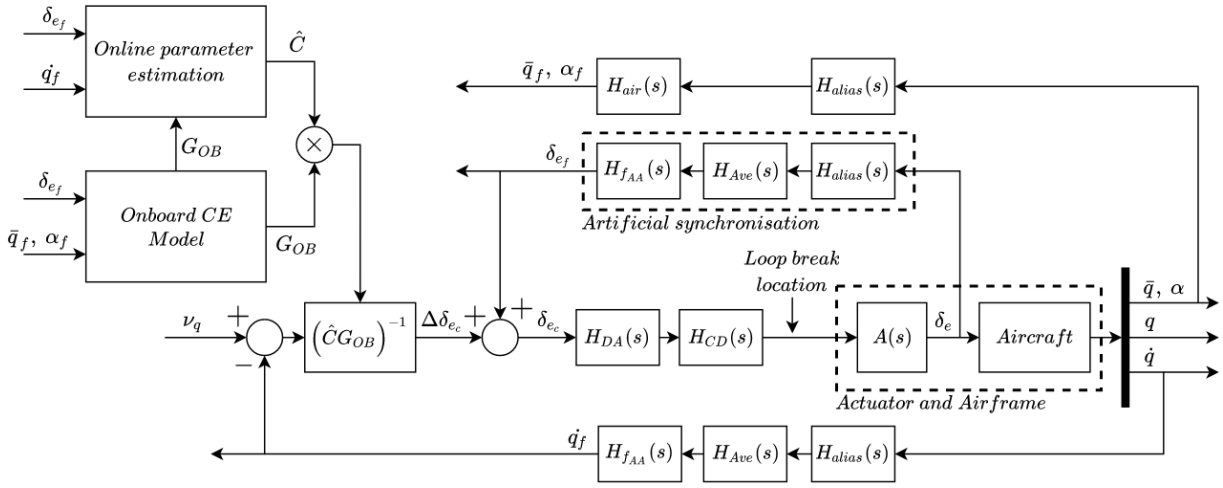

Fig. 1 Adaptive INDI control system inner loop block scheme including broken-loop location.

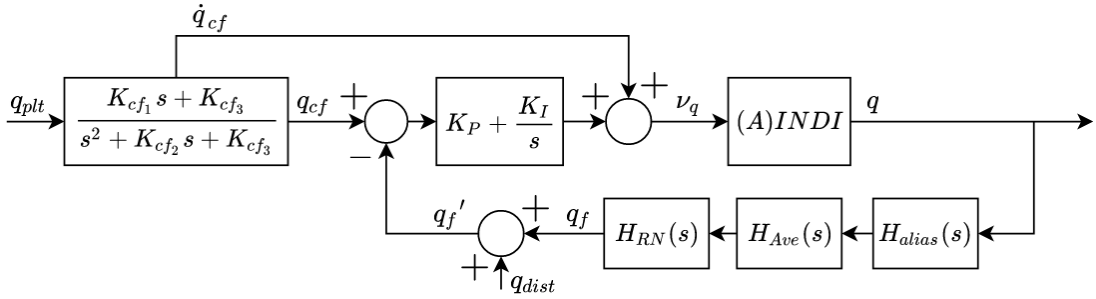

Fig. 2 Adaptive INDI control system outer loop block scheme including pitch rate disturbance input location.

A. Control System Properties

Real-world control systems are far from ideal due to the additional dynamics of sensors, filters and actuators. The derivation of an INDI-based control law assumes instantaneous deflections of the elevator and no loss of information of the feedback signals. As these characteristics cannot be achieved in real-world systems, the control performance and stability will be decreased with respect to an ideal system. Furthermore, as noise is always present filters are implemented as well which could significantly affect the feedback signals. Consequently, to improve the realism of the analysis, these aspects are also taken into account. Unfortunately, the control system of the F-16 is quite ad-hoc, which complicates the assessment of the function of each element. Therefore, the models used here are taken from Muir [39]. This research project focuses on flight control design of a high-performance aircraft as well and uses a clear description of the system elements. The sensor dynamics are specified for air data, and rate and linear accelerations:

- Air data:

$$H_{air}(s) = \frac{1}{0.02s + 1} \tag{18}$$

- Rate and linear acceleration (with notch filter):

$$H_{RN}(s) = \frac{0.0001903s^2 - 0.005346s + 1}{0.0004942s^2 + 0.03082s + 1} \tag{19}$$

Furthermore, for this control system it is assumed that the pitch acceleration can be measured directly using an angular accelerometer (AA).[43] The dynamics of this feedback signal is presumed to be mostly dominated by the filter dynamics. The filter structure used for the angular acceleration measurements is the same as used in [43]:

$$H_{f_{AA}}(s) = \frac{\omega^2_{f_{AA}}}{s^2 + 2\zeta_{f_{AA}}\omega_{f_{AA}}s + \omega^2_{f_{AA}}} \tag{20}$$

The filter parameters are set to $\omega_{f_{AA}} = 30$ rad/s and $\zeta_{f_{AA}} = 1$. Furthermore, for incremental control laws it has been observed that synchronization of the angular acceleration and control surface deflection is necessary. For this analyses, the same approach as used in Smeur et al. [19] will be adopted. Consequently. the synchronization of these signals is achieved by delaying the elevator deflection measurement using an equivalent filter which approximates the angular acceleration feedback dynamics. A more advanced approach is estimating the relative delay in real-time, as is investigated in van 't Veld et al. [44]. In addition to these models, Muir [39] specifies that the rate and linear acceleration feedback paths also contain averaging dynamics and that these can be modelled as zero-order-hold (ZOH), see Equation (21). Next to these channels it will be assumed that averaging will also be required for the angular acceleration feedback signal.

Next to the feedback dynamics described by [39], the complete control system model will also account for a limited sampling frequency of the system. This is added to the model as Fly-by-wire control systems are digital. It is assumed that the system in this study operates at 100 Hz. To incorporate the limitations of the restricted sampling rate, continuous-time models of anti-aliasing, $H_{alies}(s)$, a digital-to-analogue (DA) converter, $H_{DA}(s)$, and computational delay, $H_{CD}(s)$, are added to the simulation model. [45] The delay, assumed to be one sampling period, is implemented just before the actuator input and is modelled using a second order Padé approximant. Furthermore, the anti-aliasing filters are placed just after the sensor models. The DA converter will be modelled as a continuous-time ZOH transfer function and the anti-aliasing as a first order lag with the cut-off frequency less than half the sampling frequency, here selected at 45 Hz.[45]:

$$H_{DA}(s) = \frac{\frac{T_s^2}{60}s^2 - \frac{T_s}{10}s + 1}{\frac{T_s^2}{20}s^2 + \frac{2T_s}{5}s + 1} \tag{21}$$

$$H_{alias}(s) = \frac{\omega_{alias}}{s + \omega_{alias}} \tag{22}$$

The block diagrams describing the complete control system are shown is Figure 1 and 2.

B. Mass model

As mentioned before, the handling qualities will be analyzed for different CG locations. These CG locations will be obtained by changing the fuel distribution over the tanks. To be able to do this a geometric configuration of one front and one rear fuel tank will be assumed. According to the US Air Force official website*, the total fuel capacity of the F-16C/D, without external tanks, is approximately 3.175 kg and the airframe mass is approximately 8936 kg. The parameters used for the mass model are shown in Table 4 and the equations used to determine the CG shifts are given in Equation (23) and (24). In this model it is assumed that the mass moment of inertia of the fuel in the tank itself can be neglected and therefore only the parallel axis term is applied.

Table 4 Mass model parameters.

		Front tank (ft)	Rear tank (rt)	Airframe (af)
Longitudinal CG position (x_{cg})	[$\bar{c}$]	-0.3	0.9	0.35
Capacity (C) / Mass (M)	[kg]	1587.5	1587.5	8936
Inertia (I)	[kg·m^2]	-	-	74121

$$x_{cg,tot} = \frac{x_{cg,af}M_{af} + x_{cg,ft}C_{ft} + x_{cg,rt}C_{rt}}{M_{tot}} \tag{23}$$

$$I_{yy,tot} = I_{yy,af} + M_{af}\bar{c}^2\left(x_{cg,af} - x_{cg,tot}\right)^2 + C_{ft}\bar{c}^2\left(x_{cg,ft} - x_{cg,tot}\right)^2 + C_{rt}\bar{c}^2\left(x_{cg,rt} - x_{cg,tot}\right)^2 \tag{24}$$

*USAF, 'F-16 Fighting Falcon', *US Air Force*, Hampton, USAF, 2015, https://www.af.mil/About-Us/Fact-Sheets/Display/Article/104505/f-16-fighting-falcon/, (accessed December 10 2020)

To be able to use the values for the different CG location, inertia and total mass, the University of Minnesota F-16 Simulink model inputs have been adjusted such that these quantities could serve as model input as well. The mass and inertia properties of the aircraft at the nominal, forward, backward and low-fuel CG locations are summarized in Table 5.

Table 5 Mass and inertia properties per CG location.

		Nominal	Front	Rear	Low fuel
Longitudinal CG position ($x_{cg,tot}$)	[$\bar{c}$]	0.338	0.254	0.435	0.350
Total mass (M_{tot})	[kg]	12111	10523	10523	9253
Inertia ($I_{yy,tot}$)	[kg·m^2]	87804	80944	78941	75492

V. Results and discussion

The obtained results will be shown and discussed here. First, the control law designs for each flight condition will be treated in Section V.A. During the analysis it was found that the results of FC-1 were quite similar to those of FC-3 and the results of FC-4 showed significant resemblance to FC-2. To focus on the most relevant results, Section V.B will only display the HQ&S results of FC-2 and FC-3. Lastly, the presented results will be discussed more elaborately is Section V.C.

The analysis of the parameter estimation is performed in the time domain. Consequently, it was required to define a standard pitch rate tracking signal. The signal is shown in Figure 3. This signal was carefully constructed to keep the aircraft motion inside the linear region of the flight condition.

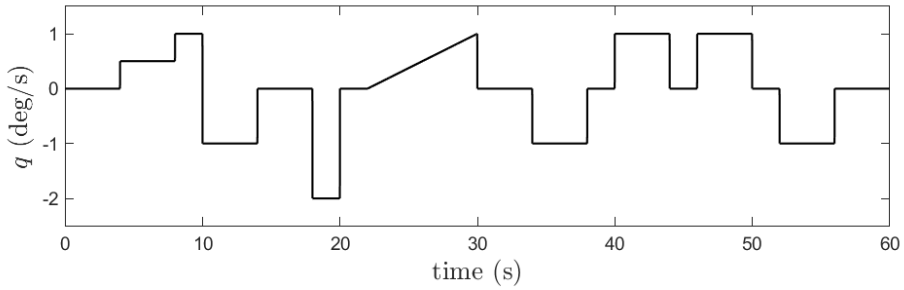

Fig. 3 Pitch rate tracking signal

A. Control law design results

After linearizing the nonlinear F-16 model at the nominal CG location and trim conditions described in Table 5 and 3, respectively, the next step is to optimize the control law design parameters. The initial parameter values and their final optimized results are shown in Table 6. Shaping the initial parameter values of the command filter is based on placing the desired short period dynamics such that the CAP and ζ_{SP} would be in the centre of the level 1 region of the CAP vs. ζ_{SP} requirement. This design point corresponds to a CAP of 1 and a ζ_{SP} of 0.7. To achieve this, the zero of the aircraft short period transfer function is used. Furthermore, the initial PI compensator gains are manually selected such that the closed loop control law followed the command model with reasonable accuracy. For all flight conditions this seemed to hold for a initial P and I gains of 4.00 and 1.00, respectively. Lastly, all final designs shown in Table 6 achieved the level 1 regions of the requirements. However, it was found that the CAP vs. short period damping, the attitude dropback and the Neal-Smith were often competing requirements and therefore ended on the boundary of the level 1 region. To comply with these requirements, it was necessary to increase the value of the zero in the command model and often decrease the natural frequency. Depending in the flight condition this leads to an increase in the short period damping or a decrease of the CAP as can be seen in Figure 13 and 15.

To select the appropriate value for the LMS adaption gain, μ, the sensitivity of the parameter estimation performance metrics described in Section III with respect to μ is analyzed for all uncertainty cases. Considering these results, the

Table 6 Control law design optimization results.

	FC-1		FC-2		FC-3		FC-4	
DP	Initial	Final	Initial	Final	Initial	Final	Initial	Final
K_P	4.00	4.22	4.00	7.07	4.00	3.93	4.00	5.45
K_I	1.00	0.91	1.00	0.00	1.00	1.04	1.00	0.28
K_{cf_1}	18.05	8.29	20.10	6.15	12.74	8.31	16.34	8.02
K_{cf_2}	2.99	3.52	5.43	2.97	2.86	3.29	3.96	2.94
K_{cf_3}	4.57	4.64	15.06	6.55	4.18	5.36	7.98	5.21

RMS CE model error and the CMSD of the correction factor estimation were most critical for selecting an appropriate value of μ. Consequently, these are presented in Figure Figure 4 till 7 and will be briefly discussed.

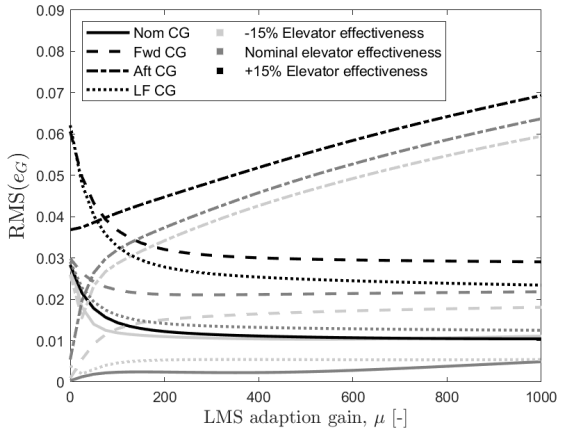

Fig. 4 RMS of the CE model error as a function of μ for all uncertainty cases at FC-2.

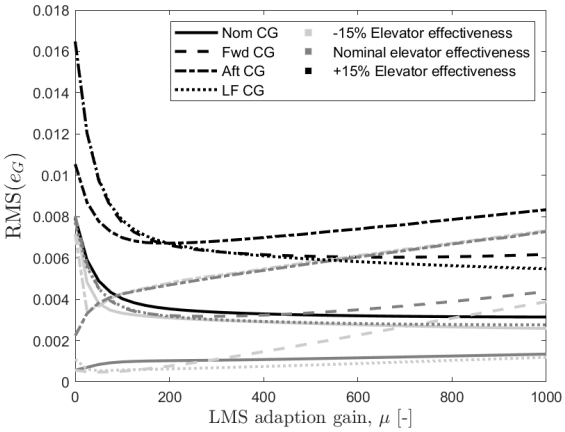

Fig. 5 RMS of the CE model error as a function of μ for all uncertainty cases at FC-3.

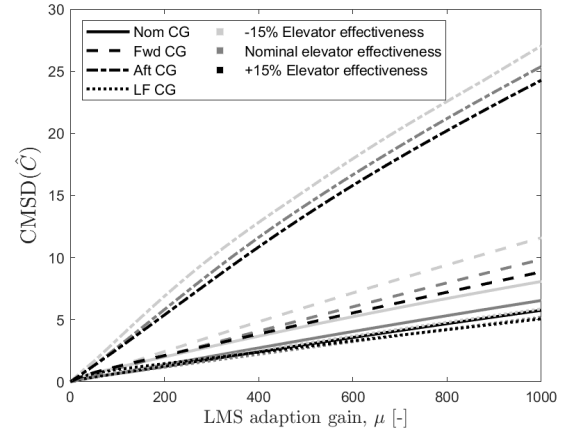

Fig. 6 CMSD of the correction factor estimation as a function of μ for all uncertainty cases at FC-2.

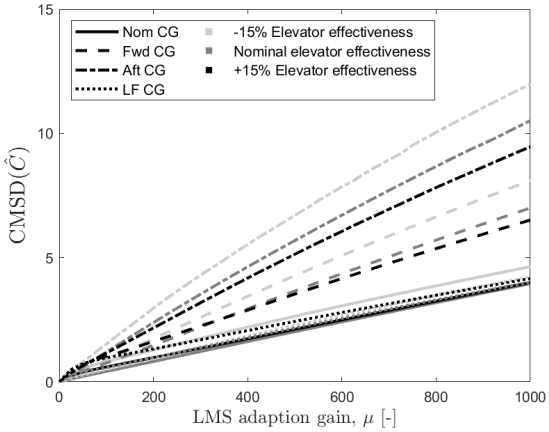

Fig. 7 CMSD of the correction factor estimation as a function of μ for all uncertainty cases at FC-3.

The RMS CE model error shows to have a flattening trend for increasing values of μ for the nominal, forward and

low-fuel CG locations. However, for a backward CG location, it is clear that the RMS value starts to rise after a certain value of μ. Considering FC-2, the RMS value even increases for all values of μ. Furthermore, from Figure 6 and 7 it can be seen that the estimation CMSD has a near linear growth with respect to the adaption gain. As explained in Section III.B this value should be as low as possible. Taking into account the increasing RMS value for a backward CG location and the always increasing CMSD, a value of 150 was deemed an appropriate choice for μ for all flight conditions.

B. Handling quality sensitivity results

The estimation of the correction factor for FC-2 and FC-3, and $\mu = 150$, are shown in Figure 8 until 11. These time responses are obtained for the scenario that the CE model has not been corrected before the start of the first episode. Furthermore, the response is resulting from following the pitch rate tracking signal displayed in Figure 3. Applying this worst case scenario, $\mu = 150$ and the tracking signal of Figure 3, it was found that approximately 20 seconds is required to reach convergence for all uncertainty cases.

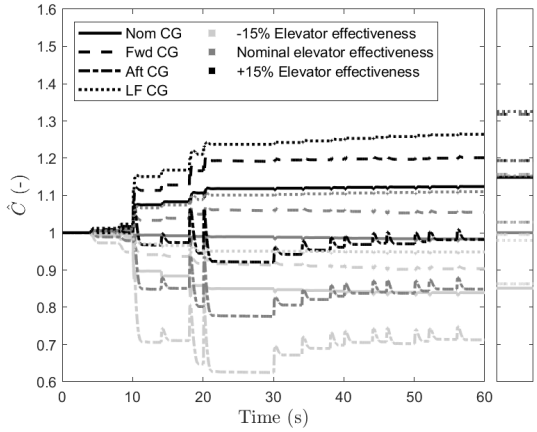

Fig. 8 Correction factor estimation over time of all uncertainty cases. First episode for μ = 150 and FC-2. The desired value is given in the window on the right side.

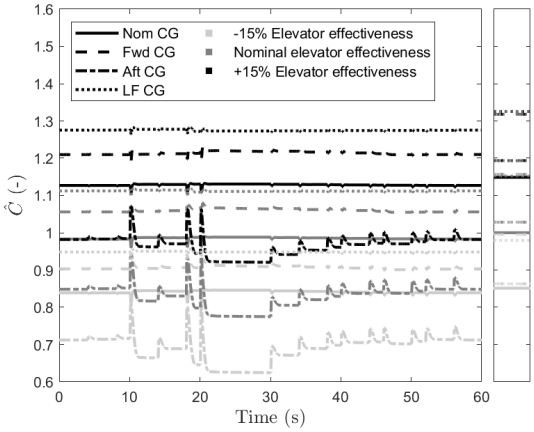

Fig. 9 Correction factor estimation over time of all uncertainty cases. Converged episode for μ = 150 and FC-2. The desired value is given in the window on the right side.

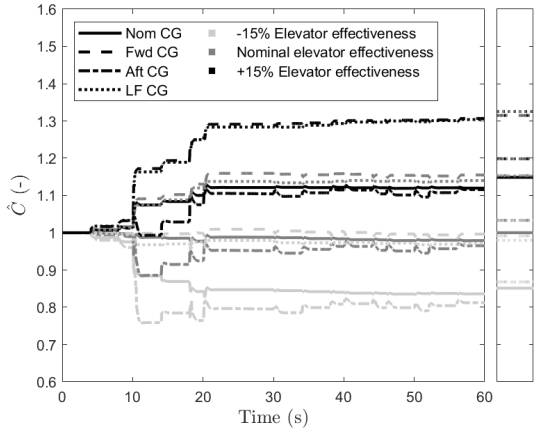

Fig. 10 Correction factor estimation over time of all uncertainty cases. First episode for μ = 150 and FC-3. The desired value is given in the window on the right side.

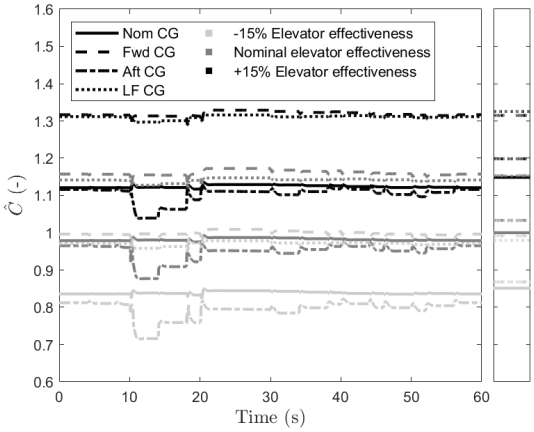

Fig. 11 Correction factor estimation over time of all uncertainty cases. Converged episode for μ = 150 and FC-3. The desired value is given in the window on the right side.

As was already predicted by the sensitivity of the RMS CE model error and the CMSD of the correction factor estimation, the backward CG location parameter estimation shows significantly more activity than the estimation of the other CG locations. Furthermore, taking the average values of the responses of Figure 9 and 11, it can be seen that the parameter estimation for some cases generate significant underestimations. Despite these results, it is clear from Figure 12 until 19 that the sensitivity of the CAP vs short period and the attitude dropback handling quality guidelines is decreased. However, the results mainly show that the added value of online parameter estimation lies in coping with the CE uncertainty. Unfortunately, it does not completely solve the sensitivity for adverse forward and backward CG shifts.

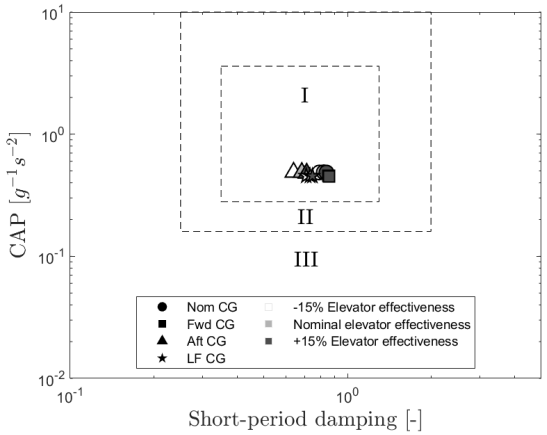

Fig. 12 CAP vs. short period damping criterion sensitivity for FC-2 and non-adaptive control

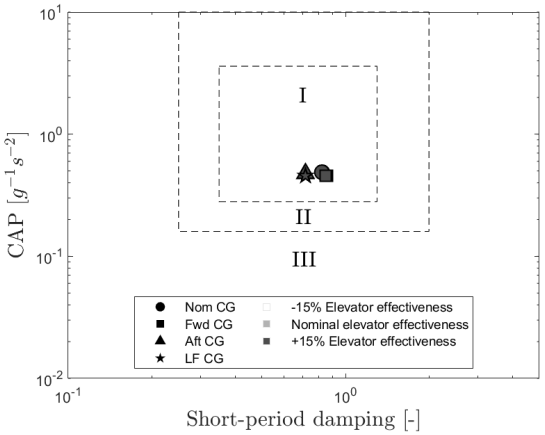

Fig. 13 CAP vs. short period damping criterion sensitivity for FC-2 and adaptive control.

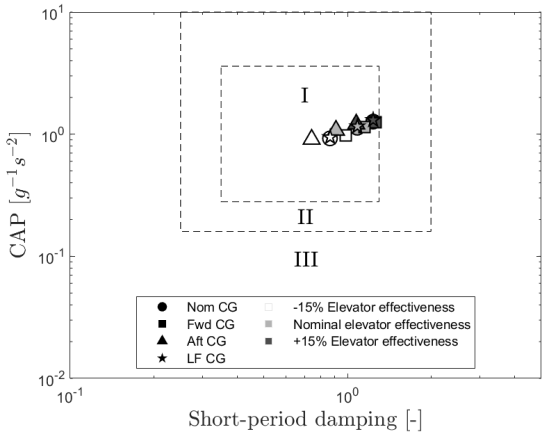

Fig. 14 CAP vs. short period damping criterion sensitivity for FC-3 and non-adaptive control.

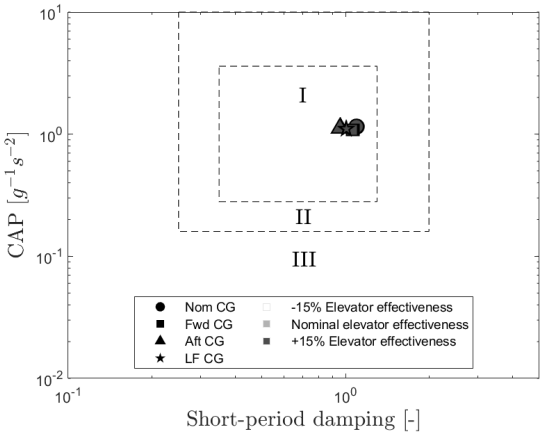

Fig. 15 CAP vs. short period damping criterion sensitivity for FC-3 and adaptive control.

C. Discussion

The results obtained in the previous section indicate that the addition of online parameter estimation and model correction using LMS can decrease the variation in HQ&S of an INDI-based pitch rate control law. However, there are some aspects related to the obtained control law designs and parameter estimation which could be further illuminated. First of all, the optimized PI compensator gains of the non-adaptive INDI pitch rate control law show a significant variation over the different flight conditions despite the relatively small analysis domain. For the design of a proper gain scheduling function, it is desired to have a smooth transition of the control gains for changes in the scheduling

variables.[46] Consequently, these gain values might not be a wise choice for use in a gain scheduling controller. However, the purpose of the design was to obtain as much robust performance as possible of the SISO control law by finding a set of gains which maximizes the broken-loop cross-over frequency.

Furthermore, a dissertation on adaptive backstepping control for modern fighter aircraft [9] proposes a scheduling method for the natural frequency of the command filter that is linearly dependent on the dynamic pressure. The command filter natural frequency changes from 2.5 rad/s for low dynamic pressure to 6.5 for high dynamic pressure. Analyzing the obtained command model natural frequencies of Table 6, it can be seen that the natural frequencies found here behave differently compared to the linear scheduling used in Sonneveldt [9]. Although a similar relation seems to be present between the dynamic pressure and the natural frequency for the initial design parameter values in Table 6, it can be seen that this relation changes considerably after the optimization. This could be resulting from the different design objective used in this study as is described in Section III.

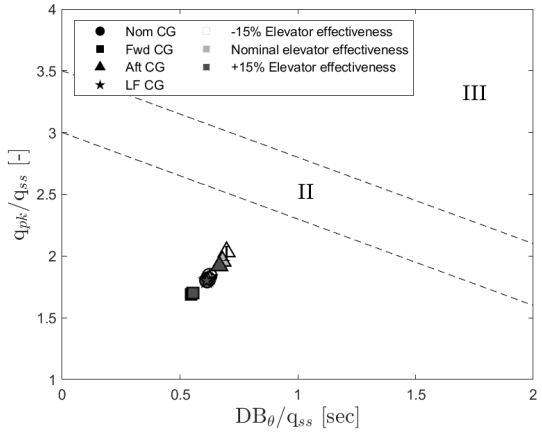

Fig. 16 Pitch attitude dropback criterion sensitivity for FC-2 and non-adaptive control.

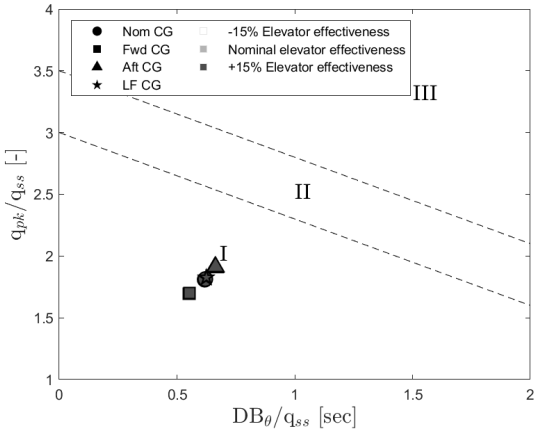

Fig. 17 Pitch attitude dropback criterion sensitivity for FC-2 and adaptive control.

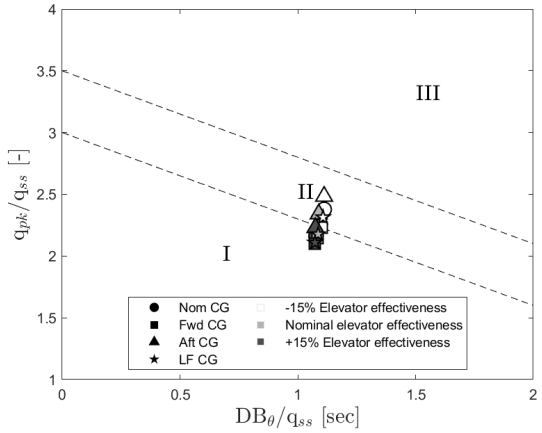

Fig. 18 Pitch attitude dropback criterion sensitivity for FC-3 and non-adaptive control.

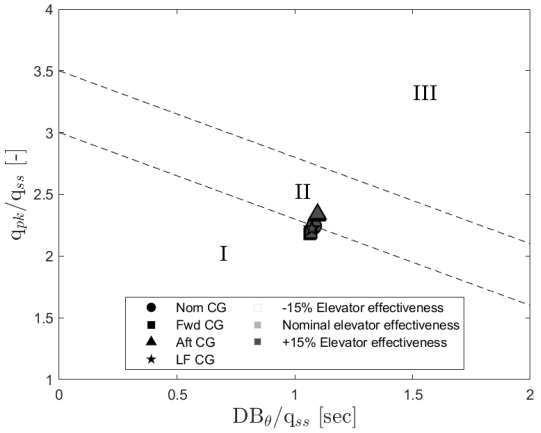

Fig. 19 Pitch attitude dropback criterion sensitivity for FC-3 and adaptive control.

However, the design performed in Sonneveldt [9] also does not consider the pitch attitude bandwidth vs. flight-path angle bandwidth. This requirement showed to be quite important for the selection of the command filter natural frequency. A high pitch attitude bandwidth following from a high natural frequency of the command filter could result in an unbalanced ratio of the pitch attitude and flight-path angle bandwidth. and a reduction in the command filter

natural frequency was able to solve this issue.

Furthermore, reconsidering the parameter estimation responses of FC-2 in Figure 9, the estimation of the correction factor for the forward and backward CG cases show larger deviations for the desired value and more activity than the correction factor estimations for same CG cases of FC-3 shown in Figure 11. Moreover, the average estimation error of the correction factor for a backward CG location and -15% elevator effectiveness at FC-2, is nearly equal to the deviation at the start of the first episode. Despite this significant deviation after convergence it was observed that the sensitivity for the CAP vs. short period damping and attitude dropback criteria still decreased, see Figure 13 and 17. Presumably, the reason behind this result lies in the fact that an underestimation of the correction factor is obtained, which is often observed in this study. The consequence of an underestimation is a lower value for the CE model. The successive result of a lower CE value is a larger elevator deflection increment determined by the INDI controller. Although this could result in an overshoot of the optimum elevator deflection, it could also result in a quicker convergence to a desired elevator deflection. Therefore, the lower CE model value could also function slightly like high-gain control for the inversion and induce some performance robustness. However, this comes at a cost of inversion loop stability.

Another pressing question is what causes the large underestimation of the correction factor estimation. Further investigation of the nominal and low-fuel CG locations for both flight conditions in Figure 9 and 11 made clear that these are not as much affected by differences in flight condition as the other CG location cases. Considering that FC-2 is a flight condition with a higher dynamic pressure than FC-3, see Table 3, the problem could be a result of an increased sensitivity in aerodynamic forces and moments for changes in the aircraft states. This can be confirmed by the linearized $\Delta\dot{q}$ model coefficients shown in Table 7. Especially the model coefficient m_α at FC-2 increases considerably in magnitude for a forward and backward CG shift. The result of this significant increase in influence of $\Delta\alpha$ on $\Delta\dot{q}$ could weaken the assumption that the $\Delta\alpha$ dependency could be neglected.

Table 7 Incremental pitch acceleration model coefficients, m_α, m_q and m_{δ_e}, for FC-2 and FC-3, and the nominal, forward and backward CG locations.

		FC-2			FC-3		
Model coefficient	Unit	nom	forward	backward	nom	forward	backward
m_α	s^{-2}	0.0529	-6.43	7.38	0.763	-0.352	3.14
m_q	s^{-2}	-0.949	-1.50	-0.514	-0.471	-0.702	-0.271
m_{δ_e}	s^{-2}	-10.9	-12.5	-11.1	-3.02	-3.40	-3.08

Figure 20 and 21 confirm that the influence of $\Delta\alpha$ on $\Delta\dot{q}$ becomes noticeably stronger when the CG has shifted to the backward location. The response shown in these figures is obtained by tracking the pitch rate ramp segment in the tracking signal of Figure 3 and using the linearized aircraft model at FC-2. Reconsidering Figure 9, the parameter estimation shows the worst performance during this period for a backward cg position. A comparison of Figure 20 and 21 shows that only accounting for the effect of $\Delta\delta_e$ after the initial transient does not give a good description of $\Delta\dot{q}$ for a backward CG location. Consequently, the assumption of neglecting the effects of $\Delta\dot{q}_{\Delta\alpha}$ and $\Delta\dot{q}_{\Delta q}$ does not hold here. This would explain the observed offset in the parameter estimation for the backward and forward CG locations at FC-2.

Although, it is presumed that the parameter estimation problems can be overcome by adding the estimation of the $\Delta\dot{q}_{\Delta\alpha}$ and $\Delta\dot{q}_{\Delta q}$ effects, it does indicate a fundamental problem of the INDI control law applied in this paper. In the derivation of this control law, it is assumed that the influence of the incremental state, $\Delta\underline{x}$, could be neglected. However, as shown in Figure 21, this might not hold for adverse CG locations and therefore could decrease the control performance. Unfortunately, adding the incremental state dependency in the INDI control law design is not possible as this would require knowledge of the state at the next time-step. Consequently, mitigating the HQ&S variation of the INDI-based control law for all cases, including adverse CG locations, cannot be achieved by finding a correct control effectiveness model alone. Therefore, robust versions of the INDI pitch rate control law, such as Incremental Sliding-mode control [47] or a more advanced robust outer loop design using μ-analysis [48], might aid the required robustness for large CG shifts. In addition, in Wang et al. [21] it is proven that the influence of the incremental state dependent part becomes less for an increasing sampling frequency, which indicates that an increased sampling frequency could resolve the remaining handling quality variations due to adverse CG shifts. However, this proof is based on the assumption that the actuators and feedback dynamics are ideal. Therefore, the control surface increment determined by the INDI control law could be tracked instantly and the feedback signal is neither delayed nor filtered. The experiments which give the results described in the previous section do include actuators and feedback dynamics. Consequently,

to verify whether the an increase in sampling frequency could improve the tracking performance of the control law analysed in this study, the robustness proof developed in Wang et al. [21] should be extended with unmodeled dynamics of actuators and the flight control computer.

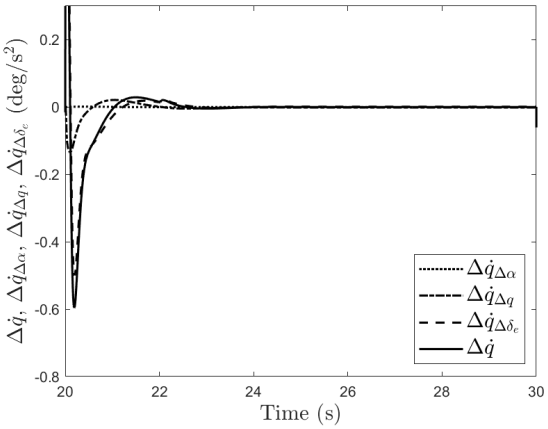

Fig. 20 Incremental pitch acceleration and corresponding incremental state dependency for the nominal CG location of FC-2.

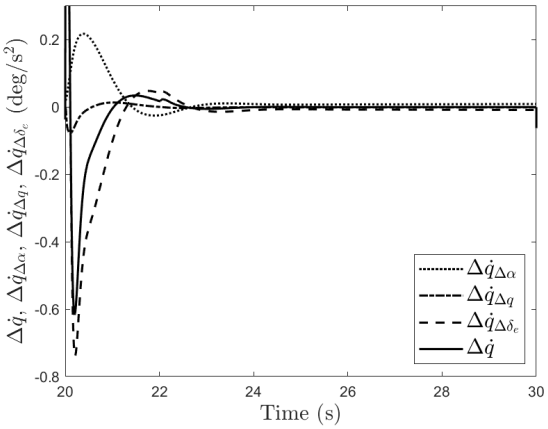

Fig. 21 Incremental pitch acceleration and corresponding incremental state dependency for the backward CG location of FC-2.

Lastly, this study does not consider the effect of noise and turbulence on the parameter estimation performance. As these phenomena distort the signals used by the parameter estimation it is presumed that the estimation performance will degrade and the HQ&S variation could increase again. Consequently, it is recommended that effects of these phenomena are investigated in future research to obtain a better understanding of the control performance of the adaptive INDI-based control law considered in this study for real-world applications.

VI. Conclusions and recommendations for future work

Incremental Nonlinear Dynamic Inversion (INDI) based control laws are known for their increased robustness for model uncertainties and disturbances with respect to control laws based on Nonlinear Dynamic Inversion (NDI). This could be achieved while requiring less knowledge of the complete system model and having similar design complexity of a NDI based control law. Despite these strengths of INDI-based control laws, it was demonstrated, during a flight test with a UAV in a recent research project, that the control performance could still vary significantly due to changes in the control effectiveness (CE). To put this observed issue in the context of full-scale high-performance aircraft, this paper presents a handling quality and stability (HQ&S) sensitivity study for an INDI-based pitch rate flight control law. The sensitivity was analyzed for system uncertainties originating from unanticipated centre of gravity (CG) shifts and elevator effectiveness uncertainty. It was confirmed that the control law still shows significant variation even though its was designed to achieve maximum performance robustness without violating important HQ&S guidelines. As an attempt to decrease this variation, an indirect adaptive version of the INDI-based pitch rate control law has been proposed and analyzed. The online identification used in this indirect adaptive control law is based on Least-Mean-Square (LMS) parameter estimation. Furthermore, the objective is to estimate a correction factor to scale the on-board CE model by only using the measured incremental pitch acceleration and incremental elevator deflection feedback. Therefore, the same time-scale separation assumption as used for the INDI control law derivation is applied.

The results obtained for the HQ&S sensitivity analysis of the adaptive control law revealed that online correction of the CE model enables a decrease of the HQ&S variation. However, it is also established that the variation induced by large backward CG shifts could not be completely solved using this approach. On top of that, for the forward and backward CG location cases at the highest dynamic pressure flight condition, the online parameter estimation performance is considerably lower and showed more activity. The reason behind this problem is an increased influence of the neglected incremental states on the incremental pitch acceleration. Due to this it is not possible to reach the desired correction factor value by using a model incorporating the time-scale separation assumption. The solution to the estimation problem is to add the incremental state terms to the identification model. However, this result reveals an

additional problem considering the INDI pitch rate control law applied in this research. As this control law is also derived using the time-scale separation assumption, the control performance is presumed to degrade for large CG shifts despite having a correct CE model.

Considering these conclusions there are still some challenges that need to be addressed. First of all, the control performance degradation caused by violation of the time-scale separation assumption due to large CG shifts. The CG range of high-performance aircraft could have a considerable range due to different store configuration. Consequently, this is a very relevant issue for these type of aircraft. Incorporating robust design frameworks such as μ-analysis or applying Incremental Sliding-mode control might aid in making the control law more robust for large CG shifts. Furthermore, the CE model correction could be improved by incorporating the incremental state influence in the identification model definition. Moreover, coping with turbulence and noise is often a challenging aspect of flight control law design. These stochastic processes can degrade handling qualities and affect parameter estimation performance. Therefore, it is valuable to extend the knowledge obtained in this study by analyzing these phenomena as well. Lastly, probably the most important and most challenging recommendation is to find a rigorous stability proof of the complete adaptive INDI-based pitch rate control law.

References

[1] Snell, S., Enns, D., and Garrard, W., "Nonlinear inversion flight control for a supermaneuverable aircraft," *Journal of Guidance, Control, and Dynamics*, Vol. 15, No. 4, 1992, pp. 976–984. https://doi.org/10.2514/3.20932.

[2] Gal-Or, B., *Vectored Propulsion, Supermaneuverability and Robot Aircraft*, Springer New York, New York, NY, 1990. https://doi.org/10.1007/978-1-4613-8961-3.

[3] Gallaway, C., and Osborn, R., "Aerodynamics perspective of supermaneuverability," *3rd Applied Aerodynamics Conference*, American Institute of Aeronautics and Astronautics, Colorado Springs,CO,U.S.A., 1985. https://doi.org/10.2514/6.1985-4068.

[4] Slotine, J., and Li, W., *Applied nonlinear control*, Prentice Hall, Englewood Cliffs, N.J, 1991.

[5] Albostan, O., and Gökaşan, M., "High Angle of Attack Manoeuvring Control of F-16 Aircraft Based on Nonlinear Dynamic Inversion and Eigenstructure Assignment," *European Conference for Aeronautics and Space Sciences*, 2017, p. 15. https://doi.org/10.13009/EUCASS2017-228.

[6] Edwards, C., Lombaerts, T., and Smaili, H. (eds.), *Fault tolerant flight control: a benchmark challenge*, 399, Springer, Berlin, 2010.

[7] Mohler, R. R., "Nonlinear Control of High Performance Aircraft," *1993 American Control Conference*, 1993, pp. 1395–1399. https://doi.org/10.23919/ACC.1993.4793100.

[8] Krstić, M., Kanellakopoulos, I., and Kokotović, P. V., *Nonlinear and adaptive control design*, Wiley, 1995.

[9] Sonneveldt, L., "Adaptive Backstepping Flight Control for Modern Fighter Aircraft," Ph.D. thesis, Delft University of Technology, Faculty of Aerospace Engineering, 2010. ISBN 978-90-8570-573-4.

[10] Harris, J., "F-35 Flight Control Law Design, Development and Verification," *2018 Aviation Technology, Integration, and Operations Conference*, American Institute of Aeronautics and Astronautics, Atlanta, Georgia, 2018. https://doi.org/10.2514/6.2018-3516.

[11] Miller, C., "Nonlinear Dynamic Inversion Baseline Control Law: Architecture and Performance Predictions," *AIAA Guidance, Navigation, and Control Conference*, American Institute of Aeronautics and Astronautics, Portland, Oregon, 2011. https://doi.org/10.2514/6.2011-6467.

[12] da Costa, R., Chu, Q., and Mulder, J., "Reentry Flight Controller Design Using Nonlinear Dynamic Inversion," *Journal of Spacecraft and Rockets*, Vol. 40, No. 1, 2003, pp. 64–71. https://doi.org/10.2514/2.3916.

[13] Härkegård, O., and Glad, S., "Flight Control Design Using Backstepping," *IFAC Proceedings Volumes*, Vol. 34, No. 6, 2001, pp. 283–288. https://doi.org/10.1016/S1474-6670(17)35187-X.

[14] Steinberg, M., and Page, A., "Nonlinear adaptive flight control with a backstepping design approach," *Guidance, Navigation, and Control Conference and Exhibit*, American Institute of Aeronautics and Astronautics, Boston,MA,U.S.A., 1998. https://doi.org/10.2514/6.1998-4230.

[15] Lombaerts, T., Huisman, H., Chu, Q., Mulder, J., and Joosten, D., "Nonlinear Reconfiguring Flight Control Based on Online Physical Model Identification," *Journal of Guidance, Control, and Dynamics*, Vol. 32, No. 3, 2009, pp. 727–748. https://doi.org/10.2514/1.40788.

[16] van Gils, P., Van Kampen, E.-J., de Visser, C. C., and Chu, Q. P., "Adaptive Incremental Backstepping Flight Control for a High-Performance Aircraft with Uncertainties," *AIAA Guidance, Navigation, and Control Conference*, American Institute of Aeronautics and Astronautics, San Diego, California, USA, 2016. https://doi.org/10.2514/6.2016-1380, URL http://arc.aiaa.org/doi/10.2514/6.2016-1380.

[17] Sieberling, S., Chu, Q., and Mulder, J., "Robust flight control using incremental nonlinear dynamic inversion and angular acceleration prediction," *Journal of guidance, control and dynamics, 33.2010 no.6*, 2010. https://doi.org/10.2514/1.49978.

[18] Smith, P., and Berry, A., "Flight test experience of a non-linear dynamic inversion control law on the VAAC Harrier," *Atmospheric Flight Mechanics Conference*, American Institute of Aeronautics and Astronautics, Denver,CO,U.S.A., 2000. https://doi.org/10.2514/6.2000-3914.

[19] Smeur, E., Chu, Q., and de Croon, G., "Adaptive Incremental Nonlinear Dynamic Inversion for Attitude Control of Micro Air Vehicles," *Journal of Guidance, Control, and Dynamics*, Vol. 39, No. 3, 2016, pp. 450–461. https://doi.org/10.2514/1.G001490.

[20] Grondman, F., Looye, G., Kuchar, R., Chu, Q., and Van Kampen, E., "Design and Flight Testing of Incremental Nonlinear Dynamic Inversion-based Control Laws for a Passenger Aircraft," *2018 AIAA Guidance, Navigation, and Control Conference*, American Institute of Aeronautics and Astronautics, Kissimmee, Florida, 2018. https://doi.org/10.2514/6.2018-0385.

[21] Wang, X., van Kampen, E., Chu, Q., and Lu, P., "Stability Analysis for Incremental Nonlinear Dynamic Inversion Control," *Journal of Guidance, Control, and Dynamics*, Vol. 42, No. 5, 2019, pp. 1116–1129. https://doi.org/10.2514/1.G003791.

[22] DoD, "Military Specification: Flying Qualities of Piloted Airplanes, MIL-F-8785C," , November 1980.

[23] Diniz, P. S. R., *Adaptive Filtering: Algorithms and Practical Implementation*, Springer US, 1997.

[24] Haykin, S., and Widrow, B., *Least-Mean-Square Adaptive Filters*, John Wiley & Sons, 2003. Google-Books-ID: U8X3mJtawUkC.

[25] DoD, *FLYING QUALITIES OF PILOTED AIRCRAFT*, MIL-HDBK-1797, Department of Defence, 1997.

[26] Tischler, M. B., *Practical Methods for Aircraft and Rotorcraft Flight Control Design: An Optimization-based Approach*, American Institute of Aeronautics and Astronautics, Incorporated, 2017.

[27] AGARD, "Handling Qualities of Unstable Highly Augmented Aircraft," *AGARD-AR-279*, AGARD, Neuilly Sur Seine, France, 1991.

[28] Mitchell, D., Hoh, R., Aponso, B., and Klyde, D., "Proposed Incorporation of Mission-Oriented Flying Qualities into MIL-STD-1797A," Tech. Rep. Wright Laboratory Technical Report (WL-TR-94-3162), 1994.

[29] AGARD, "Flying Qualities," Tech. Rep. AGARD-CP-508, AGARD, feb 1991. https://doi.org/10.14339/AGARD-CP-508-pdf.

[30] Mitchell, D., Hoh, R., Aponso, B., and Klyde, D., "Flight Control Design - Best Practices," Tech. Rep. Research and Technology Organization Technical Report (RTO-TR-029), 2000.

[31] Berger, T., Tischler, M., Hagerott, S. G., Gangsaas, D., and Saeed, N., "Longitudinal Control Law Design and Handling Qualities Optimization for a Business Jet Flight Control System," *AIAA Atmospheric Flight Mechanics Conference*, American Institute of Aeronautics and Astronautics, 2012. https://doi.org/10.2514/6.2012-4503, URL https://arc.aiaa.org/doi/abs/10.2514/6.2012-4503.

[32] Neal, T. P., and Smith, R. E., "An In-flight Investigation to Develop Control System Design Criteria for Fighter Airplanes," Tech. Rep. AFFDL-TR-70-74, Volume 2, Air Force Flight Dynamics Laboratory, Dec. 1970.

[33] Skogestad, S., and Postlethwaite, I., *Multivariable Feedback Control: Analysis and Design*, Wiley, 2005.

[34] Sun, L. G., "Model and Sensor Based Nonlinear Adaptive Flight Control with Online System Identification," Ph.D. thesis, Delft University of Technology, Faculty of Aerospace Engineering, 2014. Publisher: Ipskamp Drukkers, Enschede, The Netherlands.

[35] Heise, C. D., Leitao, M., and Holzapfel, F., "Performance and Robustness Metrics for Adaptive Flight Control - Available Approaches," *AIAA Guidance, Navigation, and Control (GNC) Conference*, American Institute of Aeronautics and Astronautics, Boston, MA, 2013. https://doi.org/10.2514/6.2013-5090.

[36] Bhardwaj, P., Akkinapalli, V. S., Zhang, J., Saboo, S., and Holzapfel, F., "Adaptive Augmentation of Incremental Nonlinear Dynamic Inversion Controller for an Extended F-16 Model," *AIAA Scitech 2019 Forum*, American Institute of Aeronautics and Astronautics, San Diego, California, 2019. https://doi.org/10.2514/6.2019-1923.

[37] Stepanyan, V., Krishnakumar, K., Nguyen, N., and Van Eykeren, L., "Stability and Performance Metrics for Adaptive Flight Control," *AIAA Guidance, Navigation, and Control Conference*, American Institute of Aeronautics and Astronautics, Chicago, Illinois, 2009. https://doi.org/10.2514/6.2009-5965.

[38] Mooij, E., "Robust Control of a Conventional Aeroelastic Launch Vehicle," *AIAA Scitech 2020 Forum*, American Institute of Aeronautics and Astronautics, Orlando, FL, 2020. https://doi.org/10.2514/6.2020-1103.

[39] Muir, E., "The GARTEUR High Incidence Research Model (HIRM) benchmark problem," *Guidance, Navigation, and Control Conference and Exhibit*, American Institute of Aeronautics and Astronautics, Boston,MA,U.S.A., 1998. https://doi.org/10.2514/6.1998-4243.

[40] DoD, *Flight Control Systems - Design,Installation and Test of Piloted Aircraft*, MIL-DTL-9490E, Department of Defence, 2008.

[41] Russel, R., "Non-linear F-16 Simulation using Simulink and Matlab," Tech. rep., University of Minnesota, June 2003.

[42] Nguyen, L., Ogburn, M. E., Gilbert, W. P., Kibler, K. S., Brown, P. W., and Deal, P. L., "Simulator study of stall/post-stall characteristics of a fighter airplane with relaxed longitudinal static stability." Tech. rep., NASA, Dec. 1979.

[43] Keijzer, T., Looye, G., Chu, Q., and van Kampen, E., "Flight testing of incremental backstepping based control laws with angular accelerometer feedback," *AIAA Scitech 2019 Forum*, 2019. https://doi.org/10.2514/6.2019-0129.

[44] van 't Veld, R., van Kampen, E., and Chu, Q., "Stability and Robustness Analysis and Improvements for Incremental Nonlinear Dynamic Inversion Control," *2018 AIAA Guidance, Navigation, and Control Conference*, American Institute of Aeronautics and Astronautics, Kissimmee, Florida, 2018. https://doi.org/10.2514/6.2018-1127.

[45] Stevens, B. L., and Lewis, F. L., *Aircraft control and simulation*, Wiley, 1992.

[46] Leith, D., and Leithead, W., "Survey of gain-scheduling analysis and design," *Int. J. Control*, Vol. 73, 2000, pp. 1001–1025. https://doi.org/10.1080/002071700411304.

[47] Wang, X., van Kampen, E., and Chu, Q. P., "Incremental Sliding-Mode Fault-Tolerant Flight Control," *Journal of Guidance, Control, and Dynamics: devoted to the technology of dynamics and control*, Vol. 42, No. 2, 2019. https://doi.org/10.2514/1.G003497, URL https://repository.tudelft.nl/islandora/object/uuid%3Ae32e92a0-8b42-44ef-8ee4-7f82e56f8f0e.

[48] Magni, J., Bennani, S., and Terlouw, J., *Robust Flight Control*, Lecture notes in control and information sciences, Springer, 1997.

II

Literature Reviews

The second part of this thesis is concerned with literature studies. The goal of this part is to gather the relevant knowledge required to fully understand the problem at hand and successfully design and analyse an adaptive INDI control law which could cope with CG shifts, inertia changes and aerodynamic modelling errors.

The first chapter of this part, Chapter 2, covers the fundamental theory of Incremental Nonlinear Dynamic Inversion. Furthermore, this chapter contains a literature study into the state-of-the-art applications and research projects which apply this control law design framework.

This will be followed by Chapter 3 which dives into the world of adaptive control. This chapter aims to give the reader a general understanding of the related aspects. Furthermore, at the end of this chapter, a concise set of adaptive laws will be selected which will be combined with the INDI control law design framework. Considering these goals, this chapter is concerned with answering the following research question and its sub-questions:

> *Which adaptive methods are suited for the integration in INDI-based pitch rate control of high-performance aircraft?*
>
> - *What are the adaptive control approaches?*
> - *What is the state-of-the-art research in the field of adaptive INDI?*
> - *Which methods are suited for INDI-based control?*

Chapter 4 focuses on modelling the aircraft dynamics while taking into account the effect of centre of gravity translations. The goal of this chapter is to show how the system dynamics are affected by CG shifts and inertia changes and how this affects the INDI control law. From the knowledge gathered in this chapter it should be possible to answer the second research question:

> *How do longitudinal centre of gravity shifts, changes in inertia and aerodynamic model mismatches affect the INDI-based pitch rate control law?*

The goal of the last chapter of this part, chapter 5, is to select a set of metrics to evaluate the adaptive control laws. Furthermore, a brief study is performed on the use of handling quality and stability guidelines and which guidelines are most appropriate for the analysis of longitudinal rotational control. The research question and sub-questions which could be answered by this information are the following:

> *Which evaluation metrics are suited for the assessment of adaptive INDI-based control?*

- *Which metrics quantify control performance in adaptive control?*
- *Which metrics quantify parameter estimation performance in adaptive control?*
- *What is the appropriate metric for assessing computational complexity of adaptive control methods?*
- *What are the appropriate handling quality and controller stability guidelines for the evaluation of the non-adaptive and adaptive INDI-based pitch rate control law?*

This work has been graded previously.

2

Incremental nonlinear dynamic inversion control

Before the theory on adaptive methods will be discussed, the fundamental theory of the INDI design framework will be covered. As mentioned in the introduction, INDI is based on NDI. Therefore, to aid the understanding of the principles behind INDI, this chapter will start with the theory on the derivation of the NDI control law design framework in section 2.1. Then, with the knowledge obtained and reformulating the dynamic equations into an incremental form, the INDI control law design approach will be derived. This derivation will be treated in section 2.2. Moreover, flight control laws based on dynamic inversion often make use of the fact that the system of dynamics can be separated slow and fast dynamics. The separation on the basis of slow and fast dynamics is called *time-scale separation*. This principle and its meaning for dynamic inversion based control laws will be explained in section 2.3. Then, in section 2.4 the effect of model uncertainty on the NDI and INDI control laws will be compared and it will be shown why the INDI control law is more robust to model uncertainties. Lastly, section 2.5 contains a literature review on the state-of-the-art researches and applications of INDI.

2.1. Nonlinear Dynamic Inversion

This section will concisely cover the derivation of a control law based on the NDI approach. A more detailed derivation can be found in Khalil (2002). For the control design based on NDI the following general multi-input-multi-output (MIMO) system description is considered:

$$\begin{aligned} \dot{\underline{x}} &= \underline{f}(\underline{x}) + g(\underline{x})\underline{u} \\ \underline{y} &= \underline{h}(\underline{x}) \end{aligned} \tag{2.1}$$

To find a solution for $\underline{u}$ it is required to have a system description in controllable canonical form. A local state coordinate transformation will be done to be able to rewrite the system description into this form. This could be achieved by the following diffeomorphism:

$$\underline{z} = \Phi(\underline{x}) = \begin{bmatrix} \underline{\phi}_1(\underline{x}) \\ \underline{\phi}_2(\underline{x}) \\ \vdots \\ \underline{\phi}_\rho(\underline{x}) \\ \underline{\phi}_{\rho+1}(\underline{x}) \\ \vdots \\ \underline{\phi}_n(\underline{x}) \end{bmatrix} = \begin{bmatrix} \underline{h}(\underline{x}) \\ L_f^1 \underline{h}(\underline{x}) \\ \vdots \\ L_f^{\rho-1} \underline{h}(\underline{x}) \\ L_f^{\rho} \underline{h}(\underline{x}) \\ \vdots \\ L_f^{n-1} \underline{h}(\underline{x}) \end{bmatrix} \tag{2.2}$$

Here, $\underline{z}$ is the transformed state, $\underline{\phi}_i(\underline{x})$ are the diffeomorphism functions and L_f^j is the j-th order Lie derivative with respect to the vector field $\underline{f}(\underline{x})$. Furthermore, ρ is the relative degree of the dynamic system, which will be discussed later in this section. $L_f\underline{h}(\underline{x})$ is the first order derivative of $\underline{h}(\underline{x})$ in the direction of vector $\underline{f}(\underline{x})$ and can be written as follows:

$$L_f\underline{h}(\underline{x}) = \nabla\underline{h}(\underline{x})\underline{f}(\underline{x}) \tag{2.3}$$

Using the definition of $\underline{z}$ of Eq. (2.2) and taking the first time derivative gives the following result:

$$\dot{\underline{z}} = \begin{bmatrix} \dot{\underline{\phi}}_1(\underline{x}) \\ \dot{\underline{\phi}}_2(\underline{x}) \\ \vdots \\ \dot{\underline{\phi}}_\rho(\underline{x}) \\ \dot{\underline{\phi}}_{\rho+1}(\underline{x}) \\ \vdots \\ \dot{\underline{\phi}}_n(\underline{x}) \end{bmatrix} = \begin{bmatrix} \frac{\partial\underline{\phi}_1(\underline{x})}{\partial\underline{x}}\dot{\underline{x}} \\ \frac{\partial\underline{\phi}_2(\underline{x})}{\partial\underline{x}}\dot{\underline{x}} \\ \vdots \\ \frac{\partial\underline{\phi}_\rho(\underline{x})}{\partial\underline{x}}\dot{\underline{x}} \\ \frac{\partial\underline{\phi}_\rho(\underline{x})}{\partial\underline{x}}\dot{\underline{x}} \\ \vdots \\ \frac{\partial\underline{\phi}_n(\underline{x})}{\partial\underline{x}}\dot{\underline{x}} \end{bmatrix} \tag{2.4}$$

The derivatives for $\underline{\phi}_i(\underline{x})$ can be further evaluated as:

$$\begin{aligned} \dot{\underline{z}}_i = \dot{\underline{\phi}}_i(\underline{x}) = \frac{\partial\underline{\phi}_i(\underline{x})}{\partial\underline{x}}\dot{\underline{x}} = \frac{\partial\underline{\phi}_i(\underline{x})}{\partial\underline{x}}\left[\underline{f}(\underline{x}) + g(\underline{x})\underline{u}\right] = \frac{\partial}{\partial\underline{x}}\left[L_f^{i-1}\underline{h}(\underline{x})\underline{f}(\underline{x}) + L_f^{i-1}\underline{h}(\underline{x})g(\underline{x})\underline{u}\right] = \\ = L_f^i\underline{h}(\underline{x}) + L_gL_f^{i-1}\underline{h}(\underline{x})\underline{u} \end{aligned} \tag{2.5}$$

For all $\dot{\underline{z}}_i$ for which $i < \rho$ it holds that $L_gL_f^{i-1}\underline{h}(\underline{x}) = 0$. As a result of this the following result is obtained:

$$\dot{\underline{z}}_i = L_f^i\underline{h}(\underline{x}) = \underline{z}_{i+1} \tag{2.6}$$

At $\dot{\underline{\phi}}_\rho(\underline{x})$ the value of $L_gL_f^{i-1}\underline{h}(\underline{x})$ will not be equal to zero. Furthermore, for all $\dot{\underline{\phi}}_i(\underline{x})$ with $\rho < i < n$ a function $\underline{\phi}_i(\underline{x})$ can be defined for which $L_gL_f^{i-1}\underline{h}(\underline{x})$ is equal to zero again. Using this, the following canonical formulation of the system dynamics is found:

$$\dot{\underline{z}} = \begin{bmatrix} \dot{\underline{z}}_1 \\ \dot{\underline{z}}_2 \\ \vdots \\ \dot{\underline{z}}_\rho \\ \dot{\underline{z}}_{\rho+1} \\ \vdots \\ \dot{\underline{z}}_n \end{bmatrix} = \begin{bmatrix} \underline{z}_2 \\ \underline{z}_3 \\ \vdots \\ L_f^\rho\underline{h}(\underline{x}) + L_gL_f^{\rho-1}\underline{h}(\underline{x})\underline{u} \\ q_{\rho+1}(\underline{x}) \\ \vdots \\ q_n(\underline{x}) \end{bmatrix} = \begin{bmatrix} \underline{z}_2 \\ \underline{z}_3 \\ \vdots \\ L_f^\rho\underline{h}(\Phi^{-1}(\underline{z})) + L_gL_f^{\rho-1}\underline{h}(\Phi^{-1}(\underline{z}))\underline{u} \\ q_{\rho+1}(\Phi^{-1}(\underline{z})) \\ \vdots \\ q_n(\Phi^{-1}(\underline{z})) \end{bmatrix} = \begin{bmatrix} \underline{z}_2 \\ \underline{z}_3 \\ \vdots \\ F(\underline{z}) + G(\underline{z})\underline{u} \\ q_{\rho+1}(\underline{z}) \\ \vdots \\ q_n(\underline{z}) \end{bmatrix} \tag{2.7}$$

With this result the system of Eq. (2.1) is fully transformed into a controllable canonical form and it could be used to determine the solution for the control input $\underline{u}$. Please note from Eq. (2.2) that $\underline{z}_1$ is defined as $\underline{h}(\underline{x})$, which means that $\underline{z}_1$ is also $\underline{y}$. Using this together with the canonical form of Eq.

(2.7) it could therefore be shown that $\dot{\underline{z}}_\rho$ is $\underline{y}^{(\rho)}$. Therefore, when solving for the control input, $\underline{u}$, in the equation for $\dot{\underline{z}}_\rho$ in Eq. (2.7), the following result could be obtained:

$$\underline{u} = G^{-1}(\underline{z})\left(\underline{y}^{(\rho)} - F(\underline{z})\right) \tag{2.8}$$

Defining $\underline{y}^{(\rho)}$ as the desired dynamics and virtual control input, ν, the final NDI control law can be written as follows:

$$\underline{u} = G^{-1}(\underline{z})\left(\underline{\nu} - F(\underline{z})\right) \tag{2.9}$$

Using this solution it is required that the inverse of $L_g L_f^{\rho-1}\underline{h}(\underline{x})$ or $G^{-1}(\underline{z})$ exists. Thus, this matrix is non-singular for all $\underline{x}$ and $\underline{z}$ and preferably square. In case the matrix is not square, it is possible to find a pseudo inverse with, for example, the Moore-Penrose method. Furthermore, note that this solution for $\underline{u}$ results in an input-output linearization of system (2.1). To obtain an input-state linearization of the system, the function description of $\underline{h}(\underline{x})$ should be the identity matrix.

Moreover, if $\rho < n$ it means the system has internal dynamics. As shown in (2.7), it is possible to determine an equation for these dynamics which is not dependent on $\underline{u}$. This can be done as follows:

$$\underline{z}_i = L_f^i \underline{h}(\underline{x}) + L_g L_f^{i-1}\underline{h}(\underline{x})\underline{u} = L_f^i \underline{h}(\underline{x}) + L_g L_f^{i-1}\underline{h}(\underline{x})\left(G^{-1}(\underline{z})\left(\underline{\nu} - F(\underline{z})\right)\right) \quad , \quad \rho < i \leq n \tag{2.10}$$

At this point almost all aspects of the controller are designed. The only thing that is left is the virtual control input, $\underline{\nu}$. As the system is fully linearized using this procedure, it is possible to use a linear controller to determine $\underline{\nu}$. Possible candidates for a stabilization problem or tracking problem are (2.11) and (2.12), respectively.

$$\underline{\nu} = -\underline{K}_0\underline{y} - \underline{K}_1\frac{d\underline{y}}{dt} - \underline{K}_2\frac{d^2\underline{y}}{dt^2} - \ldots - \underline{K}_{\rho-1}\frac{d^{\rho-1}\underline{y}}{dt^{\rho-1}} \tag{2.11}$$

$$\underline{\nu} = -\underline{K}_0\left(\underline{y} - \underline{y}_d\right) - \underline{K}_1\frac{d\left(\underline{y} - \underline{y}_d\right)}{dt} - \underline{K}_2\frac{d^2\left(\underline{y} - \underline{y}_d\right)}{dt^2} - \ldots - \underline{K}_{\rho-1}\frac{d^{\rho-1}\left(\underline{y} - \underline{y}_d\right)}{dt^{\rho-1}} + \frac{d^\rho \underline{y}_d}{dt^\rho} \tag{2.12}$$

Here, $\underline{y}_d$ is the desired system output and $\underline{K}_i$ are diagonal matrices containing positive control gains. Figure 2.1 shows a block diagram of a NDI control law for an aircraft. As indicated in the figure, there is a separation between the flying quality dependent and airframe dependent part of the control law. If the inversion on the right side of the dashed line is perfect, this part will behave as $\frac{1}{s}$. This means that the left side of the dashed line is fully responsible for the handling quality of the controller.

2.1.1. Single-input-single-output systems

For single-input-single-output (SISO) systems the system description is shown in equation (2.13). It still has the same form as (2.1), however the system input and output variables are scalar.

$$\begin{aligned} \dot{\underline{x}} &= \underline{f}(\underline{x}) + \underline{g}(\underline{x})u \\ y &= h(\underline{x}) \end{aligned} \tag{2.13}$$

Here, both $\underline{f}(\underline{x})$ and $\underline{g}(\underline{x})$ are $(n \times 1)$ vector functions and $h(\underline{x})$ is a scalar function with scalar output y. Furthermore, the elements of $\underline{z}$ are scalar as well. For the determination the elements of $\underline{z}$ and its time derivatives, the Lie derivatives can be written out as follows:

$$\begin{aligned} L_f^i h(\underline{x}) &= \nabla\left(L_f^{i-1}h(\underline{x})\right)\underline{f}(\underline{x}) = \begin{bmatrix} \frac{\partial\left(L_f^{i-1}h(\underline{x})\right)}{\partial x_1} & \cdots & \frac{\partial\left(L_f^{i-1}h(\underline{x})\right)}{\partial x_n} \end{bmatrix}\underline{f}(\underline{x}) \\ L_g L_f^{i-1} h(\underline{x}) &= \nabla\left(L_f^{i-1}h(\underline{x})\right)\underline{g}(\underline{x}) = \begin{bmatrix} \frac{\partial\left(L_f^{i-1}h(\underline{x})\right)}{\partial x_1} & \cdots & \frac{\partial\left(L_f^{i-1}h(\underline{x})\right)}{\partial x_n} \end{bmatrix}\underline{g}(\underline{x}) \end{aligned} \tag{2.14}$$

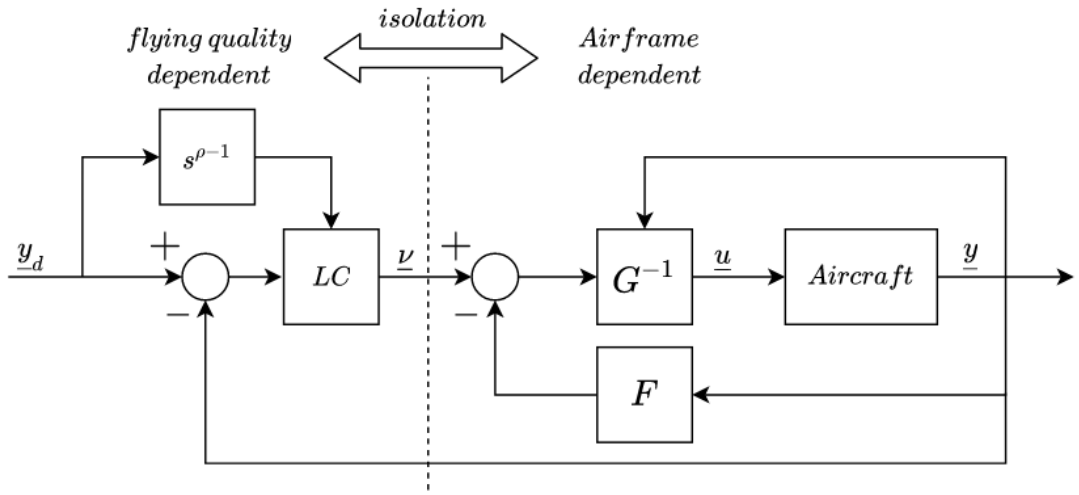

Figure 2.1: Block diagram of control loop based on NDI.

When the relative degree of the SISO system is found, the NDI control solution can be determined similarly to (2.9):

$$u = \left(L_g L_f^{\rho-1} h(\underline{x})\right)^{-1} \left(\nu - L_f^{\rho} h(\underline{x})\right) \tag{2.15}$$

2.1.2. Multi-input-multi-output systems

MIMO systems have the same description as (2.1). Here, $\underline{f}(\underline{x})$ is still a $(n \times 1)$ vector function, however $g(\underline{x})$ has become a $(n \times m)$ matrix function. Furthermore, $\underline{y}$ and $\underline{u}$ have become $(m \times 1)$ vectors. In this derivation $\underline{u}$ and $\underline{y}$ have the same size to obtain a square matrix for G.

Using vectors and a matrix for $\underline{u}$, $\underline{y}$ and $g(\underline{x})$, the derivation of the NDI control law is more elaborate. Equation (2.16) shows how the Lie derivatives are determined for every output variable of a MIMO system.

$$\begin{aligned} L_f^i h_j(\underline{x}) &= \nabla\left(L_f^{i-1} h_j(\underline{x})\right) \underline{f}(\underline{x}) = \begin{bmatrix} \frac{\partial\left(L_f^{i-1} h_j(\underline{x})\right)}{\partial x_1} & \frac{\partial\left(L_f^{i-1} h_j(\underline{x})\right)}{\partial x_2} & \cdots & \frac{\partial\left(L_f^{i-1} h_j(\underline{x})\right)}{\partial x_n} \end{bmatrix} \underline{f}(\underline{x}) \\ L_g L_f^{i-1} h_j(\underline{x}) &= \nabla\left(L_f^{i-1} h_j(\underline{x})\right) g(\underline{x}) = \begin{bmatrix} \frac{\partial\left(L_f^{i-1} h_j(\underline{x})\right)}{\partial x_1} & \frac{\partial\left(L_f^{i-1} h_j(\underline{x})\right)}{\partial x_2} & \cdots & \frac{\partial\left(L_f^{i-1} h_j(\underline{x})\right)}{\partial x_n} \end{bmatrix} g(\underline{x}) \end{aligned} \tag{2.16}$$

Furthermore, each output variable, y_j, has its own relative degree. Thus, $\rho = \{\rho_1, \rho_2, \ldots, \rho_m\}$. This means that the NDI procedure has to be repeated for all output variables to find the appropriate control law to control each output variable. This gives the following set of equations:

$$\underline{\dot{z}}_\rho = \begin{bmatrix} \dot{z}_{\rho_1} \\ \vdots \\ \dot{z}_{\rho_m} \end{bmatrix} = \begin{bmatrix} y_1^{(\rho_1)} \\ \vdots \\ y_m^{(\rho_m)} \end{bmatrix} = \begin{bmatrix} L_f^{\rho_1} h_1(\underline{x}) \\ \vdots \\ L_f^{\rho_m} h_m(\underline{x}) \end{bmatrix} + \begin{bmatrix} L_g L_f^{\rho_1 - 1} h_1(\underline{x}) \\ \vdots \\ L_g L_f^{\rho_m - 1} h_m(\underline{x}) \end{bmatrix} \underline{u} = F(\underline{x}) + G(\underline{x})\underline{u} = \underline{\nu} \tag{2.17}$$

Solving (2.17) for $\underline{u}$ gives the control law of (2.9).

2.2. Incremental Nonlinear Dynamic Inversion

As mentioned before, the INDI control design procedure is also applicable to more general nonlinear system descriptions. This section will consider its derivation and is based on the the derivation shown in Sieberling et al. (2010). Consider the following non-control-affine nonlinear system:

$$\begin{aligned} \underline{\dot{x}} &= \underline{f}(\underline{x},\underline{u}) \\ \underline{y} &= \underline{h}(\underline{x}) \end{aligned} \tag{2.18}$$

To linearize the system with an expression for $\underline{u}$ to control the system output, the diffeomorphism of (2.2) can be used. However, due to the non-control-affine structure of the model, the time derivative of $\underline{z}$ will not result in an control-affine description of $\underline{\dot{z}}_\rho$. To obtain a control-affine structure for $\underline{\dot{z}}_\rho$, the system should be linearized around the current state and input. For the INDI procedure, this is done be taking the first order Taylor expansion of the dynamic equation. This will result in the following procedure:

$$\underline{\dot{z}}_i = \underline{\dot{\phi}}_i(\underline{x}) = \frac{\partial \underline{\phi}_i(\underline{x})}{\partial \underline{x}}\underline{\dot{x}} = \frac{\partial \underline{\phi}_i(\underline{x})}{\partial \underline{x}}\underline{f}(\underline{x},\underline{u}) = \frac{\partial}{\partial \underline{x}}\left[L_f^{i-1}\underline{h}(\underline{x})\underline{f}(\underline{x},\underline{u})\right] = L_f^i\underline{h}(\underline{x}) \tag{2.19}$$

$$\downarrow$$

$$\underline{\dot{z}}_i = L_f^i\underline{h}(\underline{x}) \approx L_f^i\underline{h}(\underline{x})\Big|_{\left(\underline{x}=\underline{x}_0,\underline{u}=\underline{u}_0\right)} + \left.\frac{\partial L_f^i\underline{h}(\underline{x})}{\partial \underline{x}}\right|_{\left(\underline{x}=\underline{x}_0,\underline{u}=\underline{u}_0\right)}\left(\underline{x}-\underline{x}_0\right) + \left.\frac{\partial L_f^i\underline{h}(\underline{x})}{\partial \underline{u}}\right|_{\left(\underline{x}=\underline{x}_0,\underline{u}=\underline{u}_0\right)}\left(\underline{u}-\underline{u}_0\right) =$$

$$\underline{\dot{z}}_{i,0} + F_i\left(\underline{x}_0,\underline{u}_0\right)\Delta\underline{x} + G_i\left(\underline{x}_0,\underline{u}_0\right)\Delta\underline{u} \tag{2.20}$$

Here, $\underline{x}_0$ and $\underline{u}_0$ are the current state and control input, respectively. Furthermore, the equation was simplified by writing $L_f^i\underline{h}(\underline{x})\Big|_{\left(\underline{x}=\underline{x}_0,\underline{u}=\underline{u}_0\right)}$ as $\underline{\dot{z}}_{i,0}$, $\left.\frac{\partial L_f^i\underline{h}(\underline{x})}{\partial \underline{x}}\right|_{\left(\underline{x}=\underline{x}_0,\underline{u}=\underline{u}_0\right)}\left(\underline{x}-\underline{x}_0\right)$ as $F_i\left(\underline{x}_0,\underline{u}_0\right)\Delta\underline{x}$ and $\left.\frac{\partial L_f^i\underline{h}(\underline{x})}{\partial \underline{u}}\right|_{\left(\underline{x}=\underline{x}_0,\underline{u}=\underline{u}_0\right)}\left(\underline{u}-\underline{u}_0\right)$ as $G_i\left(\underline{x}_0,\underline{u}_0\right)\Delta\underline{u}$. This procedure should be continued until $G_i\left(\underline{x}_0,\underline{u}_0\right)$ becomes nonzero. At this point a direct control-affine relation is established between the system output and the control input. To obtain a definition for the control law a similar approach as in NDI could be used. This results in the following control law:

$$\Delta\underline{u} \approx G_\rho^{-1}\left(\underline{x}_0,\underline{u}_0\right)\left(\underline{\nu} - \underline{\dot{z}}_{\rho,0} - F_\rho\left(\underline{x}_0,\underline{u}_0\right)\Delta\underline{x}\right) \tag{2.21}$$

Note that for this control law it is required to have feedback of $\underline{\dot{z}}_{\rho,0}$. Furthermore, as this control law also linearizes the controlled system, the virtual control input could be a linear control law as well. Again, possible linear control laws for a stabilization or tracking task are (2.11) and (2.12).

This control law can be simplified by assuming that the control input changes faster than the system state. Consequently it is possible to neglect the term related to Δx. This approach is based on the time-scale separation principle. This principle will be discussed in the next section.

2.3. Time-scale separation

The main application of the principle of time-scale separation is to construct cascaded control laws. When there is a significant difference in response quickness between states for a certain control input, the states can be separated into fast and slow states. If the difference is large enough, the slow states can be regarded invariant with respect to the fast states and the fast states change instantly with respect to the slow states. In case these states are related to each other, such as rotational rate and rotation angle, it is possible to separate the full set dynamic equations for each state into individual sets. The output of the dynamic equations of the faster states then act as input of the

dynamic equations of the slower states. This separation of the dynamic equations based on fast and slow states is called time-scale separation. Using this principle in NDI- or INDI-based control designs results in a cascaded structure in which the inner loops control the fast states and the outer loops control the slow states. Here, the output of the outer loop sets the reference value for the inner loop and the inner loop determines a control output to reach the reference value.

Time-scale separation can also be applied to the dynamic equations of motion of aircraft. Examples of time-scale separated states are between the roll, pitch and yaw angles and its corresponding rates, between the angle of attack and side-slip, and roll, pitch and yaw rates, or the flight path angle and altitude (Reiner et al., 1995). This results in separate systems where the relative degree is one instead of a complete system of which the relative degree is two. Consequently, the rotational control can be designed in a cascaded structure where the angular rates and the attitude angles are controlled in separate loops. Moreover, due to the lower relative degree of each separate system, the control loop design complexity is decreased as well. On top of that, even though this control structure is simplified, flight control designs based on time scale separation have shown to have unbiased tracking and increased disturbance rejection performance (van 't Veld, 2016).

To simplify the INDI control law, the principle of time-scale separation can be used as well. However, in this case the principle is used to separate the changes in state from the changes in control input. In the INDI control law it is assumed that the control input changes much faster than the state. This can be translated to the following:

$$F_\rho\left(\underline{x}_0, \underline{u}_0\right)\Delta\underline{x} \ll G_\rho\left(\underline{x}_0, \underline{u}_0\right)\Delta\underline{u}$$

If the update rate of the control system is high enough, this assumption is applicable and the effect of $F_\rho\left(\underline{x}_0, \underline{u}_0\right)\Delta\underline{x}$ could be neglected. Using this assumption the final formulation of the INDI control law can be written as follows:

$$\Delta\underline{u} \approx G_\rho^{-1}\left(\underline{x}_0, \underline{u}_0\right)\left(\underline{\nu} - \underline{\dot{z}}_{\rho,0}\right) \tag{2.22}$$

A visualization of this control law in the form of a block diagram can be found in Figure 2.2. As can be seen in this figure, the INDI control law design framework also separates the flying quality demands from the airframe dynamics.

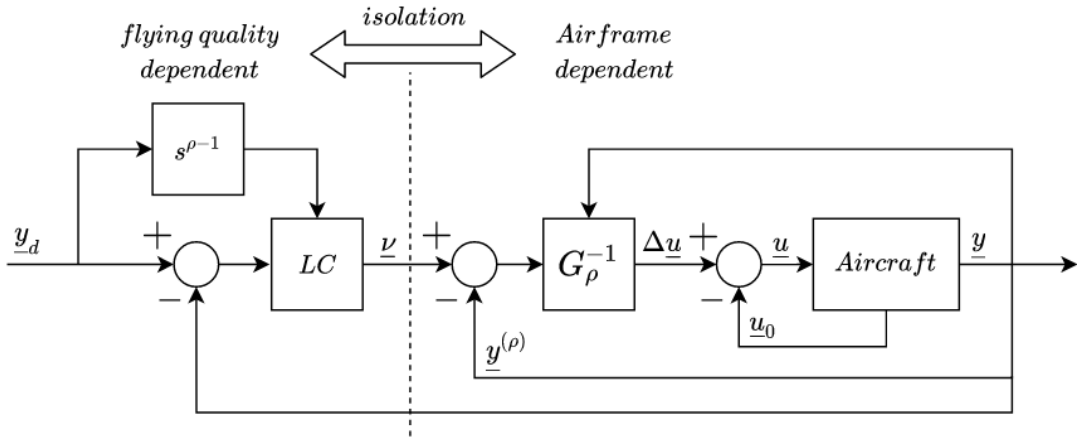

Figure 2.2: Block diagram of control loop based on INDI.

2.4. Effects of model uncertainty in ideal conditions

As mentioned before, an INDI-based controller has improved robustness to model uncertainties with respect to a NDI-based controller. To clarify why this is the case, this section will show the effect of model uncertainties in the NDI and INDI control law.

Consider the known control affine system as described in (2.23). The system output is the system state and the uncertainty is assumed to be in the system equations. Please note that the effect of actuator dynamics and signal delays is not included in this analysis.

$$\begin{aligned} \underline{\dot{x}} &= \underline{f}_{nom}(\underline{x}) + \underline{g}_{nom}(\underline{x})\underline{u} \\ \underline{y} &= \underline{x} \end{aligned} \tag{2.23}$$

Where the subscript *nom* refers to the known nominal model. Following the NDI design procedure of section 2.1, the control law can be written as:

$$\underline{u} = \underline{g}_{nom}^{-1}(\underline{x})\left(\underline{\nu} - \underline{f}_{nom}(\underline{x})\right) \tag{2.24}$$

However, the actual system will have some deviation from the known model. These deviations can be written as a Δ with respect to the known system equations as follows (Sieberling et al., 2010):

$$\underline{\dot{x}} = \left(\underline{f}_{nom}(\underline{x}) + \Delta\underline{f}\right) + \left(\underline{g}_{nom}(\underline{x}) + \Delta\underline{g}\right)\underline{u} \tag{2.25}$$

Furthermore. using the control law of (2.24), the system response can be written as:

$$\begin{aligned} \underline{\dot{x}} &= \left(\underline{f}_{nom}(\underline{x}) + \Delta\underline{f}\right) + \left(\underline{g}_{nom}(\underline{x}) + \Delta\underline{g}\right)\underline{g}_{nom}^{-1}(\underline{x})\left(\nu - \underline{f}_{nom}(\underline{x})\right) \\ &= \Delta\underline{f} - \Delta\underline{g} * \underline{g}_{nom}^{-1}(\underline{x}) * \underline{f}_{nom}(\underline{x}) + \underline{\nu} + \Delta\underline{g} * \underline{g}_{nom}^{-1}(\underline{x}) * \underline{\nu} \\ &= \Delta\underline{f} - \Delta\underline{g} * \underline{g}_{nom}^{-1}(\underline{x}) * \underline{f}_{nom}(\underline{x}) + \left[I + \Delta\underline{g} * \underline{g}_{nom}^{-1}(\underline{x})\right]\underline{\nu} \end{aligned} \tag{2.26}$$

As becomes clear from (2.26), the response of $\underline{\dot{x}}$ is not only related to $\underline{\nu}$ anymore. Furthermore, the deviations do not have to be constant and could be dependent on $\underline{x}$. Consequently, the actual system might not be completely linearized due to the existence of uncertainties.

Now consider the linearized form of (2.23) without the terms related to $\Delta\underline{x}$ in (2.27).

$$\underline{\dot{x}} = \underline{f}_{nom}(\underline{x}_0) + \underline{g}_{nom}(\underline{x}_0)\underline{u}_0 + G_{nom}\Delta\underline{u} = \underline{\dot{x}}_0 + G_{nom}\Delta\underline{u} \tag{2.27}$$

the corresponding INDI-based control law can then be written as follows:

$$\Delta\underline{u} = G_n^{-1}\left(\underline{\nu} - \underline{\dot{x}}_0\right) \tag{2.28}$$

Again, acknowledging that the actual system has a deviation with respect to the known system and using the INDI control law based on the known system model, the system response can be written as:

$$\begin{aligned} \underline{\dot{x}} &= \underline{\dot{x}}_0 + \left(G_{nom} + \Delta G\right)\Delta\underline{u} \\ &= \underline{\dot{x}}_0 + \left(G_{nom} + \Delta G\right)G_{nom}^{-1}\left(\underline{\nu} - \underline{\dot{x}}_0\right) \\ &= \underline{\nu} + \Delta G * G_{nom}^{-1} * \underline{\nu} - \Delta G * G_{nom}^{-1} * \underline{\dot{x}}_0 \\ &= \left[I + \Delta G * G_{nom}^{-1}\right]\underline{\nu} - \Delta G * G_{nom}^{-1} * \underline{\dot{x}}_0 \end{aligned} \tag{2.29}$$

Assuming the sensor measurements are ideal and the sample rate is high, $\underline{\dot{x}}_0$ can be regarded as $\underline{\dot{x}} - \Delta\underline{\dot{x}}$. This results in the following:

$$\begin{aligned} &\underline{\dot{x}} = \left[I + \Delta G * G_{nom}^{-1}\right]\underline{\nu} - \Delta G * G_{nom}^{-1} * \left(\underline{\dot{x}} - \Delta\underline{\dot{x}}\right) \\ &\downarrow \\ &\left[I + \Delta G * G_{nom}^{-1}\right]\underline{\dot{x}} = \left[I + \Delta G * G_{nom}^{-1}\right]\underline{\nu} + \Delta G * G_{nom}^{-1} * \Delta\underline{\dot{x}} \end{aligned} \tag{2.30}$$

$$\downarrow$$

$$\underline{\dot{x}} = \underline{\nu} + \left[I + \Delta G * G_{nom}^{-1} \right]^{-1} * \Delta G * G_{nom}^{-1} * \Delta \underline{\dot{x}}$$

Although this result is only true when the actuator and sensor dynamics can be neglected, it shows that the INDI control law based on the nominal model could still linearize the system despite the uncertainties if the update frequency is high enough. This is because the value of Δx decreases for increasing update frequency. At some point the term related to Δx becomes small enough compared to ν and it could be neglected.

In short, comparing equation (2.26) and (2.30), it can be concluded that the INDI control law is more robust to model uncertainties. Furthermore, when the sample rate is high, and the actuator and sensor is close to ideal, the INDI control law could still achieve the desired system response.

2.5. State-of-the-art review

This section is dedicated to a review on the INDI control design approach. Here, an overview will be given regarding the development of the theory and the suggested solutions to some of the problems.

INDI is still a relatively young design approach with one of its first introductions in Smith (1998). Here, it was postulated and shown in simulations that the use of angular acceleration measurements instead of model calculations could reduce the model dependency in flight control. Furthermore, a method to determine the new desired control deflection was introduced based on the measured control deflection and an incremental change based on the difference between the actual and desired angular acceleration and the control effectiveness. A longitudinal flight control design based on this approach was tested two years later in the VAAC Harrier (Smith and Berry, 2000). From these flight tests it was concluded that the performance was adequate at high-speed flight, but less at hovering conditions and in the transition flight regimes. In this flight regime the aircraft showed more oscillatory behaviour. One of the possible reasons given in the article stresses the phase difference between the feedback signals of which the effects could become more apparent during low speed flight.

In the years after this research, there were several projects which focused the application of INDI, on finding solutions to the observed limitations, and on finding useful additions to the theory. For example, in Bacon and Ostroff (2000) an approach to obtain the angular accelerations is proposed using three sets of linear accelerometers and differentiated angular rates. However, in the follow-up research project (Bacon et al., 2001) a washout filter was applied to obtain the angular accelerations from the angular rate measurements as ordinary differentiation amplified the noise on the angular rate signal.

Another important point of attention is the fact that the standard theory of both NDI and INDI do not take into account saturation characteristics with respect to the actuator deflection position and rate. In further research performed by A.J. Ostroff and B.J. Bacon this aspect has been considered as well. In Ostroff and Bacon (2002) a method is introduced which decreases the probability that the actuator reaches the saturation limits. Moreover, this research demonstrates the value of INDI based control in FT flight control.

In 2010 the general derivation of the INDI approach was presented next to another method to obtain the angular acceleration (Sieberling et al., 2010). This method uses a linear predictive filter to determine the angular accelerations. Furthermore, this filter has the practical benefit of compensating for signal delay as well. After this project the Delft University of Technology continued with research on INDI till this day. Multiple use cases have been studied such as helicopter control in Simplicio et al. (2013), and spacecraft control in Acquatella et al. (2012). In both studies it was shown that INDI based control could handle external disturbances, signal time-delay and model uncertainty better than NDI based control. Furthermore, in Simplicio et al. (2013) Pseudo-Control Hedging (PCH) was used in the INDI based control to prevent the system from tracking reference

signals when the actuators of the system are saturated. Although, PCH was not new, it was the first application in INDI based control and it was demonstrated to be beneficial for this type of control as well.

In more recent years more emphasis is put on the real-world implementation of INDI. In 2014 a flight test using INDI based control was performed as mentioned in Grondman et al. (2018) and van 't Veld (2016). This flight test was performed with the FASER sub-scale fixed-wing UAV in a co-operative research of the German Aerospace Centre (DLR) and the Delft University of Technology. Furthermore, two years later, in 2016, another flight test using a UAV was performed as shown in Smeur et al. (2016). Moreover, this research introduced an adaptive method to estimate the control effectiveness during flight. This was done to bypass of the required system modelling. It showed great performance and it could adequately cope with system changes related to inertia. Furthermore, in this research the importance of synchronizing the actuator and angular acceleration feedback was practically demonstrated. Moreover, using artificial delays to synchronize these signals was shown and demonstrated to work effectively.

In the same year as the micro air vehicle (MAV) flight test of Smeur et al. (2016) research was also conducted on the application of INDI in the PH-LAB Cessna Citation II. This research has been documented in van 't Veld (2016). In this research the practical aspects related to fly-by-wire (FBW) flight control are addressed and some possible solutions are proposed. Furthermore, it was shown that sampling times below 0.02 s would result in large stability margins. Besides, it was shown again that synchronization of the control variable and actuator measurements is critical for the control performance. In this research a novel method to synchronize these signals was proposed. The difference in delay of both signals were estimated on-line using an Average Square Difference Function (ASDF) and the difference in delay was used as an artificial delay for the faster signal. Moreover, it was concluded that actuator measurement bias and angular rate measurement noise were dominant factors for control performance degradation as well. The proposed solutions for these issues were using proportional-integral virtual control instead of only proportional, and applying a second-order filter. Lastly, it was concluded that currently the best option for preventing actuator saturation would to to use PCH.

The research on the practical implementation of INDI was continued and has resulted in the first successful flight test in the CS-25 certified PH-LAB Cessna Citation II (Grondman et al., 2018). This research has shown the high robustness against model uncertainties of INDI, see figure 2.3, and that it is a promising theory for future flight control design. Furthermore, it was found that using actuator measurements instead of models is more practical as difficulties could occur regarding initialization of the models. Moreover, it was concluded that the INDI law contained higher noise levels in the control signals due to the differentiation of the angular rate measurements. Even though serious effort has been put in filtering it was still concluded to be a point of attention.

Next to many more application studies, more research has been performed to advance the theory on INDI. In Wang et al. (2019b) a nonlinear stability and robustness analysis has been performed. Here, it is proven that the response of a INDI based controller is bounded when the disturbances are bounded. This result is substantiated in research on gust load alleviation of flexible aircraft using INDI based flight control (Wang et al., 2019a). This research shows that, with proper modelling of the flexible modes in an aircraft, INDI based control is able to remain stable, reduce wing root bending moment and quell wing bending modes. At the same time, a study on the application of an INDI control law for the Apache AH-64D Longbow was conducted (Pavel et al., 2020). In this paper it was shown by piloted simulation that a control system design based on INDI could improve the handling qualities of this helicopter in normal and degraded visual environment. This was demonstrated by flying the ADS-33 hover and pirouette manoeuvres in these conditions in the SIMONA flight simulator at the Delft University of Technology.

From this literature study it becomes clear that in the recent years much effort has been spent

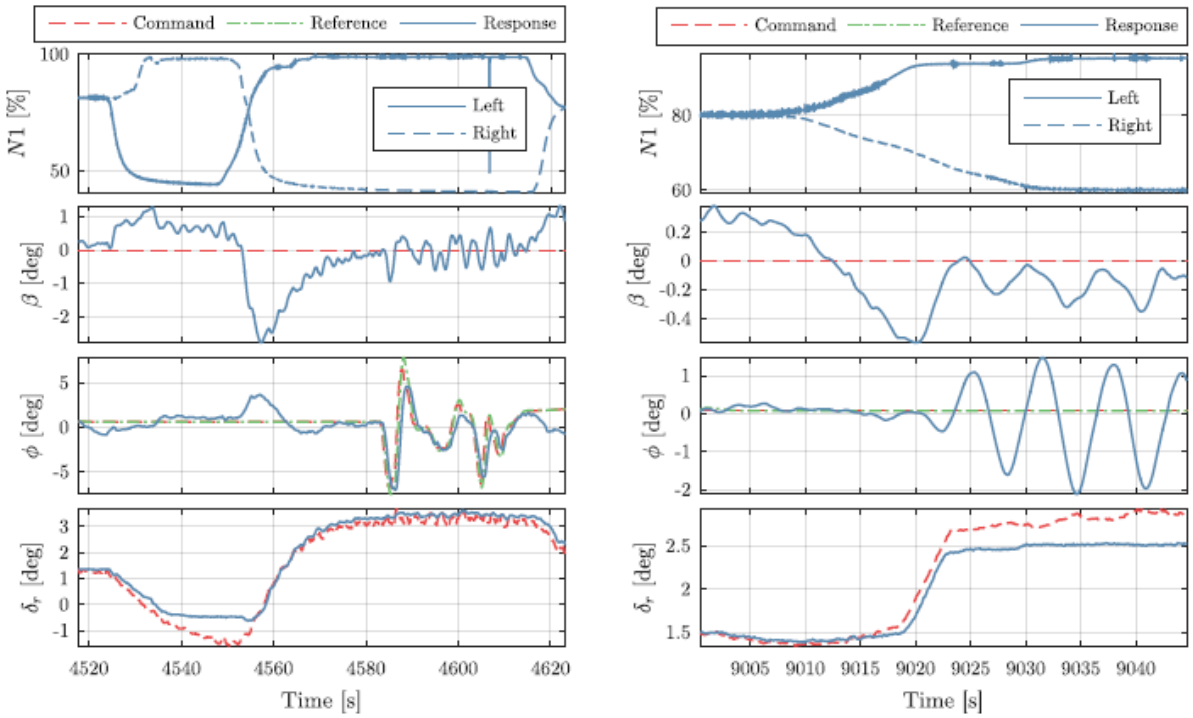

Figure 2.3: Lateral tracking response for simulated engine failure flight test at 200 KIAS and FL150 (Grondman et al., 2018).

on the practical implementation of INDI control laws. Control systems based on this design approach have shown high performance, and are robust against model uncertainties and external disturbances. Furthermore, due to the low model dependency it is an interesting method for the control design of highly nonlinear systems such as military fighter aircraft. However, as shown in Smeur et al. (2016), for agile aircraft it is important to have a good estimation of the control effectiveness. An overestimation could result in slow tracking and overshoot and an underestimation could result in sustained oscillations. Consequently, for military fighter aircraft it is important to have a good estimation of the control effectiveness to retain the demanded control performance. During this literature research no sources have been found which comment on the degradation of performance of an INDI control law due to changes in the control effectiveness. Therefore, this is of interest for the real-world application of INDI based control in military fighter aircraft and will be further investigated in this research. Moreover, it is generally known that adaptive control laws are capable of identifying changes in the system on-line and . Therefore, these methods will be further exploited to find a solution for possible performance degradation due to control effectiveness changes.

3

Adaptive control

The research on adaptive control started in the 1950's when autopilots for high-performance aircraft were investigated (Åström and Wittenmark, 2008). It was observed that the dynamic changes due to fast state transitions were not adequately treated by the conventional methods. A suggested solution to accommodate for this problem was to implement an additional law which could tune the control gains during flight. It was presumed that, using these methods, the desired control performance would be maintained even though the state transitions were fast. This led to the emergence of adaptive control. Furthermore, the adaptive law should be able to deal with any uncertainty which is normally taken into account when designing control systems. However, the additional adaptive routine transformed the linear controller into a nonlinear controller. This meant that the linear stability theories were no longer valid. At this moment in time the theory on describing stability of nonlinear controllers was not yet developed and therefore it was not possible to prove stability of the adaptive control design. Consequently, the interest in adaptive control laws decreased. However, during the 1960's stability theory based on Lyapunov stability was developed which gave insight in proving stability of nonlinear control system and therefore adaptive control systems as well (Nguyen, 2018). This increased the interest in adaptive control methods again and has resulted in the rich research field on adaptive control of today.

In literature the definition of adaptive control varies. Some surveys consider all on-line reconfiguring control laws to be adaptive while others only consider the control laws with on-line control parameter estimation to be part of adaptive control. As the definition varies, it is important to set the definition used in this research. Here, the following definition is used:

> *Adaptive control laws are control laws which modify their control parameters on-line to adhere to a predefined performance index. The adaption is performed by using on-line identification of the control parameters from a posteriori knowledge of the dynamic system. From this knowledge a certain performance index of the controller is determined, which is compared to a predefined performance index. The difference is used to drive the adaptive law (Landau et al., 2011).*

Following this definition, first an overview of the main strategies in adaptive control will be treated in section 3.1. Next to these strategies two paradigms have been developed on the used information to drive the adaptive law. These two approaches will be treated in section 3.2. Then, the focus will be drawn to the core operation of the adaptive law, which is the online identification of the model parameters. This process, and the associated matters and choices will be discussed in section 3.3.

Furthermore, research on adaptive control performed in the past decades has established that the standard adaptive law designs contain limitations. These limitations were a result of, for exam-

ple, an insufficient amount system excitation, and lacking robustness to disturbances and unmodelled dynamics. Solutions have been suggested and investigated which led to the fields of adaptive dual control and robust adaptive control. An brief introduction to these fields will be given in section 3.4.

After covering the aspects of adaptive control in general, this chapter will dive into recent and relevant research on adaptive control in combination with INDI, NDI and other model-based adaptive control laws. This state-of-the-art review will be covered in section 3.5. Lastly, using the knowledge obtained in the state-of-the art review, in section 3.6 a concise set of adaptive laws will be selected for further investigation in this research.

3.1. Direct and indirect control

Within the field of adaptive control there are two main paradigms. The adaptive law could either estimate the control parameters, $\hat{\theta}_c$, directly or the parameters of a system model, $\hat{\theta}_m$, are estimated first and these parameters are used to determine the required control parameters. These two perspectives are often referred to as *direct* / *implicit* and *indirect* / *explicit* adaptive control (Landau et al., 2011).

3.1.1. Direct adaptive control

As mentioned before, a direct adaptive control approach only estimates and adapts the control parameters, $\hat{\theta}_c$. To achieve this, the system model parameters are defined in terms of the control parameters. This results in the direct adaptive control approach also being referred to as *implicit adaptive control* (Ioannou and Fidan, 2006). A general schematic overview of the components of a direct adaptive control system is shown in Figure 3.1.

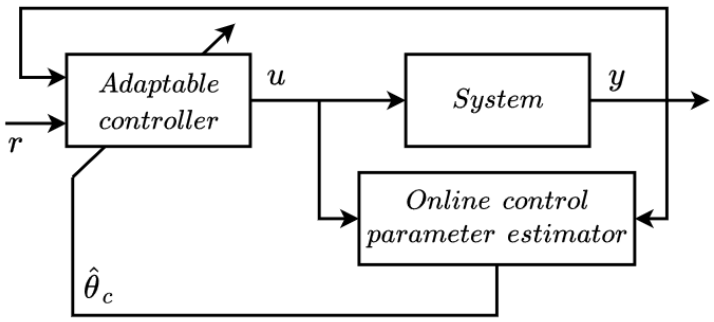

Figure 3.1: General block diagram of direct adaptive control.

One of the benefits of using direct adaptive control is the possible lower computational complexity as the control parameters are determined in one step instead of two. However, it should be possible to rewrite the system model in terms of the control parameters which is not always the case. Besides, a subsequent issue is that the dynamics characteristics, such as minimum or non-minimum phase, of the system should be known (Ioannou and Sun, 2013). If the controlled state exhibits is either minimum phase or non-minimum phase, the direct adaptive controller could still be an advantageous adaptive approach. Though, if the controlled state could behave both minimum and non-minimum phase during operation, it might be required to use extra identification algorithms to identify the change in behavior. This could reduce the advantage in computational complexity of the adaptive control law (Nguyen, 2018).

3.1.2. Indirect adaptive control

A general block scheme of an indirect adaptive control system is shown in Figure 3.2. Here, it can be seen that the control parameter estimation consists of two steps. First, the parameters of the system

model are estimated, $\hat{\theta}_m$. Secondly, the model estimate and some predefined closed loop response criteria are used to calculate the new control parameters, $\hat{\theta}_c$.

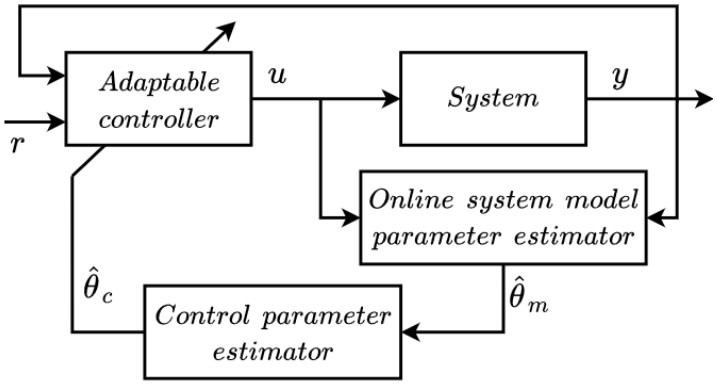

Figure 3.2: General block diagram of indirect adaptive control.

Due to the fact that indirect adaptive methods first estimate the parameters of the system model, this approach is applicable to more systems than the direct approach and it could be combined with many control laws (Landau et al., 2011). In these type of adaptive controllers the adaptive laws are basically added to the existing control law as an extra module. Therefore, the indirect adaption control laws are sometimes also referred to as modular adaptive control laws (Krstić et al., 1995).

Furthermore, this approach naturally determines whether the system dynamics are minimum or non-minimum phase which means that it is not required to actively monitor for this aspect of the system behaviour (Ioannou and Sun, 2013). Moreover, due to the determination of the model parameters it is also possible to monitor the system for possible degradation (Sun et al., 2019). This could be valuable to systems which are susceptible to wear and contain many operation critical components. However, due to the extra step in the control parameter estimation this approach could have a higher computational complexity compared to direct adaptive control. Though, despite these beneficial characteristics, it is more difficult to proof stability for these type of adaptive controllers as it fully depends on the correct convergence of the system model (Krstić et al., 1995).

3.2. Adaptive control design Methods

Next to the distinctions in paradigms of adaptive control it is also possible to make a distinction in design approach. For example, it possible to use a reference model which determines the desired system output of the closed loop system. This output will then be compared to the actual closed loop system output and based on the difference, the controller will be adapted. Adaptive control systems using this approach can be classified under *Model Reference adaptive Control* (MRAC) Systems (Nguyen, 2018). In the other branch the control parameters are adapted using other performance index forms such as the error between the adaptive prediction model and the actual system output. These adaptive control system designs are called *Self-Tuning Control* (STC) systems (Landau et al., 2011).

3.2.1. Model Reference Adaptive Control systems

This approach stems from the beginning of the research on adaptive control (Whitaker et al., 1958). A general block diagram of MRAC is shown in Figure 3.3. The essence of this approach is quite straight forward. A reference model determines a desired system output signal which should be followed by the actual system. In case the actual system output does not match the reference output, the adaptive law adjusts the control parameters such that the controlled system output follows the reference output again (Nguyen, 2018).

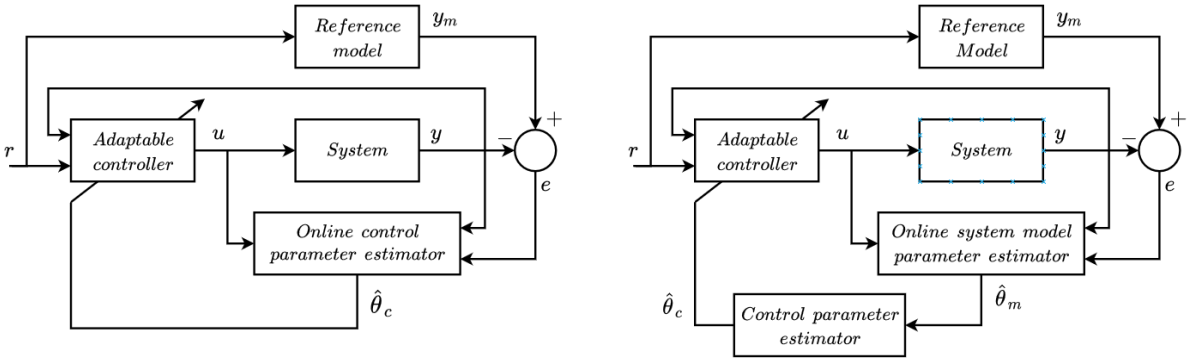

Figure 3.3: Block scheme representation of direct (left) and indirect (right) Model Reference Adaptive Control.

At first, this approach was developed for the control of LTI SISO systems. Using a rule developed at the Massachusetts Institute of Technology (MIT), also known as the *MIT rule*, it was possible to obtain a continuous-time adaptive law that could update the control parameters. The MIT rule is a scalar parameter estimation rule which was developed in the late 1950's (Mareels et al., 1987). Although MRAC control laws were developed using the MIT rule and actually tested, this method lacked proof of stability (Aström, 2014). This problem together with an accident with the X-15 decreased the interest in MRAC and other adaptive control laws as well (Dennehy et al., 2014). However, in the 1970's MRAC based on Lyapunov stability was derived, which gave a boost to the research field in the field of MRAC. Since then, the MRAC approach has been applied in many studies in industry and aerospace (Nguyen, 2018).

MRAC designs are mostly used in a direct adaptive form as this allows for an adaptive control design using Lyapunov stability functions. Consequently, it is easier to proof stability of the complete adaptive control law. For a broader view on the applications and possibilities and limitations of MRAC it is recommended to read Nguyen (2018).

3.2.2. Self-tuning Control systems

Next to MRAC systems STC systems are also introduced. This field of adaptive control system design was started by the development of the Self-tuning Regulator (STR) approach by Kalman in the late 1950's (Landau et al., 2011). The reasoning behind the STC design approach was that if the system model can be predicted online, the controller could be optimized online using the estimated model to determine the optimal control gains (Ljung and Landau, 1978).

Although the original self-tuning system was developed using an indirect adaptive approach, they can also be designed in a direct adaptive manner as is presented in Silveira et al. (2012). In this research a Generalized Minimum Variance (GMV) controller is transformed in an adaptive controller by writing the system model as an Auto-Regressive Integrated Moving Average with eXogenous input (ARIMAX) model where the controller parameters are the model parameters. However, considering that there are not many examples of the direct variants compared to the indirect ones, the direct designs are clearly less popular. The block diagram of a direct or indirect self-tuning system looks the same to the direct or indirect adaptive block diagrams shown in Figure 3.1 and 3.2. The exact process occurring in the 'Online parameter estimator' block depends on the derivation of the adaptive law. However, probably the most common version is the use of an adaptive prediction model which is adjusted based on the prediction error.

3.3. Online identification

All adaptive laws perform online identification. The algorithm which performs this can be used to update the control parameters directly or indirectly as discussed before. However, before the online identification algorithm can be implemented the designer has to make choices about the following aspects:

- State estimation
- Mathematical model
- Real-time parameter estimation algorithm

The measurements required for the control feedback and the adaptive law often contain noise and could be biased. Therefore, it could be required to perform state estimation as well. Depending on the requirements for the identification and the application the state and parameter estimation can be joint or separated. These two design option are referred to as the one-step and two-step method for system identification (Laban, 1994).

In the research of Laban (1994) it was shown that joint state and aircraft model parameter estimation requires the optimization of a nonlinear cost function. Consequently, nonlinear optimization algorithms are needed to find the correct system parameters. To find the optimum set of model parameters to optimize the cost function these algorithms require to iterate. Consequently, these algorithms are often not suitable for real-time applications. One of the few nonlinear algorithms which have been used in real-time is the *filtering method* developed at DLR (Lombaerts, 2010). Furthermore, another disadvantage of the one-step method is the fact that the state estimation could be affected by errors in the model. As the estimated state is used to estimate the system parameters the estimated parameters will also be affected again (Laban, 1994).

However, as demonstrated in Laban (1994) it is possible to separate the state and parameter estimation for the identification of the aircraft system. This approach is referred to as the *Two-step method*. The separation of the state and parameter estimation results in a nonlinear state estimation problem and a possible linear parameter estimation problem. Although, the state estimation is a nonlinear problem, due to the use of, for example, an Extended Kalman Filter (EKF) this problem is still relatively easy to solve (Laban, 1994). Besides, due to the use of the kinematic relations it is possible to omit the use of the uncertain aerodynamic model, mass and inertia (Lombaerts, 2010). Moreover, due to the possibility of using linear parameter estimation techniques as well, the Two-step method is more suitable for real-time applications, such as adaptive control.

Although state estimation will not be included in this study, the aspect of state estimation will be briefly covered to obtain a broader grasp of the aspects involved with online identification and therefore adaptive control.

3.3.1. State estimation

Sometimes it is not possible to obtain the feedback of a certain state directly from sensor measurements or the measurements are noisy and/or biased. If high quality feedback signals are required for the control system, as is the case for high-performance military aircraft, it is probably necessary to perform state estimation. State estimation could filter the noise from the signal when the noise properties are known, combine the knowledge from multiple sensors (*Sensor Fusion*), or could do both (Lombaerts, 2010). A general description of a system subjected to process and sensor noise can be written as follows:

$$\underline{\dot{x}}(t) = \underline{f}\left(\underline{\theta}(t), \underline{x}(t), \underline{u}(t), t\right) + G\underline{w}(t)$$
$$\underline{z}(t) = \underline{h}\left(\underline{\theta}(t), \underline{x}(t), \underline{u}(t), t\right) + v(t)$$

Currently, the best known state estimation algorithms in aerospace are probably based on the Kalman Filter (KF). This filter attempts to find the state using the past and current system input and output. This is achieved using a recursive weighted leas-squares formulation for the optimization of a quadratic cost function of the estimation error. Included in the recursive optimization are the process and sensor noise characteristics where it is assumed that the mean of the noise is zero (De Visser, 2011).

The standard KF is designed to find an optimal state estimate for linear systems. Consequently, this algorithm is not applicable for a nonlinear system such as an aircraft. However, to overcome this problem an extension for the standard KF has been developed which first linearizes the system around the current estimated state and then performs the standard KF routine. This algorithm is called the Extended Kalman Filter or EKF (Reif et al., 1999).

However, due to the extension to the non-linear domain the EKF becomes a non-optimal filter and it cannot be guaranteed that the state estimation will actually converge to the true system state (Wan and Merwe, 2000). To relax this problem the Kalman gain determination and measurement update phases of the algorithm have been made iterative. Due to this extra iterative layer the EKF can be adjusted for model mismatches induced during the linearization. This algorithm is called the Iterative Extended Kalman Filter (IEKF) (De Visser, 2011; Lombaerts et al., 2009). Another option is the Unscented Kalman Filter (UKF) (Wan and Merwe, 2000). This KF type carefully selects some measurement points, also known as *sigma points*, to determine the probability distribution of the state. According to the results shown in Wan and Merwe (2000) the UKF performs better in finding the mean and covariance of the states than the EKF while having a similar computational complexity.

3.3.2. Mathematical modelling

The model structures used in adaptive flight control laws depend on the prior knowledge about the system or system change, the available computational power, the required accuracy, etc. Furthermore, indirect adaptive laws for model-based control systems often make use of complete aircraft models in the form of (nonlinear) state-space formulations, transfer functions or differential equations (Lombaerts, 2010; Morelli and Klein, 2016). On the other hand, direct adaptive laws often use model structures which are more general, such as Neural Networks as shown in Rysdyk and Calise (2005). Consequently, the model structure is also dependent on the structure of the adaptive control law.

With respect to mathematical modelling of a system, there are multiple approaches. In literature the possible approaches are divided into *White-box*, *Black-box* and *Grey-box* modelling (Tangirala, 2018). White-box system modelling is possible when the prior knowledge of the system can fully describe its behaviour. The equations used in the model are based on first principles and parameters are physical constants. An example of a white-box model in the aircraft system is the relation between the body velocities, u, v and w, and the aerodynamic angles, α and β. Furthermore, black-box modelling is the approach which develops a model purely based on the input and output data of the actual system. Consequently, it is possible to obtain a system model without requiring any prior knowledge. On the other hand, the model parameters do not have any physical meaning which makes these models difficult to validate. The third type of system modelling lies in between the white- and black-box modelling and therefore has been called grey-box modelling. The models developed using this approach contain parts which are based on prior knowledge or first principles and contain parts which are purely based on data. A good example of such a model in the aircraft system is the model of the aircraft dynamics. There are terms related to the cross-coupling of the rotational motions which are based in first principles and it contains the aerodynamic model. Over the past few decades it has been established that aerodynamic model can be modelled with a certain structure, however the model parameters are obtained from flight test data.

As established in the previous chapter, without the availability of a detailed mass model to model the change in the system dynamics it is only possible to obtain knowledge of the system changes using the data gathered during flight. Consequently, in this research a black-box modelling approach will be applied. With respect to adaptive control it is very important to use as few model parameters as possible to decrease the computational demand as much as possible. Consequently, in this research the *Principle of Parsimony* is strictly followed (Lombaerts, 2010). Its definition is as follows:

Principle of Parsimony: *If there are multiple mathematical models which represent the same system at a similar accuracy, the model with the least number of parameters is preferred.*

Considering the possible black-box model structures the amount of options are vast. According to Tangirala (2018), black-box model structures could have the following characteristics:

Parametric	$\leftrightarrow$	non-parametric
Linear	$\leftrightarrow$	nonlinear
Deterministic	$\leftrightarrow$	stochastic
Static	$\leftrightarrow$	dynamic
Continuous(-time)	$\leftrightarrow$	discrete(-time)

Non-parametric models do not have a structure which can be defined by parameters such as parametric models. This does not mean that the models do not contain parameters. Mostly, the amount of model parameters of a non-parametric model is equal to the amount of data which is used to develop the model. An example of a non-parametric model is a discrete impulse response models (Tangirala, 2018):

$$y[k] = \sum_{n=-\infty}^{\infty} g[n]\, u[k-n] \tag{3.1}$$

Furthermore, within the domain of parametric models the models can be linear or nonlinear. Though, with respect to the parameters another classification is also possible. Namely, the model could be a summation of nonlinear basis functions of which each is scaled by a model parameter as shown in Eq. (3.2). These models are nonlinear, but are linear-in-the-parameters (LP). Other examples of LP models are AR(I)MAX models or multivariate B-spline models (De Visser, 2011). Nonlinear-in-the-parameters (NP) models are nonlinear models which do not posess the structure of LP models such as shown in Eq. (3.3). One of the best known NP black-box models are probably the Neural Networks (NN). With respect to system identification this distinction is more convenient as this classification immediately gives away the need for linear or nonlinear parameter estimation methods.

$$y(t) = a_0 + a_1 \cos(x) + a_2 \cos(2x) + \ldots + a_n \cos(nx) \tag{3.2}$$

$$y(t) = a_0 + a_1 \frac{1}{a_2 + x^{a_3}} \tag{3.3}$$

Deterministic models can be used for systems of which the output can be predicted accurately. This does not mean that the system does not contain randomness, but the randomness is significantly smaller than the deterministic part. For systems which have an output which cannot be accurately predicted stochastic models can be used. A clear example of a stochastic model is a model which makes weather or market forecasts.

The difference between static and dynamic models is the dependency on the past. Dynamic models in contrast to static models have a certain 'memory' as the information determined in the past is required to determine the output of the present. An example of a static model is Ohm's law and an example of a dynamic model is of course the model of the rotational dynamics of an aircraft.

With respect to dynamic systems the use of continuous or discrete-time model depends on whether the response is solved by hand of by computer simulations. By hand it is possible to find and analytical solution. However, if this cannot be done it is required to use computers. As computer operate in discrete time-steps it is required to make a discrete-time model of the the dynamic system. Other cases where discrete models are required is for example of random processes where the probability distribution is discrete. An example of such a process is the outcome of rolling dice.

3.3.3. Real-time parameter Estimation

The core activity of online identification is the parameter estimation algorithm. The goal of parameter estimation is to find the set of model parameters which results in the best approximation of a dataset considering a certain optimal criterion. Depending on the model structure and optimization criterion this optimization could be performed in one iteration or it requires several.

Parameter estimation tasks which will probably require multiple iterations are NP model identification and optimization of nonlinear cost functions. An example of the optimization of a nonlinear cost function is the optimization of the Likelihood function (De Visser, 2011):

$$\underline{\hat{\theta}}_{ML} = \arg\max_{\underline{\hat{\theta}}} L(\underline{z}\left|\underline{\hat{\theta}}\right.) = \arg\max_{\underline{\hat{\theta}}} \frac{1}{2\pi^{N/2}\sqrt{\left|\Sigma\left(\underline{\hat{\theta}}\right)\right|}} \exp\left(-\frac{1}{2}\left(\underline{z}-A(\underline{x})\underline{\hat{\theta}}\right)^T \Sigma^{-1}\left(\underline{\hat{\theta}}\right)\left(\underline{z}-A(\underline{x})\underline{\hat{\theta}}\right)\right) \tag{3.4}$$

Due to the dependency of the residual covariance matrix, Σ, on the estimated parameter(s), $\underline{\hat{\theta}}$, it is clear this function is nonlinear and therefore the optimization is nonlinear. Therefore, to find a solution to this problem it is probably required to perform iterations which could be computationally expensive. However, for adaptive control it is important that the parameter estimation can be performed in real-time. Consequently, in most cases linear optimization problems are used, as these approaches to not necessarily require iterations to find a solution. To obtain a linear optimization problem it is required to have a LP model structure and a linear cost function. Probably the best known cost function that is the quadratic cost function of Eq. (3.5).

$$J(\underline{x},\underline{z},\underline{\hat{\theta}}) = \underline{\epsilon}^T\underline{\epsilon} = \left(\underline{z}-A(\underline{x})\underline{\hat{\theta}}\right)^T\left(\underline{z}-A(\underline{x})\underline{\hat{\theta}}\right) \tag{3.5}$$

An optimization algorithm which is able to optimize this equation real time is the *Recursive Least Squares* (RLS) algorithm (Diniz, 1997). Next to this form of parameter estimation there is also the option of using Lyapunov methods as is used in MRAC. Here, the optimization criterion of to minimize the error between the reference model output and the actual system output. The parameter update will continue until this objective is achieved.

3.4. Adaptive dual and robust adaptive control

The adaptive control design approaches discussed in the beginning of this chapter are based on the assumption that the estimated parameter is also the true parameter. The principle on which this assumption is based is called the *certainty equivalence* (CE) principle (Filatov and Unbehauen, 2004). Postulated by A. Feldbaum, the performance of adaptive controllers based on this principle could be far from optimal for some systems (Ioannou and Sun, 2013). Consequently, he conducted

research on adaptive control laws which were not based on CE. In 1965 he presented the paradigm of Adaptive *Dual* control.

Furthermore, most adaptive laws are designed without considering disturbances, unmodelled dynamics and noise. Especially for MRAC based adaptive control laws the influence of unmodelled dynamics can be detrimental for the control performance. Between 1970 and 1990 many research projects have been conducted to analyse the stability of adaptive controllers in the presence of disturbances, unmodelled dynamics and noise. It was found that various adaptive control laws could become unstable and therefore effort was put in resolving these problems and developing adaptive control laws which take these factors into account. This led to the field in adaptive control now known as *robust adaptive control* (Ioannou and Sun, 2013).

3.4.1. Adaptive dual control

A dual adaptive control law is designed according to the two goals in adaptive dual control (Ioannou and Sun, 2013). First of all, the controller should *cautiously follow the reference signal.* Secondly, the control signal should *excite the system sufficiently to aid the parameter estimation.* The second goal can be achieved by adding probing signals to the control signal which is also known as *persistent excitation* (PE).

In the research of A. Feldbaum the problem for stochastic optimal control was formulated and solutions were found. However, the adaptive control designs which are designed to solve the problem are difficult to implement without setting stringent requirements on the computational power of the control computer (Wittenmark, 1995). Therefore, many sub-optimal adaptive dual control algorithms are designed. An survey containing an overview of possible dual adaptive control methods is documented in Wittenmark (1995).

With respect to the control problem of high-performance aircraft, dual adaptive control strategies might not be most appropriate. This is due to the aspect of actively influencing the control signal. Although beneficial for the parameter estimation it could disturb the control task for mission phases where accurate tracking is required. An example of an accurate tracking phase could be in-flight refueling. Consequently, in this research, the adaptive controller designs considered in this study will not include dual control elements and consequently will be based on CE.

3.4.2. Robust adaptive control

As mentioned before, most direct and indirect adaptive control laws do not take into account robustness against disturbances, unmodelled dynamics and noise. In the 1970s it was observed that many adaptive control systems would become unstable when they were subjected to these phenomena. From this moment onward there have been many research projects which focused on robustifying the adaptive laws. Already in the 1980s there were several proposed solutions for LTI systems (Ioannou and Sun, 2013). This period was the origin of the field of *robust adaptive control.*

During the past few decades, studies on adaptive law instability due to disturbances, unmodelled dynamics and noise have led to the classification of the following instability mechanisms (Ioannou and Sun, 2013):

- Parameter drift
- High-gain instability
- Fast adaption instability
- High-frequency instability
- Parameter variation effects

A clear explanation of these instability effects is given in Ioannou and Sun (2013). Possible solutions which have been investigated for these problems are for example the Dead-Zone method and the Projection method (Nguyen, 2018; Ioannou and Sun, 2013). The Dead-Zone method can be used to stop the parameter estimation when the reference model error or prediction model error is below a certain predefined threshold. On the other hand, the projection method can be used to limit the estimated parameter value within a predefined domain. For more options and solutions to these problems it is recommended to read Nguyen (2018) and Ioannou and Sun (2013).

3.5. State-of-the-art review on adaptive laws

To obtain an idea of the state-of-the-art on the field of adaptive control, this section will consider the recent and relevant research projects. As the area of research in adaptive control has become very large, it is impossible to obtain a complete grasp of the possibilities and performed work in the short state-of-the-art review written in this section. Therefore, this literature will focus on adaptive control laws used in aerospace for modern model-based nonlinear control laws. First, a state-of-the-art review will be conducted on adaptive INDI approaches. However, as the INDI control design procedure is relatively new this field is still small. Consequently, the state-of-the-art of adaptive NDI control will be considered as well. Lastly, other adaptive model-based control laws such as adaptive backstepping and adaptive incremental backstepping will be reviewed.

3.5.1. Adaptive laws in INDI control systems

As mentioned before the research on adaptive INDI is still relatively small as the INDI control law is still quite novel. The first research project considering adaptive INDI control is Lu and van Kampen (2015). Here, a fault tolerant INDI control law design is proposed and analysed in simulation, that is able to detect a rotor failure and adjust the control law to maintain safe flight. Furthermore, the first real-world application of adaptive INDI was performed in 2016 at the Faculty of Aerospace Engineering of the Delft University of Technology (Smeur et al., 2016). In this research, an adaptive INDI the control law was used for the flight control of a Bebop quadrotor from Parrot which is a MAV. The adaptive law was based on the Least-Mean-Squares (LMS) parameter estimation method. This method could be run on the computer of the drone itself due to the very low computational complexity.

In this research two critical points of the INDI control law have been treated. First of all, the requirement for synchronization in the non-adaptive INDI control law itself. It has been demonstrated that synchronization of the angular acceleration feedback and control feedback is required. Otherwise severe oscillations will be present in the control response. Furthermore, it was demonstrated that a possible solution to this problem is to add the same delay to the feedback of the control signal. Secondly, the effect of underestimating or overestimating the control effectiveness. During the experiments two tests were conducted where the control effectiveness was affected. In the first test the on-board model was tuned to a MAV without collision bumpers, but the MAV was flown with the bumpers equipped. This means that the actual control effectiveness is less then that of the on-board model. The resulting response can be seen in Figure 3.4. Due to the overestimation of the control effectiveness it has been demonstrated that the control response becomes slow and less damped. Furthermore, in the second test the conditions were switched and the MAV was flown without its collision bumpers while the model was tuned as if they were equipped. This results in an underestimation of the control effectiveness. As shown in Figure 3.5, the resulting response became significantly more oscillating. Furthermore, the oscillations were badly damped.

Lastly, in this research it was shown that the LMS parameter estimation method was very effective in estimating the correct control effectiveness parameters. Using adaptive control it was possible to obtain nearly the same roll response as the non-adaptive INDI controller without model error. The results obtained in this research are of interest in this research as in this study also con-

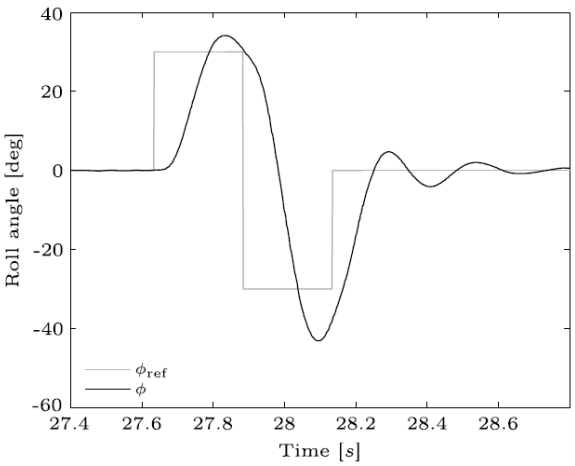

Figure 3.4: Roll angle response for overestimated control effectiveness. Source: (Smeur et al., 2016)

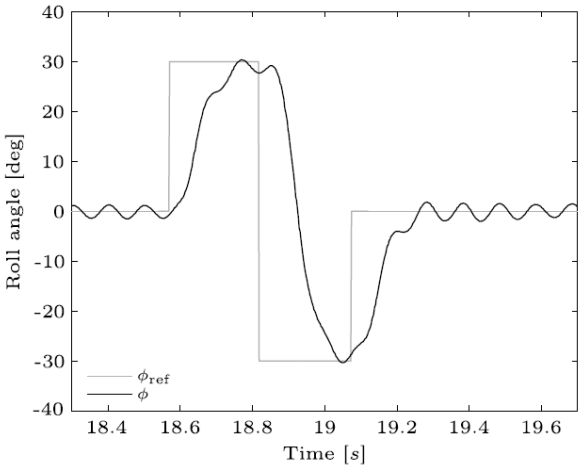

Figure 3.5: Roll angle response for underestimated control effectiveness. Source: (Smeur et al., 2016)

trol effectiveness deviation due to inertia changes will be considered. Furthermore, considering the low computational complexity of the LMS method and its high estimation performance makes it a promising application of adaptive INDI.

In 2017, the same research group conducted another study with the Bebop Parrot quadrotor controlled using LMS-based adaptive INDI (Smeur et al., 2018). In this study it was demonstrated that adaptive INDI control could also improve on the performance of standard proportional-integral-derivative (PID) controllers in severe gust load conditions. Furthermore, the adaptive control law was extended to also estimate the thrust control effectiveness. The gust load tests were conducted in a wind-tunnel and in the open air on a windy day. In both cases it was shown that the adaptive INDI controller has a higher control performance than a PID controller.

Furthermore, in the beginning of 2019 a research project on fault tolerant flight of an extended F-16 has been performed (Bhardwaj et al., 2019). In this research three INDI control laws augmented with a different version of predictor based MRAC were investigated. The first one uses the 'standard' form, the second one uses Singular Value Decomposition (SVD) update laws and the third version is based on $\mathcal{L}_1$ piece-wise adaptive augmentation. Using the test cases defined in this study, it was shown that all three adaptive laws were able to stabilize the aircraft and could compensate for the initial model deviation. Furthermore, the adaptive control laws have shown to be able to cope with unmodelled actuator dynamics adequately.

The last known research on adaptive INDI was presented in 2019 as well (Cao et al., 2019). Here, an INDI controller of a Unmanned Aerial Vehicle (UAV) was augmented with e-modified MRAC using an adaptive NN. The NN was trained online and was used to determine an augmentation signal for the INDI control law output. The goal of the control law was to be able to cope with high angle manoeuvres and uncertainties in the control effectiveness. To be able to deal with high angle manoeuvres, the reference model used the quarternion notation instead of the Euler angles to obviate singularities. The experiments performed in this study were simulation based and showed that the adaptive controller was able to follow the reference adequately for angles between $\frac{\pi}{2}$ to π radians.

From this state-of-the-art review on INDI it is clear that there is still a lot to discover with respect to adaptive control. However, the research projects performed show that adaptive INDI is able to achieve high control performance in uncertain systems. Consequently, adaptive INDI is a promising approach for the application in the INDI control law of an F-16 with time-varying dynamics.

3.5.2. Adaptive laws in NDI control systems

The NDI control law design approach already exists since the 1990's. As INDI is closely connected to NDI, adaptive forms based on this design principle will also be considered in this literature study. One of the first researches on adaptive NDI was performed in the time that NDI itself was still novel as well. In this study the NDI flight control law was augmented with a direct adaptive MRAC law based on a linear-in-the-parameters NN (Kim and Calise, 1997). In this research it was shown that indirect adaptive with a linear-in-the-parameters NN could be used to adequately correct for the inversion error. Other examples of studies in which apply linearly parameterized NNs to compensate for the model error are: (Calise et al., 1998; Calise and Rysdyk, 1998; Calise et al., 2001). In Rysdyk and Calise (2005) also a nonlinear NN with a single hidden layer was applied for the direct adaptive NDI control.

Another application of a nonlinear neural network is investigated in (Weerdt et al., 2008). Here, an adaptive nonlinear NN with tangent sigmoidal activation functions is used to compensate for the model error due to fuel sloshing in a satellite. The difference in this adaptive scheme with respect to the ones discussed before it that the NN is adapted based on the error between the prediction of the NN and the system output. Consequently, this is a Self-tuning control law. Furthermore, the estimated sloshing model is used in the system inversion loop which also makes this adaptive control law an indirect adaptive control law. In the results of the research it was shown that the neural network is able to estimate the sloshing behavior. However, when the training data of the NN does not contain much information, it was observed that the control signal contains high frequency oscillations. In this research this problem was solved using a low-pass filter on the control signal, which showed to be effective.

Furthermore, in Lombaerts (2010) research has been performed in the field of fault tolerant control using adaptive NDI. In this research, the NDI control law is made fault tolerant by estimating the aircraft model parameters online and applying these parameters in the control law. The parameter estimation method used here is the Recursive Least Squares algorithm. This adaptive control law was tested using pilot in the loop simulations in the SIMONA Research Simulator at the Faculty of Aerospace Engineering of the Delft University of Technology. It was shown that the adaptive law was able to find the correct model parameters and by using Cooper-Harper evaluations it was shown that the use of the adaptive NDI control law could reduce the workload in case of a failure. Furthermore, it was demonstrated that this adaptive INDI control law could still stabilize the aircraft for a rudder hardover case and for the failure case of Flight 1862.

The research on adaptive NDI has significantly increased during the last decade. Various research projects have been performed of which some applications studies are for UAVs (Geiser et al., 2011; Shastry et al., 2016), VTOL aircraft (Autenrieb et al., 2019) and high-performance aircraft (Rollins et al., 2013; Tol et al., 2016). Overall, it can be noted that adaptive NDI based on MRAC is very popular. This is most likely as the design follows from Lyapunov stability functions which also give some guarantee that the adaptive control law is stable. Though, despite these proofs of stability of MRAC based adaptive INDI control laws, the indirect adaptive NDI control law with RLS parameter estimation as discussed in Lombaerts (2010) is currently still the only adaptive piloted flight simulation. Therefore, this approach has proven to be practical.

3.5.3. Adaptive laws in other model-based control systems

Other model-based nonlinear flight control design methods are Backstepping (BS) and Incremental Backstepping (IBS). The adaptive versions of these methods are often integrated with Lyapunov tuning functions as the derivation of the standard BS or IBS control laws are already based on Lyapunov (Sonneveldt, 2010). These type of adaptive (I)BS control laws are also known as integrated adaptive (I)BS. These type of control laws are already in development since the late 1990's. One example is an adaptive BS control law for a high-performance aircraft is shown in Steinberg and Page

(1998). Here, it was shown in simulations that integrated adaptive BS could cope with modelling errors and system failures. However, it was noted that the control law did not adequately handle the magnitude of the actuator commands. The research project described in Li et al. (2004) is one of the examples of an adaptive BS control law which makes use of an adaptive NN. In this research it was shown that it is possible to develop a semi-global bounded control law using this design approach. Furthermore, in Ju and Tsai (2007) the performance of an adaptive BS flight control law was evaluated using handling quality guidelines. In this paper a MRAC based adaption rule was designed to ensure that the control response would follow the desired dynamics from the handling quality guidelines. It was demonstrated using computer simulations that this adaptive BS flight control law was able to achieve level 1 handling characteristics for the short-period requirement.

In Sonneveldt (2010) and van Gils et al. (2016) adaptive modular BS and IBS control designs are developed using the a new approach called Immersion and Invariance (I&I). The I&I framework defines the parameter estimation law by developing an invariant manifold on which the estimation error is zero. This manifold has a similar goal as the manifold defined in SMC and it made attractive using Lyapunov stability functions (LSF). Furthermore, the parameter estimation error is made stable by adding a stabilizing function in the definition of the manifold. This also results in the I&I framework not being based in certainty equivalence (Astolfi et al., 2007). As the I&I framework also uses an LSF for its control law design, its combination with BS comes naturally. However, this adaptive control design is not integrated as is the case with the standard adaptive BS control law.

Furthermore, in van Oort et al. (2010) an adaptive BS control law based on orthogonal least squares parameter estimation is considered. Here, the parameter estimation is used to update the on-board tensor-product B-spline model for centre of gravity shifts and actuator failure. It was demonstrated in simulations that this adaptive control law was able to give high tracking performance than the non-adaptive variant.

From this concise review on adaptive (I)BS control it could be concluded that also here Lyapunov based adaptive laws are popular. Although, this was expected as the control law design itself is also based in Lyapunov stability. With respect to this study, the modular adaptive BS approaches are most relevant as the integral approaches are specifically designed for BS control. For the modular approaches also methods as RLS parameter estimation and MRAC are used, which indicates the usefulness of these methods. Furthermore, in this literature research a modular framework for adaptive control design was discovered which was not used in the control law designs based in feedback linearization.

3.6. Selected adaptive control approaches

As seen in the previous sections in this chapter there are a vast amount of options to consider for the design of an adaptive controller. However, as it is not possible to consider all options, this section will elaborate on the selection of a concise, but diverse, set of adaptive laws which will be considered for further analysis in this thesis.

The most demanding aspect to consider in the selection is the ability of the algorithm to operate in real-time. This means that it is preferred that the steps/conversions required to obtain an parameter estimate is as low as possible. Consequently, this study will only consider approaches which use the time-domain data to obviate domain conversion steps which require extra computational time. Furthermore, it has been established that the identification algorithms based on combined state and parameter estimation, the One-Step approach, are often not suitable for real-time applications as these require several iterations per time step. On the other hand, the two step method separates the state and parameter estimation and allows for computational efficient linear parameter estimation algorithms. Consequently, to achieve a higher probability for real-time use, the identification algorithms considered in this study will be designed according to the Two-Step method.

Considering the parameter estimation methods, it has been decided to use MRAC , Immersion

and Invariance , Recursive Least Squares and Least Mean Squares. Both MRAC and I&I based adaptive control are chosen as these adaptive laws could be derived using Lyapunov stability functions. Consequently, these adaptive control laws contain a certain proof of stability in their derivation already. The differences between these adaptive control laws is that MRAC uses the error between the system output and a reference model output to drive the adaptive law and I&I adaptive control bases the adaption on only the system output information. Another interesting aspect of I&I is that it does not rely on CE which decreases the need for very accurate parameter estimation (Astolfi et al., 2007). The RLS and LMS parameter estimation routines are chosen as these adaptive laws try to find the correct model parameters by using an adjustable prediction model. As this is a completely different approach than the MRAC and II-AINDI control laws, the RLS and LMS based adaptive laws are deemed well suited for the diversity of the set of adaptive control laws considered in this study. The main difference between the RLS and LMS parameter estimation routines is that the RLS algorithm determines a variable adaption gain based on the certainty of the previous estimations whereas the LMS method has a fixed update gain. Due to this difference both parameter estimation routines have different stability and estimation characteristics which make them both interesting for this research.

4

Aircraft dynamics modelling

As mentioned in the introduction, the CG is difficult to determine accurately without making assumptions on the inertia or using unconventional sensor configurations. To still be able to correct for the changing system dynamics and maintain the control performance, this research will investigate adaptive control laws as a possible solution. To gain understanding on how the system dynamics are affected by the inertia and CG changes, a brief study on rigid body aircraft models which incorporate these factors is treated in this chapter. However, as this research only focuses on rotational control, the analysis performed here will only focus on the rotational equations of motion (EOM).

There are two approaches to model the effects in the EOM. One method is to use a geometrically fixed reference frame with respect to the aircraft. Here, the centre of gravity will not coincide with the origin of the reference frame anymore after it has shifted. This approach will be presented in section 4.1. Section 4.2 treats the second method where the reference frame origin is the CG. Lastly, section 4.3 will set the obtained knowledge into the perspective of INDI based rotational longitudinal flight control.

4.1. Aircraft fixed reference frame

According to an analysis performed in Lombaerts (2010) the moment equations for a shifted centre of gravity with respect to a geometrically fixed reference frame, in this case O, can be written as (4.1). The reference frame in which this derivation has been performed has the same orientation as the body axis reference frame shown in Figure 4.1.

$$\begin{aligned}
L^O &= I_{xx}\dot{p} + \left(I_{zz} - I_{yy}\right)qr + I_{xy}\left(pr - \dot{q}\right) - I_{xz}\left(pq + \dot{r}\right) + I_{yz}\left(r^2 - q^2\right) + mA_z^{cg}\Delta y - mA_y^{cg}\Delta z \\
M^O &= I_{yy}\dot{q} + \left(I_{xx} - I_{zz}\right)pr - I_{xy}\left(\dot{p} + qr\right) + I_{xz}\left(p^2 - r^2\right) + I_{yz}\left(pq - \dot{r}\right) - mA_z^{cg}\Delta x + mA_x^{cg}\Delta z \\
N^O &= I_{zz}\dot{r} + \left(I_{yy} - I_{xx}\right)pq - I_{xy}\left(q^2 - p^2\right) + I_{xz}\left(qr - \dot{p}\right) - I_{yz}\left(\dot{q} + pr\right) + mA_{y_{cg}}\Delta x - mA_{x_{cg}}\Delta y
\end{aligned} \tag{4.1}$$

Here, L^O, M^O and N^O are the aerodynamic moments around the X, Y and Z axis of reference frame O, and I_{xx}, I_{yy}, I_{zz}, I_{xy}, I_{xz} and I_{yz} are mass moment of inertia terms around the corresponding principle axis. Furthermore, p, q and r are the roll, pitch and yaw rate, respectively, and $\dot{p}$, $\dot{q}$ and $\dot{r}$ are their time derivatives. Then, Δx, Δy and Δz are the distances of the CG position with respect to the origin of O. A CG shift in the direction of the body axes is considered positive. Moreover, m is the aircraft mass, and A_x^{cg}, A_y^{cg} and A_z^{cg} are the specific forces at the CG with respect to the body reference frame. In these equations no assumptions are made about the symmetry of the aircraft geometry. Furthermore, no changes in mass and inertia are assumed even though the CG has shifted. To include the mass and inertia changes the mass and inertia terms, m and I can be

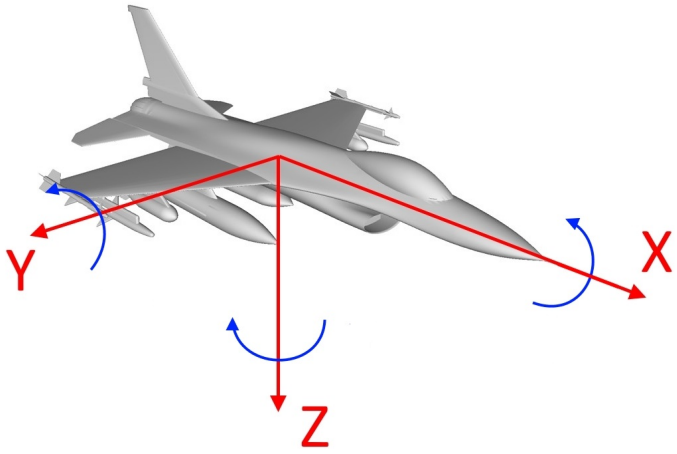

Figure 4.1: Body axis reference frame [1]

modelled as $m+\Delta m$ and $I+\Delta I$, respectively (Lombaerts, 2010). However, to limit the expansion of the derivation, the Δ-terms will not be included.

In this research the aircraft is assumed to be symmetric over the XZ plane. Furthermore, as discussed in the introduction, only the CG position change in the longitudinal direction will be considered. Therefore the inertia terms I_{xy} and I_{yz}, and the CG shift terms Δy and Δz will be neglected. This reduces (4.1) to the following set of equations:

$$\begin{aligned} L^O &= I_{xx}\dot{p} + \left(I_{zz} - I_{yy}\right) qr - I_{xz}\left(pq + \dot{r}\right) \\ M^O &= I_{yy}\dot{q} + \left(I_{xx} - I_{zz}\right) pr + I_{xz}\left(p^2 - r^2\right) - mA_z^{cg}\Delta x \\ N^O &= I_{zz}\dot{r} + \left(I_{yy} - I_{xx}\right) pq + I_{xz}\left(qr - \dot{p}\right) + mA_y^{cg}\Delta x \end{aligned} \tag{4.2}$$

Rewriting the equations of (4.2) to obtain the explicit equations for the rotational acceleration $\dot{p}$, $\dot{q}$ and $\dot{r}$ gives the following result:

$$\begin{aligned} \dot{p} &= \frac{1}{I_{xx}I_{zz} - I_{xz}^2}\Big[\left(I_{yy}I_{zz} - I_{zz}^2 - I_{xz}^2\right) qr + I_{xz}\left(I_{xx} - I_{yy} + I_{zz}\right) pq + I_{zz}L^O + I_{xz}N^O + \\ &\qquad - I_{xz}mA_y^{cg}\Delta x\Big] \\ \dot{q} &= \frac{1}{I_{yy}}\Big[\left(I_{zz} - I_{xx}\right) pr - I_{xz}p^2 + I_{xz}r^2 + M^O + mA_z^{cg}\Delta x\Big] \\ \dot{r} &= \frac{1}{I_{xx}I_{zz} - I_{xz}^2}\Big[I_{xz}\left(I_{yy} - I_{xx} - I_{zz}\right) qr + \left(I_{xx}^2 - I_{xx}I_{yy} + I_{xz}^2\right) pq + I_{xz}L^O + I_{xx}N^O + \\ &\qquad - I_{xx}mA_y^{cg}\Delta x\Big] \end{aligned} \tag{4.3}$$

This result shows that, a the proper method to predict the correct angular acceleration is to correct the model by a linear acceleration term, mA^{cg}, multiplied by the CG shift, Δx. However, it should be noted that the acceleration observed in the reference frame origin is also affected by the CG shift as shown in eq. (4.4) (Lombaerts, 2010).

[1] Kraljic, A., *Quadcopter Project.* Digital image. Github. GitHub Inc. 2017, 13-05-2020

$$\begin{aligned} A_y^O &= A_y^{cg} - \left(\dot{r} + pq\right)\Delta x \\ A_z^O &= A_z^{cg} - \left(pr - \dot{q}\right)\Delta x \end{aligned} \tag{4.4}$$

Here, A_y^O and A_z^O are the observed specific forces in the y and z direction in the origin of reference frame O, respectively. Substituting these equations in (4.3), it can be found that the change in dynamics is quadratically dependent on the CG shift.

4.2. Centre of gravity fixed reference frame

The other modelling approach sets the CG as the origin of the reference frame. Consequently, the terms related to $\Delta x, \Delta y$ and Δz remain zero in equation 4.1 and the equations can be written as in (4.5).

$$\begin{aligned} L^{cg} &= I_{xx}\dot{p} + \left(I_{zz} - I_{yy}\right)qr + I_{xy}\left(pr - \dot{q}\right) - I_{xz}\left(pq + \dot{r}\right) + I_{yz}\left(r^2 - q^2\right) \\ M^{cg} &= I_{yy}\dot{q} + \left(I_{xx} - I_{zz}\right)pr - I_{xy}\left(\dot{p} + qr\right) + I_{xz}\left(p^2 - r^2\right) + I_{yz}\left(pq - \dot{r}\right) \\ N^{cg} &= I_{zz}\dot{r} + \left(I_{yy} - I_{xx}\right)pq - I_{xy}\left(q^2 - p^2\right) + I_{xz}\left(qr - \dot{p}\right) - I_{yz}\left(\dot{q} + pr\right) \end{aligned} \tag{4.5}$$

In this set of equations the moments L, M and N are always defined relative to the CG. This means that it is not required to add the bias terms containing the specific forces acting on the CG to correct for the shift. However, the original aerodynamic model is defined with respect to another point than the shifted CG. Therefore, the aerodynamic moment terms dependent on the CG will have to be corrected. This can be achieved by writing the aerodynamic moments as follows:

$$\begin{aligned} L^{cg} &= L_0 - Z_w\left(y_{cg} - y_w\right) + Y_{fus}\left(z_{cg} - z_{fus}\right) + Y_t\left(z_{cg} - z_t\right) - Z_t\left(y_{cg} - y_t\right) \\ M^{cg} &= M_0 + Z_w\left(x_{cg} - x_w\right) - X_w\left(z_{cg} - z_w\right) - X_{fus}\left(z_{cg} - z_{fus}\right) + Z_t\left(x_{cg} - x_t\right) - X_t\left(z_{cg} - z_t\right) \\ N^{cg} &= N_0 + X_w\left(y_{cg} - y_w\right) + X_{fus}\left(y_{cg} - y_{fus}\right) - Y_{fus}\left(x_{cg} - x_{fus}\right) + X_t\left(y_{cg} - y_t\right) - Y_t\left(x_{cg} - x_t\right) \end{aligned} \tag{4.6}$$

Here, the subscript 0 indicates the pure moment due to the airframe geometry. Furthermore, w, t and *fus* refer to the wing, tail and fuselage, respectively. The reference frame used for this derivation has the same orientation as the body reference frame shown in Figure 4.1. It is assumed that the main lift forces are generated by the wings and vertical tail only. Furthermore, it is assumed that the forces in the Y direction of the wings is negligible. To include the CG shift in these equations, the terms x_{cg}, y_{cg} and z_{cg} will be rewritten in terms of a nominal CG position and a deviation, Δ. Only considering the longitudinal CG shift and defining the aerodynamic model at the nominal CG as L_{nom}, M_{nom} and N_{nom}, (4.6) can be written as follows:

$$\begin{aligned} L^{cg}\left(\Delta x\right) &= L_{nom} \\ M^{cg}\left(\Delta x\right) &= M_{nom} + Z_w\Delta x + Z_t\Delta x = M_{nom} + Z\Delta x \\ N^{cg}\left(\Delta x\right) &= N_{nom} - Y_{fus}\Delta x - Y_t\Delta x = N_{nom} - Y\Delta x \end{aligned} \tag{4.7}$$

From these equations it can be seen that the aerodynamic moment changes by the total aerodynamic force multiplied by the shift in CG. As in this research only longitudinal CG shifts are considered, only the forces Y and Z remain. Using this result in the set of equations described in (4.5) and

rewriting these equations in terms of $\dot{p}$, $\dot{q}$ and $\dot{r}$, gives the following set of equations:

$$\begin{aligned}
\dot{p} = &\frac{1}{I_{xx}I_{zz} - I_{xz}^2}\Bigg[\left(I_{yy}I_{zz} - I_{zz}^2 - I_{xz}^2\right)qr + I_{xz}\left(I_{xx} - I_{yy} + I_{zz}\right)pq + I_{zz}L_{nom} + I_{xz}N_{nom} + \\
&\qquad - I_{xz}\Delta xY\Bigg] \\
\dot{q} = &\qquad \frac{1}{I_{yy}}\Big[\left(I_{zz} - I_{xx}\right)pr - I_{xz}p^2 + I_{xz}r^2 + M_{nom} + \Delta xZ\Big] \\
\dot{r} = &\frac{1}{I_{xx}I_{zz} - I_{xz}^2}\Bigg[I_{xz}\left(I_{yy} - I_{xx} - I_{zz}\right)qr + \left(I_{xx}^2 - I_{xx}I_{yy} + I_{xz}^2\right)pq + I_{xz}L_{nom} + I_{xx}N_{nom} + \\
&\qquad - I_{xx}\Delta xY\Bigg]
\end{aligned} \tag{4.8}$$

4.3. Considering INDI-based pitch rate control

The knowledge obtained on the change in system dynamics due to CG shifts and inertia changes will be considered in the perspective of longitudinal INDI control in this section. This analysis starts by taking a first order Taylor expansion with respect to the previous time step of Eq. (4.3) and (4.8), and assuming that the difference in state between the previous and current time-step can be neglected. Furthermore, for completeness, in this formulation the change in mass, Δm, and the change in inertia, ΔI, are included. This will result in the following descriptions:

$$\dot{q} = \dot{q}_0 + \frac{\frac{\partial M^O}{\partial \delta_e} + \Delta x(m+\Delta m)\frac{\partial A_z^O}{\partial \delta_e}}{I_{yy} + \Delta I_{yy} + (m+\Delta m)(\Delta x)^2}\Delta\delta_e = \dot{q}_0 + \frac{M_{\delta_e}^O + \Delta x(m+\Delta m)A_{z_{\delta_e}}^O}{I_{yy} + \Delta I_{yy} + (m+\Delta m)(\Delta x)^2}\Delta\delta_e \tag{4.9}$$

$$\dot{q} = \dot{q}_0 + \frac{\frac{\partial M_{nom}}{\partial \delta_e} + \Delta x\frac{\partial Z}{\partial \delta_e}}{I_{yy} + \Delta I_{yy}}\Delta\delta_e = \dot{q}_0 + \frac{M_{nom_{\delta_e}} + \Delta xZ_{\delta_e}}{I_{yy} + \Delta I_{yy}}\Delta\delta_e \tag{4.10}$$

It can be seen that the obtained results, using the two reference frames, contain different factors. Though, the overall structure is equivalent. Both $A_{z_{\delta_e}}^O$ and $M_{nom_{\delta_e}}$ are negative, so a positive (forward) CG shift results in a more negative control effectiveness. This is expected as the arm between the centre of lift of the tail and the CG is increased. Furthermore, the difference in denominator between Eq. (4.9) and (4.10) is due to the fact that the specific force is considered with respect to reference frame O. Moreover, a decrease in inertia increases the control effectiveness as well. This effect is also expected as a decreased mass moment of inertia requires a lower moment to obtain a certain angular acceleration. Solving these equations for $\Delta\delta_e$ and setting $\dot{q}$ to ν, the following INDI control law descriptions can be found:

$$\Delta u = \left[\frac{M_{\delta_e}^O + \Delta x(m+\Delta m)A_{z_{\delta_e}}^O}{I_{yy} + \Delta I_{yy} + (m+\Delta m)(\Delta x)^2}\right]^{-1}\left(\nu - \dot{q}_0\right) \tag{4.11}$$

$$\Delta u = \left[\frac{M_{\delta_{e,nom}} + \Delta xZ_{\delta_e}}{I_{yy} + \Delta I_{yy}}\right]^{-1}\left(\nu - \dot{q}_0\right) \tag{4.12}$$

From the results found in this section it can be seen that the control effectiveness is indeed affected by CG shifts and inertia changes. Furthermore, modelling errors in M_{δ_e} also result in incorrect determinations of the elevator deflection increment. Moreover, it is clear that the changes in control effectiveness due to CG shifts and inertia changes cannot be decomposed into separate

terms. Consequently, nonlinear identification techniques are required to estimate the effect of each separate effect. However, as discussed in section 3.6, only linear identification methods will be used to promote the possibility for real-time operation.

The goal of the adaptive control law is to obtain a more accurate estimation of the control effectiveness to maintain constant handling qualities. Therefore, it is not required to estimate the individual influence of CG shifts and inertia changes on the control effectiveness. Consequently, it is possible to lump all causes for model deviation into one uncertain term. This approach yields a single uncertain term which could potentially be identified using the selected parameter estimation methods from the previous chapter. Therefore, in the remainder of this research, the uncertainty will be lumped together into one uncertain term. Furthermore, the nominal on-board model for the control effectiveness will be given the symbol G.

5

Evaluation metrics

To be able to compare the different adaptive control designs it is required to have a suitable set of metrics. The performance differences could be assessed by comparing, for example, the stability, robustness or disturbance rejection capabilities of each controller design. For linear systems these characteristics can be found from eigenvalue analysis or analysing the sensitivity function. However, to formally asses the stability, robustness and disturbance rejection aspects of nonlinear systems, it is required to use nonlinear stability theory as described in Slotine and Li (1991) and Wang et al. (2019a).

Using these theories to analytically proof stability, robustness and disturbance rejection capabilities would be the best approach, from a scientific point of view. However, considering that a formal systematic stability proof of adaptive controllers is not yet fully developed (Nguyen, 2018) and this study focuses on the application of adaptive nonlinear control, an analytical proof will not be covered. Consequently, this chapter will focus on metrics which could be used to evaluate and compare adaptive controllers.

The metrics involved for the adaptive control law assessment will be focused on three different aspects of the adaptive controller. First of all, the focus will be on the tracking performance and control activity. These metrics are discussed in section 5.1. Furthermore, there will also be metrics which allow for the evaluation of the parameter estimation in the adaptive law itself. The metrics used for this purpose are treated in section 5.2. Then, as the adaptive control laws should be able to run in real-time, the computational complexity is also an important aspect. Especially when it is preferred to estimate more model parameters. Therefore, section 5.3 elaborates on how the computational complexity could be analyzed and how this will be done in this study. Lastly, this chapter will dive in the control law evaluation using handling quality guidelines.

5.1. Control performance

Within the field of the assessment of nonlinear control laws there is not yet a consensus on which performance metrics are the most appropriate (Stepanyan et al., 2009). Consequently, this section will show metrics which are currently used for the control performance evaluation of nonlinear control.

A common approach is to compare the response of a nonlinear controller to the output of a reference model which receives the same reference signal as input. The error observed between the reference model and actual system could then be analysed using $\mathcal{L}$-norm metrics (Heise et al., 2013; Bhardwaj et al., 2019; Stepanyan et al., 2009). The most commonly used versions are the $\mathcal{L}_\infty$ and $\mathcal{L}_2$-norm. These norms respectively determine the maximum deviation from the reference model and the 'error energy'. The definitions of these norms are shown in Eq. (5.1) and (5.2).

$$\left\|\underline{e}\right\|_{\mathcal{L}_\infty} = \left\|\underline{y}(t) - \underline{y}_m(t)\right\|_{\mathcal{L}_\infty} \triangleq \max_{t\in T}\left\{\left|y_1(t) - y_{m,1}(t)\right|, \ldots, \left|y_n(t) - y_{m,n}(t)\right|\right\} \tag{5.1}$$

$$\left\|\underline{e}\right\|_{\mathcal{L}_2} = \left\|\underline{y}(t) - \underline{y}_m(t)\right\|_{\mathcal{L}_2} \triangleq \sqrt{\int^T \left|y_1(t) - y_{m,1}(t)\right|^2 + \ldots + \left|y_n(t) - y_{m,n}(t)\right|^2 dt} \tag{5.2}$$

Here, e is the difference between the actual system output y and the reference model output y_m, and T is the simulation time. Using the $\mathcal{L}_\infty$-norm it is possible to evaluate the transient performance of the adaptive control law. If the estimated parameter in the adaptive law is incorrect this will probably result in under or overshoot of the ideal response. The $\mathcal{L}_2$-norm can be used to evaluate the presence of oscillations and steady-state errors. Furthermore, to obtain a clear indication of the average error, the Root-Mean-Square (RMS) metric could be used as well (Heise et al., 2013):

$$RMS(e_i) = \sqrt{\frac{1}{T}\int^T \left|e_i\right|^2 dt} = \sqrt{\frac{1}{T}\int^T \left|y_i(t) - y_{m,i}(t)\right|^2 dt} \tag{5.3}$$

In this study the pitch rate, q, is the only system output variable which will be compared to a desired pitch rate. Therefore, the Eq. (5.1) till (5.3) will simplify to the following:

$$\|e\|_{\mathcal{L}_\infty} = \max_{t\in T}\left\{\left|q(t) - q_m(t)\right|\right\} \tag{5.4}$$

$$\|e\|_{\mathcal{L}_2} = \sqrt{\int^T \left|q(t) - q_m(t)\right|^2 dt} \tag{5.5}$$

$$RMS(e) = \sqrt{\frac{1}{T}\int^T \left|q(t) - q_m(t)\right|^2 dt} \tag{5.6}$$

Next to the tracking error performance it is also important to observe the control activity. It could for example be the case that the system output behaves almost exactly as the reference model, but this requires a significant amount of control activity. Although, the tracking performance is desired, it also results in faster degradation of the control actuators, which is undesired again. Furthermore, if the normal condition control activity is already high, it could be possible that the system becomes unstable when disturbances are present. Therefore, in control engineering often a trade-off is made between tracking performance and control activity as well.

To assess the control activity it is also possible to use the $\mathcal{L}_\infty$ and $\mathcal{L}_2$-norm metrics. In this case the actual control input is compared to the reference input which is required to achieve the output of $\underline{y}_m$. Although, these metrics give a good idea of how well it follows the ideal, these metrics might not be the best to analyse oscillations. Furthermore, determining the ideal control input could be a difficult task. Another metric discussed in a recently published article is the cumulative moving standard deviation (CMSD) (Mooij, 2020). This metric determines the standard deviation for a n_s amount of data samples. The definition of the CMSD metric for the control input is given in Eq. (5.7).

$$CMSD(u) = \sum_{j=n_s/2+1}^{N-n_s/2} \sqrt{\frac{1}{n_s-1}\sum_{k=0}^{n_s-1} s_j[k]}, \quad s_j[k] = \left(u[j - n_s/2 + k] - \bar{u}_j\right)^2 \tag{5.7}$$

Here, $s_j[k]$ is the squared deviation from the mean of the set of data samples of sample set j, $\bar{u}_j$. This metric can be used to observe oscillations as this would increase the standard deviation of the small dataset and this results in a quicker growing CMSD. As this is an effective approach to evaluate oscillations in the control activity, this metric will be used to assess the control activity.

5.2. Online estimation performance

Next to the tracking performance and control activity it is also important to evaluate the parameter estimation performance. As the INDI control law is robust to model uncertainties it is able to handle a certain amount of model deviation. However, it is of course desired that the parameter estimation is as close to the actual value as possible and converges without any oscillations. To be able to assess these characteristics it is possible to use similar metrics as described in the previous section. A common metric to evaluate the performance of an estimated model is the RMS estimation error (De Visser, 2011). However, as here the model parameters are estimated over time, it could be the case that there will be some transients. To evaluate the performance during a transient it is possible to use the $\mathcal{L}_\infty$-norm of the estimation error as well. Furthermore, it could be the case that the adaption gain is tuned too aggressive. This could result in drastic corrections in the estimated model parameters which again could lead to overshoot and oscillations. As this is unwanted behaviour, it is also interesting to obtain some knowledge on the oscillatory behaviour of the estimated parameter. In this study this will also be analyzed using the CMSD metric.

To use the $\mathcal{L}_\infty$-norm and RMS metrics for the evaluation of the parameter estimation, it is required to have the actual value of the parameter or model. This value can be taken from the model used in the simulation. In this study the actual value of the control effectiveness, $\dot{q}_{\delta_e} = \frac{\bar{q}S\bar{c}}{I_{yy}} C_{m_{\delta_e}}$, will be extracted for the evaluation using the $\mathcal{L}_\infty$-norm and RMS metrics. Furthermore, the CMSD will be used to evaluate the estimated parameters. Consequently, the following set of metrics will be used to evaluate stability of the parameter estimation performance:

$$\left\| e_G \right\|_{\mathcal{L}_\infty} = \max_{t \in T} \left\{ \left| \hat{G}(t) - G_{act}(t) \right| \right\} \tag{5.8}$$

$$RMS\left(e_G\right) = \sqrt{\frac{1}{T} \int^{T} \left| \hat{G}(t) - G_{act}(t) \right|^2 dt} \tag{5.9}$$

$$CMSD\left(\hat{\theta}_i\right) = \sum_{j=n_s/2+1}^{N-n_s/2} \sqrt{\frac{1}{n_s - 1} \sum_{k=0}^{n_s-1} s_j[k]}, \quad s_j[k] = \left(\hat{\theta}_i[j - n_s/2 + k] - \bar{\hat{\theta}}_{i,j} \right)^2 \tag{5.10}$$

5.3. Computational complexity

The second quantitative evaluation metric form is the analysis of the computational complexity. The study of computational complexity focuses on the increase in computation time when the input of an algorithm increases. This information can be used to evaluate whether an algorithm is able to perform the task on a certain computer or to compare algorithms with each other (Sedgewick and Flajolet, 2013).

There are several methods to perform this analysis. First of all, it is possible to use the actual computational time. In this case the algorithm is run and the time is measured for multiple sizes of the input. Using this approach it is possible to observe how the computational time increases for an increasing input size. The computational time could, for example, increase in a linear, quadratic or cubic way. although, this gives a good indication of how long it takes to process a certain amount of data on that particular computer, it does not say much about how long it will take on another computer. Except that the computation time will increase linearly, quadratically or cubically.

Another approach is to count the elementary operations of an algorithm. Using this approach often the worst case scenario will be analysed. For example, consider a sorting algorithm where the initial sequence is exactly the inverse of the target. In computational complexity analysis the elementary operations can be counted using two methods. The first method is to analyze every part of the algorithm in detail and count every elementary operation made (Sedgewick and Flajolet, 2013). This could for example lead to the conclusion that the amount of elementary operations grow in the fashion of $f(n) = 2n^2 + n + 50$. In the second approach it is already assumed that the input is

large enough that the effect of the lower order terms and scaling factors of $f(n)$ can be neglected. In this case the computational complexity is determined in the big-'O' notation (Sedgewick and Flajolet, 2013). This means that the computational complexity of $f(n)$ grows in the order of $\mathcal{O}\left(n^2\right)$.

Furthermore, counting the elementary operations can be done on different levels. It is possible to perform this low-level and count all the bit, assign, read, write operations which are performed by the computer, or the counting could be done at the level of the mathematics alone. This depends on the level of accuracy that the demanded from the analysis. However, the be able to do this, detailed knowledge about the machine architecture and compilers is required (Sedgewick and Flajolet, 2013). In this study these low level details of the flight control computer (FCC) are not available. Furthermore, it is not possible to test the required computational time on a real FCC. Therefore, the analysis of the computational complexity will be performed on the level of the mathematics used in the algorithm. Besides, in this analysis it is probably too coarse to estimate the computational complexity using the big-$\mathcal{O}$ notation. Consequently, the elementary mathematical operations of each algorithm will be counted. The basic mathematical operations are addition, subtraction, multiplication and division.

5.4. Aircraft handling quality and stability guidelines

Handling quality and stability guidelines are developed to ensure a good integration of the aircraft system with the human pilot. Its origin stems from the beginning of aircraft design (Phillips, 1989). The idea behind the development of aircraft handling quality guidelines is to give the control designer metrics to predict whether the pilot workload is adequate for the developed control system. Complying to these guidelines during the control law design phase increases the possibility that flight can be performed safely and does not require high levels of pilot workload. This section will give a concise review of the field of aircraft handling quality and stability guidelines. However, as only longitudinal control is considered in this study, this section will focus on handling quality and stability guidelines used for longitudinal control. Handling quality and stability guidelines are established for all aircraft classes. These classes are made according to their weight, size and manoeuvrability, and are defined as follows (Cook, 2012):

Class I:	Small, light
Class II:	Medium weight, low to medium manoeuvrability
Class III:	Large, heavy, low to medium manoeuvrability
Class IV:	High manoeuvrability

Furthermore, the desired handling qualities vary during flight due to different flight phases. For this reason, the assessment of the handling qualities is divided into several flight categories. These categories are labeled A, B and C and their definitions are as follows (Cook, 2012):

Category A:	Non-terminal flight phases that require rapid manoeuvring, precision tracking or precise flight path control.
Category B:	Non-terminal flight phases that require gradual manoeuvring, less precise tracking, and accurate flight path control.
Category C:	Terminal flight phases that require gradual manoeuvring and precision flight path control.

The development of handling quality requirements/guidelines is a delicate process in which the pilot opinions are transformed into mathematical quantities. One of the methods to obtain this information is using the Cooper-Harper ratings as shown in Figure 5.1 (Pratt, 2000). Using this form, the pilots provide their opinion about the handling qualities while performing a certain control task as a number between 1 and 10.

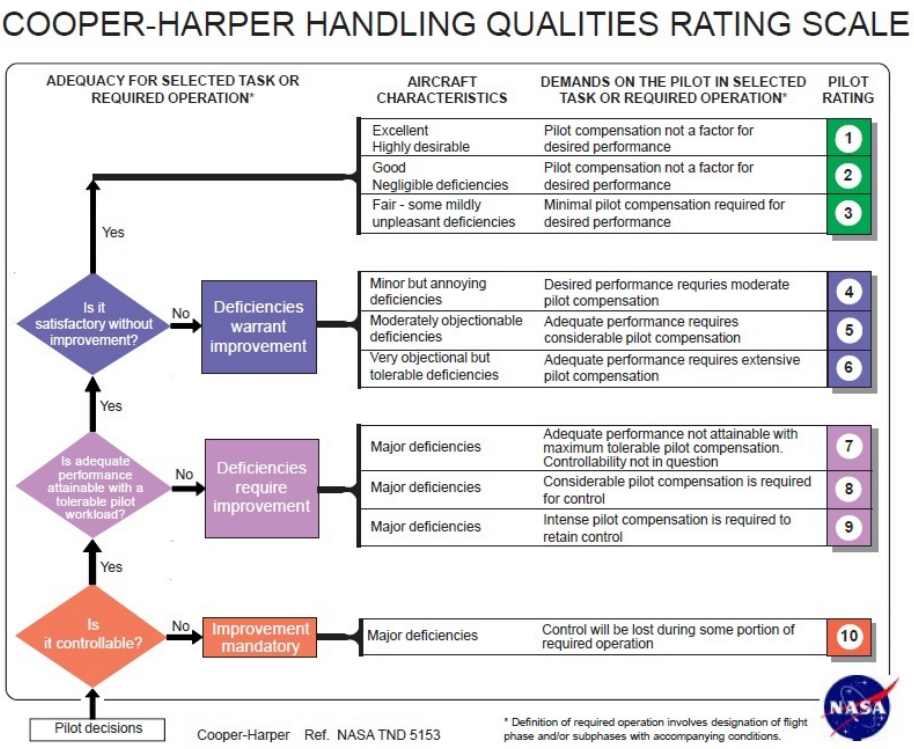

Figure 5.1: Cooper-Harper handling quality rating scale. Source: (Cooper and Harper, 1969)

Next to the Cooper-Harper pilot rating scale three levels of handling quality acceptability have been defined (DoD, 1980, 1997):

Level 1: Flying qualities clearly adequate for the mission flight phase.

Level 2: Flying qualities adequate to accomplish the mission flight phase, but some increase in pilot workload or degradation in mission effectiveness, or both, exists.

Level 3: Flying qualities such that the airplane can be controlled safely but pilot workload is excessive or mission effectiveness is inadequate, or both. Category A flight phases can be terminated safely, and Category B and C flight phases can be completed.

The handling quality level acceptability scale and the Cooper-Harper pilot rating scale have been combined to develop specifications which could be used to analyse the quality of the control system design. These specifications are based on correlations between fundamental control system aspects and Cooper-Harper ratings. The next sections will elaborate on how handling quality and stability guidelines will be applied in this study and describe the most relevant guidelines.

5.4.1. Handling quality and stability guidelines for longitudinal control

This section will discuss the relevant handling quality and stability guidelines which could be used to design and evaluate the INDI-based pitch rate control law used in this study. Guidelines used for this purpose can found in military standards, such as the MIL-STD-1797A (DoD, 1997). These guidelines consider several aspects, such as the control forces applied by the pilot, the feel system, the dynamic response of the controlled aircraft, etc.(DoD, 1997; Mitchell et al., 1994) From these aspects, only the guidelines focusing on the dynamic response of the aircraft will be applied in this thesis. This approach has been chosen as the adaptive control law is still in a conceptual stage and actual interaction with a test pilot is not considered.

The handling quality and stability guidelines mainly focus on the short term behaviour of the aircraft for the pilot input. Reviewing several sources, such as the military standards (DoD, 1997, 1980), best practices (Mitchell et al., 2000) and studies Mitchell et al. (1994); AGARD (1991b); Berger et al. (2012), it was found that the following handling quality and stability guidelines are considered to be important for longitudinal control design:

- Control Anticipation Parameter (CAP) vs. Short period damping
- Equivalent time delay
- Pitch attitude dropback
- Gibson phase rate
- Pitch attitude bandwidth vs. phase delay
- Neal-Smith
- Flight-path angle bandwidth vs. pitch attitude bandwidth

Consequently, this section will continue with briefly covering each specification. Furthermore, note that the phugoid motion will not be considered. This is because pitch rate control naturally suppresses this motion and the short period is considered most important.

CAP vs. short period damping and Equivalent time delay

The CAP vs. short period damping and equivalent time delay guidelines will be treated together as these are both based on a Lower Order Equivalent System (LOES) fit of the more complex and higher order control system. The paradigm of LOES fitting was developed to be able to quickly analyze the short term pitch response characteristics of fly-by-wire (FBW) control systems.(DoD, 1997; Mitchell et al., 1994) The addition of computers, sensors, filters, actuators and other mechanical and digital subsystems in these type of control systems results in a control law with a much higher order response than the aircraft. Before the application of LOES models, the short period frequency and damping of the controlled aircraft were selected from the frequency response by hand. Although this could work, it also resulted in wrongly selected frequencies and damping which resulted in a wrong prediction of these short term handling qualities. The idea behind a LOES fit is to find an equivalent lower order model which closely resembles the high order system within a limited frequency range. An example of a LOES model for the pitch rate response for a longitudinal stick input is shown in Eq. (5.11).(DoD, 1997; Cook, 2012)

$$\frac{q}{\delta_s} = \frac{K_\delta \left(s + \frac{1}{T_{\theta_2}} \right)}{s^2 + 2\zeta_{sp}\omega_{sp}s + \omega_{sp}^2} e^{-\tau_e s} \tag{5.11}$$

Using this model it is possible to determine an equivalent value for the short period frequency, ω_{sp}, the short period damping, ζ_{sp}, the short period zero, $\frac{1}{T_{\theta_2}}$ and the equivalent time delay, τ_e within small frequency range, often chosen between 0.1 and 10 rad/s.(DoD, 1997) Despite this simple concept of making an equivalent fit and using the model parameters in handling quality guidelines, it has been observed that it is not as easy as it sounds.(DoD, 1997; Mitchell et al., 1994) Although a fit is easily obtained, the fit could be deviating significantly form the actual aircraft response and therefore give a bad prediction of the handling qualities based on LOES model coefficients. To confront these problems, studies have been performed on how much the response is allowed to deviate before the pilot will notice. This lead to the definition of the *Maximum unnoticeable added dynamics* or MUAD bounds, see Figure 5.2 and 5.3, and the preferred LOES fitting cost of less than 10 according to the following cost function given in Eq. (DoD, 1997).

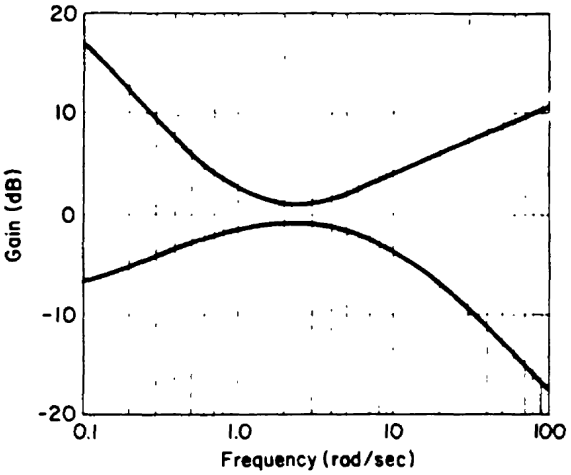

Figure 5.2: MUAD bounds for gain mismatch of LOES fit w.r.t. the full order system.

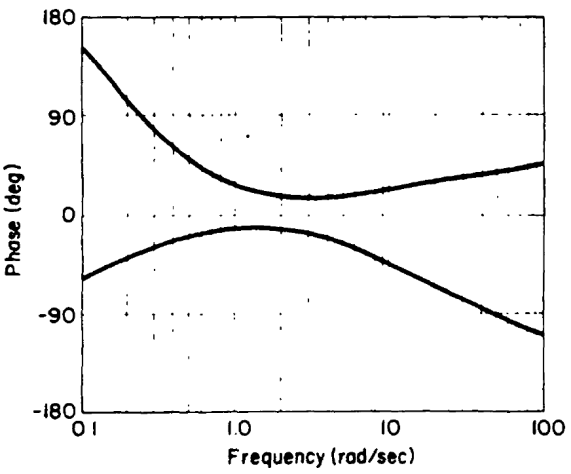

Figure 5.3: MUAD bounds for phase mismatch of LOES fit w.r.t. the full order system.

$$J = \frac{20}{N_\omega} \sum_{k=1}^{N_\omega} \left[\left(\left| H_{HOS}(\omega_k) \right| - \left| H_{LOES}(\omega_k) \right| \right)^2 + 0.01745 \left(\angle H_{HOS}(\omega_k) - \angle H_{LOES}(\omega_k) \right)^2 \right] \tag{5.12}$$

Furthermore, next to this issue there is also an ongoing discussion on the calculation of $\frac{1}{T_{\theta_2}}$. The zero of the LOES model is closely related to the lift curve at the considered flight condition. Consequently, there is a difference in opinion among control system developers and scientists whether this value should be fixed and determined beforehand with the knowledge of the aircraft model or keep it 'free' and use the result from the equivalent fit.(DoD, 2008) Both approaches do give a different prediction of the handling qualities. Though both approaches seem to be of value.(DoD, 2008) This study will not dive deeper in this discussion and will use a 'free' parameter in the future applications, though it is considered important to consider these uncertainties or limitations. However, to assure that an adequate value for $\frac{1}{T_{\theta_2}}$ is obtained, it is recommended to perform a simultaneous LOES fit of the longitudinal stick to load-factor and stick to pitch rate responses (DoD, 1997). Note that for load-factor response fit the load-factor at the instantaneous centre of rotation (ICR) should be used.

Once a LOES fit is obtained, there are two important guidelines which can be assessed. As mentioned before, these are the CAP vs. short period damping and the equivalent time delay criteria. The level 1 until 3 boundaries for τ_e are defined as follows (DoD, 1997):

Level 1:	$\tau_e \geq 0.10$
Level 2:	$\tau_e \geq 0.20$
Level 3:	$\tau_e \geq 0.25$

The definition of CAP is the ratio of the initial pitch acceleration divided by the steady state load factor response as shown in Eq. (5.13). Furthermore, this equation shows how the CAP could be determined from the LOES fit model coefficients and the airspeed, V, of the considered flight condition. The rationale of this parameter is that when the pilot is able to experience the pitch acceleration and load-factor response of the short period motion, he or she receives cues which improve the ability to make small adjustments to the pitch motion.(Cook, 2012) The CAP vs. short period damping criteria has two boundary definitions. One for the CAP and one for ζ_{sp} (DoD, 1997):

Level 1:	$0.28 \leq CAP \leq 3.60$,	$0.35 \geq \zeta_{sp} \geq 1.30$
Level 2:	$0.16 \leq CAP \leq 10.0$,	$0.25 \geq \zeta_{sp} \geq 2.00$
Level 3:	$0.16 \geq CAP \geq 10.0$,	$0.15 \geq \zeta_{sp}$

$$CAP = \frac{\dot{q}(t=0)}{n_z(t=\infty)} \quad \rightarrow \quad CAP = \frac{\omega_{n_{sp}}^2}{n_\alpha} = \frac{\omega_{n_{sp}}^2}{\frac{V}{g}\frac{1}{T_{\theta_2}}} \tag{5.13}$$

Pitch attitude dropback

The pitch attitude dropback criterion is developed by J.C. Gibson for the evaluation of highly augmented flight control systems.AGARD (1982) The definition of attitude dropback is given in Figure 5.4. From these responses the ratio of peak pitch rate over steady-state pitch rate, $\frac{\Delta\theta_{peak}}{q_{ss}}$, and the ratio of pitch attitude dropback over steady-state pitch rate, $\frac{q_{max}}{q_{ss}}$, are extracted and used to predict the handling quality. For high-precision tracking performance, a low pitch rate overshoot and pitch attitude dropback are desired. However, achieving this goal could lead to a small flight path bandwidth (AGARD, 1991b). Furthermore, Figure 5.5 shows a boundary which separates the excessive Pilot Induced Oscillation (PIO) region from the acceptable PIO region for different combinations of pitch rate overshoot and pitch attitude dropback. The definition of a PIO is *the sustained or uncontrollable oscillation resulting from efforts of the pilot to control the aircraft.*(DoD, 1997) These oscillations can differ from small and stable till heavy and unstable oscillations and are therefore potentially very dangerous. With the introduction of highly augmented aircraft PIO has become an even more important part of the control law design (Gibson, 1999).

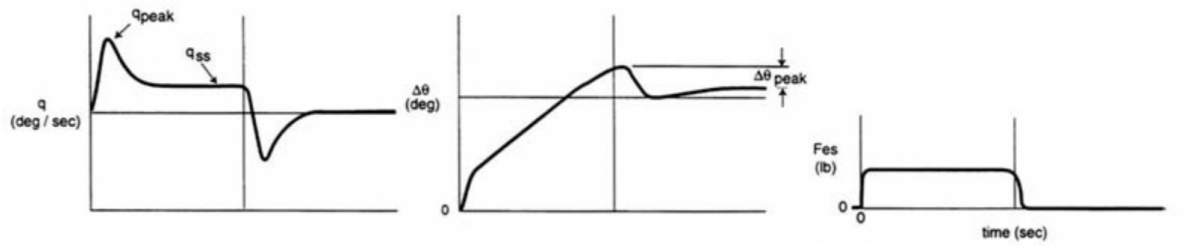

Figure 5.4: Definition of dropback in the attitude dropback criterion. Source: (Mitchell et al., 1994)

The pitch attitude dropback criterion parameters are obtained for a time-domain analysis. During this analysis, the control law is subjected to a block-shaped longitudinal stick input, as shown in the lower curve of Figure 5.4, and the response will be further analyzed to find the values for q_{ss}, q_{peak} and $\Delta\theta_{peak}$. One of the objectives of this criterion is to predict the possibility of PIO. However, as explained in National Research Council (1997), the dropback criterion alone is not a very good predictor as it is not easily affected by high-frequency delays. It is advised to use this criterion in combination with the bandwidth versus phase delay criterion as this combination could result in a good prediction of PIO susceptibility.(National Research Council, 1997; Mitchell et al., 1994) Furthermore, this criterion is only suited for rate command type control laws. This is because flight path or attitude hold types exhibit a zero steady-state pitch rate response to is step input given at the stick.(Mitchell et al., 1994)

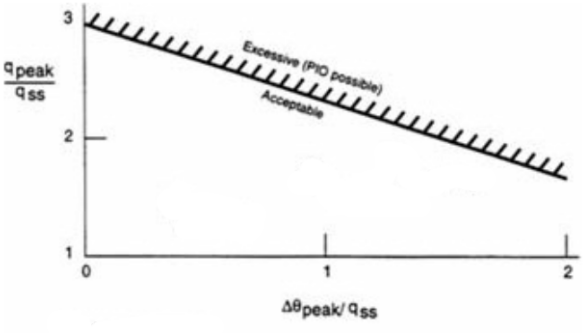

Figure 5.5: Acceptable dropback and pitch rate overshoot boundary. Source: (Mitchell et al., 1994)

Gibson phase rate

As mentioned in the previous section, the Gibson phase rate criterion could be used for the prediction of PIO occurrence (Mitchell et al., 2000). This metric focuses on the frequencies around the -180 degrees phase frequency of the open-loop attitude to pitch input response. For this handling quality criterion the gradient of the phase curve at the -180° phase frequency, $\left(\frac{\partial\phi}{\partial\omega}\right)_{\phi=-180^\circ}$, is determined which is defined as phase rate by J.C. Gibson (AGARD, 1991a). The mathematical definition of the phase rate is as follows (Gibson, 1999):

$$Average\ phase\ rate = \frac{-\left(\phi_{2\omega_{-180}} + 180\right)}{\omega_{-180}} \tag{5.14}$$

Here, $\phi_{2\omega_{-180}}$ is the phase at two times the frequency where the phase is -180 degrees. Note that the frequency is defined in Hz and not rad/s. The boundaries of this criterion are shown in Figure 5.6. Using this definition the phase rate is proportional to the phase delay determined in the pitch attitude bandwidth criterion shown later on.

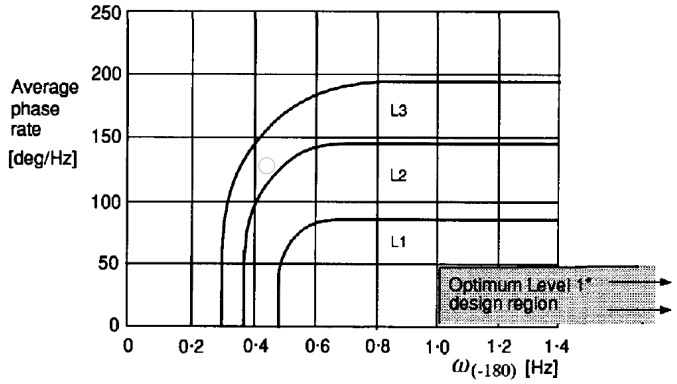

Figure 5.6: Phase rate criterion boundaries for level 1, 2 and 3 handling quality ratings. Source: Gibson (1999)

The rationale behind this handling quality criterion is that closed-loop instabilities appear noticeably more often near the -180 degrees phase frequencies AGARD (1991a). It was found empirically that the gradient of the phase curve at this frequency had a strong correlation with the occurrence of the instabilities (AGARD, 1991b). The explanation for this is when a pilot increases his or her cross-over frequency, a large decrease in phase margin follows due to the large phase rate. Furthermore, the frequency at -180 degrees phase itself is important as well. The frequency has a

minimum as the pilot tends to overdrive the aircraft due to its 'sluggish' behaviour. This also could lead to PIO (Gibson, 1999).

Pitch attitude bandwidth versus phase delay

Another well-known PIO related criterion developed for highly augmented aircraft is the *bandwidth criterion* (DoD, 1997; Mitchell et al., 1994; AGARD, 1991b). This specification indicates the highest frequency at which the control including the pilot can be closed without compromising the stability and gives a boundary on the phase delay to prevent PIO (AGARD, 1991b). The bandwidth is determined for the fully augmented frequency response and is the smallest frequency where the gain margin is at least 6 dB and the phase margin is at least 45°. The complete criterion combines the phase delay and the bandwidth as can be seen in Figure 5.7. The phase delay is determined in a similar fashion as the average phase rate (AGARD, 1991b,a):

$$\tau_p = \frac{\Delta\phi_{2\omega_{180}}}{57.3(2\omega_{180})} \tag{5.15}$$

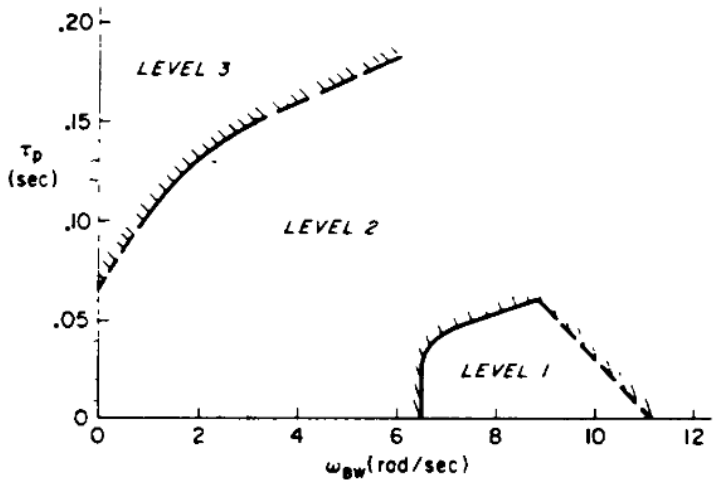

Figure 5.7: The pitch attitude bandwidth criterion bounds. Source: (DoD, 1997)

Here, ω_1 and ϕ_1 are a larger frequency and its corresponding phase close to $\omega_{\phi=-180}$. This frequency is commonly taken as $2\omega_{\phi=-180}$ as well. It it recommended in AGARD (1991b); Mitchell et al. (1994) that this specification is used together with the attitude dropback criterion as a high bandwidth could lead to increased attitude dropback. This should be avoided as high attitude dropback leads to decreased tracking performance and possibly PIO. Furthermore, the benefit of this criterion is its applicability to all control response types (AGARD, 1991b).

Flight-path angle bandwidth versus pitch attitude bandwidth

The idea behind this criterion is that the flight path angle response for a change in pitch attitude matches the pilot's expectations. If the flight path response is slow compared to the pitch attitude response or too fast, adequate control for precise tracking tasks could be degraded. Furthermore, there is an increase possibility for PIO (Mitchell et al., 1994). As the control law considered in this study does not consider the flight path response directly, this criterion might therefore be important to maintain a correct balance between both responses. The boundaries of the criterion are depicted in Figure 5.8.

The flight path angle bandwidth is defined as the frequency where the flight-path angle bandwidth to pilot input response has a phase of -135 degrees (Mitchell et al., 1994). Furthermore, the definition of the pitch attitude bandwidth is the same as explained in the previous section.

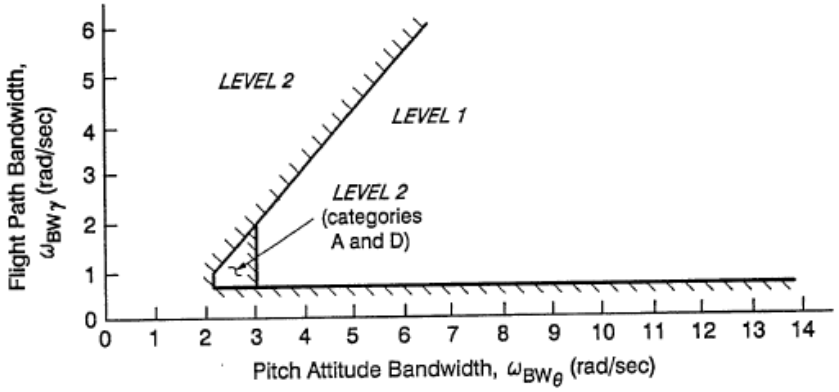

Figure 5.8: Flight-path angle bandwidth versus Pitch attitude bandwidth criteria boundaries. Source: (Mitchell et al., 1994)

Neal-Smith

The Neal-Smith criterion is a PIO prediction criterion which takes into account the required pilot compensation for a desired closed loop pitch angle response for precision attitude tracking tasks (Mitchell et al., 2000). The pilot compensation is determined such that the closed-loop pitch angle response has a bandwidth of 3.5 rad/s (Category A) and a maximum droop of 3 dB (Neal and Smith, 1970; DoD, 1997). This bandwidth is defined as the frequency at which the closed-loop phase, ($\angle(\theta/\theta_c)$), is -90 degrees. Furthermore, the simple pilot model applied for the evaluation of this criterion is shown in Figure 5.9. This figure also shows that the pilot model contains a fixed time delay. In Neal and Smith (1970) this fixed delay is set at 0.3 seconds, however the MIL-STD-1797A uses 0.25 seconds (DoD, 1997). Moreover, the frequency bandwidth for which this criterion is developed is approximately 0.5 - 10 rad/s.

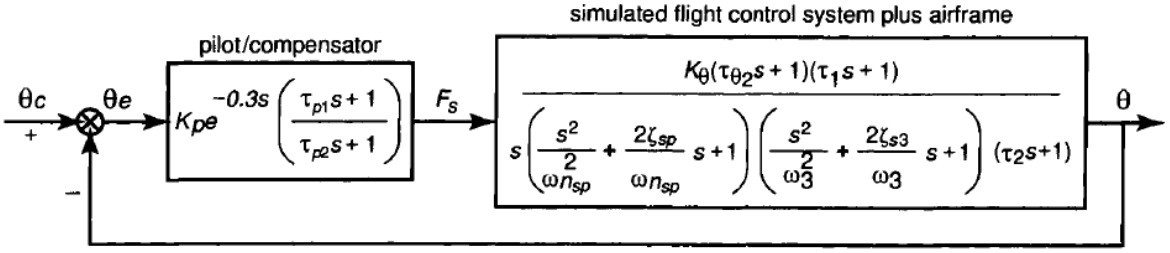

Figure 5.9: Neal-Smith pilot model and aircraft system block diagram. Source: (Cook, 2012)

The approach to find the suited pilot model parameters to obtain a bandwidth of 3.5 rad/s and a maximum droop of 3 dB is thoroughly documented in Neal and Smith (1970) or AGARD (1991b). Furthermore, the boundaries of this criterion, with extra explanation of the combined pilot-aircraft behaviour for certain combinations of pilot compensation and closed-loop peak magnitude, are shown in Figure 5.10. The x-axis indicates the pilot compensation in terms of lead or lag phase at the bandwidth frequency (here 3.5 rad/s).

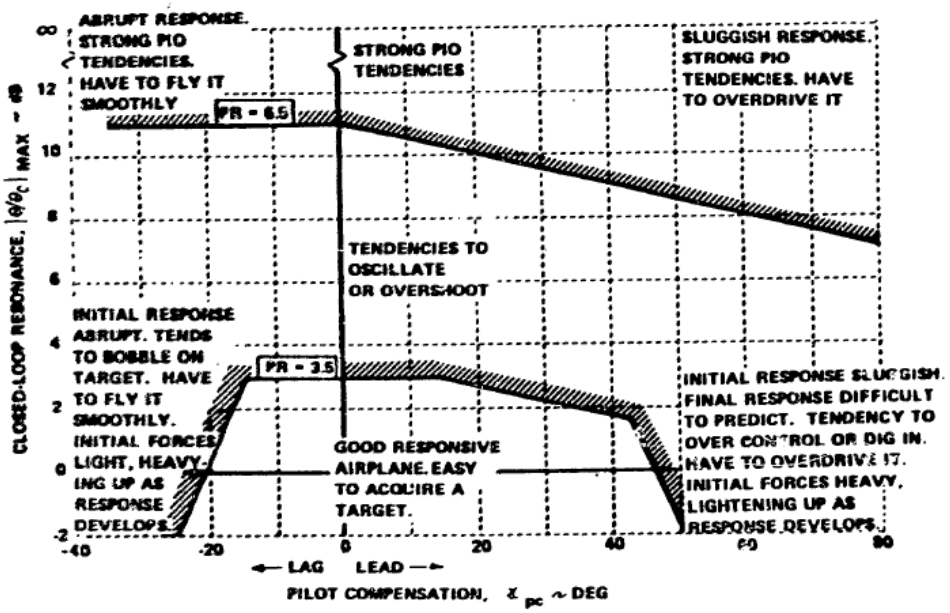

Figure 5.10: Neal-Smith criteria boundaries with explanations. Source: (Neal and Smith, 1970)

Despite the quite accurate prediction of PIO and handling qualities, this specification lacks the description of the sensitivity in changes of the target parameters or pilot model architectures (Mitchell et al., 1994, 2000). However, this could be performed by determining the required pilot compensation and resonance peak magnitude for different values of the maximum droop or bandwidth.

III

Preliminary Experiments

The third part of this thesis contains the preliminary experiments. Here, the non-adaptive and adaptive control laws are designed and analysed. The purpose of this part is to find the most suited longitudinal rotational adaptive INDI control law that is able to cope with system dynamics changes due to CG shift and inertia changes and could correct for aerodynamic modelling errors.

This goal is achieved by first designing the non-adaptive and adaptive control laws in chapter 6. Then, in chapter 7, the non-adaptive control law is tested for an ideal control system, which only contains the control law and the airframe dynamics, and a more realistic control system. This realistic control system includes actuator dynamics, sensor dynamics, filters and computational delay. The knowledge obtained from the analysis in this chapter will be used to answer research question four:

> *How is the non-adaptive INDI-based pitch rate control performance affected when actuator dynamics, sensor dynamics, filters and computational delay are added to the system model?*

Lastly, Chapter 8 will consider the performance analysis of the adaptive INDI control laws and the selection of the most suitable one. The knowledge gained from this analysis it is possible to formulate an answer for the fifth research question:

> *Which adaptive INDI-based pitch rate control law is most suited for coping with aerodynamic model mismatches and system model changes due to centre of gravity shifts and inertia changes?*

This work has been graded previously.

6

Control law design

This chapter will consider the designs of the control laws considered in this study. Furthermore, the theory of the parameter estimation algorithms and the adaptive control law design will be covered. This chapter will start with the design of the non-adaptive INDI control law in section 6.1. Then, the theory and design of the RLS-AINDI, LMS-AINDI, MR-AINDI and II-AIDNI control laws will be covered in the subsequent sections.

6.1. Non-adaptive INDI

This section will treat the baseline INDI rotational control design with the focus on the longitudinal motion. Following the design procedure shown in Chapter 2, first it is necessary to define the control variable. After this it is required to find a relation which is input affine for the control input after linearization. As only rotational rate will be considered for the longitudinal control the control variable is the pitch rate, q. As shown in Chapter 4, the EOM of the longitudinal rotational motion, without shifted CG, can be written as follows:

$$\dot{q} = \frac{1}{I_{yy}} \left[\left(I_{zz} - I_{xx} \right) pr - I_{xz} p^2 + I_{xz} r^2 + M_O \right] \tag{6.1}$$

Linearizing this equation with respect to the previous state, $\underline{x}_0 = [V_0, \alpha_0, \beta_0, p_0, q_0, r_0]$, and control input, $\underline{u}_0 = [\delta_{a,0}, \delta_{e,0}, \delta_{r,0}]$, and already neglecting $\Delta\underline{x}$ using the time-scale separation principle gives the following result:

$$\dot{q} = \dot{q}_0 + \left.\frac{\partial q}{\partial \underline{x}}\right|_{\left(\underline{x}_0, \underline{u}_0\right)} \Delta\underline{x} + \left.\frac{\partial q}{\partial \underline{u}}\right|_{\left(\underline{x}_0, \underline{u}_0\right)} \Delta\underline{u} \approx \dot{q}_0 + \left.\frac{\partial q}{\partial \underline{u}}\right|_{\left(\underline{x}_0, \underline{u}_0\right)} \Delta\underline{u} \tag{6.2}$$

Considering Eq. (6.1), the derivative of q with respect to $\underline{u}$ is basically the same as the derivative of the aerodynamic moment, M_O, with respect to $\underline{u}$ divided by the inertia term, I_{yy}. Using this, the derivative term can be written as follows:

$$\left.\frac{\partial q}{\partial \underline{u}}\right|_{\left(\underline{x}_0, \underline{u}_0\right)} = \frac{1}{I_{yy}} \left.\frac{\partial M_O}{\partial \underline{u}}\right|_{\left(\underline{x}_0, \underline{u}_0\right)} = \frac{1}{I_{yy}} \left[\left.\frac{\partial M_O}{\partial \delta_a}\right|_{\left(\underline{x}_0, \underline{u}_0\right)} \quad \left.\frac{\partial M_O}{\partial \delta_e}\right|_{\left(\underline{x}_0, \underline{u}_0\right)} \quad \left.\frac{\partial M_O}{\partial \delta_r}\right|_{\left(\underline{x}_0, \underline{u}_0\right)} \right] \tag{6.3}$$

Furthermore, taking that the longitudinal motion is only excited by the elevator and normalizing the aerodynamic moment, Eq. (6.2) can be written as the last part of Eq. (6.4).

$$\dot{q} \approx \dot{q}_0 + \frac{1}{I_{yy}} \left.\frac{\partial M_O}{\partial \delta_e}\right|_{\left(\underline{x}_0, \underline{u}_0\right)} \Delta\delta_e = \dot{q}_0 + \frac{\bar{q}_0 S \bar{c}}{I_{yy}} \left.\frac{\partial C_{m_O}}{\partial \delta_e}\right|_{\left(\underline{x}_0, \underline{u}_0\right)} \Delta\delta_e = \dot{q}_0 + \frac{\bar{q}_0 S \bar{c}}{I_{yy}} C_{m_{\delta_e}} \left(\underline{x}_0, \underline{u}_0\right) \Delta\delta_e \tag{6.4}$$

Where, $\bar{q}$ is the dynamics pressure, S is the reference surface area and $\bar{c}$ is the mean aerodynamic chord (MAC). Using this approach it is possible to use the dimensionless aerodynamic moment model and $\bar{q}$ can be obtained from sensor measurements. Then, to obtain the incremental control law, $\dot{q}$ is set to the desired pitch acceleration, ν, and Eq. (6.4) is inverted to obtain an expression for $\Delta\delta_e$ as shown in Eq. (6.5).

$$\Delta\delta_e = \left[\frac{\bar{q}_0 S\bar{c}}{I_{yy}} C_{m_{\delta_e}}\left(\underline{x}_0, \underline{u}_0\right)\right]^{-1}\left(\dot{q}_{des} - \dot{q}_0\right) = G^{-1}\left(\underline{x}_0, \underline{u}_0\right)\left(\nu - \dot{q}_0\right) \tag{6.5}$$

To obtain the value of the full elevator deflection the elevator deflection of the previous time-step, $\delta_{e,0}$, is added to the incremental deflection:

$$\delta_e = \delta_{e,0} + \Delta\delta_e \tag{6.6}$$

The remaining part of the controller design is to find an expression to determine the virtual control input. As shown in Chapter 2 the virtual control can be determined using a linear control law. To keep the performance analysis of the control law as clear as possible, this virtual control law will be designed as a simple PI controller. It has been found that using a proportional-integral (PI) control design increases the controller robustness against actuator measurement bias (van 't Veld, 2016). Therefore, the integrator action will already be implemented in this phase of the control design. This will result in the following virtual control law:

$$\nu = K_P\left(q_r - q_0\right) + K_I\int\left(q_r - q_0\right)dt \tag{6.7}$$

Assuming that the inversion loop is perfect and it can be modelled as $\frac{1}{s}$, the actual pitch rate will follow the reference pitch rate according to this transfer function:

$$\frac{q}{q_r} = \frac{K_P s + K_I}{s^2 + K_P s + K_I} \tag{6.8}$$

6.2. Recursive least squares adaptive INDI

The RLS parameter estimation algorithm attempts, just as the standard Least Squares (LS) method, to optimize the cost function of Eq. (6.9). However, unlike the standard LS algorithm the RLS algorithm is able to do this while recursively progressing through the data. As shown in Lombaerts (2010) it is therefore applicable for on-line system identification and consequently for adaptive flight control.

$$J\left(\underline{x}, \underline{z}, \underline{\hat{\theta}}\right) = \underline{\epsilon}^T\underline{\epsilon} = \left(\underline{z} - A\left(\underline{x}\right)\underline{\hat{\theta}}\right)^T\left(\underline{z} - A\left(\underline{x}\right)\underline{\hat{\theta}}\right) \tag{6.9}$$

Here, ϵ is the sum of the errors between the measurements, $\underline{z}$, and the output of the prediction model, $A\underline{\hat{\theta}}$. The prediction model contains the estimated model parameters $\hat{\theta}$ and the regression matrix Φ. The regression matrix is constructed from basis functions, ϕ_i of the prediction model. This looks as follows:

$$A\left(\underline{x}\right) = \begin{bmatrix} \phi_1\left(\underline{x}_1\right) & \phi_2\left(\underline{x}_1\right) & \cdots & \phi_n\left(\underline{x}_1\right) \\ \phi_1\left(\underline{x}_2\right) & \phi_2\left(\underline{x}_2\right) & \cdots & \phi_n\left(\underline{x}_2\right) \\ \vdots & \vdots & \ddots & \vdots \\ \phi_1\left(\underline{x}_k\right) & \phi_2\left(\underline{x}_k\right) & \cdots & \phi_n\left(\underline{x}_k\right) \end{bmatrix}$$

Here $\underline{x}_k$ is the regression model input vector at time-step k. Furthermore, from the structure of Φ it is clear that the prediction model should have a LP structure. The basis functions are not restricted to be linear functions. This means that, as long as the models are LP, the LS parameter estimation

method is not restricted to linear models. To achieve recursive parameter estimation using the LS method, the cost function of Eq. (6.9) has to be rewritten in terms of the estimated model from the old data and the estimated model using the new data. This leads to the cost function of Eq. (6.10).

$$J\left(\underline{x}_{k+1},\underline{\hat{\theta}}_{k+1}\right)=\left(\underline{z}_k-\Phi_k\underline{\hat{\theta}}_{k+1}\right)^T\left(\underline{z}_k-\Phi_k\underline{\hat{\theta}}_{k+1}\right)+\left(z_{k+1}-\underline{\phi}_{k+1}^T\underline{\hat{\theta}}_{k+1}\right)^T\left(z_{k+1}-\underline{\phi}_{k+1}^T\underline{\hat{\theta}}_{k+1}\right) \tag{6.10}$$

Where, ϕ_{k+1}^T is essentially a new row of the matrix A. However, the algorithm that is able to optimize this cost function is only valid for the estimation of time-invariant model parameters. To be able to estimate the parameters of a model for a time-varying system it is required to reduce the importance, or weight, of older data. This is possible by multiplying the older data by a weight smaller than 1 at each time step. Using this approach, the cost function of Eq. (6.10) should be written as follows:

$$J\left(\underline{x}_{k+1},\underline{\hat{\theta}}_{k+1}\right)=\sum_{i=0}^{k}\left(z_i-\underline{\phi}_i^T\underline{\hat{\theta}}_k\right)^T\lambda^{k+1-i}\left(z_i-\underline{\phi}_i^T\underline{\hat{\theta}}_k\right)+\left(z_{k+1}-\underline{\phi}_{k+1}^T\underline{\hat{\theta}}_{k+1}\right)^T\left(z_{k+1}-\underline{\phi}_{k+1}^T\underline{\hat{\theta}}_{k+1}\right) \tag{6.11}$$

Here, λ is an exponential factor which decreases the weight of older data in the parameter estimation. It essentially results in the "forgetting" the older data. Consequently, this parameter is often called the *forgetting factor* in literature. The value of the forgetting factor can be chosen between 0 and 1, where 1 indicates that all data should be treated equally and 0 means that all previous data should not be used anymore. The recursive algorithm which could optimize the cost function of Eq. (6.11) is the following:

$$\begin{aligned}K_{k+1}&=P_k\underline{\phi}_{k+1}\left(\lambda+\underline{\phi}_{k+1}^TP_k\underline{\phi}_{k+1}\right)^{-1}\\ \hat{\theta}_{k+1}&=\hat{\theta}_k+K_{k+1}\left(z_{k+1}-\underline{\phi}_{k+1}^T\hat{\theta}_k\right)\\ P_{k+1}&=\frac{1}{\lambda}\left(I-K_{k+1}\underline{\phi}_{k+1}\right)P_k\end{aligned} \tag{6.12}$$

For a complete derivation of this algorithm the reader is referred to Hayes (1996). In the algorithm of (6.12) P is the inverse of the autocorrelation matrix. For the initialization of the algorithm both an initial guess of the model parameter(s) and the matrix P (P_0) should be given. P_0 is often set as δI where δ is a small value when $\hat{\theta}_0$ is accurate and large when $\hat{\theta}_0$ is uncertain. A large value for P_0 results in fast initial adaption capabilities. These adaptive capabilities will reduce over time as P will converge to a value close to zero as the model will becomes more certain. To increase the adaptive abilities during the complete operation the value of λ could be reduced. A lower value for λ decreases the effective length of the dataset on which the regression model is fit. Consequently, the parameter estimation is more capable of following the changes in the system. Though, choosing a too small value will result in highly oscillatory estimations. Therefore, λ should be selected carefully. Common values for the forgetting factor are between 0.98 and 1.

6.2.1. RLS-AINDI control law design

To be able to identify the control effectiveness using the RLS estimation algorithm a LP prediction model should be formulated where the control effectiveness is (one of) the model parameters. Fortunately, as was established in section 4.3, this is possible by lumping all causes for uncertainty together in one uncertain parameter. Using this approach the following prediction model could be set up:

$$\dot{q}=\dot{q}_0+\tilde{G}\left(\underline{x}_0,\underline{u}_0\right)\Delta\delta_e \tag{6.13}$$

Here, $\tilde{G}\left(\underline{x}_0, \underline{u}_0\right)$ is the uncertain parameter. This prediction model is usable provided that pitch acceleration feedback should be available. However, as the INDI control law itself cannot operate without pitch acceleration feedback, this problem is automatically solved. Furthermore, there are two ways to handle to identification problem. Firstly, it is possible to fully estimate the value of $\tilde{G}\left(\underline{x}_0, \underline{u}_0\right)$. This results in estimating a physical parameter which makes the estimation more suitable for validation. However, this approach does not use of a prior known model for the control effectiveness, so the estimation is fully dependent on the acquired data. The second method is to define a correction term which scales of the on-board (nonlinear) control effectiveness model, $G\left(\underline{x}_0, \underline{u}_0\right)$, based in the observed data. This does result in the estimation of a non-physical parameter which decreases its suitability for validation. Though, it does allow for the use of the (nonlinear) on-board model of the control effectiveness in the estimation process. Furthermore, in case the estimation procedure malfunctions, it is still possible to use the on-board model. Because of this inherent safety feature, the second method for the estimation parameter formulation will be adopted. This gives the following prediction model description:

$$\dot{q} = \dot{q}_0 + c \cdot G\left(\underline{x}_0, \underline{u}_0\right) \Delta\delta_e \tag{6.14}$$

Where, $G\left(\underline{x}_0, \underline{u}_0\right)$ is the known model of the control effectiveness and c is the correction factor which will be estimated. Furthermore, moving $\dot{q}_0$ to the left side of the equality sign it is possible to formulate a prediction model which determine the increment of the pitch acceleration between time-steps:

$$\dot{q} - \dot{q}_0 = \Delta\dot{q} = c \cdot G\left(\underline{x}_0, \underline{u}_0\right) \Delta\delta_e \tag{6.15}$$

However, using this equation it is required to know the pitch acceleration and elevator deflection at the current time-step. As these are not measured yet, these values are not available. Therefore, the information of one time-step earlier will be used:

$$\Delta\dot{q}_0 = \dot{q}_0 - \dot{q}_{-1} = c \cdot G\left(\underline{x}_{-1}, \underline{u}_{-1}\right) \Delta\delta_{e,0} \tag{6.16}$$

Using this approach it is assumed that the value of c at the current time-step does not differ too much from the one of the previous time-step. To use this model in the RLS parameter estimation algorithm, it should be decomposed in a parameter, θ, and a basis function, ϕ. This is achieved as follows:

$$\phi = G\left(\underline{x}_{-1}, \underline{u}_{-1}\right) \Delta\delta_{e,0}, \quad \theta = \hat{c} \tag{6.17}$$

Using the RLS parameter estimation algorithm as shown in (6.12), it is possible to obtain an estimate of the correction factor which can be used to correct the known control effectiveness model. This is of course provided that the data used in the regression data contains enough information. Using the estimated correction factor, the rotational longitudinal RLS-AINDI control law will become:

$$\Delta\delta_e = \left(\hat{c} \cdot G\left(\underline{x}_0, \underline{u}_0\right)\right)^{-1} \left(\nu - \dot{q}_0\right) \tag{6.18}$$

6.3. Least mean squares adaptive INDI

The LMS algorithm is very well known in the domain of adaptive filtering. One of the reasons for its popularity is because of its low computational complexity and still adequate convergence properties (Diniz, 1997). As the name of the algorithm already indicates, it attempts to optimize the mean-square error (MSE) of the estimated model output and the measured system output. In this

section a brief version of the derivation will given for the LMS parameter estimation algorithm. For a more detailed coverage of the derivation or other properties, please consult Diniz (1997) or Hayes (1996). In the optimization it is endeavoured to find the optimal Wiener solution:

$$\underline{\theta} = R^{-1}\underline{p}, \quad \text{where} \quad R = E\left[\underline{\phi}_k\underline{\phi}_k^T\right], \quad \underline{p} = E\left[\underline{\phi}_k z_k\right] \tag{6.19}$$

Here $E[\cdot]$ is the expectation operator. The optimal Wiener solution will be searched by adjusting the steepest-decent algorithm as follows:

$$\underline{\hat{\theta}}_{k+1} = \underline{\hat{\theta}}_k - \mu\hat{g}_{\underline{\hat{\theta}},k} = \underline{\hat{\theta}}_k + 2\mu\left(\hat{p}_k - \hat{R}_k\underline{\hat{\theta}}_k\right) \tag{6.20}$$

Furthermore, taking the instantaneous estimations of $\hat{R}_k$ and $\hat{p}_k$ as described in (6.21) gives the final result of the parameter estimation algorithm of Eq. (6.22).

$$\hat{R}_k = \underline{\phi}_k\underline{\phi}^T, \quad \hat{p}_k = \underline{\phi}_k z_k \tag{6.21}$$

$$\begin{aligned}\underline{\hat{\theta}}_{k+1} &= \underline{\hat{\theta}}_k + 2\mu\left(\underline{\phi}_k z_k - \underline{\phi}_k\underline{\phi}_k^T\underline{\hat{\theta}}_k\right)\\ &= \underline{\hat{\theta}}_k + 2\mu\underline{\phi}_k\left(z_k - \underline{\phi}_k^T\underline{\hat{\theta}}_k\right)\\ &= \underline{\hat{\theta}}_k + 2\mu\underline{\phi}_k\epsilon_k\end{aligned} \tag{6.22}$$

For this parameter estimation law the parameters which could be adjusted by the designer are the initial estimate $\underline{\hat{\theta}}_0$ and the adaption gain μ. According to Diniz (1997) the value of μ should be chosen between zero and the inverse of the maximum eigenvalue of R. Larger values of μ will result in faster adaption and therefore quicker convergence to the true model parameters. However, just as for low values of the RLS forgetting factor, high values for the adaption gain will probably result in more oscillations in the estimation and too high values will induce instability. Consequently, the value of μ should also be selected with care.

6.3.1. LMS-AINDI control law design

As is discussed in the previous section, this parameter estimation method also bases its parameter update on the error between the prediction model output and a measurement of the real output. Consequently, the same prediction model could be used as for the RLS-AINDI control law:

$$\Delta\dot{q} = c \cdot G\left(\underline{x}_0, \underline{u}_0\right)\Delta\delta_e \tag{6.15 revisited}$$

Using this definition of the prediction model, the following decomposition for the uncertain parameter and basis function will be used again:

$$\phi = G\left(\underline{x}_{-1}, \underline{u}_{-1}\right)\Delta\delta_{e,0}, \quad \theta = \hat{c} \tag{6.23}$$

Implementing the same definition of the corrected control effectiveness as used in the RLS-AINDI control law, the LMS-AINDI control law can be defined as follows:

$$\Delta\delta_e = \left(\hat{c} \cdot G\left(\underline{x}_0, \underline{u}_0\right)\right)^{-1}\left(\nu - \dot{q}_0\right)$$

$$\hat{c} = \hat{\theta}_{k+1} = \hat{\theta}_k + \mu G\left(\underline{x}_{-1}, \underline{u}_{-1}\right)\Delta\delta_{e,0}\left[\Delta\dot{q}_0 - G\left(\underline{x}_{-1}, \underline{u}_{-1}\right)\Delta\delta_{e,0}\theta_k\right]$$

Looking at the parameter update rule of Eq. (6.3.1) it can be seen that it depends on the increment of the elevator deflection. This results in an parameter update rule that does not adapt when

the system is in a steady state. Consequently, the parameter estimation does not drift away when PE conditions are not satisfied. On the other hand, the correct value for the control effectiveness will not be found either.

6.4. Model reference adaptive INDI

Adaptive control using Lyapunov tuning functions are commonly used in adaptive BS control law designs (Krstić et al., 1995; Sonneveldt, 2010; Van Oort, 2011). This is because both the control law and the adaptive law can be designed using LSFs. Consequently, it is possible to proof stability of the complete adaptive control law.

In combination with a reference model which determines the desired response of the system, it is possible to use the Lyapunov-based tuning function parameter estimation approach for other adaptive control laws as well (Hanson et al., 2011; Nguyen, 2018; Bhardwaj et al., 2019). This can be achieved when it is possible to write the error dynamics between the reference model output and actual system output as follows:

$$\underline{\dot{e}} = A_m \underline{e} + B_m \underline{\phi}^T \tilde{\underline{\theta}} \tag{6.24}$$

The error e is also known as the reference model tracking dynamics. In Eq. (6.24) $\underline{e}$ is the vector containing the states of the reference model tracking error dynamics, A_m and B_m are the A and B matrices of the state-space of the reference model, and $\tilde{\underline{\theta}}$ is the parameter estimation error, $\underline{\phi}$ is a vector of basis functions, and $\hat{\underline{\theta}} - \underline{\theta}$. The estimated parameters could be both control gains or system model parameters. Once this form is obtained, the design of the parameter tuning function can be continued by setting up a Lyapunov stability function for the reference model tracking error:

$$\mathcal{V} = \underline{e}^T P \underline{e} + \tilde{\underline{\theta}}^T \Gamma^{-1} \tilde{\underline{\theta}} \tag{6.25}$$

$$PA_m + A_m^T P = -Q \tag{6.26}$$

Here, $P = P^T$ is a positive definite matrix which is obtained from solving equation Eq. (6.26) and Γ is a diagonal matrix containing the positive adaption gains of the tuning functions. In this equation Q is also a positive definite matrix which can be chosen by the designer. Taking the time derivative of Eq. (6.25) the following result is found:

$$\begin{aligned}
\dot{\mathcal{V}} &= \underline{e}^T P \left(A_m \underline{e} + B_m \underline{\phi}^T \tilde{\underline{\theta}} \right) + \left(A_m \underline{e} + B_m \underline{\phi}^T \tilde{\underline{\theta}} \right)^T P \underline{e} + \tilde{\underline{\theta}}^T \Gamma^{-1} \dot{\tilde{\underline{\theta}}} + \dot{\tilde{\underline{\theta}}}^T \Gamma^{-1} \tilde{\underline{\theta}} \\
&= \underline{e}^T \left(P A_m + A_m^T P \right) \underline{e} + \underline{e}^T P B_m \underline{\phi}^T \tilde{\underline{\theta}} + \tilde{\underline{\theta}}^T \underline{\phi} B_m^T P \underline{e} + \tilde{\underline{\theta}}^T \Gamma^{-1} \dot{\tilde{\underline{\theta}}} + \dot{\tilde{\underline{\theta}}}^T \Gamma^{-1} \tilde{\underline{\theta}} \\
&= -\underline{e}^T Q \underline{e} + \left(\underline{e}^T P B_m \underline{\phi}^T + \dot{\tilde{\underline{\theta}}}^T \Gamma^{-1} \right) \tilde{\underline{\theta}} + \tilde{\underline{\theta}}^T \left(\underline{\phi} B_m^T P \underline{e} + \Gamma^{-1} \tilde{\underline{\theta}} \right) \\
&= -\underline{e}^T Q \underline{e} + 2 \tilde{\underline{\theta}}^T \left(\underline{\phi} \underline{e}^T P B_m + \Gamma^{-1} \tilde{\underline{\theta}} \right)
\end{aligned} \tag{6.27}$$

To be able to find a result for the parameter estimation rule and obtain a negative definite solution for $\dot{\mathcal{V}}$ it will be assumed that the rate of change of the true model parameters, $\dot{\underline{\theta}}$, is much smaller than adaption rate of the set of estimated parameters. Therefore, $\dot{\underline{\theta}}$ will be neglected and the following result can be formulated:

$$\dot{\mathcal{V}} = -\underline{e}^T Q \underline{e} + 2 \left(\underline{\phi} \underline{e}^T P B_m + \Gamma^{-1} \dot{\tilde{\underline{\theta}}} \right) \tilde{\underline{\theta}} \tag{6.28}$$

To attain a negative definite function for $\dot{\mathcal{V}}$ one of the possible solutions for the parameter estimation update rule is the following:

$$\dot{\underline{\hat{\theta}}} = -\Gamma \underline{\phi} \underline{e}^T P B_m \tag{6.29}$$

Using this parameter estimation update rule, the control gains or model parameters are adjusted until the actual system perfectly follows the reference model. Consequently, the use of this adaptive control approach is highly dependent on the assumption that all unmodelled dynamics are fast enough and that other forms of uncertainties or unanticipated disturbances, noise for example, are insignificant and can be neglected. If this is not the case, it is possible that the parameter estimation does not converge and finally becomes unstable.

As described in Nguyen (2018) research on finding a stable adaptive law despite the unstructured uncertainties have resulted in several solutions. A few of these solutions are the Dead-Zone, σ-modification and e-modification methods. The Dead-zone method stops the update when the estimated parameter grows outside a certain predefined range. Furthermore, the σ- or e-modification add an extra $-\sigma\underline{\hat{\theta}}$ or $-\mu \left\| \underline{e}^T P B_m \right\| \underline{\hat{\theta}}$ term to the parameter estimation update rules of Eq. (6.29), respectively. Although, these improvement methods are relatively simple and make sure that the parameter estimation remain bounded, they do not improve the parameter estimation in the sense that the true set of parameters will be reached. Besides, the parameter estimation methods which include these additions should be specifically tuned for the expected amount of parameter deviation to maintain a good response of the adaptive control law.

Furthermore, if the unmodelled dynamics would affect the system response significantly, such as relatively slow actuator or strict filter dynamics, there are some methods which could allow to take these dynamics into account (Nguyen, 2018). However, these methods require extra prediction models and will introduce more design parameters into the parameter estimation law. Furthermore, the mathematical complexity will be significantly increased. Consequently, if the update law of Eq. (6.29) does not give satisfactory results and another considered adaptive law in this study does, this approach will disregarded.

6.4.1. MR-AINDI control law design

In this section the parameter update law of the MRAC-INDI control law is defined. As explained in Chapter 3, this adaptive law makes sure that the system will behave as a reference model. For this case the reference model for the pitch rate is defined as:

$$q_m = \frac{k_p s + k_I}{s^2 + k_P s + k_I} q_r \tag{6.30}$$

To start the derivation of the parameter update law it is required to define the structure of the uncertainty. For the MRAC laws the lumped uncertainty in the rotational longitudinal equations of motion will be written as follows:

$$\dot{q} = \dot{q}_0 + \left(G\left(\underline{x}_0, \underline{u}_0\right) + \Delta G\left(\underline{x}_0, \underline{u}_0\right) \right) \Delta\delta_e = \dot{q}_0 + G\left(\underline{x}_0, \underline{u}_0\right) \Delta\delta_e + \Delta G\left(\underline{x}_0, \underline{u}_0\right) \Delta\delta_e \tag{6.31}$$

Regarding the control of the system with the non-adaptive control, the control input is based on the knowledge of the nominal model. Due to the change in the control effectiveness, the determined control increment using the nominal model is not able to fully linearize the system anymore. To be able to correct for the change in the control effectiveness the control law will be given an extra adaptive term. This gives the following new definition of the control law:

$$\Delta\delta_{e_c} = \Delta\delta_{e_{INDI}} - \Delta\delta_{e_{ad}} \tag{6.32}$$

Here, $\Delta\delta_{e_{INDI}}$ is the incremental elevator deflection determined by the INDI control law using the on-board control effectiveness model and $\Delta\delta_{e_{ad}}$ is the additionally required elevator deflection increment estimated by the adaptive law. Using that the model deviation is dependent on the nominal

control increment and substituting this control law in Eq. (6.31), the deviating system dynamics can be written as:

$$\dot{q} = \dot{q}_0 + G\left(\underline{x}_0, \underline{u}_0\right)\Delta\delta_{e_{INDI}} - G\left(\underline{x}_0, \underline{u}_0\right)\Delta\delta_{e_{ad}} + \Delta G\left(\underline{x}_0, \underline{u}_0\right)\Delta\delta_{e_{INDI}} \tag{6.33}$$

Defining $\Delta\delta_{e_{ad}}$ as the nominal control increment but corrected by a term called $\hat{c}$ and modelling the control effectiveness deviation as a scaling term multiplied by the nominal control effectiveness model:

$$\begin{aligned} \Delta\delta_{e_{ad}} &= \hat{c}\cdot\Delta\delta_{e_{INDI}} \\ \Delta G\left(\underline{x}_0, \underline{u}_0\right) &= c\cdot G_{nom}\left(\underline{x}_0, \underline{u}_0\right) \end{aligned} \tag{6.34}$$

With this notation the system model will look as follows:

$$\dot{q} = \dot{q}_0 + G\left(\underline{x}_0, \underline{u}_0\right)\Delta\delta_{e_{INDI}} - \hat{c}\cdot G\left(\underline{x}_0, \underline{u}_0\right)\Delta\delta_{e_{INDI}} + c\cdot G\left(\underline{x}_0, \underline{u}_0\right)\Delta\delta_{e_{INDI}} \tag{6.35}$$

From this definition it can be seen that with the correct estimation of $\hat{c}$ it is possible to make the system behave as the nominal system again. The remainder of this section will elaborate on the derivation of the parameter estimation law which will estimate $\hat{c}$. To start the derivation the last two terms of Eq. (6.35) will be written as follows:

$$\begin{aligned} \hat{c}\cdot G\left(\underline{x}_0, \underline{u}_0\right)\Delta\delta_{e_{INDI}} &= \hat{\theta}\cdot\phi(\underline{x}_0, \underline{u}_0, \Delta\delta_{e_{INDI}}) \\ c\cdot G\left(\underline{x}_0, \underline{u}_0\right)\Delta\delta_{e_{INDI}} &= \theta\cdot\phi(\underline{x}_0, \underline{u}_0, \Delta\delta_{e_{INDI}}) \end{aligned} \tag{6.36}$$

Furthermore, taking the nominal definition of the INDI control law and the definition of the virtual control input of Eq. (6.37), the system dynamics can be written as shown in Eq. (6.38).

$$\nu = \dot{q}_m + k_P\left(q_m - q\right) + k_I\int_0^T\left(q_m - q\right)dt \tag{6.37}$$

$$\dot{q} = \dot{q}_m + k_P\left(q_m - q\right) + k_I\int_0^T\left(q_m - q\right)dt - \hat{\theta}\cdot\phi(x_0, u_0, \Delta\delta_{e_{INDI}}) + \theta\cdot\phi(x_0, u_0, \Delta\delta_{e_{INDI}}) \tag{6.38}$$

In this control law the virtual control will be driven by the error between the reference model output and the system output. Note that in this virtual control law the time derivative of the reference model output is included. This makes sure that the system immediately follows the reference model. At this moment it is possible to define the reference model tracking error dynamics. This can be done by defining $e = q_m - q$. Furthermore, the estimation error will be defined as $\tilde{\theta} = \hat{\theta} - \theta$. Using these definitions and rewriting Eq. (6.38) accordingly gives the following result:

$$\dot{e} = -k_p e - k_I\int_0^T e\cdot dt + \tilde{\theta}\cdot\phi(x_0, u_0, \Delta\delta_{e_{INDI}}) \tag{6.39}$$

Writing this equation in matrix form gives the structure as shown in Eq. (6.40). Transforming the reference model transfer function described in Eq. (6.30) into a state-space and comparing the A and B matrices to the matrices obtained in Eq. (6.40), it can be seen that the reference model tracking error dynamics are the same as the reference model dynamics. This means that the reference model error dynamics are stable and if $\hat{c}$ can be estimated correctly the error will asymptotically converge to zero.

$$\begin{aligned} \begin{bmatrix} e \\ \dot{e} \end{bmatrix} &= \begin{bmatrix} 0 & 1 \\ -k_I & -k_p \end{bmatrix}\begin{bmatrix} \int_0^t e\cdot dt \\ e \end{bmatrix} + \begin{bmatrix} 0 \\ 1 \end{bmatrix}\left[\tilde{\theta}\cdot\phi(x_0, u_0, \Delta\delta_{e_{INDI}})\right] \\ \underline{\dot{e}} &= A_m\underline{e} + B_m\left[\tilde{\theta}\cdot\phi(x_0, u_0, \Delta\delta_{e_{INDI}})\right] \end{aligned} \tag{6.40}$$

To find a parameter update law which reduces the estimation error to zero and guarantees asymptotic tracking of the reference model, the following positive definite Lyapunov function is defined using Lyapunov's direct method (Nguyen, 2018):

$$\mathcal{V} = \underline{e}^T P \underline{e} + \tilde{\theta}\gamma^{-1}\tilde{\theta} \tag{6.41}$$

Here, $P = P^T$ is a 2-by-2 and positive definite matrix which solves the Lyapunov equation defined in (6.42). Where $c > 0$ and I is the identity matrix. A solution to this problem is presented in Eq. (6.43) (Nguyen, 2018).

$$PA_m + A_m^T P = -Q = -cI \tag{6.42}$$

$$P = c \begin{bmatrix} k_I^{-1} k_p + k_P^{-1}\left(k_I + 1\right) & k_I^{-1} \\ k_I^{-1} & k_P^{-1}\left(k_I^{-1} + 1\right) \end{bmatrix} \tag{6.43}$$

Using the definition of P as in Eq. (6.42) and taking the first derivative of the Lyapunov function defined in Eq. (6.41), the following result is found:

$$\dot{\mathcal{V}} = -\underline{e}^T Q \underline{e} + 2\left(\phi\left(x_0, u_0, \Delta\delta_{e_{INDI}}\right)\underline{e}^T P B_m + \gamma^{-1}\dot{\tilde{\theta}}\right)\tilde{\theta} \tag{6.44}$$

The parameter update law could now be defined. Though, first it has to be assumed that the parameter update converges much faster to the unknown parameter value than the value of the unknown parameter changes. If this is true, the time variance of the unknown parameter could be neglected and the parameter error dynamics, $\dot{\underline{\tilde{\theta}}}$ can defined as $\dot{\underline{\hat{\theta}}}$. Using this, the parameter update law, which results in a negative definite derivative of the Lyapunov function, can be written as follows:

$$\dot{\hat{\theta}} = -\gamma\phi\left(x_0, u_0, \Delta\delta_{e_{INDI}}\right)\underline{e}^T P B_m \tag{6.45}$$

With the estimated parameter the adaptive INDI control law will look as follows:

$$\Delta\delta_{e_c} = \left(1 - \hat{c}\right)\left[G\left(\underline{x}_0, \underline{u}_0\right)\right]^{-1}\left(\nu - \dot{q}_0\right) \tag{6.46}$$

In the derivation of the adaptive law the actuator and filter dynamics are not taken into account. It is assumed that the bandwidth of the actuator and filters is large enough such that they will not interfere with the parameter estimation. These dynamics could be included in the derivation if it is required for proper performance. However, the mathematical complexity of the derivation will increase significantly and the number of parameters in the adaptive law will increase as well. An example of a MRAC-based adaptive controller which integrates the actuator dynamics is shown in section 9.12 of Nguyen (2018). In case the sign of the system changes is not known a priori, the adaptive law requires three estimation rules and an extra predictor model. This gives an indication of how the MRAC adaptive laws easily become very complex.

6.5. Immersion and Invariance adaptive INDI

I&I is a relatively new paradigm in the field of adaptive control. It has been combined with BS control in Sonneveldt (2010) and Astolfi et al. (2007) and with IBS in van Gils et al. (2015). In these studies it has shown to be an easy tuneable and well-performing adaptive law. This method allows for the integration of stable estimation dynamics in the parameter estimation rule by designing an invariant manifold on which the estimation error is zero. This manifold looks as follows:

$$\mathcal{M} = \left\{\left(x, \theta\right) \in \mathbb{R}^2 \,\middle|\, \hat{\theta} - \theta + \beta\left(x\right) = 0\right\} \tag{6.47}$$

Here, $\hat{\theta}$ is again the estimated set of model parameters and $\beta\left(\underline{x}\right)$ is a continuous stabilization function which will follow from the parameter estimation law derivation. The form of the parameter estimation law depends on the system dynamics description and the modelling of the uncertainty. Therefore, consider the following uncertain incremental dynamic equation:

$$\dot{\underline{x}} = \dot{\underline{x}}_0 + G\left(\underline{x}_0, \underline{y}_0, \underline{u}_0\right)\Delta\underline{u} \tag{6.48}$$

Here, $\underline{x} \in \mathbb{R}^n$ and $\dot{\underline{x}} \in \mathbb{R}^n$ are the states to be controlled and its first time derivative, $\underline{u}_0 \in \mathbb{R}^m$ and $\Delta\underline{u} \in \mathbb{R}^m$ are the total control input and the control increment, respectively, and $\underline{y}_0 \in \mathbb{R}^l$ are other system output variables which affect G. To be able to start the I&I design, each element of $\dot{\underline{x}}$ will be considered separately:

$$\dot{x}_i = \dot{x}_{i,0} + G_i\left(\underline{x}_0, \underline{y}_0, \underline{u}_0\right)\Delta\underline{u} = \dot{x}_{i,0} + \underline{\phi}_i^T\left(\underline{x}_0, \underline{y}_0, \underline{u}_0, \Delta\underline{u}\right)\underline{\theta}_i \tag{6.49}$$

Where, $\underline{\phi} \in \mathbb{R}^r$ is a vector containing regression basis functions and $\underline{\theta} \in \mathbb{R}^r$ is the vector containing the true model parameters. Using this description, the manifold, $\mathcal{M}_i$, can be defined as:

$$\mathcal{M}_i = \left\{\left(\underline{x}_0, \underline{y}_0, \underline{u}_0, \Delta\underline{u}, \underline{\theta}_i\right) \in \mathbb{R}^{n+l+m+m+r} \,\middle|\, \hat{\theta}_i - \theta_i + \underline{\beta}_i\left(\underline{x}_0, \underline{y}_0, \underline{u}_0, \Delta\underline{u}\right) = 0\right\} \tag{6.50}$$

Using this definition of the manifold and the description of the uncertain incremental dynamic system, the INDI control law for x_i looks as follows:

$$\Delta\underline{u} = \left[\underline{\phi}_i^T\left(\underline{\hat{\theta}}_i + \underline{\beta}_i\left(\underline{x}_0, \underline{y}_0, \underline{u}_0, \Delta\underline{u}\right)\right)\right]^{-1}\left(\nu_i - \dot{x}_{i,0}\right) \tag{6.51}$$

The next steps of the adaptive law design are concerned with making the manifold of Eq. (6.62) invariant. This will be done by designing stable off-manifold dynamics. To do this the off-manifold error and its corresponding dynamics are defined as Eq. (6.52) and (6.53). Furthermore, for a better overview of the equations $\left(\underline{x}_0, \underline{z}_0, \underline{u}_0, \Delta\underline{u}\right)$ will from now on be written as $(\cdot)$.

$$\underline{\sigma}_i = \underline{\hat{\theta}}_i - \underline{\theta}_i + \underline{\beta}_i(\cdot) \tag{6.52}$$

$$\begin{aligned}
\dot{\underline{\sigma}}_i &= \dot{\underline{\hat{\theta}}}_i + \frac{\partial\underline{\beta}_i(\cdot)}{\partial x_i}\dot{x}_i + \sum_{j=1\neq i}^{n}\frac{\partial\underline{\beta}_i(\cdot)}{\partial x_j}\dot{x}_j + \frac{\partial\underline{\beta}_i(\cdot)}{\partial\underline{y}}\dot{\underline{y}}_0 + \frac{\partial\underline{\beta}_i(\cdot)}{\partial\underline{u}}\dot{\underline{u}}_0 + \frac{\partial\underline{\beta}_i(\cdot)}{\partial\Delta\underline{u}}\Delta\dot{\underline{u}}_0 \\
&= \dot{\underline{\hat{\theta}}}_i + \frac{\partial\underline{\beta}_i(\cdot)}{\partial x_i}\left[\dot{x}_{i,0} + \underline{\phi}_i^T(\cdot)\underline{\theta}_i\right] + \sum_{j=1\neq i}^{n}\frac{\partial\underline{\beta}_i(\cdot)}{\partial x_j}\dot{x}_j + \frac{\partial\underline{\beta}_i(\cdot)}{\partial\underline{y}}\dot{\underline{y}}_0 + \frac{\partial\underline{\beta}_i(\cdot)}{\partial\underline{u}}\dot{\underline{u}}_0 + \frac{\partial\underline{\beta}_i(\cdot)}{\partial\Delta\underline{u}}\Delta\dot{\underline{u}}_0 \\
&= \dot{\underline{\hat{\theta}}}_i + \frac{\partial\underline{\beta}_i(\cdot)}{\partial x_i}\left[\dot{x}_{i,0} + \underline{\phi}_i^T(\cdot)\left(\underline{\hat{\theta}}_i + \underline{\beta}_i(\cdot) - \underline{\sigma}_i\right)\right] + \sum_{j=1\neq i}^{n}\frac{\partial\underline{\beta}_i(\cdot)}{\partial x_j}\dot{x}_j + \frac{\partial\underline{\beta}_i(\cdot)}{\partial\underline{y}}\dot{\underline{y}}_0 + \frac{\partial\underline{\beta}_i(\cdot)}{\partial\underline{u}}\dot{\underline{u}}_0 + \frac{\partial\underline{\beta}_i(\cdot)}{\partial\Delta\underline{u}}\Delta\dot{\underline{u}}_0
\end{aligned} \tag{6.53}$$

For the derivation of the off-manifold dynamics it is also assumed that the rate of change of the true model parameters, $\dot{\underline{\theta}}_i$, is much smaller than the rate of change of the estimated parameters. A suitable equation for the parameter estimation law can now be defined as follows:

$$\dot{\underline{\hat{\theta}}}_i = -\frac{\partial\underline{\beta}_i(\cdot)}{\partial x_i}\left[\dot{x}_{i,0} + \underline{\phi}_i^T(\cdot)\left(\underline{\hat{\theta}}_i + \underline{\beta}_i(\cdot)\right)\right] - \sum_{j=1\neq i}^{n}\frac{\partial\underline{\beta}_i(\cdot)}{\partial x_j}\dot{x}_j - \frac{\partial\underline{\beta}_i(\cdot)}{\partial\underline{y}}\dot{\underline{y}}_0 - \frac{\partial\underline{\beta}_i(\cdot)}{\partial\underline{u}}\dot{\underline{u}}_0 - \frac{\partial\underline{\beta}_i(\cdot)}{\partial\Delta\underline{u}}\Delta\dot{\underline{u}}_0 \tag{6.54}$$

Due to this choice, the off-manifold error dynamics can be described by:

$$\underline{\dot{\sigma}}_i = -\frac{\partial \underline{\beta}_i(\cdot)}{\partial x_i} \underline{\phi}_i^T(\cdot)\, \underline{\sigma}_i \tag{6.55}$$

At this point it is possible to find a formulation for $\beta(\cdot)$. This can be done by defining a LSFs for σ. This procedure is shown in Eq. (6.56) till (6.59).

$$\mathcal{V}_i = \underline{\sigma}_i^T \Gamma^{-1} \underline{\sigma}_i \tag{6.56}$$

$$\dot{\mathcal{V}}_i = -2\underline{\sigma}_i^T \Gamma^{-1} \frac{\partial \underline{\beta}_i(\cdot)}{\partial x_i} \underline{\phi}_i^T(\cdot)\, \underline{\sigma}_i \tag{6.57}$$

$$\frac{\partial \underline{\beta}_i(\cdot)}{\partial x_i} = \Gamma \underline{\phi}_i(\cdot) \tag{6.58}$$

$$\underline{\beta}_i(\cdot) = \Gamma \int_0^{x_i} \underline{\phi}_i(\cdot, \chi)\, d\chi \tag{6.59}$$

In these equations Γ is a positive diagonal matrix with the adaption gains for each parameter on the diagonal. Using the definitions for $\beta(\cdot)$ of Eq. (6.59) and the parameter update rule of Eq. (6.54) it is possible to make Eq. (6.57) negative definite and give σ a stable equilibrium at 0. This does not mean that $\underline{\hat{\theta}}_i$ will become equal to $\underline{\theta}$, but it does mean that $\lim_{t\to\infty} \underline{\sigma}_i = 0$.

6.5.1. II-AINDI control law design

To start the derivation of the II-AINDI control law, the uncertain pitch dynamics will be defined as Eq. (6.60). Furthermore, using the regression model of Eq. (6.17), the uncertain dynamics can be written as in the second part of Eq. (6.60).

$$\dot{q} = \dot{q}_0 + c \cdot G_{nom}\left(\underline{x}_0, \underline{u}_0\right) \Delta\delta_e \tag{6.60}$$

However, for the application in adaptive control it is not possible to obtain the $\Delta\delta_e$. Therefore, the adaptive law will operate with the knowledge obtained from one time-step back. Furthermore, the correction factor and control effectiveness multiplied by the elevator deflection increment will again be described by a regression function:

$$\dot{q}_0 = \dot{q}_{-1} + c \cdot G_{nom}\left(\underline{x}_{-1}, \underline{u}_{-1}\right) \Delta\delta_{e,0} = \dot{q}_{-1} + \theta \cdot \phi\left(\underline{x}_{-1}, \underline{u}_{-1}, \Delta\delta_{e,0}\right) \tag{6.61}$$

To start with the derivation of the parameter update law, a manifold will be defined on which the parameter estimation error is zero.

$$\mathcal{M} = \left\{ \left(\underline{x}_{-1}, \underline{u}_{-1}, \Delta\delta_{e,0}, \hat{\theta}\right) \in \mathbb{R}^4 \,\middle|\, \hat{\theta} - \theta + \beta\left(\underline{x}_{-1}, \underline{u}_{-1}, \Delta\delta_{e,0}\right) = 0 \right\} \tag{6.62}$$

Here, θ is the actual correction factor and $\hat{\theta}$ its estimate from the I&I parameter estimator. Furthermore, $\beta\left(\underline{x}_{-1}, \underline{u}_{-1}, \Delta\delta_{e,0}\right)$ is a stabilization function which will be defined later on. The next steps are to determine the estimation error dynamics and determine a functions for $\dot{\hat{\theta}}$ and $\beta\left(\underline{x}_{-1}, \underline{u}_{-1}, \Delta\delta_{e,0}\right)$ which make the manifold invariant. This is done by taking the time derivative of Eq. (6.63) and assuming that the real parameter changes much slower in time than the estimated parameter converges. Then, the resulting estimation error dynamics can be written as in Eq. (6.64) and (6.65). To promote the overview of the derivation $\left(\underline{x}_{-1}, \underline{u}_{-1}, \Delta\delta_{e,0}\right)$ will be written as $(\cdot)$

$$\sigma = \hat{\theta} - \theta + \beta(\cdot) \tag{6.63}$$

$$\dot{\sigma} = \dot{\hat{\theta}} - \dot{\theta} + \frac{\partial \beta(\cdot)}{\partial q} \dot{q}_0 + \sum_{j=1}^{n} \frac{\partial \beta(\cdot)}{\partial x_j} \dot{x}_{j,0} + \frac{\partial \beta(\cdot)}{\partial \underline{u}} \underline{\dot{u}}_0 + \frac{\partial \beta(\cdot)}{\partial \Delta\delta_e} \Delta\dot{\delta}_{e,0} \tag{6.64}$$

$$\dot{\sigma} = \dot{\hat{\theta}} + \frac{\partial \beta(\cdot)}{\partial q}\left(\dot{q}_{-1} + \phi(\cdot)^T\left(\hat{\theta} + \beta(\cdot) - \sigma\right)\right) + \sum_{j=1}^{n} \frac{\partial \beta(\cdot)}{\partial x_j}\dot{x}_{j,0} + \frac{\partial \beta(\cdot)}{\partial \underline{u}}\dot{\underline{u}}_0 + \frac{\partial \beta(\cdot)}{\partial \Delta\delta_e}\Delta\dot{\delta}_{e,0} \tag{6.65}$$

A possible choice for the parameter update law is presented in Eq. (6.66). This choice results in the parameter estimation error dynamics of Eq. (6.67).

$$\dot{\hat{\theta}} = -\frac{\partial \beta(\cdot)}{\partial q}\left(\dot{q}_{-1} + \phi(\cdot)^T\left(\hat{\theta} + \beta(\cdot)\right)\right) - \sum_{j=1}^{n} \frac{\partial \beta\left(\underline{x}, \Delta u_0\right)}{\partial x_j}\dot{x}_{j,0} - \frac{\partial \beta(\cdot)}{\partial \underline{u}}\dot{\underline{u}}_0 - \frac{\partial \beta(\cdot)}{\partial \Delta\delta_e}\Delta\dot{\delta}_{e,0} \tag{6.66}$$

$$\dot{\sigma} = -\frac{\partial \beta(\cdot)}{\partial q}\phi(\cdot)^T\sigma \tag{6.67}$$

At this point the continuous function $\beta(\cdot)$ can be derived. This can be done by first defining a LSF for the parameter estimation error. This function will be defined as follows:

$$V = \frac{1}{2\gamma}\sigma^2, \quad \gamma > 0 \tag{6.68}$$

Then, taking the time derivative of this LSF, the result of Eq. (6.69) is obtained. To make this function negative definite, the choice for $\beta(\cdot)$ as defined in Eq. (6.70) can be used.

$$\dot{V} = \frac{1}{\gamma}\sigma\dot{\sigma} = -\frac{1}{\gamma}\frac{\partial \beta(\cdot)}{\partial q}\phi(\cdot)^T\sigma^2 \tag{6.69}$$

$$\frac{\partial \beta(\cdot)}{\partial q} = \gamma\phi(\cdot) \quad \rightarrow \quad \beta(\cdot) = \gamma\int_0^q \phi(\cdot)\,d\chi = \gamma\phi(\cdot)\,q \tag{6.70}$$

As a result of this choice the final parameter update law has become as presented in Eq. (6.72). It can be seen that the update law contains the time derivative of the dynamic pressure, $\bar{q}$. This is required as this is in fact also a time-varying variable of the regression function:

$$\phi(\cdot) = \frac{\bar{q}_{-1}S\bar{c}}{I_{yy}}C_{m_{\delta_e}}\Delta\delta_{e,0} \tag{6.71}$$

$$\begin{aligned}\dot{\hat{\theta}} &= -\gamma\left[\phi(\cdot)\left(\dot{q}_{-1} + \phi(\cdot)^T\left(\hat{\theta} + \beta(\cdot)\right)\right) + \frac{\partial \phi(\cdot)}{\partial \bar{q}}q_{-1}\dot{\bar{q}}_0 + \frac{\partial \phi(\cdot)}{\partial \Delta\delta_e}q_{-1}\Delta\dot{\delta}_{e,0}\right] \\ &= -\gamma\left[\frac{\bar{q}_{-1}S\bar{c}}{I_{yy}}C_{m_{\delta_e}}\Delta\delta_{e,0}\left(\dot{q}_{-1} + \frac{\bar{q}_{-1}S\bar{c}}{I_{yy}}C_{m_{\delta_e}}\Delta\delta_{e,0}\left(\hat{\theta} + \beta(\cdot)\right)\right) + \frac{S\bar{c}}{I_{yy}}C_{m_{\delta_e}}q_{-1}\left(\Delta\delta_{e,0}\dot{\bar{q}}_{-1} + \bar{q}_{-1}\Delta\dot{\delta}_{e,0}\right)\right]\end{aligned} \tag{6.72}$$

The estimated parameter will be used in the II-AINDI control law as follows:

$$\Delta\delta_e = \left[\left(\hat{\theta} + \beta(\cdot)\right)\cdot G_{nom}\left(\underline{x}_0, \underline{u}_0\right)\right]^{-1}\left(\nu - \dot{q}_0\right) = \left[\hat{c}\cdot G_{nom}\left(\underline{x}_0, \underline{u}_0\right)\right]^{-1}\left(\nu - \dot{q}_0\right) \tag{6.73}$$

7

Non-adaptive INDI control law analysis

This chapter will treat the non-adaptive INDI control law analysis of the rotational control of the F-16 aircraft. This will be performed for an ideal and a more realistic control system model. First of all, the bare airframe dynamics and ideal control system model will be covered in section 7.1. Then, the system elements of the more realistic system model and the complete model itself are treated in section 7.2. This will be followed by the setup of the analysis in section 7.3. Here,the test cases and the simulation initialization will be discussed. Furthermore, section 7.4 will present and elaborate on the simulation results. Finally, this chapter will be ended with a concise conclusion in section 7.5.

7.1. Ideal control system description

This section elaborates on the elements of the ideal control system, which are the bare airframe dynamics and the INDI control law. Though, as the INDI control law is already covered in section 6.1, this section will mainly focus on the bare airframe dynamics. However, only longitudinal rotational control is treated in this study. Consequently, this section will only treat the longitudinal rotational equations of motion. The pitching motion can be described as follows:

$$\dot{q} = \frac{1}{I_{yy}} \left[\left(I_{zz} - I_{xx} \right) pr + I_{xz} \left(r^2 - p^2 \right) + M \right] \tag{7.1}$$

The aerodynamic moment, M, can be defined as shown in Eq. (7.2). Furthermore, the nonlinear model used to describe the dependency of C_m on the aerodynamic angles and control surface deflection is the low-fidelity taken from Nguyen et al. (1979). The equation used in this model are shown in Eq. (7.3) and (7.4).

$$M = \bar{q} S \bar{c} C_{m,T} \tag{7.2}$$

$$C_{m,T} = f\left(\alpha, \beta, q, \delta_e\right) = C_m\left(\alpha, \delta_e\right) + C_{Z,T}\left(\alpha, \beta, q, \delta_e\right) \left[x_{cg_r} - x_{cg} \right] + C_{m_q}(\alpha) \frac{\bar{c} q}{2V} \tag{7.3}$$

$$C_{Z,T} = C_Z\left(\alpha, \beta, \delta_e\right) + C_{Z_q}(\alpha) \frac{\bar{c} q}{2V} \tag{7.4}$$

The aerodynamic coefficients, C_m, C_{m_q}, C_Z and C_{Z_q} are obtained by interpolating the low-fidelity look-up tables from Nguyen et al. (1979). Furthermore, the value of the CG in Eq. (7.3) is normalized by the MAC and defined with respect to the leading edge of the wing at the MAC location on the wing. The reference CG value, x_{cg_r}, used in the model is $0.35\bar{c}$. Furthermore, the values for $\bar{c}$ and S are 11.32 ft and 300.0 ft^2, respectively. Moreover, as the analysis only considers longitudinal motion, the values of β, p and r will remain small. Consequently, thesis states will not affect the longitudinal motion.

As discussed before, this model has been set up in a Simulink format by the University of Minnesota (UoM) and Honeywell (Russel, 2003). This model also contains a International Standard Atmosphere (ISA) model which can be used to determined the atmospheric properties around the aircraft. Therefore, the output of the aircraft model also contains the dynamic and static pressure. Using the discussed aircraft model, the ISA model and the INDI control law, the control system shown in Figure 7.1 can be set up. A more detailed description of the '*Aircraft*' block is presented in Figure 7.2.

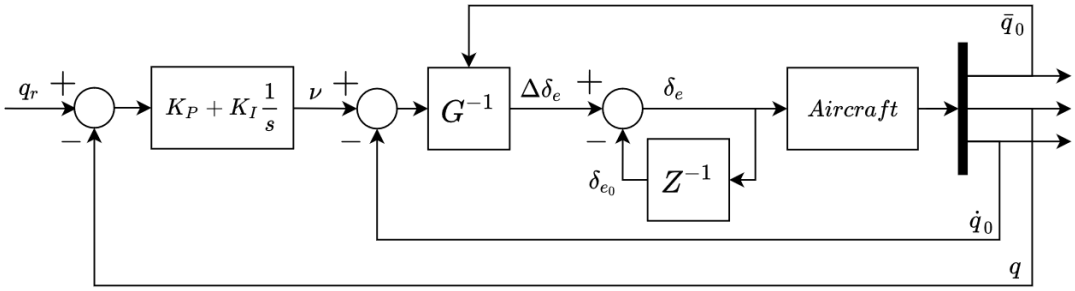

Figure 7.1: Block diagram of the INDI control loop in an ideal control system.

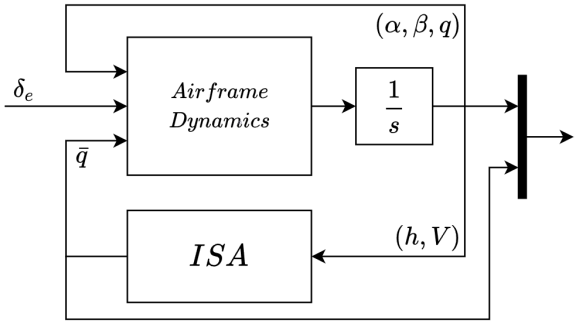

Figure 7.2: Block of the bare airframe dynamics plus ISA.

7.2. Non-ideal control system description

In reality the control system also contains non-ideal elements such as actuator dynamics and filters. These elements change the bandwidth of the feed-forward and feedback paths and therefore change the overall control performance. As demonstrated by actual flight tests in Smeur et al. (2016), it is required to have an accurate estimation of the control effectiveness in order to have adequate flight performance. Although, this research was performed with a small drone, it does indicate that real-world aspects of the control loop do affect the robustness of the control performance to uncertainties in the on-board model. To analyse whether this also applies for high-performance military aircraft real-world aspects of control systems will be added to the control loop to be able to perform more realistic simulations. However, the knowledge on the actual control system of an F-16 is not publicly available, which makes it impossible to evaluate the controller for the actual F-16. Consequently, a publicly available control system model of a similar aircraft type will be used, which is the flight control system model of the High Incidence Research Model (HIRM). This FCC model has been used in the benchmark flight control design problem set by the Group for Aeronautical Research and Technology in EURope (GARTEUR) and is described in Muir (1998). The modelled elements and corresponding transfer functions are shown in Table 7.2. Furthermore, the block diagram of the non-ideal control system is shown in Figure 7.3. The remainder of this section will elaborate on the models used for the simulated non-ideal control system of this research.

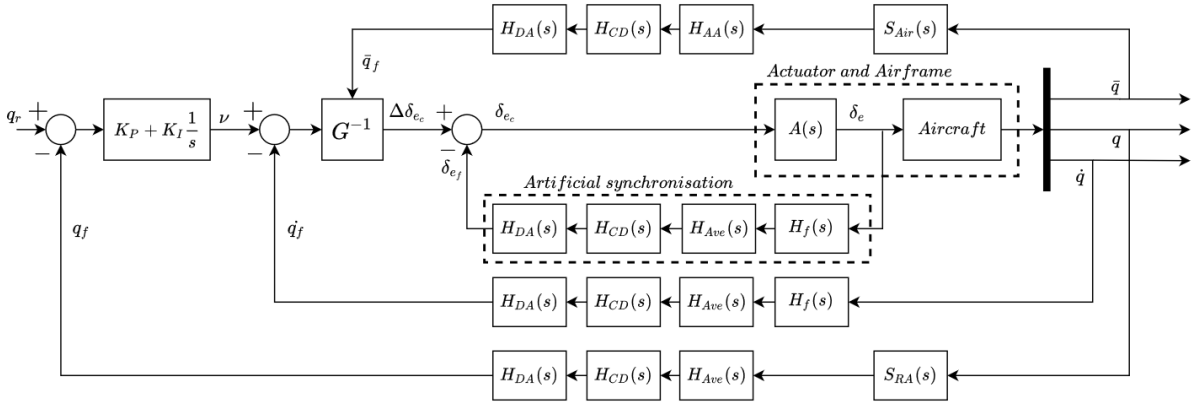

Figure 7.3: Block diagram of the INDI control loop for the non-ideal system.

7.2.1. Actuator dynamics

In the standard F-16 model of the UoM a the actuators are modelled using first-order low-pass dynamics (Russel, 2003). For this research this model type will be adopted as well because first-order dynamics are considered to be accurate enough for the analysis performed in this study. Consequently, the transfer function of the actuator dynamics is as follows:

$$A(s) = \frac{\omega_{act}}{s + \omega_{act}} \tag{7.5}$$

Here, ω_{act} is the bandwidth of the actuator dynamics. Furthermore, the actuators also have a deflection and rate limit. To incorporate these factors in the actuator model, the transfer function is transformed to a block diagram as shown in Figure 7.4.

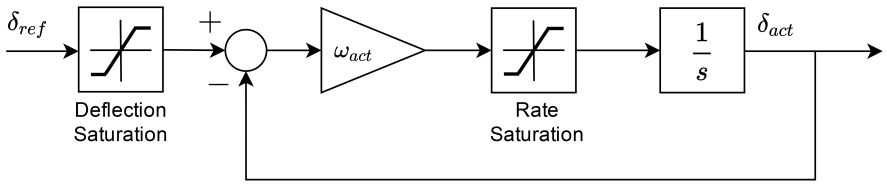

Figure 7.4: Block diagram of actuator dynamics including deflection and rate saturation.

The standard actuator bandwidth of the elevator in the UoM F-16 model is set to 20.2 rad/s. This bandwidth is significantly lower than the bandwidth used in Zhang et al. (2019) and Muir (1998) which use a bandwidth between approximately 60 and 80 rad/s. Therefore, the default bandwidth of the model is considered too low and a larger bandwidth will be used. A higher bandwidth is beneficial for following fast changing commands or rejecting disturbances. However, too much bandwidth could excite the structural vibration modes of the airframe, which should be avoided as this deteriorates the control performance (Pratt, 2000). Considering these points and the bandwidth used in other research projects, the bandwidth in this research will be set to 60 rad/s. The actuator properties used in this research are summarised in Table 7.1.

7.2.2. Feedback loop and FCC dynamics

As mentioned before, the non-ideal flight control system model defined for the HIRM control system design problem by GARTEUR will be used for the control system analysis in this research. The processes which are considered and the corresponding transfer functions are listed below in Table 7.2.

Table 7.1: Actuator properties of the F-16 model (Russel, 2003).

Control effector	**Unit**	**Min.**	**Max.**	**Rate limit** [*/s]	ω_n [rad/s]
Elevator	deg	-25	25	± 60	60
Aileron	deg	-21.5	21.5	± 80	60
Rudder	deg	-30	30	± 120	60
thrust	N	4448	84516	± 44482	1

Table 7.2: Non-ideal Feed-forward and feedback process transfer functions (Muir, 1998).

Process	**Symbol**	**Transfer function**
Air data sensors	$S_{Air}(s)$	$\frac{1}{0.02s+1}$
Anti-aliasing filter (at 100 Hz FCC frequency)	$H_{AA}(s)$	$\frac{1}{0.00001013s^2+0.0032s+1}$
Rate and acceleration sensors	$S_{RA}(s)$	$\frac{0.00019s^2-0.00173s+1}{0.000704s^2+0.0401s+1}$
Averaging on rate and acceleration	$H_{Ave}(s)$	$\frac{-0.00208s+1}{0.00417s+1}$
Computational delay	$H_{CD}(s)$	$\frac{-0.0062s+1}{0.0062s+1}$
D/A converter	$H_{DA}(s)$	$\frac{-0.00208s+1}{0.00417s+1}$

The bandwidth of the sensor models are all between approximately 30 and 50 rad/s. As this is rather low for sensor dynamics alone, it is supposed that these models include filter dynamics already. Therefore, no extra filter dynamics will be added to these feedback paths.

The INDI control law also requires feedback of the angular acceleration. Possible methods to obtain this feedback are linear accelerometers (Bacon and Ostroff, 2000), prediction filters (Sieberling et al., 2010) or using differentiation of the filtered angular rate (Smeur et al., 2016). Furthermore, due to the development in angular accelerometers it is possible to to directly obtain this feedback (Keijzer et al., 2019). Using these sensors it has been shown that the control performance remains the same, but the fault tolerance performance is improved. Assuming that future high-performance military aircraft could be equipped with these sensors as well, this research will suppose that an angular accelerometer is present in the control system. This means that a model for the angular acceleration feedback dynamics is necessary as well. In this FCS model the assumed non-ideal elements of the angular acceleration feedback path are the filter dynamics, averaging dynamics, computational delay and delay due to analogue to digital conversion. From data-sheets of commercial off-the-shelf angular acceleration sensors[1][2], it was found that the bandwidth is in the order of 100 - 200 Hz. This bandwidth is significantly larger than that of the control system itself. Consequently, the dynamics of the sensor itself are assumed to be negligible and the sensor dynamics will be left

[1]Jewell Instruments, *ASB Series Angular Accelerometer*, `http://jewellinstruments.com/wp-content/uploads/2012/07/Jewell_SC_Data-Sheet_ASB-Series-Angular-Accelerometer_Dec-2013.pdf`

[2]Columbia Research Laboratories, *Angular Accelerometers*, `https://www.crlsensors.com/prodDocs/sr-207rfr.pdf`

out of the system model. The filter dynamics will be modelled as a second order low-pass filter as shown in Eq. (7.6). This architecture has been chosen because there are no design requirements and it has been shown to be applicable in Keijzer et al. (2019). The natural frequency and damping of this filter are selected to be 30 rad/s and 1, respectively. This bandwidth is the lowest possible bandwidth before significant performance degradation was observed.

$$H_f(s) = \frac{\omega_f^2}{s^2 + 2\zeta_f \omega_f s + \omega_f^2} \tag{7.6}$$

7.2.3. Complete non-ideal control system

Combining all previously described non-ideal elements of a control system into a block diagram gives the result of Figure 7.3. Please note that this control law is already designed taking into account synchronisation of the actuator and pitch acceleration signals. This is performed by adding the models of the non-ideal elements of the angular acceleration feedback path to the actuator deflection measurement as 'artificial synchronization'. There are more advanced methods to perform the synchronization, such as the average square difference function (ASDF) or the average magnitude difference function (AMDF) (van 't Veld, 2016; Jacovitti and Scarano, 1993). However, this would significantly increase the control system design complexity, which is not desired at this stage of the analysis. As shown in Smeur et al. (2016) it is also possible to synchronise the signals using the filter dynamics in the feedback path of the actuator signal. As this is a practical and validated method it will be used in the current control design as well.

7.3. Analysis setup

This section elaborates on the test cases used for the analysis of the non-adaptive INDI control law performance. Furthermore, the flight condition on which the aircraft is trimmed in the simulation and other relevant simulation settings are discussed.

7.3.1. Test cases

The test cases will be quite straight forward. To analyse the robustness against model mismatches the simulations will be performed for having the correct value of the control effectiveness, a 30% underestimation and a 30% overestimation. The effect of the model mismatch will be evaluated for two different airframe static stability conditions. As high-performance military aircraft, such as an F-16, should also be able to operate at negative static margins (SM) the effects of model mismatches will also be considered for such conditions. Consequently, the effect of model mismatches will be analysed at a 5% positive static margin and at a 5% negative static margin. A summary of the test cases is presented in Table 7.3.

Table 7.3: Test cases for the model deviation robustness analysis.

Variable	**Unit**	**Value**					
SM	%	+5			-5		
Cont. eff. dev.	%	0	-30	+30	0	-30	+30

7.3.2. Control system/simulation specifications

Next to the elements of the control system discussed above there are some other practical aspects regarding the controller design and simulation which are used in the analysis. These aspect will be covered here.

First of all, the update frequency of the FCC. In real-world control systems this update frequency

is limited. Therefore, this simulation will also be performed using a limited update frequency. Other research projects using a modern high-performance military aircraft have been consulted to find an appropriate value (Knapp et al., 2018; Muir, 1998). From these research projects it became clear that update frequencies between 64 and 100 Hz are used. Assuming that the computation power of FCC's has advanced during the past decades it will be assumed in this research that a flight control update frequency of 100 Hz could be achieved.

Table 7.4: Aircraft system properties and trim condition for both stable and unstable aircraft dynamics.

Simulation variable	Unit	Stable AC	Unstable AC
Aircraft properties			
mass	kg	9295	9295
CG position	$\bar{c}$	0.26	0.36
Static margin	%	5	-5
I_{xx}	kg· m^2	12875	12875
I_{yy}	kg· m^2	75674	75674
I_{zz}	kg· m^2	85552	85552
I_{xz}	kg· m^2	1331	1331
Flight condition			
Altitude	m	1500	1500
Velocity	m/s	150	150
Mach number	-	0.45	0.45
Control setting			
Thrust	N	10026	8487
δ_e	deg	-3.27	-0.46
δ_a	deg	0.00	0.00
δ_r	deg	0.00	0.00
Aerodynamics angles			
α	deg	3.15	2.81
β	deg	0.00	0.00
Aerodynamic model			
$C_{m_{\delta_e}}$	-	-1.031e-2	-9.551e-3

Furthermore, the analysis will be performed for one flight condition starting from steady, wings-level flight. As mentioned in the introduction the model used in this research is considered valid up to a Mach number of 0.6. Consequently, a Mach number below 0.6 will be chosen. The altitude is selected such that the trim conditions result in low angle of attack. An example of a flight conditions which complies to both preferences is at an altitude of 1500 m and a velocity of 150 m/s. A summary of this trim point and the control system parameters for both test cases is given in Table 7.4 and 7.5.

Table 7.5: Control system properties.

Controller parameters	unit	Value
Proportional gain	-	5
Integral gain	-	5.3
Ang. acc. filter parameters		
bandwidth	rad/s	30
damping ratio	-	1

The control gains during the simulations are set to 5 and 5.3 for the proportional and integral

gain, respectively. These values have been found from manually finding a solution where overshoot was within reasonable limits and the damping was considered adequate. Although, the control gain is not determined from flying quality requirements, these values are deemed appropriate for the current analysis.

7.4. Numerical simulation

This section will treat the analysis results of non-adaptive INDI control design for the ideal and non-ideal control system. First, the analysis will be performed for the ideal INDI control system. As will become clear from the results presented later on, this case will show that the ideal INDI controller is very robust against control effectiveness model mismatches. However, it will be shown that this robustness will significantly decrease when realistic control system elements are taken into account in the simulation. This is a result which is in line with the flight test results of Smeur et al. (2016) where it was shown that a change in inertia, unknown to the controller, resulted in reduced control performance.

7.4.1. Ideal system

The results of the robustness analysis for the ideal control system will be presented and discussed here. What is meant by "ideal" in this analysis is the absence of signal bandwidth limiting and delay inducing processes, such as sensors, filters and computers, in the control loop. The ideal control system is the system model as discussed in section 7.1. For this case it is allowed that the controller has a limited sampling time. As discussed in 7.3.2, the FCC sampling time is set to 0.01 s. The time-domain and frequency-domain plots are determined for the system shown in Figure 7.1 and for the test cases described in Table 7.3.

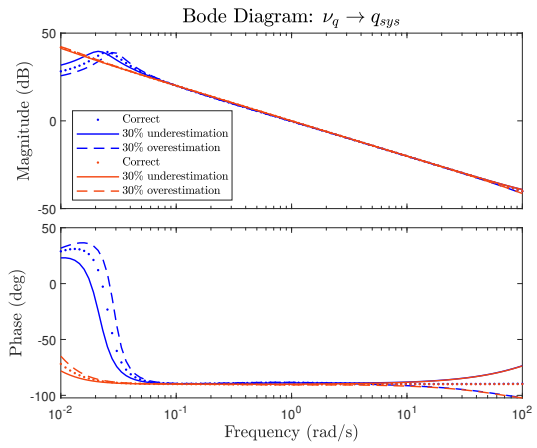

Figure 7.5: Inversion loop frequency response of the ideal control system for stable (blue) and unstable airframe dynamics (orange).

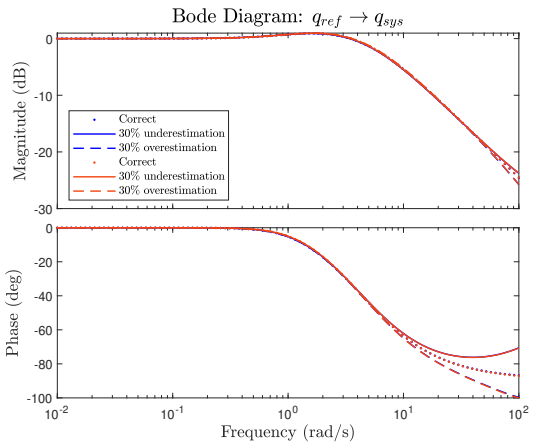

Figure 7.6: Closed-loop INDI frequency response of the ideal control system for stable (blue) and unstable airframe dynamics (orange). Blue and orange lines are overlapping.

The results for the model deviation analysis are presented in figure 7.5 to 7.8. Figure 7.5 shows the inversion loop frequency response for varying control effectiveness model deviations and airframe dynamics. Furthermore, Figure 7.6 shows the closed control loop frequency response for the same variations in the model and airframe dynamics.

Analyzing Figure 7.5 it can be seen that the airframe stability does not significantly affect the inversion loop dynamics within bandwidth of 0.1 and 10 rad/s. However, for frequencies below this region a clear difference is visible for changing airframe stability. Here, the stable airframe dynamics clearly deviates from the pure integrator dynamics, while the unstable airframe dynamics response

remains relatively close. Figure 7.7 shows that this is also a consequence of the limited sampling time of the flight control computer. In Chapter 2 an important assumption was made by neglecting the terms related to Δx based in the time-scale separation of the state and the control input. Here, it can be seen that this assumption slowly becomes violated. Though, considering the closed-loop response in Figure 7.6 these low-frequency deviations do not results in a different closed-loop response at the same frequencies.

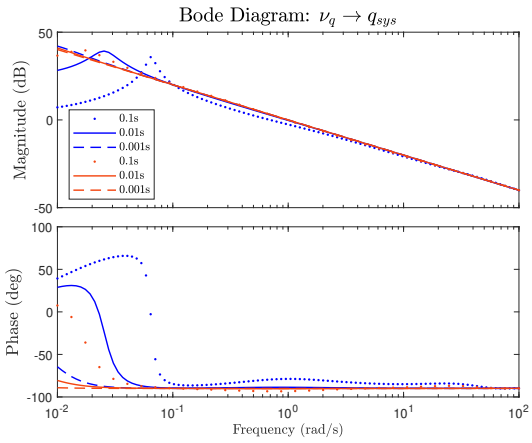

Figure 7.7: Inversion loop dynamics for different values of the FCC sampling time for stable (blue) and unstable airframe dynamics (orange).

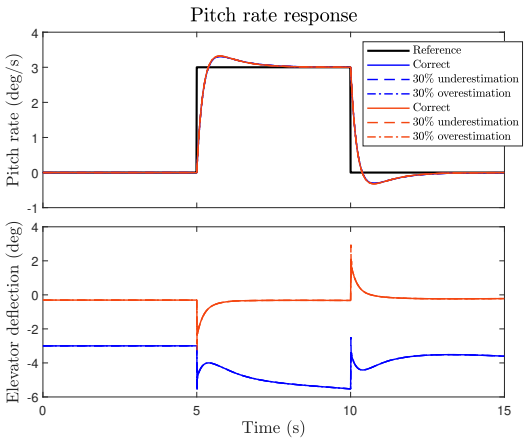

Figure 7.8: Time-domain pitch rate response for stable (blue) and unstable (orange) airframe dynamics following a block reference pitch rate signal.

The effect of model deviation on the inversion loop response for both stable and unstable airframe dynamics are similar for frequencies above 0.1 rad/s. Below this frequency the effect of model deviation affects the stable airframe inversion loop response more than the unstable airframe inversion loop response. Though, this again does not affect the closed-loop response. For frequencies above 10 rad/s an underestimation of the control effectiveness results in less phase shift and an overestimation in more phase shift. This could be a consequence of the larger incremental control deflection resulting from the underestimation. Due to this the control deflection overshoots the desired deflection which induces a larger pitch acceleration. As the control system is not limited by actuators this effect could therefore lead to less phase shift at high frequencies. For an overestimation of the control effectiveness this will be the other way around. This will result in smaller incremental control deflections which lead to a slower convergence to the desired control deflection and therefore slower convergence to the desired pitch acceleration and so on. Furthermore, the change in frequency response is also dependent on the flight control sampling time. A Lower sampling time results in better observations of the higher frequencies in the feedback signal and therefore allow for better control of these frequencies. Despite this difference, the time domain response will probably not deviate significantly from the time response where the correct control effectiveness model is used. This is because the magnitude for 10 rad/s and higher is already below -10 dB.

Figure 7.8 shows the system pitch rate response for all test cases. During the simulation the aircraft was commanded to follow a block signal reference as indicated by the black line. Despite the overshoot, it was found that for all test cases the response was similar as already predicted by the result shown in figure 7.6.

These results show that an INDI based control system without actuators, sensors and filters is robust against control effectiveness model uncertainties. Consequently, the necessity of adding an adaptive law to maintain constant handling qualities does not follow clearly from analysing an INDI control system which is close to ideal. However, as will be shown later on, including extra non-ideal

control system dynamics into the control loop will increase the sensitivity for model mismatches.

7.4.2. Non-ideal system

The analysis results for the model mismatch sensitivity study including non-ideal control system elements are shown and discussed in this section. As discussed before, the flight controller update frequency is set to 100 Hz. The non-ideal analysis the actuator bandwidth is 60 rad/s, the proportional and integrator gains are 5 and 5.3, and the filter bandwidth is set to 30 rad/s with a damping ratio of 1. Furthermore, using the values and the dynamics of the actuators, sensors and computers of section 7.2.2, the results of figure 7.9 and 7.10 are obtained.

Comparing the non-ideal control system inversion loop results to the results obtained for the ideal control system, it can be seen that for frequencies below 0.1 rad/s the stable airframe response is very similar. However, the unstable airframe response has changed and has become similar to the stable airframe dynamics response. This can be explained by the fact that the feedback signal has been delayed. This results in inversion mismatches as has been proven in Sieberling et al. (2010). Though, these differences are not influencing the closed-loop response. Furthermore, for frequencies between 0.1 rad/s and 10 rad/s it can be seen that the extra control system elements slightly affect the magnitude and phase of the stable airframe inversion loop. Lastly, the effects of the added control system elements become most apparent for frequencies above 10 rad/s. Here it can be seen that the gain decreases faster and the phase shift is significantly increased. This is expected as the extra elements are decreasing the bandwidth of the control loop and introduces extra delay of which the effects become more dominant for higher frequencies.

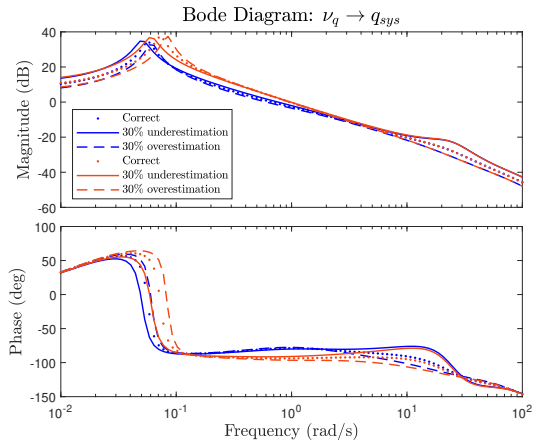

Figure 7.9: Inversion loop frequency response of the non-ideal control system for stable (blue) and unstable (orange) airframe dynamics.

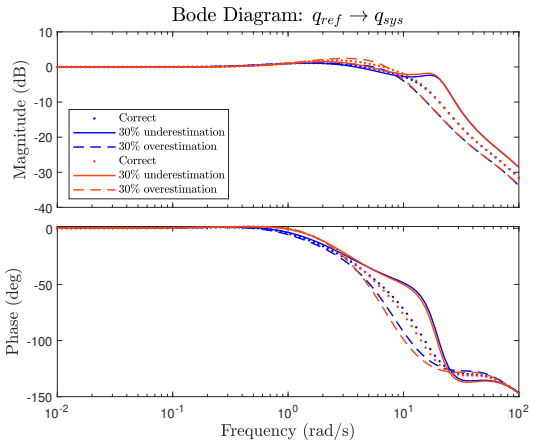

Figure 7.10: Closed-loop INDI frequency response of the non-ideal control system for stable (blue) and unstable (orange) airframe dynamics.

In Figure 7.10 it could be observed that there is a small difference between the closed loop response of stable and unstable airframe dynamics. Though, considering that the control system gains are not obtained from handling quality requirements, it cannot be concluded whether this will also occur for a properly tuned control system. Nevertheless, if the difference is still present for a proper tuned controller, it might be required to adjust the controller settings during flight to compensate for the changing aircraft stability.

Furthermore, considering this control system, it can be seen that the model mismatch has more effect on the system response for the non-ideal case. It can be seen in Figure 7.10 that an underestimation results in some of the higher frequencies having a larger gain. Consequently, an extra high frequency response could be observed in the time-domain response as shown in Figure 7.12. On the other hand, an overestimation results in more overshoot, which essentially means that the

controller becomes more sluggish.

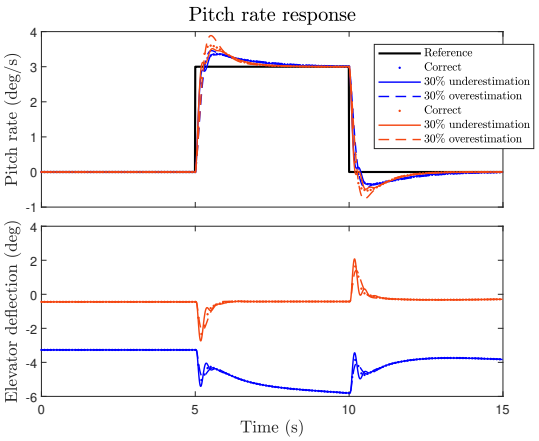

Figure 7.11: Time-domain pitch rate response of the non-ideal control system for stable (blue) and unstable (orange) airframe dynamics..

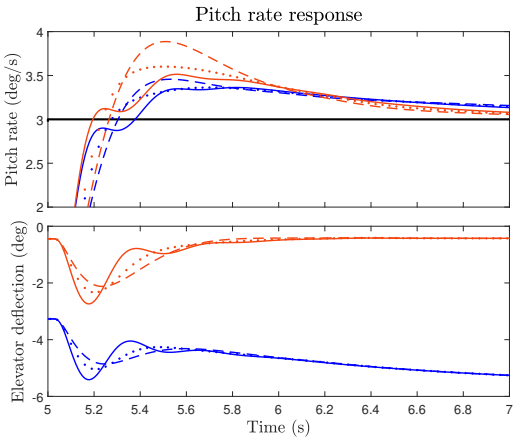

Figure 7.12: Zoomed in time-domain pitch rate response of the non-ideal control system for stable (blue) and unstable (orange) airframe dynamics.

The detailed changes in the frequency response cannot be generalized as the controller is not designed according to handling quality requirements. Though, it can be concluded that introducing realistic control system processes results in higher sensitivity to mismatches in the control effectiveness model. In the upcoming chapters it will be shown that this problem can be handled using adaptive laws which adjust the model parameters on-line to maintain an accurate estimate and therefore prevent control performance degradation.

7.5. Conclusion

From the analysis performed in this chapter it can be concluded that an ideal INDI based control system is very robust against model uncertainties. However, it has been shown that this robustness will reduce when models of real-world elements, such as actuators, filters and computational delay, are included in the system model. Therefore, the need for adaptive control becomes more apparent for non-ideal control systems. Consequently, the non-ideal control system model will also be used for the evaluation of the adaptive INDI control laws.

Using the non-ideal control system model it was shown that the pitch rate and elevator response become more oscillatory for a 30% underestimation of the control effectiveness model. A 30% overestimation results in a slower control response which induces slightly more overshoot. Considering these results it can be concluded that there is a need for an accurate model of the control effectiveness.

8

Adaptive INDI control law analysis

The evaluation of the adaptive INDI control laws designed in Chapter 6 will be performed in this chapter. The tracking performance, control activity and parameter estimation performance will be evaluated using the metrics selected in Chapter 5. First of all, the setup of the analysis will be treated in section 8.1. In this section the simulated system deviation will be covered together with the tracking objectives. Then the simulation results are presented and discussed separately for each adaptive control law in section 8.2. Then a study concerning the sensitivity of the results obtained from simulations will be performed in section 8.3. Furthermore, this section will also treat the comparison between the adaptive laws. Lastly, the main findings will be briefly recapped in the conclusion in section 8.4

8.1. Analysis setup

As shown in Chapter 4, the control effectiveness could be affected by errors in the aerodynamic model, CG shifts and inertia changes. In the analysis performed in this chapter all these factors will be varied simultaneously to evaluate the parameter estimation methods developed in Chapter 5. The variations in CG and inertia will be gradual because these also change gradually during normal flight. Furthermore, the aerodynamic model deviation will be set as an initial offset. This is done as it is assumed that the aerodynamic model for $C_{m_{\delta_e}}$ deviates at the flight condition.

To evaluate the adaptive control laws, two test cases will be set up. In both tests the same aerodynamic modelling error and the same CG shift and inertia change will be applied. The applied modelling error, CG shift and inertia change are shown in Table 8.1. The arrows in the table indicate that the simulated cause for model deviation is time-varying and changes during the first 100 seconds and that the simulation is initialized at the values left from the arrow. This time interval has been chosen because simulating the actual time for such a deviation to occur due to fuel consumption, will make the experiments impractical. From Table 8.1 it can be seen that the CG and inertia are time-varying and the aerodynamic modelling error is already present at the start of the simulation. Lastly, during the simulation the total mass remains constant.

The difference between the test cases will be the tracking objective (TO). Each TO will take 200 seconds in which the tracking task of Figure 8.1 will be repeated a different amount of times. The first tracking objective consist of continuously repeating the tracking task and in the second the tracking task will only be repeated at 0, 67 and 140 seconds. In between the execution of the tracking tasks, the reference signal will be zero. The second tracking objective is used to evaluate the difference in parameter estimation performance for a significant decrease in PE conditions.

Table 8.1: CG and inertia variations, and aerodynamic model deviation for the adaptive control law evaluation test case. The arrows in the ' deviation' column indicate that the deviation is time varying. The time-varying deviations will occur within the first 100 seconds of the simulation.

Variable	Unit	deviation
SM	%	-5 → 5
CG	$\bar{c}$	0.36 → 0.26
I_{yy}	kg· m^2	75674 → 68107
$C_{m_{\delta_e},nom}$	deg^{-1}	0.8·$C_{m_{\delta_e},act}$

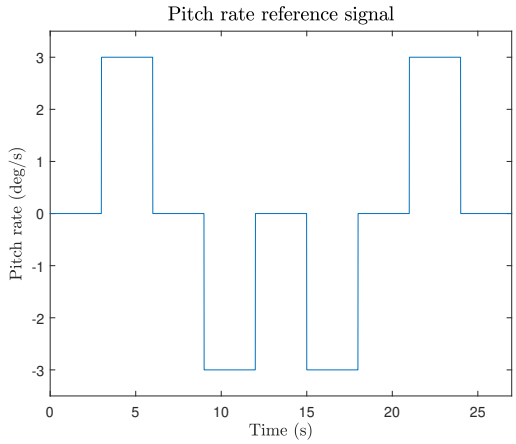

Figure 8.1: Test case pitch rate reference signal. This signal will repeat during the simulation.

8.2. Numerical simulation

In this section the results of the numerical simulations of the test cases are presented. In these simulations the non-ideal system as described in Chapter 7 is used. Furthermore, the values of $C_{m_{\delta_e}}$ used in the simulations is constant. It can be seen in Figure 8.4 the value of $C_{m_{\delta_e}}$ contains some oscillations on top of the change due to the CG shift. However, as the oscillations are mostly within one percent of the actual value, the model inaccuracy is regarded negligible compared to the model deviation due to the CG shift, inertia change and aerodynamic model error offset. Therefore, the use of a constant is deemed accurate enough for the current analysis.

For each adaptive control law the simulation will be performed for multiple values of the adaption gain or forgetting factor to observe the effect on the estimation performance. The results of the multiple simulations give the possibility to inspect some important aspects of the adaptive control law. First of all, it is possible to analyse whether the adaptive INDI control law has the ability to achieve higher performance than the baseline INDI control law. Furthermore, it is possible to observe how the control performance changes for the different values of the adaption gain or forgetting factor. Moreover, using a broad domain it is possible to investigate whether the effect of decreasing or increasing values result in a gradual roll-off or result in a sudden large drop in control performance. The former behaviour is preferred from a control design perspective as this increases the reliability of the adaptive control law.

The tracking performance of each adaptive law will be analyzed according to the metrics defined in Chapter 5. For this analysis a reference model is required. This reference model is defined as the ideal performance which could be obtained if the dynamic inversion would be perfect and the inversion loop could be modelled as a perfect integrator. This transfer function is show is Eq.

(8.1). Here, q_r is the commanded pitch rate from the pilot. Furthermore, the performance of the parameters estimation will be assessed. This will be done using similar metrics such as the maximum and the RMS of the error between the estimated and actual control effectiveness, and the cumulative standard deviation of the estimated parameter.

$$\frac{q_m}{q_r} = \frac{5.0s + 5.3}{s^2 + 5.0s + 5.3} \tag{8.1}$$

8.2.1. Non-adaptive INDI

First the performance of the baseline INDI pitch rate controller will be analysed for the test cases as defined in the previous section. The effect of the increasing model error on the pitch rate and elevator deflection response will be shown. Furthermore, the baseline values of the performance metrics as defined in Chapter 5 will be determined. These can be used to evaluate how much the adaptive controller will improve the performance of the controller. The figures shown in this section are the result from tracking objective 1. This is done to limit the amount of figures in this section. Furthermore, the visual results of the tracking are quite similar despite the difference in tracking objectives.

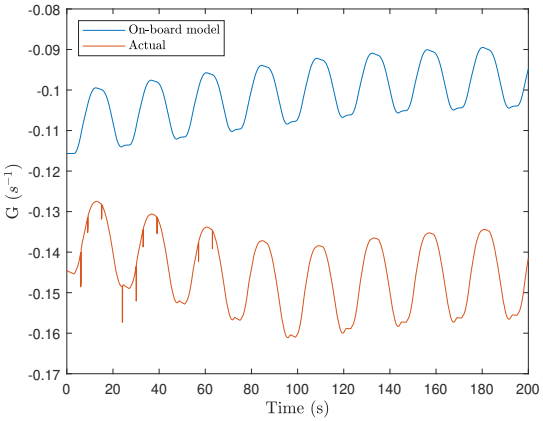

Figure 8.2: Control effectiveness during the simulation.

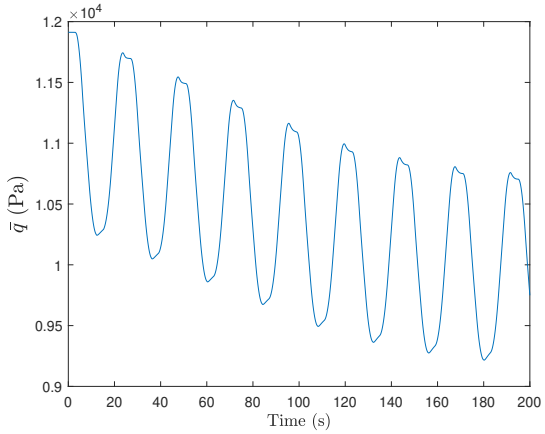

Figure 8.3: Dynamic pressure during the simulation.

The envelope of the control effectiveness of the actual aircraft and the on-board model can be seen in Figure 8.2 and 8.4. It can be seen that the actual control effectiveness becomes more negative until 100 seconds. This is due to the forward shifting CG and decreasing inertia. Furthermore, the extra oscillation which is visible in the control effectiveness envelope is due to the change in dynamic pressure as can be seen in Figure 8.3. The changing dynamic pressure is a result of the changing velocity. As the control design is only focused on rotational control, the velocity, and consequently the thrust, is not controlled during the simulation. This means that only the trim thrust is used, which results in a velocity decrease when pitching upward and increase when pitching downward. Next to the oscillations in the dynamic pressure due to the pitching motion, there is also an decreasing trend. This is due to the decrease in velocity which is a consequence of the extra drag induced due to the larger elevator deflection required to control the aircraft at a static margin of 5%. This overall decrease in dynamic pressure decreases the overall control effectiveness as can be seen when inspecting the on-board model control effectiveness curve in Figure 8.2. Furthermore, there are a few spikes visible in the curve of the actual control effectiveness during the first 80 seconds. This is due to the fact that the elevator deflection becomes greater than zero at these moments. This can be verified by inspecting Figure 8.7 and 8.4. Moreover, Figure 8.4 shows that the value of

$C_{m_{\delta_e}}$ becomes approximately 8% larger due to the CG shift. The other oscillations in the value are a consequence of the change in angle of attack. As the angle of attack does not become large during the simulation, the influence is still small. Lastly, as defined in the test case, the on-board model starts with an underestimation in the aerodynamic model of 20%. This results in the initial offset as visible in Figure 8.2. All together, these deviations result into an increase in control effectiveness of approximately 50%.

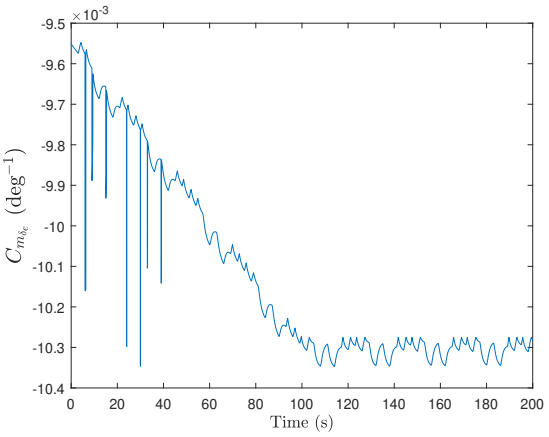

Figure 8.4: Change in the value of $C_{m_{\delta_e}}$.

The effect of the increased deviation of the on-board control effectiveness can be seen in Figure 8.5 till 8.8. The 'reference' curve in Figure 8.5 and 8.6 is the pilot input and the 'ideal' response is the output of the ideal system to the reference signal input. The dynamics of the ideal system is described by Eq. (8.1). Furthermore, the curve labeled with 'actual' is the actual system response to the reference signal input. The initial offset due to the aerodynamic modelling error already induces an additional small amplitude higher frequency oscillation in the pitch rate response. These oscillations become worse over time as can be seen in Figure 8.6. As shown in Chapter 7 the additional oscillations are a consequence of the on-board control effectiveness model being significantly lower than the actual control effectiveness. This results in too large elevator deflection increments which result in elevator deflection overshoot. This leads to oscillations in the elevator response, see Figure 8.8. In this case the oscillations are large enough that they are able to affect the pitch rate response and therefore decrease the control performance.

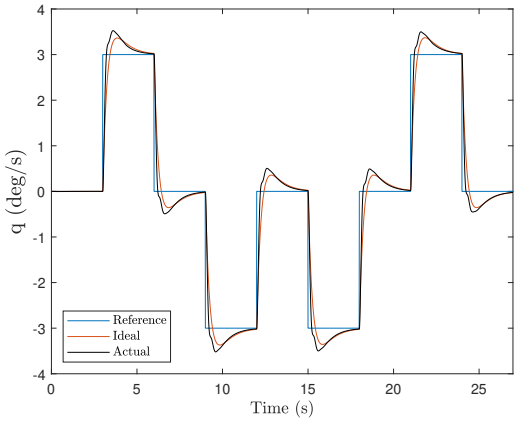

Figure 8.5: Pitch rate response of the non-adaptive INDI pitch rate controller for the first 27 seconds.

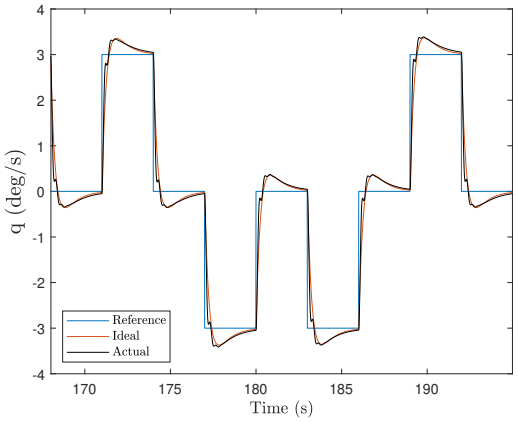

Figure 8.6: Pitch rate response of the non-adaptive INDI pitch rate controller for the last 27 seconds.

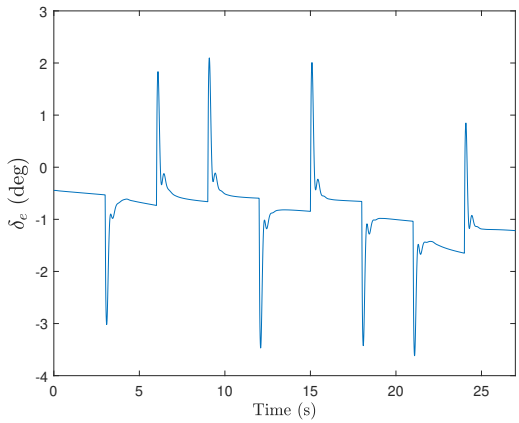

Figure 8.7: Elevator response of the non-adaptive INDI pitch rate controller for the first 27 seconds.

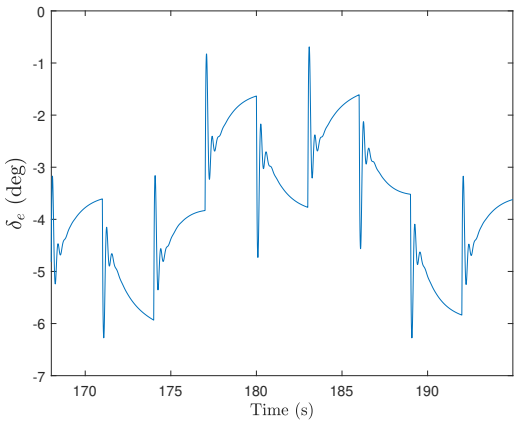

Figure 8.8: Elevator response of the non-adaptive INDI pitch rate controller for the last 27 seconds.

Lastly, the baseline values of the control performance metrics are shown in Table 8.2. These values will be used to normalize the results in the assessment of the adaptive control laws. This will be done to be able to compare the performance of the different Tracking objectives. As can be seen in Table 8.2 the values differ. This is a consequence of the difference between the tracking objectives. The second tracking objective contains less variations which makes it easier to follow. Therefore, most metric results are lower than the results obtained in the first tracking objective.

Table 8.2: Baseline control performance metric values for both tracking objectives TO-1 and TO-2.

Metric	TO-1	TO-2
$\|e\|_{\mathcal{L}_\infty}$	0.86	0.86
$\|e\|_{\mathcal{L}_2}$	2.59	1.62
$RMS(e)$	0.18	0.12
$CMSD(\delta_e)$	1372	489

8.2.2. Recursive Least Squares adaptive INDI

The performance of the RLS-AINDI control law depends on the value of the forgetting factor, λ, and the initial setting of the parameter covariance matrix, P_0. As discussed before, the short-term adaption abilities of the RLS parameter estimator are high when the values of the P are high. However, in this simulation it is assumed that the adaptive law was already activated before the simulation started and the P had already converged. This assumption will be made because the design of the adaptive controller does not include an algorithm which activates the adaptive law or resets P. Therefore, the adaptive law is assumed to be activated at all times and the values of P are only changed by the RLS method itself.

Consequently, $0.1 \cdot I$ was chosen for P_0. Furthermore, the forgetting factor is normally selected between 0.98 and 1. Low values of λ are capable of faster adaption and therefore in following fast system changes. However, lower values also increase the necessity for PE. Consequently, more information should be present in the reference signal to maintain adequate performance of the estimation. If the amount of information is not sufficient, the estimation is more likely to drift and oscillate, which decreases the estimation performance.

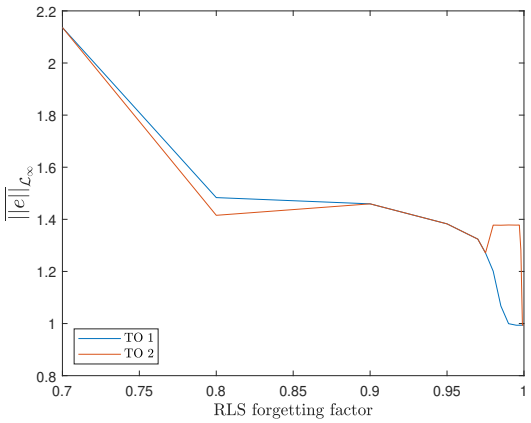

Figure 8.9: Normalized $\mathcal{L}_\infty$-norm of the deviation from the reference model as a function of the RLS forgetting factor.

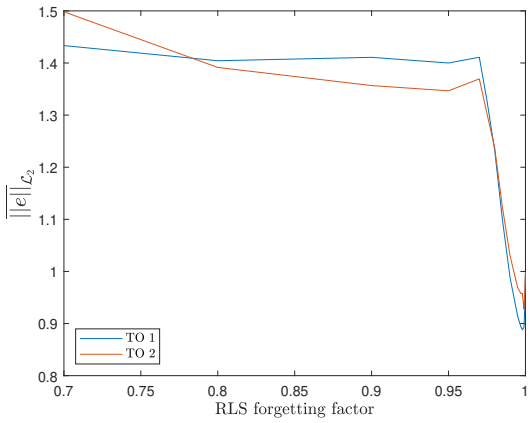

Figure 8.10: Normalized $\mathcal{L}_2$-norm of the deviation from the reference model as a function of the RLS forgetting factor.

Figure 8.9 and 8.10 show the normalized values of $\|e\|_{\mathcal{L}_\infty}$ and $\|e\|_{\mathcal{L}_2}$ as a function of the forgetting factor for both tracking objectives. The normalization is done with respect the to baseline control law result. Simulations have been run for forgetting factor values between 0.7 and 1.0. Considering the common lower boundary of 0.98, a value of 0.7 is very low. Though, this large range was chosen to show how the control performance changes for low values of the forgetting factor. For both tracking objectives it can be seen that $\overline{\|e\|}_{\mathcal{L}_\infty}$ and $\overline{\|e\|}_{\mathcal{L}_2}$ remain bounded. This means that the controller did not become unstable despite the very low value of the forgetting factor or significant decrease in excitation during the second tracking task. Furthermore, it can be seen that the degradation of the performance due a too low forgetting factor does not result in a drastic decrease in tracking performance. Considering control system design, this is a preferable characteristic. Knowing this characteristic the remainder of the analysis will focus on the metric results for which the forgetting factor is between 0.98 and 1.0.

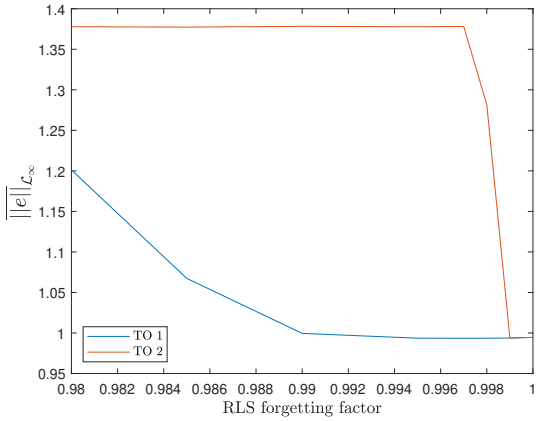

Figure 8.11: Normalized $\mathcal{L}_\infty$-norm of the deviation from the reference model as a function of the RLS forgetting factor.

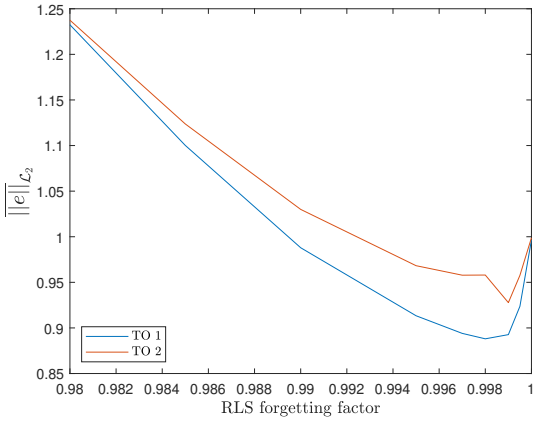

Figure 8.12: Normalized $\mathcal{L}_2$-norm of the deviation from the reference model as a function of the RLS forgetting factor.

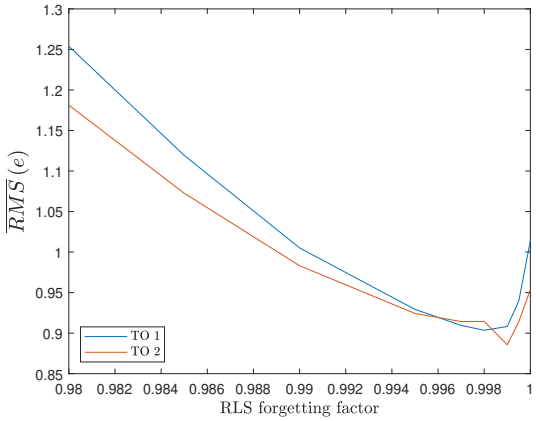

Figure 8.13: Normalized RMS of the deviation from the reference model as a function of the RLS forgetting factor.

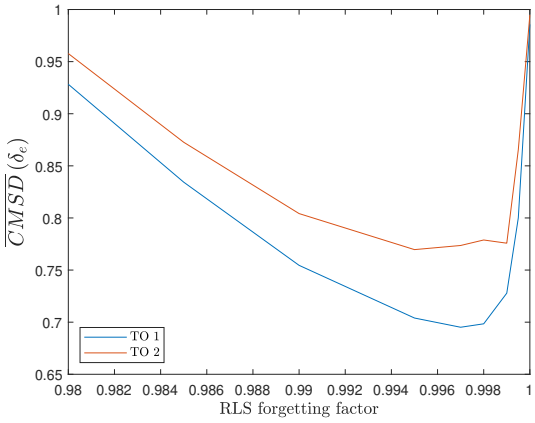

Figure 8.14: Normalized CMSD of the elevator deflection as a function of the RLS forgetting factor.

Figure 8.11 till 8.14 show the normalized results of the tracking performance and control activity metrics for forgetting factors between 0.98 and 1.0. Considering the results for TO-1, it is possible to improve on the baseline controller using the RLS parameter estimator in the adaptive control law. Though, the performance is also dependent on the amount of excitation in the reference signal as is shown by the results of TO-2. This is especially visible in Figure 8.11 and 8.14. The values of $\overline{\|e\|}_{\mathcal{L}_2}$ and $\overline{RMS}(e)$ seem to be less sensitive. This indicates that the oscillations and steady state values of e are not very sensitive to a decrease in excitation.

Looking at the parameter estimation performance in Figure 8.15 till 8.17, it can be seen that the parameter estimation is strongly affected by the decrease in excitation. The maximum deviation from the actual control effectiveness, $\|e_G\|_{\mathcal{L}_\infty}$, already increases for a forgetting factor below 0.999. Furthermore, the maximum deviation is still finite which means that the decrease in excitation did not results into instability of the parameter estimation.

Next to the maximum deviation, the values of $\text{RMS}(e_G)$ show that the reduction in excitation leads the significant deviation from the actual control effectiveness. Furthermore, the fact that the values of $\text{CMSD}(\hat{c})$ in TO-2 are similar to the ones obtained in TO-1 indicates that the estimation activity is almost equal. This should not be the case as TO-2 contains less excitation. Therefore, it can be concluded that the parameter estimation is oscillating. This is also visible in Figure 8.18 which shows the development of $\hat{c}$ with a forgetting factor of 0.995 for both TO-1 and TO-2. This figure shows what happens to the parameter estimation using the RLS algorithm when the signals used for the estimation contain little information, e.g. a small amount or low amplitude frequencies. In these situations, the covariance matrix, P, is not significantly changed by the new data, but at each iteration it is multiplied by $\frac{1}{\lambda}$. As λ, the forgetting factor, is less than one, this means that the covariance matrix grows. This again results in an increasing value of the adaptive gain, K, which results in large corrections of the estimated parameter even when the error is small. Consequently, a certain uncontrolled behaviour appears in the parameter estimation as can be seen in Figure 8.18.

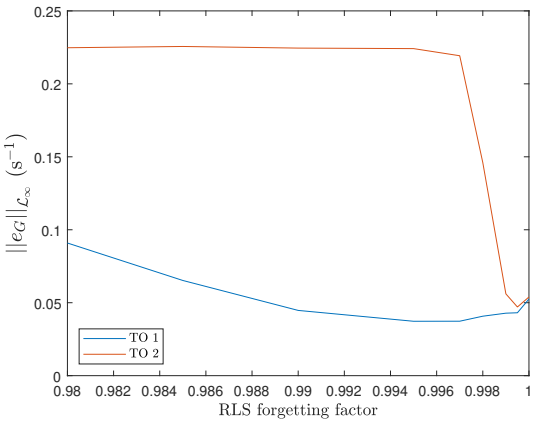

Figure 8.15: $\mathcal{L}_\infty$-norm of the control effectiveness model error as function of the RLS forgetting factor.

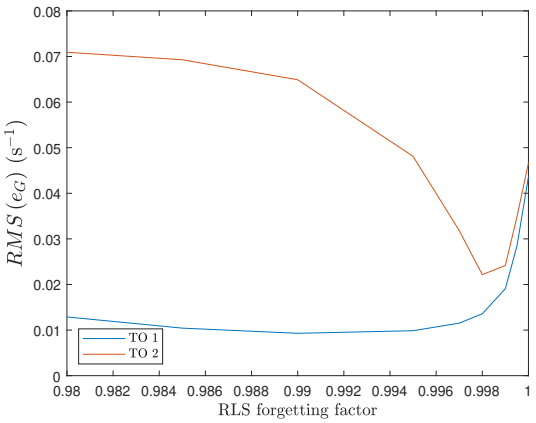

Figure 8.16: RMS of the control effectiveness model error as function of the RLS forgetting factor.

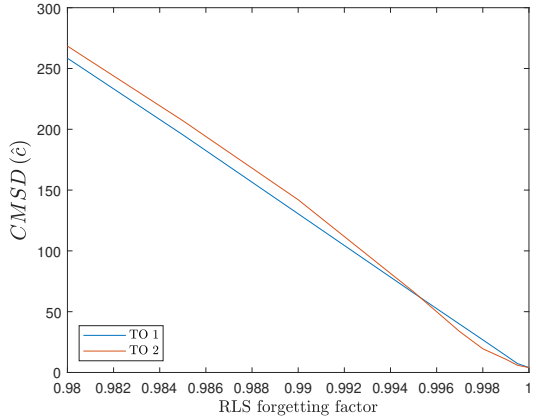

Figure 8.17: CMSD of the estimated correction factor as function of the RLS forgetting factor.

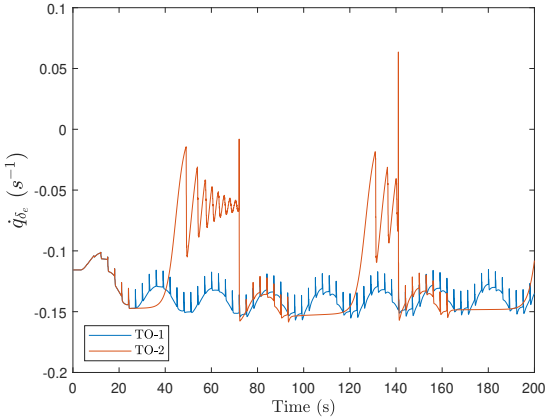

Figure 8.18: Estimated control effectiveness for TO-1 and TO-2. λ= 0.995.

The computational complexity will be determined from analysing the algorithm listed below. Each line has a certain amount of elementary mathematical operations which will be counted. Though, while counting the amount of parameters is regarded to be a variable amount. Consequently, it is possible to observe how the computational complexity grows for a growing number of parameters. It should be noted that the counting does not take into account algorithms which could speed up the process. Therefore, the resulting dependency on computational complexity is a worst case scenario. In this algorithm $\underline{\beta}(\underline{x})$ is a vector containing basis functions which can multiplied with $\underline{\hat{\theta}}$ to obtain the correction factor, $\hat{c}$. Although, the determined correction factor in the used in the previous analysis is a constant, this approach would have been applied if $\hat{c}$ would have had more dependencies. Using this definition of the variables, the worst case would grow as follows:

$$CC_{RLS}(n) = 9n^2 + 7n + 9 \tag{8.2}$$

Algorithm 1: Recursive Least Squares parameter estimation

input : $\delta_{e,k}$, $\delta_{e,k-1}$, $\dot{q}_k$, $\dot{q}_{k-1}$, $\bar{q}_k$, $C_{m_{\delta_e}}$, $\underline{\hat{\theta}}_k$, P_k, $\underline{x}$

initialization: $\underline{\hat{\theta}}_0$, P_0, λ, $\frac{S\bar{c}}{I_{yy}}$;

while $k \leq N$ **do**

$$z_{k+1} = \dot{q}_k - \dot{q}_{k-1};$$
$$\Delta\delta_{e,k} = \delta_{e,k} - \delta_{e,k-1};$$
$$\underline{\phi}_{k+1} = \underline{\beta}(\underline{x}) \frac{S\bar{c}}{I_{yy}} C_{m_{\delta_e}} \bar{q}_k \Delta\delta_{e,k};$$
$$e_k = z_{k+1} - \underline{\phi}_{k+1}^T \underline{\hat{\theta}}_k;$$
$$K_{k+1} = P_k \underline{\phi}_{k+1} \left(\lambda + \underline{\phi}_{k+1}^T P_k \underline{\phi}_{k+1}\right)^{-1};$$
$$\underline{\hat{\theta}}_{k+1} = \underline{\hat{\theta}}_k + K_{k+1} e_k;$$
$$P_{k+1} = \lambda^{-1}\left(P_k - K_{k+1} \underline{\phi}_{k+1}^T P_k\right);$$
$$\dot{q}_{\delta_e} = \frac{S\bar{c}}{I_{yy}} C_{m_{\delta_e}} \bar{q}_k \underline{\hat{\theta}}_{k+1}^T \underline{\beta}(\underline{x});$$

end

8.2.3. Least Mean Squares Adaptive INDI

The parameter that influences the adaptive abilities of the LMS-AINDI control law is the adaption gain μ. Increasing this value increases the correction response when there is a difference between the measured incremental pitch acceleration and the estimated incremental pitch acceleration. Too low values lead to slow convergence and too large values lead to overshoot and possibly instability. To observe how sensitive the tracking and parameter estimation performance is for different values of the adaption gain, multiple values have been analysed. The learning gain has been changed between 10 and 4600 and the corresponding results are shown in Figure 8.19 till 8.25. This range was found as from a adaptive gain of approximately 4600 the parameter estimation quickly becomes unstable. Although this characteristic is highly undesired for control law design, it can be seen that this value is relatively quite far from the optimal value which is somewhere between 50 and 500. Consequently, the adaptive law itself also has a significant gain margin.

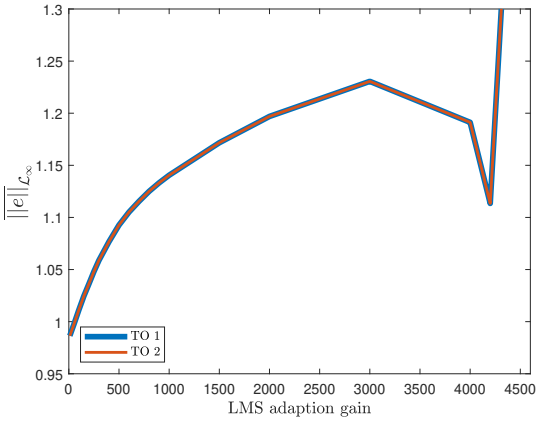

Figure 8.19: Normalized LMS learning gain versus the $\mathcal{L}_\infty$ norm of the tracking error.

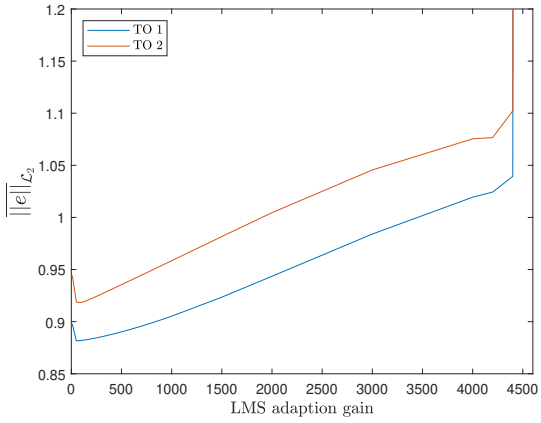

Figure 8.20: Normalized LMS learning gain versus the $\mathcal{L}_2$ norm of the tracking error.

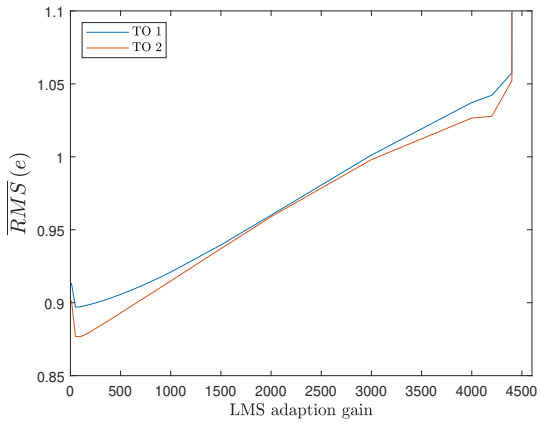

Figure 8.21: Normalized root mean square pitch rate tracking error.

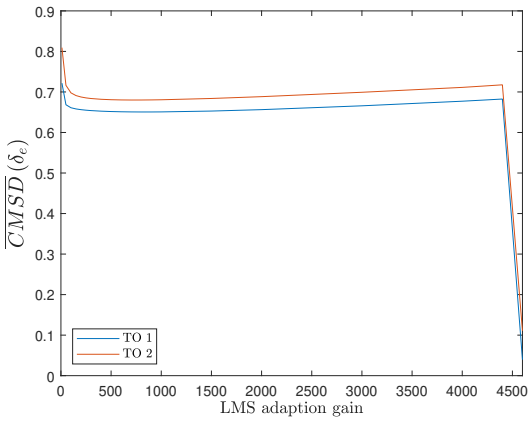

Figure 8.22: Normalized cumulative moving standard deviation of the elevator deflection during each simulation.

The results of the normalized tracking performance and control activity are shown in figure 8.19 till 8.22. First of all, it is clear that the LMS-AINDI control law is able to improve on the performance of the non-adaptive baseline control law as well. Though, the range for which this is possible depends on the metric. Furthermore, it can be concluded that this adaptive control law is very robust against changes in PE. This was already expected as the parameter estimation rule will only adjust the correction factor when the elevator deflection is changing. The result is a very similar response between TO-1 and TO-2. Regarding the results shown in Figure 8.19 it is quite interesting that in both TOs the values for $\overline{\|e\|}_{\mathcal{L}_\infty}$ are the same. This is a consequence of the fact that this deviation occurs during the first occurrence of the reference signal of Figure 8.1. For both TO-1 and TO-2 the first occurrence happens at the start and here the adaptive law converges exactly the same for both cases, which induces the same response. However, it can be concluded that the difference in PE conditions do not result in larger deviations between the reference model pitch response and the actual pitch response.

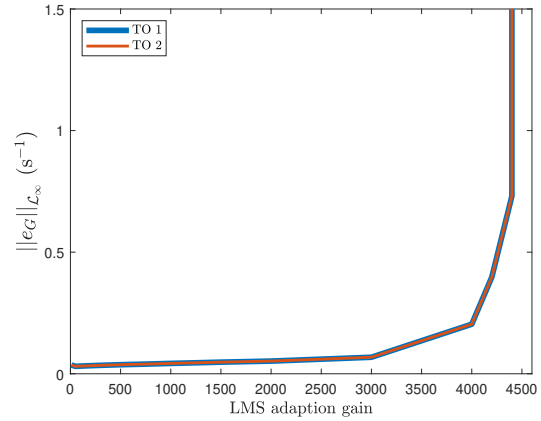

Figure 8.23: $\mathcal{L}_\infty$ norm of the control effectiveness error.

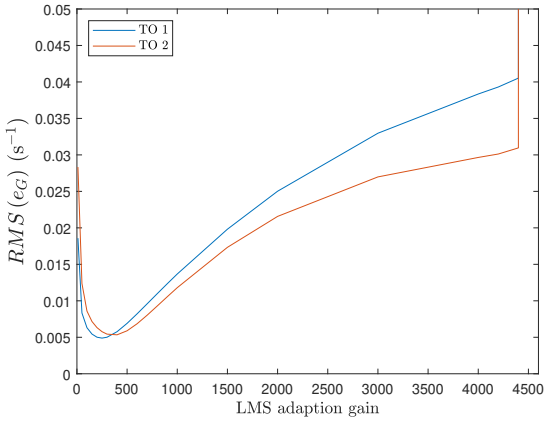

Figure 8.24: Root mean square of the control effectiveness error.

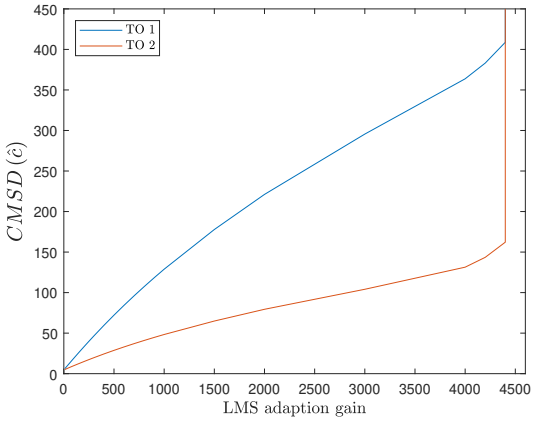

Figure 8.25: Cumulative moving standard deviation of the estimation correction factor.

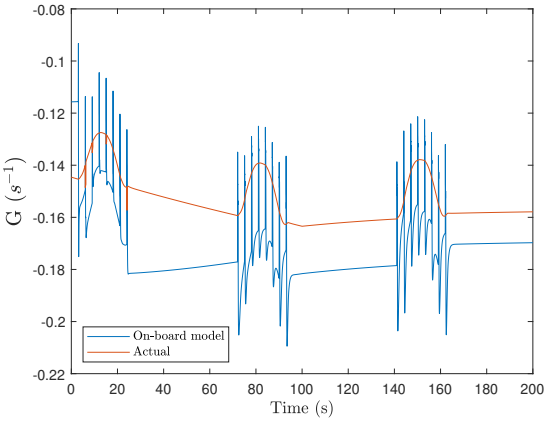

Figure 8.26: Control effectiveness development for simulating TO-2 with an adaption gain of 2000.

The parameter estimation performance results are shown in Figure 8.23 till 8.25. Also from these results it stands out that the $\mathcal{L}_\infty$-norm metric is exactly the same for both TO-1 and TO-2. This is again due to the first occurrence of the reference signal of Figure 8.1. It seems that the largest deviation always occurs in this period. This probably has a strong relation to the maximum reference model deviation. Furthermore, it seems that the RMS estimation error remains quite similar as well, despite the change in PE. As it is expected that the control effectiveness estimation does not change in the stationary periods of TO-2, the RMS value then results from an estimation error during these periods. As shown in Figure 8.26 this is indeed the case. Lastly, the results presented in Figure 8.25 confirm that the LMS parameter estimation law becomes less active when the controller itself is less active.

Algorithm 2: Least Mean Squares parameter estimation

Input : $\delta_{e,k}$, $\delta_{e,k-1}$, $\dot{q}_k$, $\dot{q}_{k-1}$, $\bar{q}_k$, $C_{m_{\delta_e}}$, $\underline{\hat{\theta}}_k$, $\underline{x}$
Output: $\underline{\hat{\theta}}_{k+1}$, $\dot{q}_{\delta_e}$
initialization: $\underline{\hat{\theta}}_0$, μ, $\frac{S\bar{c}}{I_{yy}}$;
while $k \leq N$ **do**
$z_{k+1} = \dot{q}_k - \dot{q}_{k-1}$;
$\Delta\delta_{e,k} = \delta_{e,k} - \delta_{e,k-1}$;
$\underline{\phi}_{k+1} = \underline{\beta}(\underline{x}) \frac{S\bar{c}}{I_{yy}} C_{m_{\delta_e}} \bar{q}_k \Delta\delta_{e,k}$;
$e_k = z_{k+1} - \underline{\phi}_{k+1}^T \underline{\hat{\theta}}_k$;
$\underline{\hat{\theta}}_{k+1} = \underline{\hat{\theta}}_k + \mu \underline{\phi}_{k+1} e_k$;
$\dot{q}_{\delta_e} = \frac{S\bar{c}}{I_{yy}} C_{m_{\delta_e}} \bar{q}_k \underline{\hat{\theta}}_{k+1}^T \underline{\beta}(\underline{x})$;
end

The algorithm of the LMS parameter estimation routine is shown above. In this algorithm $\underline{\beta}(\underline{x})$ has the same definition as used in the algorithm of the RLS parameter estimation. Furthermore, μ will be a square matrix with size $n \times n$. Using the same counting procedure are before, the computational complexity will grow as follows:

$$CC_{LMS}(n) = 2n^2 + 6n + 7 \tag{8.3}$$

8.2.4. Model Reference Adaptive INDI

In this section the numerical simulation results of the MR-AINDI control law are presented and analysed. The adaptive characteristics of this adaptive control law can be tuned by adjusting the adaption parameter γ. In Figure 8.27 and 8.28 the results are presented for simulations run with the non-ideal aircraft model and with the ideal aircraft model, respectively. From the results shown in Figure 8.27 it first of all has to be concluded that the MR-AINDI control law is not able to find the correct value for $\hat{c}$ for the non-ideal aircraft. As already noted about the derived parameter update law, it does not take into account the effect of actuator dynamics and filters. It was therefore assumed that the influence these elements on the control performance could be neglected. Unfortunately this is not the case. This can be concluded from the fact that the parameter estimation does converge to the correct value for the ideal aircraft model. This is shown in Figure 8.28.

The reason why the parameter estimation in the non-ideal system grows to values smaller than zero it that it probably thinks that the control effectiveness is less than the known control effectiveness. This is a consequence of the latency in pitch rate response due to the inclusion of actuator and filter dynamics in the control loop. Unfortunately, this latency cannot be corrected by increasing the commanded elevator increment. As discussed before, this problem could be solved by including the dynamics of the actuators and filters in the adaptive control law design. However, this significantly increases the mathematical complexity of the adaptive law. As the RLS-AINDI and LMS-ANDI control laws are able to produce satisfactory results in their most basic form, it is therefore decided to exclude the MR-AINDI control law from further investigation.

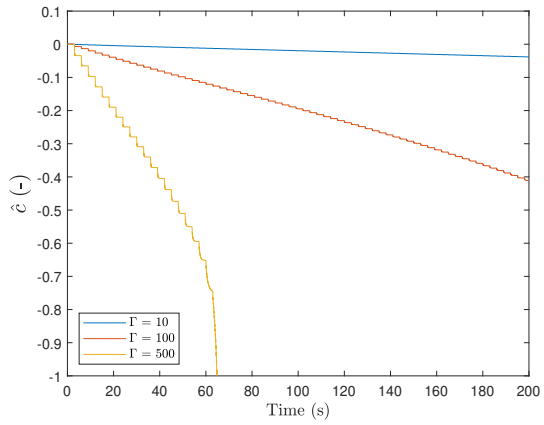

Figure 8.27: Estimated correction factor for the non-ideal system.

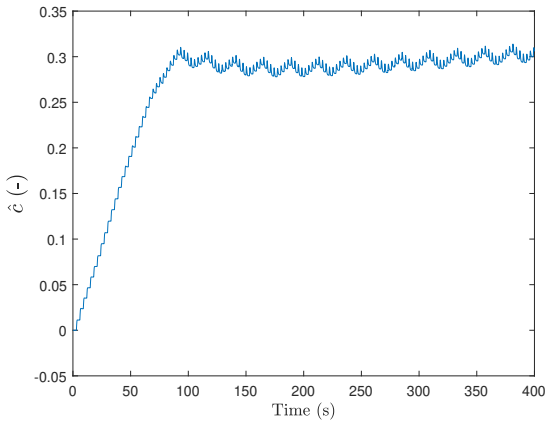

Figure 8.28: Estimated correction factor for the ideal system.

8.2.5. Immersion and Invariance Adaptive INDI

The results of the parameter estimation from several numerical simulations of TO-1 using the non-ideal aircraft model are presented in Figure 8.29. In the simulations the adaption gain has been changed in increasing steps of 50. Considering the results the II-AINDI control law does not deliver satisfactory results either. In this case the exact reason for the incorrect and not converging parameter estimation is unknown. Despite the high performance in an IBS control law as demonstrated in van Gils et al. (2016), it does not seem to work with the current design in combination with an INDI control law.

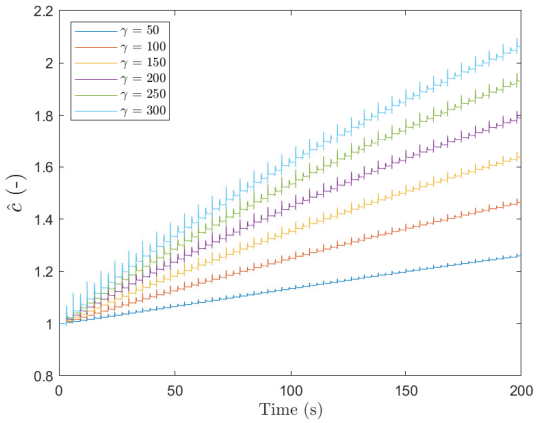

Figure 8.29: Estimated correction factor using the Immersion and Invariance parameter estimation law.

To track down the reason of the unsatisfactory performance, an adaptive INDI control design based the I&I framework was also developed for a much simpler dynamic system. This dynamic system was defined as in Eq. 8.4. The actual value for a was set to 5 and the 'on-board board model' was set to 8. Though despite the reduction in complexity, it was not possible to obtain satisfactory results. Though, using the full nonlinear system equation it was possible to obtain the correct estimate. Albeit with a very slow convergence rate. Though, it was also tested how the estimation performance would also contain model error in the remaining nonlinear model. It was found that this would significantly affect the parameter estimation. Consequently, the approach of using the full nonlinear model in parameter estimation law will not be pursued in this study. Moreover, this would again require the full model to be present, while this need was circumvented with the selection of INDI control.

$$\dot{x} = x^2 + a \cdot u \tag{8.4}$$

The I&I adaptive control design framework has been demonstrated for feedback linearizable systems in the past. However, to the best knowledge of the author this is the first application in INDI control. Furthermore, the derivation of the adaptive law is very flexible as the definition of β is free to choose by the designer as long as it facilitates the attractiveness of the manifold. Due to the limited amount of time it was not possible to try several possible derivations. Therefore, there is still room for improvement for the design of an adaptive control law consisting from I&I and INDI. Despite this fact, II-AINDI control will not be considered for further analysis in this study.

8.3. Comparison and sensitivity

In this section the results of the RLS-AINDI and LMS-AINDI adaptive laws are compared. Furthermore, the sensitivity of the results will be analysed. This is done by introducing measurement noise, ν, and input time delay, τ_d. These forms of uncertainty are common in real control systems and could result in parameter drift phenomena as discussed in chapter 3. Consequently, the effects of these factors are important to consider as well when selecting an adaptive control design. The measurement noise considered in the sensitivity analysis will be added to the pitch acceleration measurement. This signal has been chosen as this will result in the most uncorrelated uncertainty between the elevator deflection increment data and the pitch acceleration data for the parameter estimation. Furthermore, the delay will be added to the actuator command signal.

First of all, the computational complexity will be compared. As determined the the previous section the computational complexity of the RLS estimator and the LMS estimator grow as shown

in Eq. (8.5).

$$\begin{aligned} CC_{RLS}(n) &= 9n^2 + 7n + 9 \\ CC_{LMS}(n) &= 2n^2 + 6n + 7 \end{aligned} \tag{8.5}$$

From these results it can be seen that the complexity of both adaptive laws grows quadratically with the amount of model parameters. Though, due the the difference in the term before n^2, the computational complexity of the RLS parameter estimator will always be approximately 4.5 times larger than the LMS. This means that the LMS parameter estimation could have circa two times as much model parameters before it reaches the computational complexity of the RLS parameter estimation.

Table 8.3: Control performance metric values for both tracking objectives TO-1 and TO-2 and for each noise and delay condition for the non-adaptive control law.

Metric	TO-1						TO-2					
	var(ν) [$(°/s^2)^2$]			τ_d [s]			var(ν) [$(°/s^2)^2$]			τ_d [s]		
	0	0.01	0.1	0	0.02	0.05	0	0.01	0.1	0	0.02	0.05
$\|e\|_{\mathcal{L}_\infty}$	0.86	0.90	1.04	0.86	1.05	1.39	0.86	0.87	0.94	0.86	1.05	1.39
$\|e\|_{\mathcal{L}_2}$	2.59	2.60	2.72	2.59	3.13	4.41	1.62	1.65	1.83	1.62	1.95	2.72
$RMS(e)$	0.18	0.18	0.19	0.18	0.22	0.31	0.12	0.12	0.13	0.12	0.14	0.19
$CMSD(\delta_e)$	1372	1510	2000	1372	1549	1926	489	719	1279	489	584	676

Regarding the non-adaptive control performance for the noise and delay cases and TO-1 and TO-2, the results are summarized in Table 8.3. Furthermore, the raw values of the results visualized in the figures of this section can be found in Appendix A. It can be seen that when either the noise or the delay increases, the performance metric values increase as well. Consequently, the non-adaptive control performance always degrades.

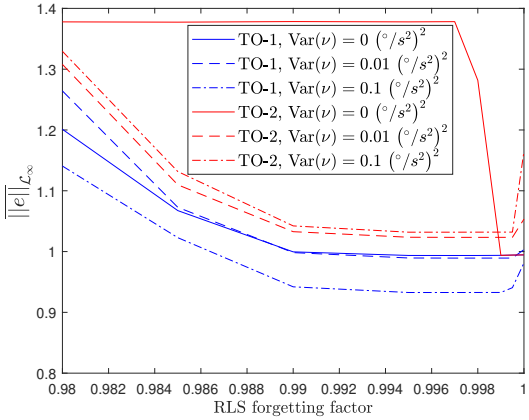

Figure 8.30: Normalized $\mathcal{L}_\infty$-norm of the reference model deviation as a function of the RLS forgetting factor for multiple noise levels.

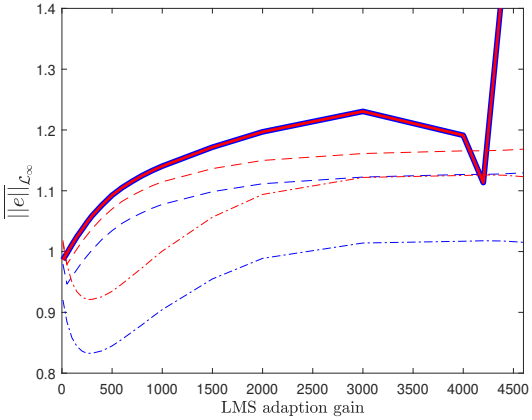

Figure 8.31: Normalized $\mathcal{L}_\infty$-norm of the reference model deviation as a function of the LMS adaption gain for multiple noise levels.

First of all, both the RLS-AINDI and LMS-AINDI control laws are coping well with the non-ideal control system elements. However, with respect to the amount of excitation in the control signal, the LMS-AINDI control law shows more consistent performance than the RLS-AINDI control law. This is a consequence of the fact that the LMS-AINDI control law doesn not adapt when the aircraft is flying steady conditions. However, the tests without noise or delay for the LMS-AINDI show that the

performance could suddenly decease drastically. Although, this behaviour is highly undesirable it is preceded by a gradual decrease in performance and is relatively far away from the optimal region which is in the range of 100 to 400.

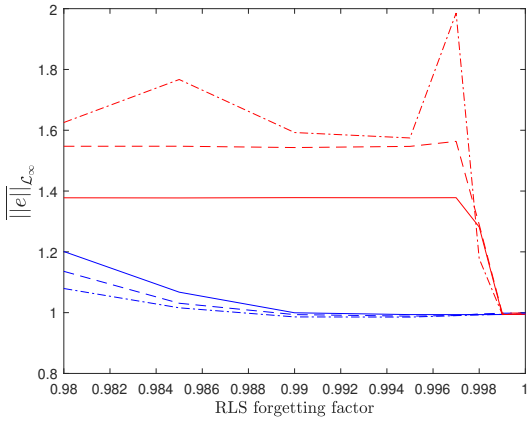

Figure 8.32: Normalized $\mathcal{L}_\infty$-norm of the reference model deviation as a function of the RLS forgetting factor for multiple input delay values.

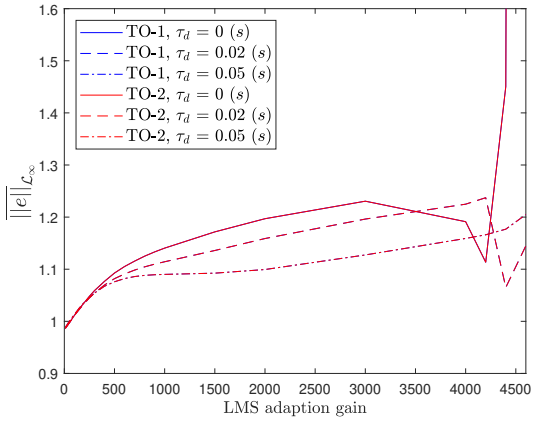

Figure 8.33: Normalized $\mathcal{L}_\infty$-norm of the reference model deviation as a function of the LMS adaption gain for multiple input delay values.

The results for the $\mathcal{L}_\infty$-norm tracking performance metric for the sensitivity analysis of both the RLS- and LMS-AINDI control laws are shown in Figure 8.30 till 8.33. In these figures the normalization is done with respect to the non-adaptive control law subjected to the same TO, noise or delay conditions. Regarding the addition of noise it can be seen that both adaptive laws are able to improve more on the non-adaptive INDI control law when the noise level increases. Though, this does not mean that the adaptive control law performs better than the non-adaptive without sensor noise. Furthermore, for this case study it can be seen that the LMS-AINDI is able to achieve the highest improvement in the case of measurement noise. Moreover, this adaptive control law shows the most consistent behaviour. With respect the to time delay, also the LMS-AINDI control law shows to have the most consistent performance.

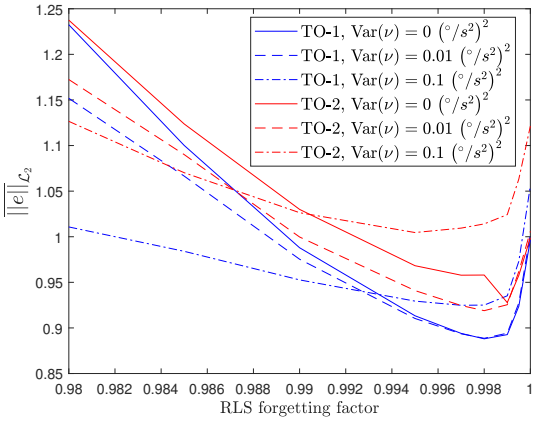

Figure 8.34: Normalized $\mathcal{L}_2$-norm of the reference model deviation as a function of the RLS forgetting factor for multiple noise levels.

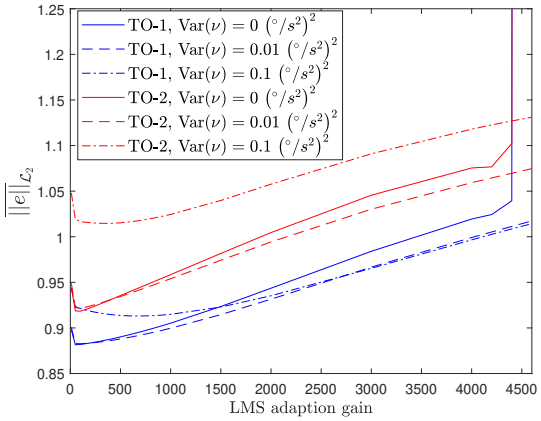

Figure 8.35: Normalized $\mathcal{L}_2$-norm of the reference model deviation as a function of the LMS adaption gain for multiple noise levels.

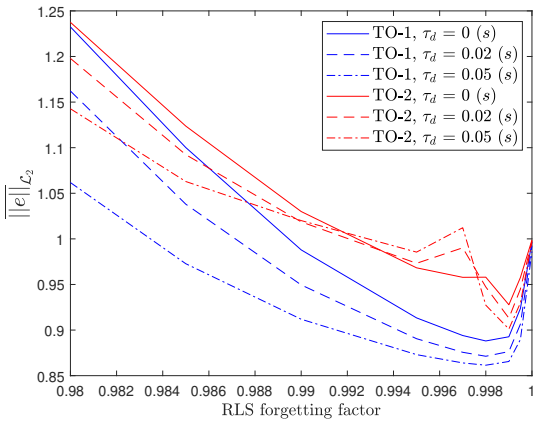

Figure 8.36: Normalized $\mathcal{L}_2$-norm of the reference model deviation as a function of the RLS forgetting factor for multiple input delay values.

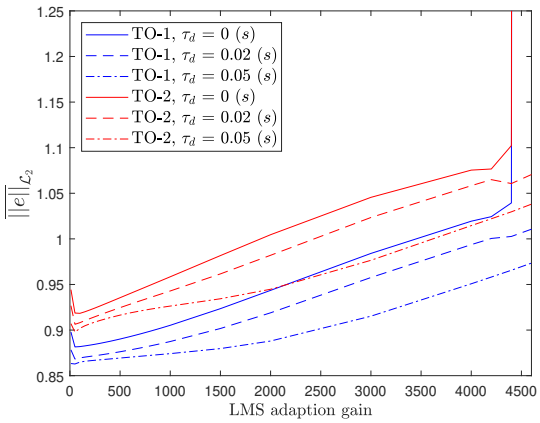

Figure 8.37: Normalized $\mathcal{L}_2$-norm of the reference model deviation as a function of the LMS adaption gain for multiple input delay values.

Considering the $\mathcal{L}_2$-norm of the tracking performance it can be said that both adaptive control laws have quite consistent performance. Though, considering the noise sensitivity the RLS-AINDI control law shows to be slightly more consistent. Furthermore, both laws also have a very similar optimal performance increase. With respect to the extra input delay, both adaptive control laws are able to significantly improve on the oscillations. This can be concluded as the $\mathcal{L}_2$-norm metric especially penalizes oscillations in the reference model deviation.

Regarding the analysis and sensitivity results of the RMS(e) metric it can be seen that both adaptive laws have similar improvement performance within their optimal range. However, it can be seen that the LMS-AINDI control law gives a more consistent response for this metric result as well. Though, for high noise levels it seems to lose its ability to improve on the non-adaptive controller. However, a similar response is shown for the RLS-AINDI for the same noise level.

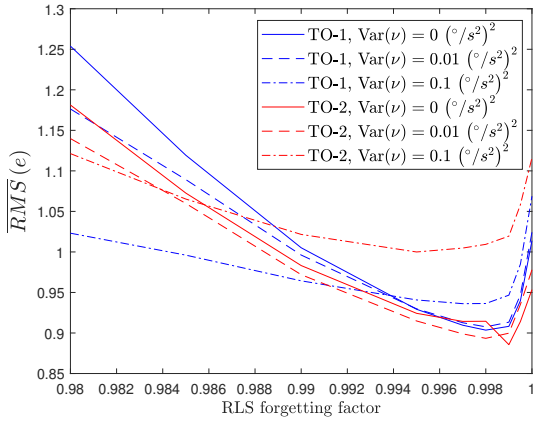

Figure 8.38: Normalized RMS of the reference model deviation as a function of the RLS forgetting factor for multiple noise levels.

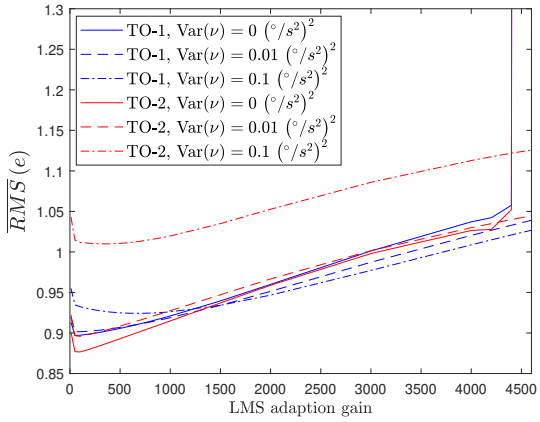

Figure 8.39: Normalized RMS of the reference model deviation as a function of the LMS adaption gain for multiple noise levels.

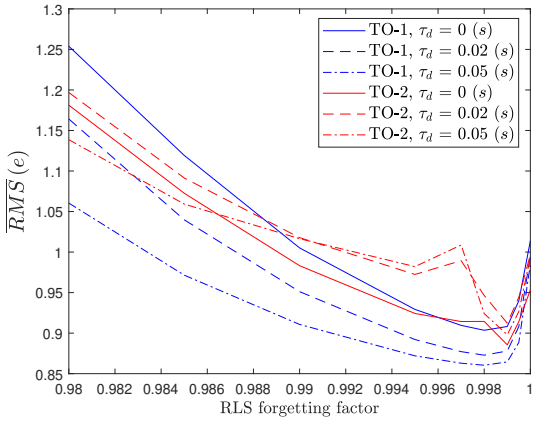

Figure 8.40: Normalized RMS of the reference model deviation as a function of the RLS forgetting factor for multiple input delay values.

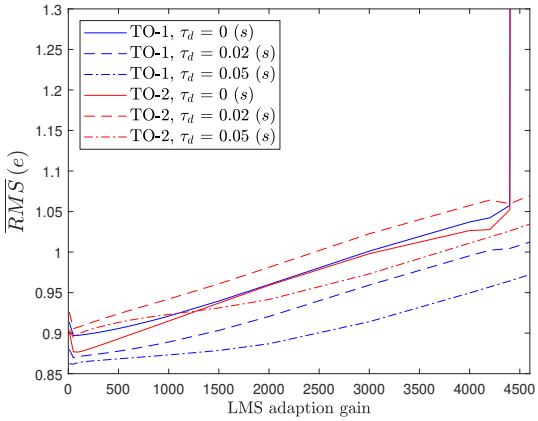

Figure 8.41: Normalized RMS of the reference model deviation as a function of the LMS adaption gain for multiple input delay values.

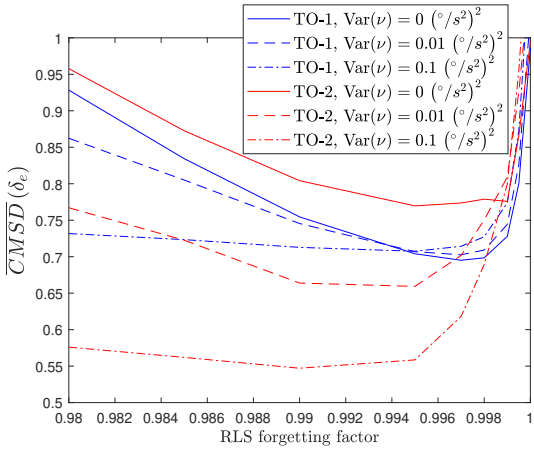

Figure 8.42: Normalized CMSD of the elevator deflection as a function of the RLS forgetting factor for multiple noise levels.

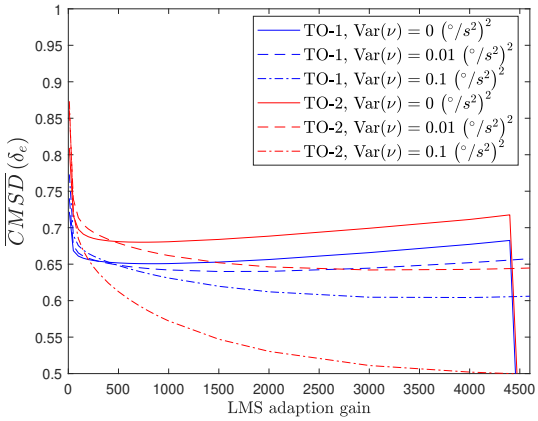

Figure 8.43: Normalized RMS of the elevator deflection as a function of the LMS adaption gain for multiple noise levels.

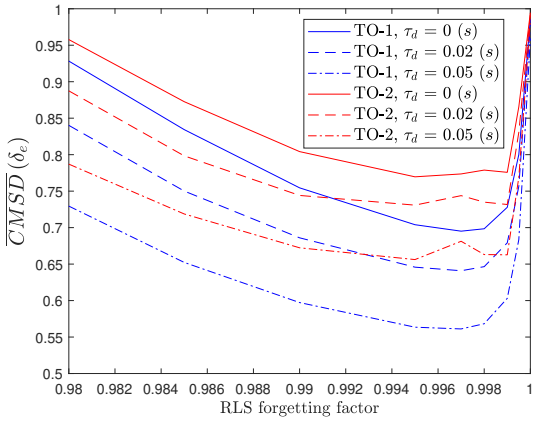

Figure 8.44: Normalized CMSD of the Elevator deflection as a function of the RLS forgetting factor for multiple input delay values.

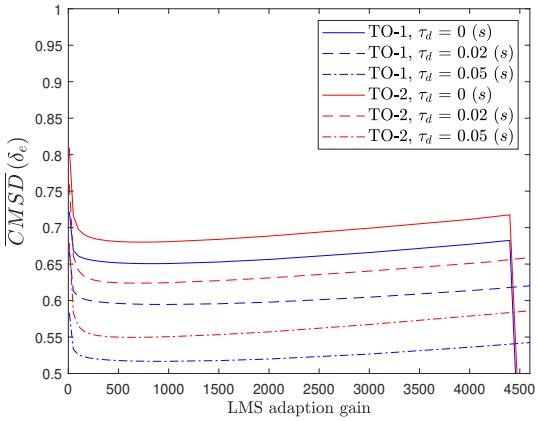

Figure 8.45: Normalized CMSD of the elevator deflection as a function of the LMS adaption gain for multiple input delay values.

The responses of the RLS-AINDI and LMS-INDI for the CMSD of the elevator deflection are shown in Figure 8.42 till 8.45. It stands out that both adaptive control laws are able to achieve large improvements with respect to the non-adaptive controller. However, the LMS-AINDI control law shows again more consistent behaviour in its response. Furthermore, with respect to the time delay it can be seen that the relative improvement of adaptive control only increases for increasing time delay. From this it can be deduced that adaptive control is able to increase the phase margin of the non-adaptive controller subjected to the same time delay.

With respect to the parameter estimation stability it can be seen that LMS parameter estimation clearly is much more robust against reduced PE conditions than RLS parameter estimation. The CMSD of the parameter estimation for the different noise or delay cases are shown in Figure 8.46 till 8.49. During the second tracking objective there are two periods of steady flight. In these periods it is not required to adapt the model parameters as no control inputs are required. The lower value of the CMSD of $\hat{c}$ for the LMS parameter estimator for TO-2 shows that this approach does adhere to this property and the RLS parameter estimator does not.

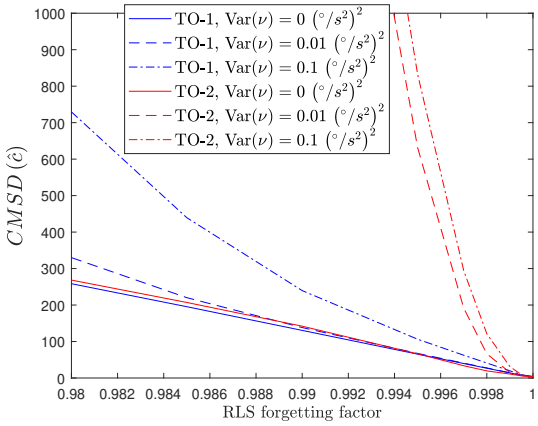

Figure 8.46: CMSD of the control effectiveness model error as a function of the RLS forgetting factor for multiple noise levels.

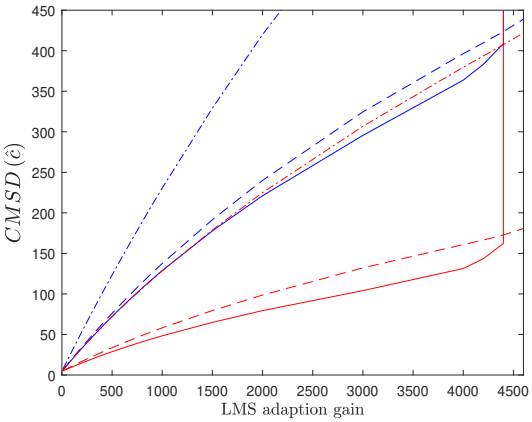

Figure 8.47: CMSD of the control effectiveness model error as a function of the LMS adaption gain for multiple noise levels.

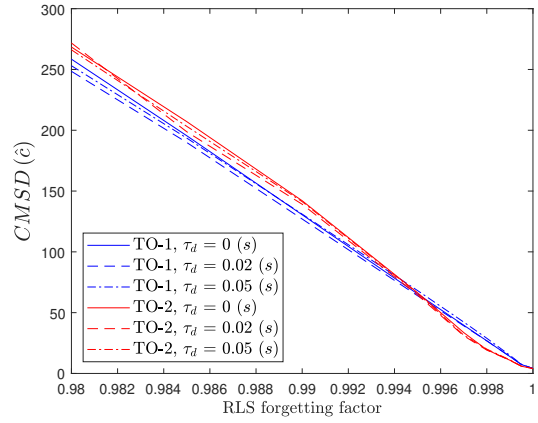

Figure 8.48: CMSD of the control effectiveness model error as a function of the RLS forgetting factor for multiple input delay values.

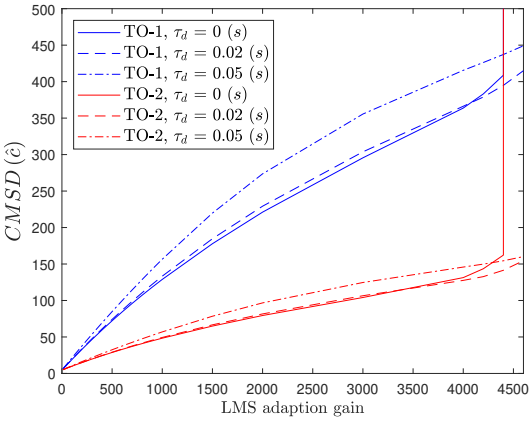

Figure 8.49: CMSD of the control effectiveness model error as a function of the LMS adaption gain for multiple input delay values.

Furthermore, the stability of both the RLS and LMS parameter estimation is affected by noise.

For the first tracking objective the performance degradation of the RLS and LMS methods are very similar. However if the noise is combined with low PE conditions, it can be seen that the RLS parameter estimation performance significantly decreases.

Figure 8.50 till 8.53 show the sensitivity of the maximum RLS and LMS parameter estimation error to noise and input delay. Considering the noise, it can be seen that a small amount of noise actually helps the LMS parameter estimation as it remains stable for adaption values larger than 4600. Furthermore, it can be seen that a reduction in PE does result in a larger maximum error. However, as shown in Figure 8.50, the maximum estimation error for the RLS estimator in this condition is much more sensitive. Furthermore, it can be seen that for TO-1 without noise or delay, the RLS parameter estimation performs better than the LMS approach. However, for the cases with delay it can be seen that the LMS parameter estimator shown more consistent behaviour again.

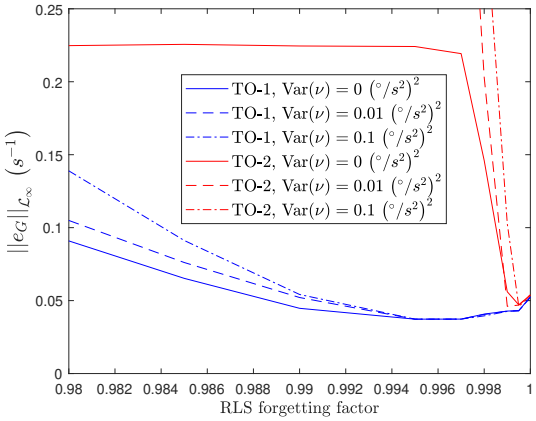

Figure 8.50: $\mathcal{L}_\infty$-norm of the control effectiveness model error as a function of the RLS forgetting factor for multiple noise levels.

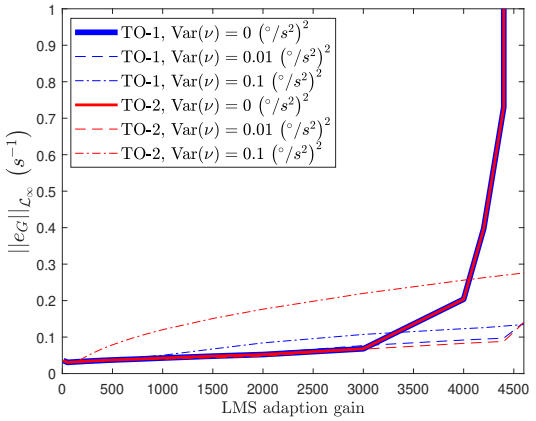

Figure 8.51: $\mathcal{L}_\infty$-norm of the control effectiveness model error as a function of the LMS adaption gain for multiple noise levels.

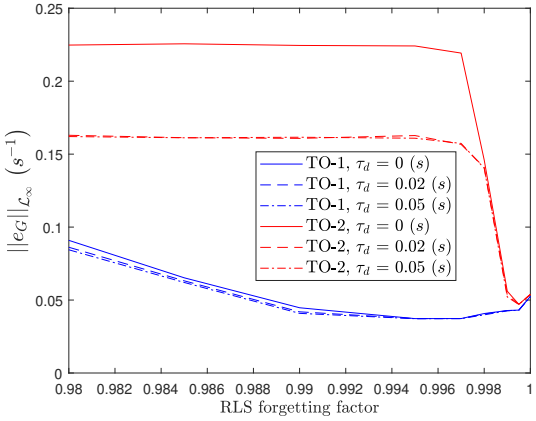

Figure 8.52: $\mathcal{L}_\infty$-norm of the control effectiveness model error as a function of the RLS forgetting factor for multiple input delay values.

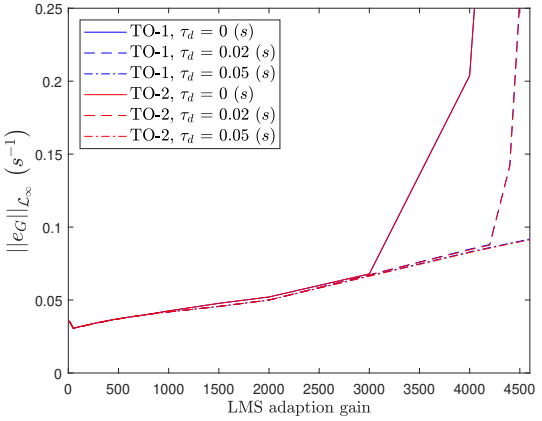

Figure 8.53: $\mathcal{L}_\infty$-norm of the control effectiveness model error as a function of the LMS adaption gain for multiple input delay values.

The sensitivity analysis results for the RMS error in the control effectiveness estimation are presented in Figure 8.54 till 8.57. Considering only TO-1 it can be seen that the RLS estimator performs well and very consistent despite the addition of noise or delay. However, as was observed in all the metrics treated before, this performance degrades significantly when reducing the PE conditions.

Consequently, considering all factors involved in the analysis, the LMS parameter estimator has the most consistent behaviour.

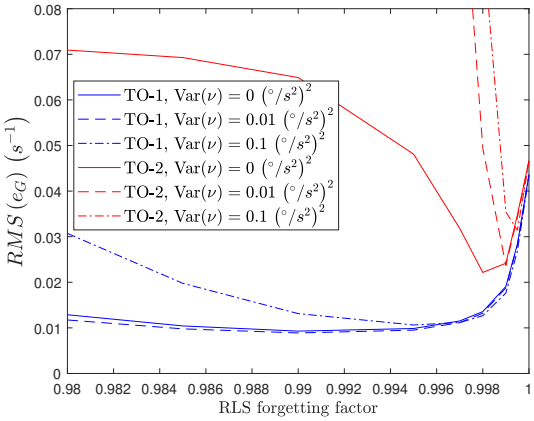

Figure 8.54: RMS of the control effectiveness model error as a function of the RLS forgetting factor for multiple noise levels.

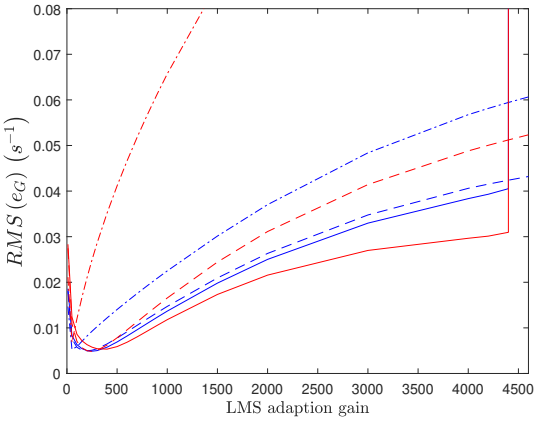

Figure 8.55: RMS of the control effectiveness model error as a function of the LMS adaption gain for multiple noise levels.

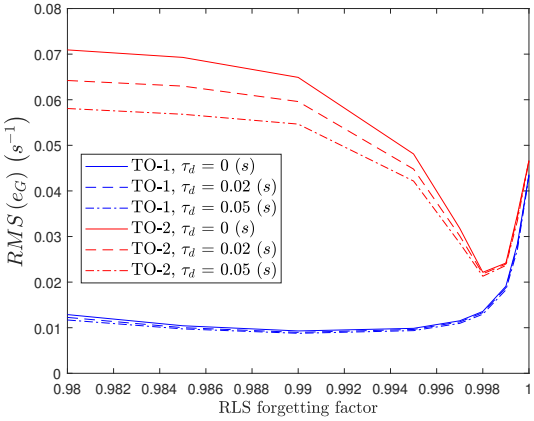

Figure 8.56: RMS of the control effectiveness model error as a function of the RLS forgetting factor for multiple input delay values.

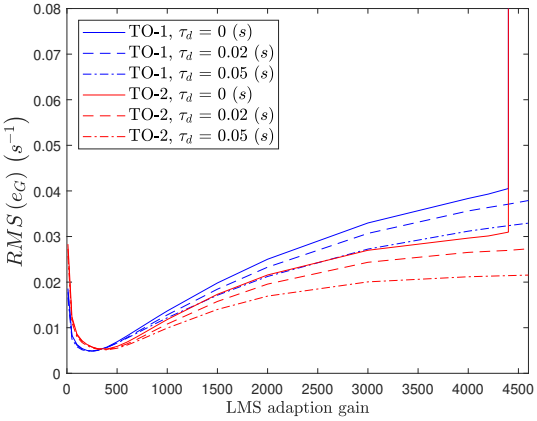

Figure 8.57: RMS of the control effectiveness model error as a function of the LMS adaption gain for multiple input delay values.

Considering the noise and time delay sensitivity of the RLS-AINDI and LMS-AINDI control laws it can be noted that it is quite similar. Though also taking into account the sensitivity of the adaptive control laws to differences in excitation of the reference signal, it can be seen that the LMS-AINDI control law is more consistent. Though, high noise levels are recommended to be avoided. In short, considering the results gathered in this chapter, the LMS-AINDI is regarded to be the most suitable adaptive INDI control law from the adaptive control laws considered in this thesis.

8.4. Conclusion

In this chapter the adaptive control laws are evaluated for their tracking performance, control activity and parameter estimation performance. First of all, from the set of adaptive INDI control laws considered in this study the MR-AINDI and the II-AINDI control laws were not able to give satisfactory results. For the MR-AINDI control law this is due to the neglect of the filter and actuator dynamics in the derivation of the parameter estimation rule. Taking these dynamics into account results

in a significantly more complex adaptive law. As the results of the RLS-AINDI and LMS-AINDI were satisfactory, it was decided to discard the MR-AINDI from further analysis.

The exact reason of the unsatisfactory result of the II-AINDI control law is not known. The adaptive control law design framework was also tested for a much simpler system and also in this case the adaptive INDI control law did not converge. As a last try the adaptive control of the simple system was developed using the complete nonlinear model. This did result in a converging adaptive control law. However, if this approach would be used as well for the adaptive INDI flight control law, it would mean that the full aerodynamic model would be required. As this again increases the model dependency of the control law, this approach is not pursued and the II-AINDI control law was also discarded from further analysis. However, as this is probably the first application of the I&I framework for the design of adaptive INDI control and the I&I framework allows for some flexibility in the design of the adaptive rule, it is recommended that the research on the combination of the I&I framework and INDI will be continued.

From the comparison and sensitivity analysis it first of all became clear that the RLS-AINDI control law is much more sensitive than the LMS-AINDI control law for changes in the amount of excitation in the reference signal. Though, this was expected considering the derivation of the parameter estimation. Overall, both RLS-AINDI and LMS-AINDI are capable of making significant improvement on the non-adaptive control operating in the same conditions. Though, the sensitivity on the LMS-AINDI control law was overall lower to the induced uncertainties. Consequently, the LMS-AINDI control law is regarded to be the most suitable control law for coping with model uncertainties related to aerodynamics model deviations, CG shifts and inertia changes.

IV

Additional derivations and results

This part focuses on the additional derivations and results for this thesis project. To perform the optimization of the control law parameters it was required to apply more criteria than the handling quality and stability guidelines described in Chapter 5 alone. Consequently, this part is dedicated to the additional optimization guidelines to obtain a satisfactory design of the control system.

9

Additional criteria for control law design optimization

The set of criteria for the design parameter optimization often does not consist of the handling quality requirements described in Section 5.4 alone. Next to these requirements it is highly recommended by Tischler (2017) to add criteria regarding controller stability and stability robustness. These specifications are important because they ensure that the overall control system is stable and the stability is robust for situations where the stability margins decrease.

Furthermore, the control system architecture for which the design will be optimized is shown in Figure 9.1. This architecture separates the feed-forward path and the feedback path. The rationale behind this structure is that the command filter could induce the desired control response and the closed-loop part could follow the command filter output in a robust manner. To accomplish the robustness, the closed-loop part is accommodated with a PI compensator. To make sure that the closed-loop part mainly follows the command filter output and does not distort it, a specification will be added which monitors the difference between the command filter output and the actual output. Furthermore, due to the dynamics of the command filter and the dynamics of the closed-loop part, the response could easily deviate from the desired secons order response, needed to make a good LOES fit. Consequently, to assure that the LOES fit is reasonable, a specification which evaluates the LOES fit cost will be added as well.

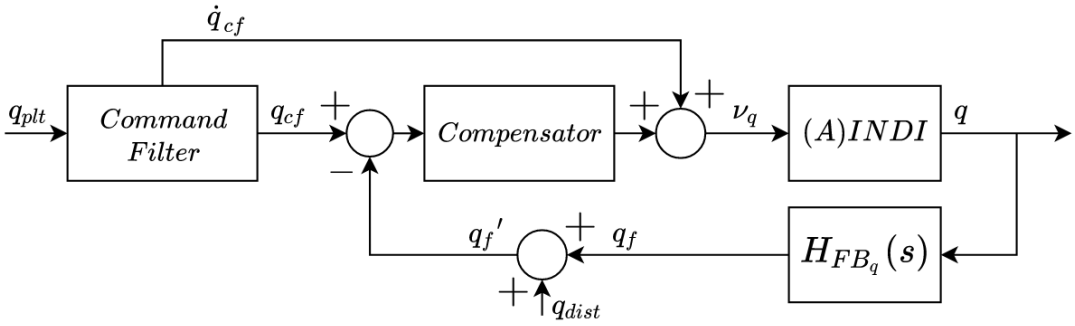

Figure 9.1: (Adaptive) INDI control system outer loop block scheme including pitch rate disturbance input location.

On top of that, actuator activity is an important property to take into account during the control system design as well. This specification can be used to find a design with minimal actuator usage while complying to all demands. Moreover, reduced actuator usage results in less wear and could decrease the likeliness of PIO due to actuator saturation.

This chapter will explain and describe the additional specifications required to obtain a feasible design. Section 9.1 will cover the specifications which consider stability and stability robustness.

Then, Section 9.2 will treat the specifications related to command model following and LOES fit cost. Lastly, Section 9.3 will elaborate on the specification which take into account actuator activity.

9.1. Controller stability

Regarding the stability of the control law, first of all, a criterion which constrains the real part of all the eigenvalues of the control system will be applied. When the real part of one or more of the eigenvalues have a significant positive value the design is immediately regarded as level 3, the boundary is set at 10^{-3}. Consequently, this specification ensures that the obtained stability of the design is within the capabilities of the pilot.

Furthermore, to incorporate stability robustness into the design, a requirement which limits the gain and phase margin to be at least 6 dB and 45 degrees, respectively, will be added as well. These stability margins are defined in the military flight control systems specification MIL-DTL-9490E and should be met even for the most critical centre of gravity locations (DoD, 2008). The margins are determined for the broken-loop response where the control loop is broken just before the actuator input. Considering Figure 9.1 this location is within the $(A)INDI$ block. This block scheme for the non-adaptive INDI control law is displayed more detailed in Figure 9.2. Furthermore, the boundaries which define the level 1, 2 and 3 regions for this requirement can be found in Figure 9.3. Moreover, for the optimization it is required to define a frequency range in which the stability margins will be evaluated. In this study the frequencies between 0.01 and 100 rad/s are analysed as this range usually covers the full range of the aircraft dynamics (Tischler, 2017).

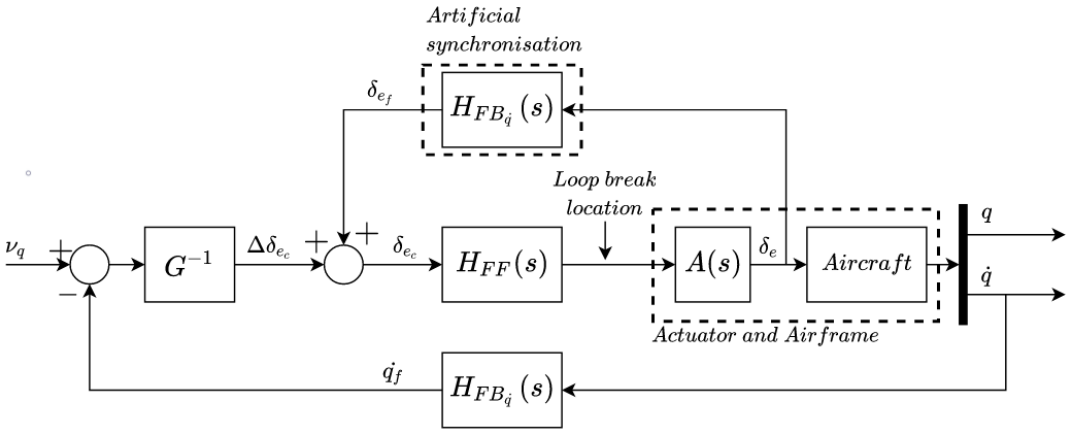

Figure 9.2: INDI control system inner loop block scheme including loop break input location.

Next to the gain/phase margins, the Nichols stability margin requirement is applied. This criterion ensures that the control law is also robust when both the broken-loop gain and phase margin change at the same time (Tischler, 2017). The specification guides the optimization such that the broken-loop frequency response displayed in a Nichols plot remains outside the so-called *exclusion zone*. This zone is defined in Muir (1998) and the boundaries are shown in Figure 9.4. As this specification also uses a frequency-domain response, it again required to define a frequency range as well. This frequency range is chosen to be the same as the range used for the stability margin analysis to evaluate the robust stability for the full broken-loop response.

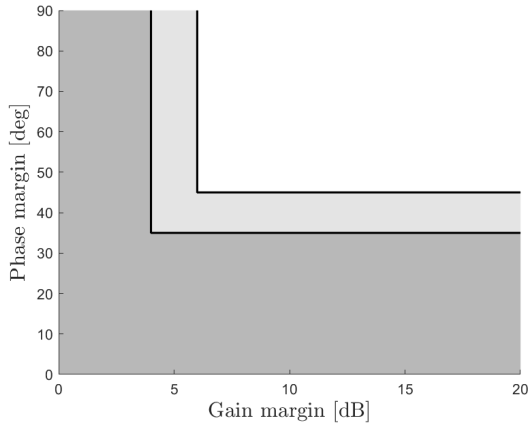

Figure 9.3: Stability margin guideline boundaries

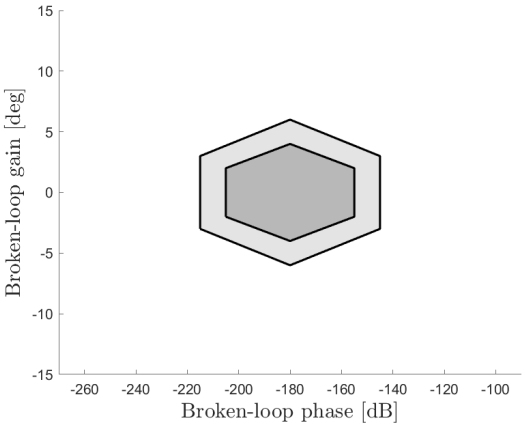

Figure 9.4: Nichols margins guideline boundaries

9.2. LOES fit and model following

The goal of the command filter is to shape the pilot input such that output of the filter is the desired aircraft response for the given pilot command. Consequently, the part of the control law after the command filter should accurately follow this signal to obtain an aircraft response which behaves as the desired response dictated by the command filter. To assure that this goal is achieved a specification which determines the difference between the command filter and the complete control law response will be added to the optimization as well. This specification analyzes the differences between the magnitude and phase of both frequency responses. The difference of error is penalized by a cost function, J_{mf}, which is the same cost function as used for the calculation of the LOES fit cost and is defined as follows (Tischler, 2017):

$$J_{mf} = \frac{20}{N_\omega} \sum_{i=1}^{N_\omega} \left[\left(\left| H_{full}(\omega_i) \right| - \left| H_{cf}(\omega_i) \right| \right)^2 + 0.01745 \left(\angle H_{full}(\omega_i) - \angle H_{cf}(\omega_i) \right)^2 \right] \tag{9.1}$$

Here, N_ω is again the amount of frequency points used in the analysis, H_{full} is the pilot input to the aircraft pitch rate transfer function and H_{cf} is the transfer function of the command filter. Furthermore, to make a fair comparison between both transfer functions, the effect of the equivalent delay found by the LOES fit of the full control loop is added to the command filter transfer function. The level 1 and 2 regions of this specification are shown in Figure 9.5.

Furthermore, to guide the LOES fit, a specification which constrains the LOES fit cost will be incorporated as well. According to the MIL-STD-1797A the LOES fit cost should be less than or equal to 10 to have an adequate fit. However, from experience it was found that this bound would lead to a non-existing design space. Using the MUAD bounds, Figure 5.2 and 5.3, as the driving factor for the LOES fit resulted in a relaxed bound of the level 1 region of the cost specification and led to a design space again. This approach was adopted as the cost of the LOES fit could be resulting from a fitting error at the edges of the fitting domain. As can be seen from Eq. (9.1), the weight of the error does not change with frequency. Furthermore, considering the MUAD bounds, the pilot becomes less sensitive to fitting errors for frequencies far from the pilot cross-over frequency range. Therefore, it is possible that the fitting cost becomes larger than 10 while the fitting error is still within the MUAD bounds (Hodgkinson and Johnston, 1979). As these bounds represent the sensitivity of the pilot for the deviation from second order behaviour, it is therefore chosen to regard these bounds as leading for the LOES fit. Though, to minimize the mismatch between the full order system and the LOES fit, a LOES fit cost guideline is still applied albeit with a relaxed level 1 boundary. The boundary is set to 20 instead of 10 as shown in Figure 9.6.

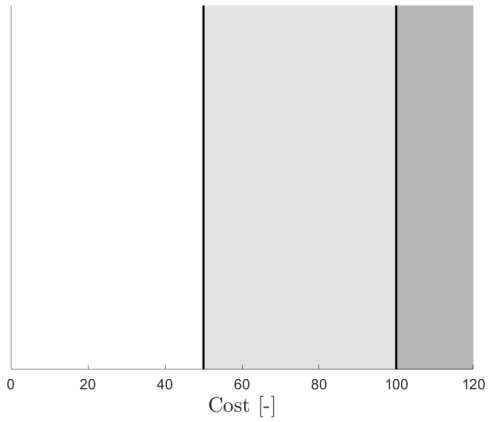

Figure 9.5: Model following cost guideline boundaries

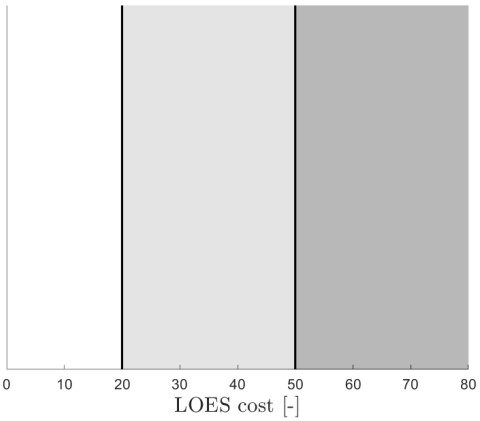

Figure 9.6: LOES fit cost guideline boundaries

9.3. Actuator activity

The actuator activity is taken into account by adding a specification which determines the actuator deflection RMS. This value is determined by calculating the area below the autospectrum of the considered signal which is proportional to the RMS value. As described in Tischler (2017) the actuator RMS is determined by analysing the signal from the pilot input to the actuator position. Furthermore, the feed-forward and feedback path in this control law are separated due to the additional command filter. Therefore, it is recommended to analyse the actuator activity resulting from disturbances as well (Tischler, 2017). To do this the actuator RMS for disturbances is determined by analysing the signal from the disturbance to the actuator position. The input of the disturbance signal in the control loop is located after the feedback path dynamics as shown in Figure 9.1. This disturbance input is used as a general source and therefore it is located after the the sensors and filters. Boundaries of the level 1 and 2 regions of the specification are displayed in Figure 9.7. The x-axis displays the normalized actuator RMS value.

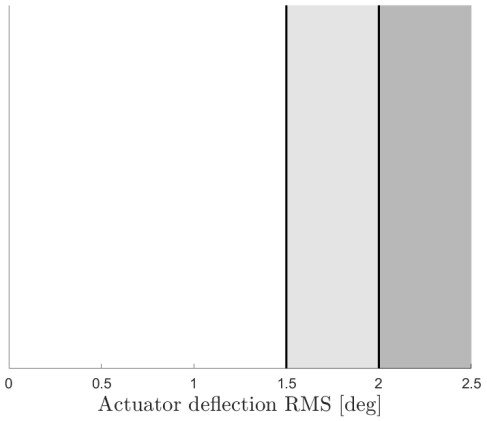

Figure 9.7: Actuator deflection RMS guideline boundaries.

V

Conclusions and recommendations

10

Conclusions and recommendations

This final part will conclude the thesis by answering the research questions and elaborating on the impact of the findings on INDI-based control research as a whole. Finally, the recommendations for future research on adaptive INDI-based control will be treated.

10.1. Answers to research questions

1. **Which adaptive methods are suited for the integration in INDI-based pitch rate control of high-performance aircraft?**

   (a) **What are the adaptive control approaches?**
   A literature survey has established that several approaches have been developed. The uncertain model parameter could be estimated directly or indirectly. In the direct approach, the uncertainty is defined in such a way that the adaptive control law could estimate the uncertainty model parameters directly. The indirect approach first estimates the system model parameters. The new estimation of the system model can then be applied to determine the correct control law parameters. Within these design approaches there is the option to use a reference model which determines the desired dynamic response of the aircraft. This approach is called *Model Reference Adaptive Control* (MRAC) and the error between the actual system output and the reference model output is used to drive the adaptive law. The derivations of the update laws are often based on Lyapunov stability functions (LSF). Furthermore, it is also possible to use an adaptive prediction model of which the model parameters are estimated online. This prediction model often represents the system itself. A third option is based on the *Immersion and Invariance* (I&I) framework. This approach does not use a self tuning prediction model or a reference model but bases its derivation on an invariant manifold on which the estimation error is zero.

   (b) **What is the state-of-the-art research in the field of adaptive INDI?**
   The research on adaptive INDI is still a young field. Consequently, the list of finished research projects is still short. One of these projects has considered an indirect adaptive approach based on the Least-Mean-Square (LMS) parameter estimation applied to a micro air vehicle (MAV). The control objective was to track an attitude command and the adaptive method was used to correct the on-board control effectiveness model. Another project has developed an MRAC design for an extended F-16 simulation model. In this research continuous parameter update rules were derived using LSFs. The third and last research project also considered MRAC. However, here the adaptive method is used train a Neural Network. The output of the Neural network can determine a correction term to augment the output of the INDI contor law.

(c) **Which methods are suited for INDI-based control?**
Based on a state-of-the-art review on adaptive INDI it was established that both direct and indirect adaptive approaches have been investigated in recent research projects. Furthermore, as INDI is a control law which uses part of the aircraft model, the combination with indirect adaptive methods comes naturally. On the other hand, an adaptive approach such as integrated adaptive Backstepping cannot be applied as here the adaptive law is designed together with the control law using LSFs.

Furthermore, with respect to real-time operation it is preferred that the model structure of the estimated uncertainty is linear-in-the-parameters (LP). LP models allow for the use of linear parameter estimation algorithms which are more suited for real-time applications than nonlinear parameter estimation methods. The parameter estimation methods which were regarded most suited for application in adaptive control were the Recursive Least Squares (RLS) method, the Leas-Mean-Square method, MRAC and I&I.

2. **How do longitudinal centre of gravity shifts, changes in inertia and aerodynamic model mismatches affect the INDI-based pitch rate control law?**
A literature review is conducted on modelling the aircraft equations of motion while taking into account the possibility of centre of gravity shifts. From this study it is established that there are two options to go about this. The first approach describes the change in dynamics with respect to a reference frame that is fixed to the geometry of the aircraft and the second method uses a centre of gravity fixed reference frame. After linearization and applying the time-scale separation assumption, both approaches yield a model in which only the CE term will be affected by CG shifts, inertia changes and aerodynamic model mismatches. These models reveal that the longitudinal centre of gravity (CG) shifts could increase or decrease the CE depending on a shift in the direction of the nose or the tail. Furthermore, changes in inertia have an inverse proportional effect and aerodynamic model mismatches have a direct proportional effect on the CE. However, the CE will be affected in a nonlinear manner when all uncertainty factors are combined. Despite the nonlinear dependency on these factors, the CE model will either be larger or smaller than the actual CE. When the actual CE model is larger than the actual CE, the control response will be slower than what is achievable. Furthermore, in case the CE model is lower than the actual CE, the response will be quicker with respect to having a correct model.

Though, if the difference in too much, there is a possibility for instability. Lastly, it has been established that large CG shifts could result in a lower validity of the time-scale separation assumption. This is the consequence of an increased influence of the incremental angle-of-attack on the incremental pitch acceleration. The violation of this assumption will result in decreased control performance despite having a correct CE model. As it was incorrectly presumed that the time-scale separation assumption would hold for all uncertainty cases, this problem was not identified by the models described above. Consequently, this model is not comprehensive enough to analysis the change in control performance of INDI-based pitch rate control.

3. **Which evaluation metrics are suited for the assessment of adaptive INDI-based control?**

(a) **Which metrics quantify control performance in adaptive control?**
The metric which are used most often for nonlinear control are the $\mathcal{L}_\infty$- and $\mathcal{L}_2$-norm of the temporal error between a reference model and the real system output. The former is suitable to evaluate the maximum error and the latter for oscillations in the error signal. Furthermore, the Root-Mean-Square (RMS) of the temporal error is a suitable metric as well. This metric could be used to evaluate the average error during the simulation.

However, considering the sensitivity of the $\mathcal{L}_2$-norm and RMS metrics, it was found that both metrics showed a similar trend. Consequently, using one of the two is sufficient. Lastly, the cumulative moving standard deviation (CMSD) is a suitable metric to evaluate control activity and parameter estimation activity.

(b) **Which metrics quantify parameter estimation performance in adaptive control?**
The same metrics as used for the control performance are applicable. However, to be able these for parameter estimation assessment as well, it should be possible to extract the actual value of the parameter from the simulation model.

(c) **What is the appropriate metric for assessing computational complexity of adaptive control methods?**
There are several approaches to estimate the computational complexity of an algorithm. A commonly used method is to simply measuring the time a computer needs to execute an algorithm and monitor the change in the required execution time when the size of the data changes. Another option is to use the big-$\mathcal{O}$ notation which characterizes the growth rate of the elementary operations for an increasing dataset. Though, as the algorithms of the adaptive control methods considered in this research are not computationally intensive and the dataset at each iteration is small, both measuring the iteration time and using the big-$\mathcal{O}$ notation are not very practical metrics. Therefore, the appropriate metric adopted here is to count the number of elementary operations performed during each iteration. To obtain its sensitivity the counted number of operations is determined as a function of the number of estimated parameters.

(d) **What are the appropriate handling quality and controller stability guidelines for the evaluation of the non-adaptive and adaptive INDI-based pitch rate control law?**
The study on handling quality and stability guidelines, revealed that there are several handling quality and stability guidelines for longitudinal control. The most important criteria with respect to the short-term dynamic response are found to be the short period damping versus Control anticipation parameter (CAP), the equivalent time delay and the pitch attitude dropback. Furthermore, there are important guidelines which focus on the prediction of pilot induced oscillations. These are the Gibson phase rate, the pitch attitude bandwidth versus phase delay, the Neal-Smith and the flight path angle bandwidth versus pitch attitude bandwidth.

4. **How is the non-adaptive INDI-based pitch rate control performance affected when actuator dynamics, sensor dynamics, filters and computational delay are added to the system model?**
Simulations with the system model that includes these more realistic control system elements show that the robustness to model uncertainties is decreased. Although, the non-adaptive control law is still quite robust, it is observed that a CE value that is lower than the actual CE induces a significant increase in control activity and additional oscillations in the pitch rate response. Consequently, the need for an accurate CE model increases when actuator dynamics, sensor dynamics, filters and computational delays are added to the system model.

5. **Which adaptive INDI-based pitch rate control law is most suited for coping with aerodynamic model mismatches and system model changes due to centre of gravity shifts and inertia changes?**
The analysis of the adaptive INDI-based control laws considered in this study has revealed that the direct adaptive design based on LMS parameter estimation is the most suited. This algorithm is able to converge close to the desired value quickly and does not drift even when the information in the estimation data is low. From the analysis results and sensitivity analysis of this approach, it is concluded that this adaptive control law gives the most consistent

response while being subjected to aerodynamic model uncertainties, centre of gravity shifts and inertia changes.

6. **What are the differences in handling qualities and stability between the non-adaptive and adaptive INDI-based pitch rate control law, considering aerodynamic model mismatches and system variation due to longitudinal centre of gravity shifts?**
   It is observed that the adaptive control law is able to decrease the variation in handling qualities and stability with respect to the non-adaptive control law. However, it is found that large forward and backward CG shifts could result in a decrease of the validity of the time-scale separation assumption. As the applied adaptive control law attempts to correct the CE model by only using the measured incremental pitch acceleration and incremental elevator deflection, this leads to a decrease in the estimation performance. On top of that, the decreased validity of the time-scale separation assumption impairs the control performance of the INDI control law despite having a correct CE model. Consequently, the proposed adaptive control solution in this thesis is not suited to solve the variation in handling qualities and stability for large CG shifts.

10.2. Contribution to research on INDI-based control

This section will make an effort to put the observations and conclusions made in this thesis into the perspective of INDI-based control development. In a recent study on indirect adaptive INDI-based control, based on LMS parameter estimation, applied to a MAV has already demonstrated that the control performance could be made more robust against model uncertainties. Furthermore, the results obtained from the simulations performed in this thesis confirm that a similar adaptive method could retain the INDI-based control law performance of a high-performance aircraft subjected to CG location, inertia and aerodynamic model uncertainties. Consequently, this thesis contributes to the knowledge on applicability of LMS parameter estimation and model correction for INDI-based control in uncertain high-performance aircraft and airborne systems is a whole.

However, the results also revealed that a large CG shift can lead to weakening of the time-scale separation assumption. This is a consequence of the significant increase of the angle-of-attack influence on the aircraft pitching motion. Variations in HQ&S following from this problem could not be solved by using the correct CE model in the INDI-based control law. Furthermore, the change in the angle-of-attack influence due to CG shifts occurs to all fixed-wing aircraft. Therefore, it is possible that this issue arises for all fixed-wing aircraft which are subjected to large CG shifts. Moreover, this result stresses that it is important to analyse the validity of the time-scale separation assumption when the control performance variation, due to system uncertainties, of an INDI-based controller is explored.

10.3. Recommendations

The results obtained from the simulations performed in this thesis project show that an indirect adaptive method based on LMS parameter estimation is able to decrease the HQ&S variation of an INDI-based pitch rate control law following from CG shift, inertia changes and aerodynamic model error. Consequently, this first step in the validation process of this adaptive control law shows that there is potential. However, to increase the validity, there are still challenges that should be faced.

First of all, the mass model used to simulate the CG shifts and inertia changes only considers the influence of fuel. The mass distribution of actual high-performance military aircraft is also altered by different store configurations. Therefore, as one of the aspects to expand the validation of the adaptive INDI-based pitch rate control law considered in this thesis, it is recommended to add the effect of stores to the mass model.

Furthermore, the aerodynamic model of the aircraft considered in this thesis is limited to Mach

numbers between 0.2 and 0.6. Therefore, it was not possible to analyse the performance of the control laws for trans-sonic and supersonic velocities. Consequently, to expand the validity of the simulations it is recommended to apply a more comprehensive aerodynamic model as well. In addition, structural vibrations are not considered either. As these vibrations impose high demands on filter design for the angular rate and presumably on angular acceleration feedback, it is advised to incorporate this aspect in the simulation model as well in future validation studies.

Moreover, it is established that the time-scale separation assumption can be violated for large CG shifts. This results in a residual HQ&S variation that cannot be mitigated by having the correct CE model. Consequently, to pursue the objective of further decreasing the HQ&S variation it is recommended that further research on robustifying the outer loop will be performed. For example, an adaptive design based on MRAC, which does account for the extra dynamics of actuators, sensors and filter, might be suited as this framework does allow for adaption of the outer loop output. Furthermore, the outer loop of the adaptive control law proposed in this thesis could be augmented with sliding-mode control or a more advanced robust framework, such as μ-analysis, could be used for the design of the outer loop.

In addition, another direction for future research is to consider the performance of the adaptive control law in a stochastic environment. The research performed in this thesis does not consider the phenomena of turbulence. As this factor distorts the information in the parameter estimation input signals, it will affect the estimation performance. As handling turbulence is a common aspects of real-world flight control laws, a study in this field would add to the validation process of the implementation of the adaptive INDI-based control laws considered in this thesis.

Finally, one of the most important steps in the validation of the adaptive control laws applied in this thesis, is a rigorous closed-loop stability proof. Without this proof it is not safe to perform piloted flight tests in actual aircraft. Consequently, this aspect is strongly recommended for future research.

Bibliography

P. Acquatella, W. Falkena, E. van Kampen, and Q.P. Chu. Robust Nonlinear Spacecraft Attitude Control using Incremental Nonlinear Dynamic Inversion. In *AIAA Guidance, Navigation, and Control Conference*, Minneapolis, Minnesota, August 2012. American Institute of Aeronautics and Astronautics. ISBN 978-1-60086-938-9. doi: 10.2514/6.2012-4623.

AGARD. Criteria for handling qualities of military aircraft. Number AGARD Conference Proceedings No. 333 (AGARD-CP-333). AGARD, apr 1982. ISBN 92-835-0313-8/AD-A118596.

AGARD. Flying qualities. Technical Report AGARD-CP-508, AGARD, feb 1991a.

AGARD. Handling qualities of unstable highly augmented aircraft. In *AGARD-AR-279*, Neuilly Sur Seine, France, May 1991b. AGARD. ISBN 92-835-0609-X.

O. Albostan and M. Gökaşan. High Angle of Attack Manoeuvring Control of F-16 Aircraft Based on Nonlinear Dynamic Inversion and Eigenstructure Assignment. *European Conference for Aeronautics and Space Sciences*, page 15, 2017. doi: 10.13009/EUCASS2017-228.

A. Astolfi, D. Karagiannis, and R. Ortega. *Nonlinear and Adaptive Control with Applications*. Springer Science & Business Media, December 2007. ISBN 978-1-84800-066-7.

Karl Aström. History of Adaptive Control. In J. Baillieul and T. Samad, editors, *Encyclopedia of Systems and Control*, pages 1–9. Springer, London, 2014. ISBN 978-1-4471-5102-9. doi: 10.1007/978-1-4471-5102-9_120-1.

J. Autenrieb, H. Shin, and M. Bacic. Development of a Neural Network-based Adaptive Nonlinear Dynamic Inversion Controller for a Tilt-wing VTOL Aircraft. pages 44–52, November 2019. doi: 10.1109/REDUAS47371.2019.8999700.

B.J. Bacon and A.J. Ostroff. Reconfigurable flight control using nonlinear dynamic inversion with a special accelerometer implementation. In *AIAA Guidance, Navigation, and Control Conference and Exhibit*, Dever,CO,U.S.A., August 2000. American Institute of Aeronautics and Astronautics. ISBN 978-1-62410-301-8. doi: 10.2514/6.2000-4565.

B.J. Bacon, A.J. Ostroff, and S.M. Joshi. Reconfigurable NDI controller using inertial sensor failure detection isolation. *IEEE Transactions on Aerospace and Electronic Systems*, 37(4):1373–1383, October 2001. ISSN 1557-9603. doi: 10.1109/7.976972. Conference Name: IEEE Transactions on Aerospace and Electronic Systems.

T. Berger, M. Tischler, S. G. Hagerott, D. Gangsaas, and N. Saeed. Longitudinal Control Law Design and Handling Qualities Optimization for a Business Jet Flight Control System. In *AIAA Atmospheric Flight Mechanics Conference*. American Institute of Aeronautics and Astronautics, Aug 2012. doi: 10.2514/6.2012-4503. URL `https://arc.aiaa.org/doi/abs/10.2514/6.2012-4503`.

P. Bhardwaj, V. S. Akkinapalli, J. Zhang, S. Saboo, and F. Holzapfel. Adaptive Augmentation of Incremental Nonlinear Dynamic Inversion Controller for an Extended F-16 Model. In *AIAA Scitech 2019 Forum*, San Diego, California, January 2019. American Institute of Aeronautics and Astronautics. ISBN 978-1-62410-578-4. doi: 10.2514/6.2019-1923.

A. Calise, S. Lee, and M. Sharma. Direct adaptive reconfigurable control of a tailless fighter aircraft. In *Guidance, Navigation, and Control Conference and Exhibit*, Boston,MA,U.S.A., August 1998. American Institute of Aeronautics and Astronautics. doi: 10.2514/6.1998-4108.

A. J. Calise, N. Hovakimyan, and M. Idan. Adaptive output feedback control of nonlinear systems using neural networks. *Automatica*, 37(8):1201–1211, August 2001. ISSN 0005-1098. doi: 10.1016/S0005-1098(01)00070-X.

A.J. Calise and R.T. Rysdyk. Nonlinear adaptive flight control using neural networks. *IEEE Control Systems Magazine*, 18(6):14–25, December 1998. ISSN 1941-000X. doi: 10.1109/37.736008. Conference Name: IEEE Control Systems Magazine.

Su Cao, Lincheng Shen, Renshan Zhang, Huangchao Yu, and Xiangke Wang. Adaptive Incremental Nonlinear Dynamic Inversion Control Based on Neural Network for UAV Maneuver. In *2019 IEEE/ASME International Conference on Advanced Intelligent Mechatronics (AIM)*, pages 642–647, July 2019. doi: 10.1109/AIM.2019.8868510. ISSN: 2159-6247.

M. V. Cook. *Flight Dynamics Principles: A Linear Systems Approach to Aircraft Stability and Control*. Butterworth-Heinemann, October 2012. ISBN 978-0-08-098276-2.

G. Cooper and R. Harper. The use of pilot ratings in evaluation of aircraft handling qualities. *NASA Ames Technical Report*, May 1969.

C. C. De Visser. *Global Nonlinear Model Identification with Multivariate Splines*. Phd thesis, Delft University of Technology, Faculty of Aerospace Engineering, 2011. Publisher: C.C. de Visser ISBN: 978-90-8570-770-7.

C. J Dennehy, J. S. Orr, Draper Laboratories, Immanuel Barshi, and Irving C. Statler. A Comprehensive Analysis of the X-15 Flight 3-65 Accident. Technical report, NASA, 2014.

P. S. R. Diniz. *Adaptive Filtering: Algorithms and Practical Implementation*. Springer US, May 1997. ISBN 978-0-7923-9912-4.

DoD. Military specification: Flying qualities of piloted airplanes, MIL-F-8785C, November 1980.

DoD. *FLYING QUALITIES OF PILOTED AIRCRAFT*. MIL-HDBK-1797. Department of Defence, December 1997.

DoD. *Flight Control Systems - Design,Installation and Test of Piloted Aircraft*. MIL-DTL-9490E. Department of Defence, April 2008.

D. Enns, D. Bugajski, R. Hendrick, and G. STEIN. Dynamic inversion: an evolving methodology for flight control design. *International Journal of Control*, 59(1):71–91, January 1994. ISSN 0020-7179. doi: 10.1080/00207179408923070.

N.M. Filatov and H. Unbehauen. *Adaptive Dual Control: Theory and Applications*. Springer Science & Business Media, April 2004. ISBN 978-3-540-21373-4.

Benjamin Gal-Or. *Vectored Propulsion, Supermaneuverability and Robot Aircraft*. Springer New York, New York, NY, 1990. ISBN 978-0-387-97161-2 978-1-4613-8961-3. doi: 10.1007/978-1-4613-8961-3.

C. Gallaway and R. Osborn. Aerodynamics perspective of supermaneuverability. In *3rd Applied Aerodynamics Conference*, Colorado Springs,CO,U.S.A., October 1985. American Institute of Aeronautics and Astronautics. doi: 10.2514/6.1985-4068.

M. Geiser, E. Xargay, N. Hovakimyan, T. Bierling, and F. Holzapfel. L1 Adaptive Augmented Dynamic Inversion Controller for a High Agility UAV. In *AIAA Guidance, Navigation, and Control Conference*, Portland, Oregon, August 2011. American Institute of Aeronautics and Astronautics. ISBN 978-1-60086-952-5. doi: 10.2514/6.2011-6457.

J. C. Gibson. *Development of a design methodology for handling qualities excellence in fly by wire aircraft*. Delft University Press, Delft, 1999. ISBN 90-407-1841-5.

F. Grondman, G. Looye, R.O. Kuchar, Q.P. Chu, and E. Van Kampen. Design and Flight Testing of Incremental Nonlinear Dynamic Inversion-based Control Laws for a Passenger Aircraft. In *2018 AIAA Guidance, Navigation, and Control Conference*, Kissimmee, Florida, January 2018. American Institute of Aeronautics and Astronautics. ISBN 978-1-62410-526-5. doi: 10.2514/6.2018-0385.

C. Hanson, M. Johnson, J. Schaefer, N.T. Nguyen, and J. Burken. Handling Qualities Evaluations of Low Complexity Model Reference Adaptive Controllers for Reduced Pitch and Roll Damping Scenarios. In *AIAA Guidance, Navigation, and Control Conference*, Portland, Oregon, August 2011. American Institute of Aeronautics and Astronautics. ISBN 978-1-60086-952-5. doi: 10.2514/6.2011-6607.

J.J. Harris. F-35 Flight Control Law Design, Development and Verification. In *2018 Aviation Technology, Integration, and Operations Conference*, Atlanta, Georgia, June 2018. American Institute of Aeronautics and Astronautics. ISBN 978-1-62410-556-2. doi: 10.2514/6.2018-3516.

M. H. Hayes. *Statistical Digital Signal Processing and Modeling*. Wiley, April 1996. ISBN 978-0-471-59431-4.

C. D. Heise, M. Leitao, and F. Holzapfel. Performance and Robustness Metrics for Adaptive Flight Control - Available Approaches. In *AIAA Guidance, Navigation, and Control (GNC) Conference*, Boston, MA, August 2013. American Institute of Aeronautics and Astronautics. ISBN 978-1-62410-224-0. doi: 10.2514/6.2013-5090.

A. Hodel, M. Whorton, and J. Zhu. Stability Metrics for Simulation and Flight-Software Assessment and Monitoring of Adaptive Control Assist Compensators. In *AIAA Guidance, Navigation and Control Conference and Exhibit*, Honolulu, Hawaii, August 2008. American Institute of Aeronautics and Astronautics. ISBN 978-1-60086-999-0. doi: 10.2514/6.2008-7005.

J. Hodgkinson and K. Johnston. Initial results of an inflight simulation of augmented dynamics in fighter approach and landing. In *Guidance and Control Conference*, Boulder,CO,U.S.A., August 1979. American Institute of Aeronautics and Astronautics. doi: 10.2514/6.1979-1783.

Y. Hou, Q. Wang, and C. Dong. Gain Scheduled Control: Switched Polytopic System Approach. *Journal of Guidance, Control, and Dynamics*, 34(2):623–629, March 2011. ISSN 0731-5090, 1533-3884. doi: 10.2514/1.51699.

P. Ioannou and B. Fidan. *Adaptive Control Tutorial*. SIAM, January 2006. ISBN 978-0-89871-615-3.

P. Ioannou and J. Sun. *Robust Adaptive Control*. Courier Corporation, September 2013. ISBN 978-0-486-32072-4.

S. Jacklin. Closing the Certification Gaps in Adaptive Flight Control Software. In *AIAA Guidance, Navigation and Control Conference and Exhibit*, Honolulu, Hawaii, August 2008. American Institute of Aeronautics and Astronautics. ISBN 978-1-60086-999-0. doi: 10.2514/6.2008-6988.

G. Jacovitti and G. Scarano. Discrete time techniques for time delay estimation. *IEEE Transactions on Signal Processing*, 41(2):525–533, February 1993. ISSN 1941-0476. doi: 10.1109/78.193195.

H. Ju and C. Tsai. Longitudinal axis flight control law design by adaptive backstepping. *IEEE Transactions on Aerospace and Electronic Systems*, 43(1):311–329, January 2007. ISSN 1557-9603. doi: 10.1109/TAES.2007.357136. Conference Name: IEEE Transactions on Aerospace and Electronic Systems.

Twan Keijzer, Gertjan Looye, Q. Chu, and E. van Kampen. Flight testing of incremental backstepping based control laws with angular accelerometer feedback. *AIAA Scitech 2019 Forum*, 2019. doi: 10.2514/6.2019-0129.

H.K. Khalil. *Nonlinear Systems*. Prentice Hall, 2002. ISBN 978-0-13-067389-3.

B. S. Kim and A. J. Calise. Nonlinear Flight Control Using Neural Networks. *Journal of Guidance, Control, and Dynamics*, 20(1):26–33, January 1997. ISSN 0731-5090, 1533-3884. doi: 10.2514/2.4029.

M. E. Knapp, T. Berger, M. Tischler, and M. C. Cotting. Development of a Full Envelope Flight Identified F-16 Simulation Model. In *2018 AIAA Atmospheric Flight Mechanics Conference*, Kissimmee, Florida, January 2018. American Institute of Aeronautics and Astronautics. ISBN 978-1-62410-525-8. doi: 10.2514/6.2018-0525.

Miroslav Krstić, Ioannis Kanellakopoulos, and Petar V. Kokotović. *Nonlinear and adaptive control design*. Wiley, June 1995. ISBN 978-0-471-12732-1.

M. Laban. *On-Line Aircraft Aerodynamic Model Identification*. Phd thesis, Delft University of Technology, Faculty of Aerospace Engineering, May 1994. ISBN: 90-6275-987-4.

I.D. Landau, R. Lozano, M. M'Saad, and A. Karimi. *Adaptive Control: Algorithms, Analysis and Applications*. Springer Science & Business Media, June 2011. ISBN 978-0-85729-664-1.

D. Leith and W.E. Leithead. Survey of gain-scheduling analysis and design. *Int. J. Control*, 73:1001–1025, January 2000a. doi: 10.1080/002071700411304.

D.J. Leith and W.E. Leithead. Gain-Scheduled Control: Relaxing Slow Variation Requirements by Velocity-Based Design. *Journal of Guidance, Control, and Dynamics*, 23(6):988–1000, November 2000b. ISSN 0731-5090, 1533-3884. doi: 10.2514/2.4667.

Y. Li, S. Qiang, X. Zhuang, and O. Kaynak. Robust and adaptive backstepping control for nonlinear systems using RBF neural networks. *IEEE Transactions on Neural Networks*, 15(3):693–701, May 2004. ISSN 1941-0093. doi: 10.1109/TNN.2004.826215. Conference Name: IEEE Transactions on Neural Networks.

L. Ljung and I. D. Landau. Model Reference Adaptive Systems and Self-Tuning Regulators - Some Connections. *IFAC Proceedings Volumes*, 11(1):1973–1979, January 1978. ISSN 1474-6670. doi: 10.1016/S1474-6670(17)66173-1.

T. J. J. Lombaerts. *Fault Tolerant Flight Control: A Physical Model Approach*. PhD thesis, Delft University of Technology, Faculty of Aerospace Engineering, 2010. Publisher: T.J.J. Lombaerts. ISBN: 9789081544313.

T.J.J. Lombaerts, H.O. Huisman, Q.P. Chu, J.A. Mulder, and D.A. Joosten. Nonlinear Reconfiguring Flight Control Based on Online Physical Model Identification. *Journal of Guidance, Control, and Dynamics*, 32(3):727–748, May 2009. ISSN 0731-5090, 1533-3884. doi: 10.2514/1.40788.

P. Lu and E. van Kampen. Active fault-tolerant control for quadrotors subjected to a complete rotor failure. In *2015 IEEE/RSJ International Conference on Intelligent Robots and Systems (IROS)*, pages 4698–4703, Hamburg, Germany, September 2015. IEEE. ISBN 978-1-4799-9994-1. doi: 10.1109/IROS.2015.7354046.

A. D. Manshadi and F. Saghafi. In-Flight Estimation of Time-Varying Aircraft Center of Gravity Position Based on Kinematics Approach. *Journal of Aircraft*, 55(5):2037–2049, September 2018. ISSN 0021-8669, 1533-3868. doi: 10.2514/1.C034973.

I. M. Y. Mareels, B. D. O. Anderson, R. R. Bitmead, M. Bodson, and S. S. Sastry. Revisiting the Mit Rule for Adaptive Control. *IFAC Proceedings Volumes*, 20(2):161–166, July 1987. ISSN 1474-6670. doi: 10.1016/S1474-6670(17)55954-6.

I. Matamoros and C. C. de Visser. Incremental Nonlinear Control Allocation for a Tailless Aircraft with Innovative Control Effectors. In *2018 AIAA Guidance, Navigation, and Control Conference*, Kissimmee, Florida, January 2018. American Institute of Aeronautics and Astronautics. ISBN 978-1-62410-526-5. doi: 10.2514/6.2018-1116.

D.T. Mitchell, R.H. Hoh, B.L. Aponso, and D.H. Klyde. Proposed Incorporation of Mission-Oriented Flying Qualities into mil-std-1797a. Technical Report Wright Laboratory Technical Report (WL-TR-94-3162), 1994.

D.T. Mitchell, R.H. Hoh, B.L. Aponso, and D.H. Klyde. Flight Control Design - Best Practices. Technical Report Research and Technology Organization Technical Report (RTO-TR-029), 2000.

E. Mooij. Robust Control of a Conventional Aeroelastic Launch Vehicle. In *AIAA Scitech 2020 Forum*, Orlando, FL, January 2020. American Institute of Aeronautics and Astronautics. ISBN 978-1-62410-595-1. doi: 10.2514/6.2020-1103.

E. Morelli and V. Klein. *Aircraft System Identification: Theory and Practice*. Sunflyte Enterprises, November 2016. ISBN 978-0-9974306-1-5.

E. Muir. The GARTEUR High Incidence Research Model (HIRM) benchmark problem. In *Guidance, Navigation, and Control Conference and Exhibit*, Boston,MA,U.S.A., August 1998. American Institute of Aeronautics and Astronautics. doi: 10.2514/6.1998-4243.

National Research Council. *Aviation Safety and Pilot Control: Understanding and Preventing Unfavorable Pilot-Vehicle Interactions*. 1997. ISBN 978-0-309-05688-5. doi: 10.17226/5469.

T. Peter Neal and Rogers E. Smith. An In-flight Investigation to Develop Control System Design Criteria for Fighter Airplanes. Technical Report AFFDL-TR-70-74, Volume 2, Air Force Flight Dynamics Laboratory, December 1970.

L.T. Nguyen, M. E. Ogburn, W. P. Gilbert, K. S. Kibler, P. W. Brown, and P. L. Deal. Simulator study of stall/post-stall characteristics of a fighter airplane with relaxed longitudinal static stability. Technical report, NASA, December 1979.

N.T. Nguyen. *Model-Reference Adaptive Control: A Primer*. Advanced Textbooks in Control and Signal Processing. Springer International Publishing, 2018. ISBN 978-3-319-56392-3. doi: 10.1007/978-3-319-56393-0.

A.J. Ostroff and B.J. Bacon. Enhanced NDI strategies for reconfigurable flight control. In *Proceedings of the 2002 American Control Conference (IEEE Cat. No.CH37301)*, volume 5, pages 3631–3636 vol.5, May 2002. doi: 10.1109/ACC.2002.1024492. ISSN: 0743-1619.

M.D. Pavel, P. Shanthakumaran, Q.P. Chu, O. Stroosma, M. Wolfe, and H. Cazemier. Incremental Nonlinear Dynamic Inversion for the Apache AH-64 Helicopter Control. *Journal of the American Helicopter Society*, 65(2):1–16, April 2020. ISSN 2161-6027. doi: 10.4050/JAHS.65.022006.

W. H. Phillips. Flying qualities from early airplanes to the Space Shuttle. *Journal of Guidance, Control, and Dynamics*, May 1989. doi: 10.2514/3.20432.

R. Pratt. *Flight Control Systems: Practical Issues in Design and Implementation*. IET, 2000. ISBN 978-0-85296-766-9.

K. Reif, S. Gunther, E. Yaz, and R. Unbehauen. Stochastic stability of the discrete-time extended Kalman filter. *IEEE Transactions on Automatic Control*, 44(4):714–728, April 1999. ISSN 1558-2523. doi: 10.1109/9.754809.

J. Reiner, G.J. Balas, and W.L. Garrard. Robust Dynamic Inversion for Control of Highly Maneuverable Aircraft. *Journal of Guidance, Control, and Dynamics*, 18(1):18–24, January 1995. ISSN 0731-5090, 1533-3884. doi: 10.2514/3.56651.

E. Rollins, J. Valasek, J. A. Muse, and M. A. Bolender. Nonlinear Adaptive Dynamic Inversion Applied to a Generic Hypersonic Vehicle. In *AIAA Guidance, Navigation, and Control (GNC) Conference*, Boston, MA, August 2013. American Institute of Aeronautics and Astronautics. ISBN 978-1-62410-224-0. doi: 10.2514/6.2013-5234.

W.J. Rugh. Analytical framework for gain scheduling. *IEEE Control Systems Magazine*, 11(1):79–84, January 1991. ISSN 1941-000X. doi: 10.1109/37.103361.

R.S. Russel. Non-linear f-16 simulation using simulink and matlab. Technical report, University of Minnesota, June 2003.

R. Rysdyk and A.J. Calise. Robust nonlinear adaptive flight control for consistent handling qualities. *IEEE Transactions on Control Systems Technology*, 13(6):896–910, November 2005. ISSN 2374-0159. doi: 10.1109/TCST.2005.854345.

R. Sedgewick and P. Flajolet. *An introduction to the analysis of algorithms*. Addison-Wesley, Upper Saddle River, NJ, 2nd ed edition, 2013. ISBN 978-0-321-90575-8.

J. Shamma and M. Athans. Gain Scheduling: Potential Hazards and Possible Remedies. *Control Systems, IEEE*, 12:101–107, July 1992. doi: 10.1109/37.165527.

A. K. Shastry, A. Pattanaik, and M. Kothari. Neuro-adaptive Augmented Dynamic Inversion Controller for Quadrotors. *IFAC-PapersOnLine*, 49(1):302–307, January 2016. ISSN 2405-8963. doi: 10.1016/j.ifacol.2016.03.070.

S. Sieberling, Q.P. Chu, and J.A. Mulder. Robust flight control using incremental nonlinear dynamic inversion and angular acceleration prediction. *Journal of guidance, control and dynamics, 33.2010 no.6*, 2010. ISSN 1533-3884. doi: 10.2514/1.49978.

A. S. Silveira, J. E. N. Rodríguez, and A. A. R. Coelho. Robust design of a 2-DOF GMV controller: A direct self-tuning and fuzzy scheduling approach. *ISA Transactions*, 51(1):13–21, January 2012. ISSN 0019-0578. doi: 10.1016/j.isatra.2011.07.006.

P. Simplicio, M. Pavel, E. Van Kampen, and Q.P. Chu. An acceleration measurements-based approach for helicopter nonlinear flight control using Incremental Nonlinear Dynamic Inversion. *Control Engineering Practice*, 21:1065–1077, August 2013. doi: 10.1016/j.conengprac.2013.03.009.

J.J.E. Slotine and W. Li. *Applied nonlinear control*. Prentice Hall, Englewood Cliffs, N.J, 1991. ISBN 978-0-13-040890-7.

E. J. J. Smeur, G. C. H. E. de Croon, and Q. Chu. Cascaded incremental nonlinear dynamic inversion for MAV disturbance rejection. *Control Engineering Practice*, 73:79–90, April 2018. ISSN 0967-0661. doi: 10.1016/j.conengprac.2018.01.003.

E.J.J. Smeur, Q.P. Chu, and G.C.H.E. de Croon. Adaptive Incremental Nonlinear Dynamic Inversion for Attitude Control of Micro Air Vehicles. *Journal of Guidance, Control, and Dynamics*, 39(3): 450–461, March 2016. ISSN 0731-5090, 1533-3884. doi: 10.2514/1.G001490.

M. Smit and I. Craig. Robust flight controller design using H-infinity loop-shaping and dynamic inversion techniques. In *Guidance, Navigation, and Control Conference and Exhibit*, Boston,MA,U.S.A., August 1998. American Institute of Aeronautics and Astronautics. doi: 10.2514/6.1998-4132.

P. Smith and A. Berry. Flight test experience of a non-linear dynamic inversion control law on the VAAC Harrier. In *Atmospheric Flight Mechanics Conference*, Denver,CO,U.S.A., August 2000. American Institute of Aeronautics and Astronautics. doi: 10.2514/6.2000-3914.

P.R. Smith. A simplified approach to nonlinear dynamic inversion based flight control. In *23rd Atmospheric Flight Mechanics Conference*, Boston,MA,U.S.A., August 1998. American Institute of Aeronautics and Astronautics. doi: 10.2514/6.1998-4461.

S.A. Snell, D.F. Enns, and W.L. Garrard. Nonlinear inversion flight control for a supermaneuverable aircraft. *Journal of Guidance, Control, and Dynamics*, 15(4):976–984, July 1992. ISSN 0731-5090, 1533-3884. doi: 10.2514/3.20932.

L. Sonneveldt. *Adaptive Backstepping Flight Control for Modern Fighter Aircraft*. PhD thesis, Delft University of Technology, Faculty of Aerospace Engineering, 2010. ISBN 978-90-8570-573-4.

A. Stanley. *State estimation of in-flight aircraft centre of gravity*. thesis, Loughborough University, January 2011.

M. Steinberg and A. Page. Nonlinear adaptive flight control with a backstepping design approach. In *Guidance, Navigation, and Control Conference and Exhibit*, Boston,MA,U.S.A., August 1998. American Institute of Aeronautics and Astronautics. doi: 10.2514/6.1998-4230.

R.F. Stengel. Toward intelligent flight control. *IEEE Transactions on Systems, Man, and Cybernetics*, 23(6):1699–1717, December 1993. ISSN 00189472. doi: 10.1109/21.257764.

V. Stepanyan, K. Krishnakumar, N. Nguyen, and L. Van Eykeren. Stability and Performance Metrics for Adaptive Flight Control. In *AIAA Guidance, Navigation, and Control Conference*, Chicago, Illinois, August 2009. American Institute of Aeronautics and Astronautics. ISBN 978-1-60086-978-5. doi: 10.2514/6.2009-5965.

J. Sun, C. Li, C. Liu, Z. Gong, and R. Wang. A data-driven health indicator extraction method for aircraft air conditioning system health monitoring. *Chinese Journal of Aeronautics*, 32(2):409–416, February 2019. ISSN 1000-9361. doi: 10.1016/j.cja.2018.03.024.

A.K. Tangirala. *Principles of System Identification: Theory and Practice*. CRC Press, October 2018. ISBN 978-1-4398-9602-0.

M. B. Tischler. *Practical Methods for Aircraft and Rotorcraft Flight Control Design: An Optimization-based Approach*. American Institute of Aeronautics and Astronautics, Incorporated, 2017. ISBN 978-1-62410-443-5.

H. J. Tol, C. C. de Visser, L. G. Sun, E. van Kampen, and Q. P. Chu. Multivariate Spline-Based Adaptive Control of High-Performance Aircraft with Aerodynamic Uncertainties. *Journal of Guidance, Control, and Dynamics*, 39(4):781–800, April 2016. ISSN 0731-5090, 1533-3884. doi: 10.2514/1.G001079.

P. van Gils, E. van Kampen, C.C. de Visser, and Q.P. Chu. Adaptive Incremental Backstepping Flight Control for a High-Performance Aircraft with Uncertainties. 2015.

Pieter van Gils, Erik-Jan Van Kampen, Coen C. de Visser, and Q Ping Chu. Adaptive Incremental Backstepping Flight Control for a High-Performance Aircraft with Uncertainties. In *AIAA Guidance, Navigation, and Control Conference*, San Diego, California, USA, January 2016. American Institute of Aeronautics and Astronautics. ISBN 978-1-62410-389-6. doi: 10.2514/6.2016-1380. URL `http://arc.aiaa.org/doi/10.2514/6.2016-1380`.

E. R. Van Oort. *Adaptive Backstepping Control and Safety Analysis for Modern Fighter Aircraft*. PhD thesis, Delft University of Technology, Faculty of Aerospace Engineering, 2011. ISBN 978-90-8570-735-6.

E. R. van Oort, L. Sonneveldt, Q. P. Chu, and J. A. Mulder. Full-Envelope Modular Adaptive Control of a Fighter Aircraft Using Orthogonal Least Squares. *Journal of Guidance, Control, and Dynamics*, 33(5):1461–1472, September 2010. ISSN 0731-5090, 1533-3884. doi: 10.2514/1.48175.

R.C. van 't Veld. Incremental Nonlinear Dynamic Inversion Flight Control: Stability and Robustness Analysis and Improvements. 2016.

E. Wan and R. Merwe. The Unscented Kalman Filter for Nonlinear Estimation. volume 153-158, pages 153–158, February 2000. ISBN 978-0-7803-5800-3. doi: 10.1109/ASSPCC.2000.882463.

X. Wang, E. Van Kampen, Q.P. Chu, and R. De Breuker. Flexible Aircraft Gust Load Alleviation with Incremental Nonlinear Dynamic Inversion. *Journal of Guidance, Control, and Dynamics*, 42(7): 1519–1536, July 2019a. ISSN 0731-5090, 1533-3884. doi: 10.2514/1.G003980.

X. Wang, E. van Kampen, Q.P. Chu, and P. Lu. Stability Analysis for Incremental Nonlinear Dynamic Inversion Control. *Journal of Guidance, Control, and Dynamics*, 42(5):1116–1129, May 2019b. ISSN 0731-5090, 1533-3884. doi: 10.2514/1.G003791.

E. Weerdt, E. Kampen, D. Gemert, Q.P. Chu, and J.A. Mulder. Adaptive Nonlinear Dynamic Inversion for Spacecraft Attitude Control with Fuel Sloshing. In *AIAA Guidance, Navigation and Control Conference and Exhibit*, Honolulu, Hawaii, August 2008. American Institute of Aeronautics and Astronautics. ISBN 978-1-60086-999-0. doi: 10.2514/6.2008-7162.

H.P. Whitaker, J. Yamron, and A. Kezer. *Design of model-reference adaptive control systems for aircraft*. Massachusetts Institute of Technology, Instrumentation Laboratory : Jackson & Moreland, Cambridge, Mass., 1958.

B. Wittenmark. Adaptive Dual Control Methods: An Overview. *IFAC Proceedings Volumes*, 28(13): 67–72, June 1995. ISSN 1474-6670. doi: 10.1016/S1474-6670(17)45327-4.

V. Wüest, V. Kumar, and G. Loianno. Online Estimation of Geometric and Inertia Parameters for Multirotor Aerial Vehicles. In *2019 International Conference on Robotics and Automation (ICRA)*, pages 1884–1890, May 2019. doi: 10.1109/ICRA.2019.8794274. ISSN: 2577-087X.

J. Zhang, J.and Wang, F. Zhang, and F. Holzapfel. Modeling and Incremental Nonlinear Dynamic Inversion Control for a Highly Redundant Flight System. In *AIAA Scitech 2019 Forum*, San Diego, California, January 2019. American Institute of Aeronautics and Astronautics. ISBN 978-1-62410-578-4. doi: 10.2514/6.2019-1922.

K.J. Åström and B. Wittenmark. *Adaptive Control*. Courier Corporation, January 2008. ISBN 978-0-486-46278-3.

Appendices

A

Preliminary experiments sensitivity results

Table A.1: $\mathcal{L}_\infty$-norm of the tracking error (RLS-AINDI).

	TO-1					TO-2				
		var(v) $[(^\circ/s^2)^2]$		τ_d [s]			var(v) $[(^\circ/s^2)^2]$		τ_d [s]	
λ	Initial	0.01	0.10	0.02	0.05	Initial	0.01	0.10	0.02	0.05
non-adaptive	0.86	0.90	1.04	1.05	1.39	0.86	0.87	0.94	1.05	1.39
0.9800	1.03	1.14	1.19	1.19	1.50	1.18	1.14	1.25	1.62	2.26
0.9850	0.92	0.97	1.06	1.08	1.41	1.18	0.97	1.06	1.62	2.46
0.9900	0.86	0.90	0.98	1.04	1.37	1.19	0.90	0.98	1.62	2.21
0.9950	0.85	0.89	0.97	1.04	1.37	1.18	0.89	0.97	1.62	2.19
0.9970	0.85	0.89	0.97	1.04	1.38	1.19	0.89	0.97	1.64	2.76
0.9980	0.85	0.89	0.97	1.05	1.38	1.10	0.89	0.97	1.35	1.64
0.9990	0.85	0.89	0.97	1.05	1.38	0.85	0.89	0.97	1.05	1.38
0.9995	0.86	0.89	0.98	1.05	1.38	0.86	0.89	0.97	1.05	1.38
1.0000	0.86	0.90	1.02	1.05	1.38	0.86	0.92	1.10	1.05	1.38

Table A.2: $\mathcal{L}_\infty$-norm of the tracking error (LMS-AINDI).

	TO-1					TO-2				
		var(ν) $[(^\circ/s^2)^2]$		τ_d [s]			var(ν) $[(^\circ/s^2)^2]$		τ_d [s]	
μ	Initial	0.01	0.10	0.02	0.05	Initial	0.01	0.10	0.02	0.05
non-adaptive	0.86	0.90	1.04	1.05	1.39	0.86	0.87	0.94	1.05	1.39
10	0.85	0.88	0.96	1.04	1.37	0.85	0.88	0.96	1.04	1.37
50	0.86	0.85	0.92	1.05	1.39	0.86	0.85	0.92	1.05	1.39
100	0.87	0.86	0.89	1.06	1.41	0.87	0.86	0.89	1.06	1.41
150	0.88	0.87	0.88	1.07	1.43	0.88	0.87	0.88	1.07	1.43
200	0.89	0.88	0.87	1.09	1.44	0.89	0.88	0.87	1.09	1.44
250	0.90	0.89	0.87	1.10	1.45	0.90	0.89	0.87	1.10	1.45
300	0.91	0.90	0.87	1.11	1.47	0.91	0.90	0.87	1.11	1.47
400	0.93	0.92	0.87	1.12	1.48	0.93	0.92	0.87	1.12	1.48
500	0.94	0.93	0.88	1.14	1.50	0.94	0.93	0.88	1.14	1.50
600	0.95	0.94	0.89	1.15	1.50	0.95	0.94	0.89	1.15	1.50
700	0.96	0.95	0.90	1.15	1.51	0.96	0.95	0.90	1.15	1.51
800	0.97	0.96	0.92	1.16	1.51	0.97	0.96	0.91	1.16	1.51
900	0.98	0.96	0.93	1.17	1.51	0.97	0.96	0.93	1.16	1.51
1000	0.98	0.97	0.94	1.17	1.52	0.98	0.97	0.94	1.17	1.52
1500	1.01	0.99	0.99	1.19	1.52	1.01	0.99	0.99	1.19	1.52
2000	1.03	1.00	1.03	1.22	1.53	1.03	1.00	1.03	1.22	1.53
3000	1.06	1.01	1.06	1.26	1.57	1.06	1.01	1.05	1.26	1.57
4000	1.02	1.01	1.06	1.29	1.61	1.02	1.01	1.06	1.29	1.61
4200	0.96	1.01	1.06	1.30	1.62	0.96	1.01	1.06	1.30	1.62
4400	1.25	1.02	1.06	1.12	1.64	1.25	1.02	1.06	1.12	1.64
4600	13.20	1.02	1.06	1.20	1.68	9.85	1.02	1.06	1.20	1.67

Table A.3: $\mathcal{L}_2$-norm of the tracking error (RLS-AINDI).

	TO-1					TO-2				
		var(ν) $[(^\circ/s^2)^2]$		τ_d [s]			var(ν) $[(^\circ/s^2)^2]$		τ_d [s]	
λ	Initial	0.01	0.10	0.02	0.05	Initial	0.01	0.10	0.02	0.05
non-adaptive	2.59	2.60	2.72	3.13	4.41	1.62	1.65	1.83	1.95	2.72
0.9800	3.16	2.99	2.75	3.64	4.68	2.00	1.93	2.06	2.34	3.11
0.9850	2.85	2.77	2.68	3.25	4.29	1.82	1.80	1.96	2.13	2.89
0.9900	2.56	2.54	2.59	2.97	4.02	1.67	1.65	1.88	1.99	2.77
0.9950	2.37	2.37	2.53	2.79	3.85	1.57	1.55	1.84	1.90	2.68
0.9970	2.32	2.32	2.52	2.74	3.81	1.55	1.53	1.85	1.93	2.75
0.9980	2.30	2.31	2.52	2.73	3.80	1.55	1.52	1.86	1.85	2.52
0.9990	2.31	2.33	2.54	2.74	3.81	1.50	1.53	1.87	1.78	2.45
0.9995	2.39	2.41	2.65	2.84	3.92	1.55	1.59	1.95	1.84	2.53
1.0000	2.58	2.61	2.87	3.11	4.35	1.61	1.66	2.05	1.95	2.71

Table A.4: $\mathcal{L}_2$-norm of the tracking error (LMS-AINDI).

	TO-1					TO-2				
		var(v) $[(^\circ/s^2)^2]$		τ_d [s]			var(v) $[(^\circ/s^2)^2]$		τ_d [s]	
μ	Initial	0.01	0.10	0.02	0.05	Initial	0.01	0.10	0.02	0.05
non-adaptive	2.59	2.60	2.72	3.13	4.41	1.62	1.65	1.83	1.95	2.72
10	2.33	2.34	2.57	2.75	3.80	1.53	1.57	1.92	1.81	2.47
50	2.28	2.30	2.51	2.72	3.80	1.49	1.52	1.87	1.77	2.44
100	2.28	2.30	2.51	2.72	3.82	1.49	1.52	1.86	1.77	2.45
150	2.29	2.30	2.50	2.73	3.82	1.49	1.52	1.86	1.78	2.46
200	2.29	2.30	2.50	2.73	3.82	1.49	1.52	1.86	1.78	2.47
250	2.29	2.30	2.49	2.73	3.82	1.50	1.53	1.86	1.78	2.47
300	2.29	2.30	2.49	2.73	3.82	1.50	1.53	1.86	1.79	2.48
400	2.30	2.30	2.49	2.74	3.83	1.51	1.54	1.86	1.80	2.49
500	2.31	2.31	2.49	2.74	3.83	1.52	1.54	1.86	1.80	2.49
600	2.31	2.31	2.48	2.75	3.84	1.53	1.55	1.86	1.81	2.50
700	2.32	2.32	2.48	2.76	3.84	1.53	1.55	1.86	1.82	2.51
800	2.33	2.33	2.48	2.76	3.84	1.54	1.56	1.87	1.82	2.51
900	2.34	2.33	2.49	2.77	3.85	1.55	1.57	1.87	1.83	2.52
1000	2.35	2.34	2.49	2.78	3.85	1.55	1.57	1.87	1.84	2.52
1500	2.39	2.38	2.51	2.82	3.88	1.59	1.61	1.90	1.88	2.54
2000	2.44	2.42	2.54	2.88	3.91	1.63	1.64	1.94	1.91	2.57
3000	2.55	2.51	2.63	3.00	4.03	1.69	1.70	2.00	2.00	2.66
4000	2.64	2.60	2.71	3.11	4.19	1.74	1.75	2.05	2.06	2.76
4200	2.65	2.61	2.73	3.13	4.22	1.74	1.76	2.05	2.08	2.78
4400	2.69	2.63	2.74	3.14	4.26	1.79	1.76	2.06	2.07	2.80
4600	50.58	2.65	2.76	3.16	4.29	42.97	1.77	2.07	2.09	2.82

Table A.5: RMS of the tracking error (RLS-AINDI).

	TO-1					TO-2				
		var(v) $[(^\circ/s^2)^2]$		τ_d [s]			var(v) $[(^\circ/s^2)^2]$		τ_d [s]	
λ	Initial	0.01	0.10	0.02	0.05	Initial	0.01	0.10	0.02	0.05
non-adaptive	0.180	0.180	0.190	0.221	0.312	0.120	0.120	0.130	0.138	0.193
0.9800	0.226	0.212	0.194	0.257	0.331	0.142	0.137	0.146	0.165	0.220
0.9850	0.202	0.196	0.189	0.230	0.303	0.129	0.127	0.139	0.151	0.204
0.9900	0.181	0.179	0.183	0.210	0.284	0.118	0.117	0.133	0.141	0.196
0.9950	0.167	0.167	0.179	0.197	0.272	0.111	0.110	0.130	0.134	0.190
0.9970	0.164	0.164	0.178	0.194	0.269	0.110	0.108	0.131	0.137	0.195
0.9980	0.163	0.163	0.178	0.193	0.268	0.110	0.107	0.131	0.131	0.178
0.9990	0.164	0.164	0.180	0.194	0.270	0.106	0.108	0.133	0.126	0.173
0.9995	0.169	0.171	0.187	0.201	0.277	0.110	0.112	0.138	0.130	0.179
1.0000	0.183	0.184	0.203	0.220	0.307	0.114	0.117	0.145	0.138	0.192

Table A.6: RMS of the tracking error (LMS-AINDI).

	TO-1					TO-2				
		var(v) $[(^\circ/s^2)^2]$		τ_d [s]			var(v) $[(^\circ/s^2)^2]$		τ_d [s]	
μ	Initial	0.01	0.10	0.02	0.05	Initial	0.01	0.10	0.02	0.05
non-adaptive	0.180	0.180	0.190	0.221	0.312	0.120	0.120	0.130	0.138	0.193
10	0.164	0.166	0.182	0.194	0.269	0.108	0.111	0.136	0.128	0.174
50	0.161	0.162	0.178	0.192	0.270	0.105	0.108	0.132	0.125	0.173
100	0.162	0.162	0.177	0.193	0.270	0.105	0.108	0.132	0.125	0.174
150	0.162	0.162	0.177	0.193	0.270	0.105	0.108	0.132	0.126	0.174
200	0.162	0.162	0.177	0.193	0.270	0.106	0.108	0.131	0.126	0.174
250	0.162	0.163	0.176	0.193	0.270	0.106	0.108	0.131	0.126	0.175
300	0.162	0.163	0.176	0.193	0.270	0.106	0.108	0.131	0.126	0.175
400	0.163	0.163	0.176	0.194	0.271	0.107	0.109	0.131	0.127	0.176
500	0.163	0.163	0.176	0.194	.0271	0.107	0.109	0.131	0.128	0.176
600	0.164	0.164	0.176	0.194	0.271	0.108	0.110	0.132	0.128	0.177
700	0.164	0.164	0.176	0.195	0.272	0.108	0.110	0.132	0.129	0.177
800	0.165	0.164	0.176	0.195	0.272	0.109	0.110	0.132	0.129	0.178
900	0.165	0.165	0.176	0.196	0.272	0.109	0.111	0.132	0.130	0.178
1000	0.166	0.165	0.176	0.197	0.272	0.110	0.111	0.133	0.130	0.178
1500	0.169	0.168	0.178	0.200	0.274	0.112	0.114	0.135	0.133	0.180
2000	0.173	0.171	0.180	0.203	0.277	0.115	0.116	0.137	0.135	0.182
3000	0.180	0.178	0.186	0.212	0.285	0.120	0.120	0.141	0.141	0.188
4000	0.187	0.184	0.192	0.220	0.296	0.123	0.124	0.145	0.146	0.195
4200	0.188	0.185	0.193	0.222	0.299	0.123	0.124	0.145	0.147	0.197
4400	0.190	0.186	0.194	0.222	0.301	0.126	0.125	0.146	0.146	0.198
4600	3.577	0.187	0.195	0.224	0.303	3.039	0.125	0.146	0.148	0.200

Table A.7: CMSD of the elevator deflection (RLS-AINDI).

	TO-1					TO-2				
		var(v) $[(^\circ/s^2)^2]$		τ_d [s]			var(v) $[(^\circ/s^2)^2]$		τ_d [s]	
λ	Initial	0.01	0.10	0.02	0.05	Initial	0.01	0.10	0.02	0.05
non-adaptive	1372	1510	2000	1549	1926	489	719	1279	548	676
0.9800	1274	1302	1463	1301	1405	468	552	770	486	532
0.9850	1145	1216	1447	1162	1256	427	520	737	438	486
0.9900	1035	1126	1426	1063	1150	393	477	719	408	454
0.9950	966	1067	1415	1000	1085	376	474	700	400	444
0.9970	954	1061	1429	993	1081	378	505	714	408	461
0.9980	958	1071	1455	1001	1094	381	540	791	403	448
0.9990	999	1124	1547	1052	1162	379	582	881	401	448
0.9995	1097	1247	1745	1172	1316	423	666	1222	455	520
1.0000	1352	1556	2227	1515	1848	486	781	1508	544	666

Table A.8: CMSD of the elevator deflection (LMS-AINDI).

	TO-1					TO-2				
		var(ν) $[(^\circ/s^2)^2]$		τ_d [s]			var(ν) $[(^\circ/s^2)^2]$		τ_d [s]	
μ	Initial	0.01	0.10	0.02	0.05	Initial	0.01	0.10	0.02	0.05
non-adaptive	1372	1510	2000	1549	1926	489	719	1279	548	676
10	990	1118	1546	1033	1123	396	619	1117	416	459
50	917	1020	1380	950	1027	350	531	921	362	394
100	907	1005	1351	938	1013	341	513	876	351	382
150	903	998	1338	933	1008	338	506	855	348	378
200	900	994	1329	930	1005	336	502	839	346	375
250	899	990	1322	928	1003	335	499	827	344	374
300	897	988	1316	927	1001	334	496	816	344	373
400	895	983	1305	925	999	333	492	798	343	372
500	894	980	1296	923	997	333	488	783	342	372
600	893	977	1288	922	996	333	485	770	342	372
700	893	974	1281	922	996	333	482	759	342	372
800	893	972	1274	921	995	333	480	749	342	372
900	893	971	1268	921	995	333	478	740	342	372
1000	893	970	1262	921	995	333	476	732	342	372
1500	896	966	1239	923	997	334	469	700	344	374
2000	901	967	1224	926	1001	337	465	678	346	377
3000	913	973	1209	937	1014	342	462	654	351	383
4000	929	985	1209	951	1032	348	462	642	357	391
4200	933	987	1210	954	1036	349	463	641	358	393
4400	936	990	1211	957	1041	351	463	640	360	394
4600	54	993	1212	961	1045	54	464	639	361	396

Table A.9: CMSD of the correction factor estimation (RLS-AINDI).

	TO-1					TO-2				
		var(ν) $[(^\circ/s^2)^2]$		τ_d [s]			var(ν) $[(^\circ/s^2)^2]$		τ_d [s]	
λ	Initial	0.01	0.10	0.02	0.05	Initial	0.01	0.10	0.02	0.05
0.9800	258	330	729	248	253	268	8441	9521	272	266
0.9850	195	220	439	190	194	207	5277	5784	199	203
0.9900	131	138	240	127	131	142	2411	2764	139	141
0.9950	65	67	106	64	68	66	632	833	65	66
0.9970	40	41	62	39	42	34	192	294	31	32
0.9980	27	28	41	27	29	20	66	121	19	20
0.9990	14	14	20	14	15	11	15	31	11	11
0.9995	7	7	9	7	8	6	6	9	6	6
1.0000	4	4	4	4	4	4	4	4	4	4

Table A.10: CMSD of the correction factor estimation (LMS-AINDI).

	TO-1					TO-2				
		var(ν) $[(^\circ/s^2)^2]$		τ_d [s]			var(ν) $[(^\circ/s^2)^2]$		τ_d [s]	
μ	Initial	0.01	0.10	0.02	0.05	Initial	0.01	0.10	0.02	0.05
10	6	6	7	6	6	5	5	6	5	5
50	12	12	17	12	13	7	8	12	7	8
100	19	20	29	19	21	10	11	19	10	11
150	26	27	42	27	30	12	14	26	13	13
200	33	35	54	34	38	15	17	33	15	16
250	40	42	66	41	46	17	20	40	17	19
300	47	49	77	48	54	20	23	47	20	22
400	60	63	101	61	69	24	28	59	25	27
500	72	76	123	74	85	29	34	72	29	32
600	84	89	146	87	100	33	39	84	33	38
700	96	102	167	99	114	37	44	95	38	43
800	107	144	189	111	129	41	49	107	42	48
900	118	126	210	122	143	45	54	118	46	52
1000	129	138	231	133	157	48	58	128	49	57
1500	178	192	329	185	220	65	80	179	67	78
2000	221	240	420	229	274	79	99	225	82	97
3000	296	325	582	304	356	104	132	307	107	125
4000	364	396	726	366	415	131	161	380	128	146
4200	383	410	753	379	426	144	166	394	133	150
4400	409	424	780	395	437	162	173	407	141	154
4600	2.246e7	439	808	415	449	2.246e7	181	422	155	160

Table A.11: $\mathcal{L}_\infty$-norm of the control effectiveness estimation deviation (RLS-AINDI).

	TO-1					TO-2				
		var(ν) $[(^\circ/s^2)^2]$		τ_d [s]			var(ν) $[(^\circ/s^2)^2]$		τ_d [s]	
λ	Initial	0.01	0.10	0.02	0.05	Initial	0.01	0.10	0.02	0.05
0.9800	0.091	0.105	0.139	0.086	0.084	0.225	22.241	24.597	0.163	0.162
0.9850	0.065	0.076	0.091	0.063	0.062	0.226	14.413	14.597	0.161	0.161
0.9900	0.045	0.052	0.054	0.042	0.041	0.225	5.763	6.219	0.161	0.161
0.9950	0.037	0.037	0.037	0.037	0.037	0.224	1.113	1.396	0.163	0.161
0.9970	0.037	0.037	0.037	0.037	0.037	0.219	0.457	0.607	0.157	0.157
0.9980	0.041	0.041	0.040	0.040	0.040	0.146	0.203	0.326	0.141	0.140
0.9990	0.043	0.043	0.043	0.043	0.043	0.056	0.046	0.103	0.053	0.052
0.9995	0.043	0.043	0.043	0.043	0.043	0.047	0.047	0.046	0.047	0.047
1.0000	0.053	0.053	0.052	0.052	0.052	0.054	0.054	0.054	0.054	0.054

Table A.12: $\mathcal{L}_\infty$-norm of control effectiveness estimation deviation (LMS-AINDI).

	TO-1					TO-2				
		var(ν) $[(°/s^2)^2]$		τ_d [s]			var(ν) $[(°/s^2)^2]$		τ_d [s]	
μ	Initial	0.01	0.10	0.02	0.05	Initial	0.01	0.10	0.02	0.05
10	0.036	0.036	0.036	0.036	0.035	0.036	0.036	0.036	0.036	0.035
50	0.031	0.031	0.031	0.031	0.031	0.031	0.031	0.031	0.031	0.031
100	0.032	0.031	0.029	0.031	0.031	0.032	0.031	0.029	0.031	0.031
150	0.032	0.032	0.029	0.032	0.032	0.032	0.032	0.033	0.032	0.032
200	0.033	0.033	0.029	0.033	0.033	0.033	0.033	0.041	0.033	0.033
250	0.034	0.033	0.029	0.034	0.034	0.034	0.033	0.049	0.034	0.034
300	0.035	0.034	0.029	0.034	0.035	0.035	0.034	0.056	0.034	0.035
400	0.036	0.035	0.030	0.036	0.036	0.036	0.035	0.068	0.036	0.036
500	0.037	0.036	0.034	0.037	0.037	0.037	0.036	0.079	0.037	0.037
600	0.038	0.037	0.038	0.038	0.038	0.038	0.037	0.088	0.038	0.038
700	0.039	0.038	0.042	0.039	0.039	0.039	0.038	0.097	0.039	0.039
800	0.040	0.038	0.045	0.040	0.040	0.040	0.038	0.105	0.040	0.040
900	0.041	0.039	0.048	0.041	0.041	0.041	0.039	0.113	0.041	0.041
1000	0.043	0.040	0.050	0.042	0.042	0.043	0.040	0.120	0.042	0.042
1500	0.048	0.43	0.067	0.046	0.046	0.048	0.043	0.151	0.046	0.046
2000	0.052	0.056	0.084	0.050	0.050	0.052	0.048	0.177	0.050	0.050
3000	0.068	0.077	0.107	0.067	0.067	0.068	0.067	0.220	0.067	0.066
4000	0.204	0.092	0.123	0.085	0.083	0.204	0.083	0.256	0.085	0.083
4200	0.398	0.095	0.126	0.088	0.086	0.398	0.086	0.263	0.088	0.086
4400	0.731	0.097	0.130	0.142	0.089	0.731	0.088	0.269	0.142	0.089
4600	1.145e6	0.140	0.134	0.371	0.092	1.146e6	0.140	0.276	0.371	0.091

Table A.13: RMS of the control effectiveness estimation deviation (RLS-AINDI).

	TO-1					TO-2				
		var(ν) $[(°/s^2)^2]$		τ_d [s]			var(ν) $[(°/s^2)^2]$		τ_d [s]	
λ	Initial	0.01	0.10	0.02	0.05	Initial	0.01	0.10	0.02	0.05
0.9800	0.013	0.012	0.031	0.012	0.012	1.00	34.45	36.87	0.064	0.058
0.9850	0.010	0.010	0.020	0.010	0.010	0.98	25.16	25.61	0.063	0.057
0.9900	0.009	0.009	0.013	0.009	0.009	0.92	12.80	13.85	0.060	0.055
0.9950	0.010	0.010	0.011	0.010	0.009	0.68	4.27	5.37	0.045	0.042
0.9970	0.012	0.011	0.011	0.011	0.011	0.45	1.68	2.59	0.030	0.029
0.9980	0.014	0.013	0.013	0.013	0.013	0.31	0.70	1.34	0.022	0.021
0.9990	0.019	0.019	0.018	0.019	0.018	0.34	0.33	0.50	0.024	0.024
0.9995	0.028	0.028	0.027	0.028	0.027	0.49	0.48	0.44	0.034	0.034
1.0000	0.044	0.044	0.043	0.044	0.043	0.66	0.65	0.66	0.047	0.047

Table A.14: RMS of the Control effectiveness estimation deviation (LMS-AINDI).

	TO-1					TO-2				
		var(ν) $[(^\circ/s^2)^2]$		τ_d [s]			var(ν) $[(^\circ/s^2)^2]$		τ_d [s]	
μ	Initial	0.01	0.10	0.02	0.05	Initial	0.01	0.10	0.02	0.05
10	0.019	0.018	0.015	0.018	0.017	0.028	0.027	0.021	0.027	0.026
50	0.008	0.008	0.005	0.008	0.008	0.012	0.011	0.007	0.012	0.011
100	0.006	0.006	0.006	0.006	0.006	0.009	0.007	0.012	0.008	0.008
150	0.005	0.005	0.007	0.005	0.005	0.007	0.006	0.017	0.007	0.007
200	0.005	0.005	0.008	0.005	0.005	0.006	0.005	0.021	0.006	0.006
250	0.005	0.005	0.009	0.005	0.005	0.006	0.005	0.025	0.006	0.006
300	0.005	0.005	0.010	0.005	0.005	0.005	0.005	0.029	0.005	0.005
400	0.006	0.007	0.012	0.006	0.006	0.005	0.006	0.035	0.005	0.005
500	0.007	0.008	0.014	0.007	0.007	0.006	0.008	0.041	0.006	0.006
600	0.008	0.009	0.016	0.008	0.008	0.007	0.010	0.047	0.007	0.006
700	0.010	0.011	0.018	0.009	0.009	0.008	0.011	0.052	0.008	0.007
800	0.011	0.012	0.019	0.010	0.010	0.009	0.013	0.057	0.009	0.008
900	0.012	0.013	0.021	0.012	0.011	0.011	0.015	0.061	0.010	0.009
1000	0.014	0.015	0.023	0.013	0.012	0.012	0.017	0.066	0.011	0.010
1500	0.020	0.021	0.030	0.019	0.017	0.017	0.024	0.085	0.016	0.014
2000	0.025	0.026	0.037	0.023	0.021	0.022	0.031	0.102	0.020	0.017
3000	0.033	0.035	0.048	0.031	0.027	0.027	0.041	0.129	0.024	0.020
4000	0.038	0.041	0.057	0.036	0.031	0.030	0.049	0.149	0.027	0.021
4200	0.039	0.042	0.058	0.036	0.032	0.030	0.050	0.152	0.027	0.021
4400	0.041	0.042	0.059	0.037	0.032	0.031	0.051	0.156	0.027	0.021
4600	6.266e5	0.043	0.061	0.038	0.033	6.262e5	0.052	0.159	0.027	0.022